NUI MAYNOOTH

Ollscoil na hÉireann Má Nuad

Topics in Automotive Rollover Prevention: Robust and Adaptive Switching Strategies for Estimation and Control

A dissertation

submitted for the degree of

Dodoctor of Philosophy

by

Selim Solmaz, B.Sc., M.Sc.

Supervisor: Prof. Robert Shorten

Hamilton Institute

National University of Ireland, Maynooth

Ollscoil na hÉireann, Má Nuad

Maynooth, December 2007

For my wife Aslı, and my daughter Melis Naz

&

For my mother, father and all the family.

Sevgili eşim Aslı Solmaz ve biricik kızımız Melis Naz Solmaz'a

&

annem Hafize Solmaz, babam Mehmet Solmaz ve tüm aileme...

Acknowledgements

First and foremost, as provider of my research guidance and focus, Professor Robert Shorten deserves thanks that go beyond anything that can be expressed here. I would like to convey my sincere gratitude to him for being an excellent supervisor and a good friend with his constant support, great patience, generous assistance and enthusiastic encouragement throughout the past four years. His confidence in me and my work will forever be appreciated. His emphasis on "leaving no stones unturned" produced an enjoyable work environment and a challenging yet great learning experience, where the constant feeling of accomplishment is an integral part of the process. With a healthy combination of theoretical and applied research, this experience has helped me mature as a researcher. I feel especially grateful to him for creating numerous and generous opportunities for me to learn, as well as helping me to interact and benefit from the experience of many international researchers.

Many thanks are also due to Professor Martin Corless of Purdue University, for his friendship, hospitality, and many helpful conversations during the last few years, which contributed greatly to my project. Particularly, I am indebted to him for his contributions to Chapter 3 as well as many useful chats we had regarding the *dynamic LTR*, during my visit to Purdue in 2006. Also, I am sincerely grateful to him for recommending me to Hamilton Institute at the first place. I would also like to thank Dr. Oliver Mason, and Dr. Fiacre O'Cairbre for conversations which have helped to clear up subtle points of mathematical confusion that I encountered during the course of my project. I especially thank Dr. Oliver Mason for his invaluable suggestions and the great support he provided with the preparations of my thesis. I extend many thanks to Dr. Jens Kalkkuhl and DaimlerChrysler Forschung for hosting me as a visiting researcher in Esslingen during the first year of my Ph.D, where I had an opportunity to experience the cutting-edge vehicular technology first-hand, and also learned a lot about the open problems in the automotive industry. This visit has motivated many of the automotive estimation and control applications we analyze in this thesis. The last but not the least, I am grateful to Dr. Mehmet Akar for his contributions

to Chapter 2 as well as his support for my Ph.D project, and I particularly thank him for the useful conversations we had regarding the automotive CG estimation problem.

I feel truly fortunate and honored to have had the opportunity to work in an environment as stimulating as that provided by the Hamilton Institute here at NUI Maynooth. Not the least of the advantages that this has afforded me has been the chance to meet and interact with researchers of extremely high calibre and considerable experience across many fields. Special thanks are due to Professor Douglas Leith, the director of the Hamilton Institute, and Professor Robert Shorten, whose great efforts help to make the Institute the positive working environment that it is today. Also, I hereby thank all the Hamilton Institute family for contributing to create a vibrant, interactive and a fun work place. In this context, I would like to especially thank Rosemary Hunt and Kate Moriarty, whose patience and good-natured professional help with the various administrative issues that need to be dealt with in the course of a Ph.D has made my task considerably easier. I extend many thanks to Dr. John Scanlan at the NUIM commercialization office, as well as to Cathy Holahan at Enterprise Ireland for their great help and support for commercializing some of our research results. I also gratefully acknowledge the financial support that I have received from Science Foundation Ireland, Enterprise Ireland, and the European Union.

I feel greatly indebted to my dear wife Aslı, and my lovely daughter Melis Naz as they have been the greatest source of joy, inspiration, and support at many occasions during the preparation of this thesis. Finally, no words can overstate the debt of gratitude that I owe to my parents, my brother and the family for their unconditional love, support, encouragement and kindness through all the years of my life.

Abstract

The main focus in this thesis is the analysis of alternative approaches for estimation and control of automotive vehicles based on sound theoretical principles. Of particular importance is the problem rollover prevention, which is an important problem plaguing vehicles with a high center of gravity (CG). Vehicle rollover is, statistically, the most dangerous accident type, and it is difficult to prevent it due to the time varying nature of the problem. Therefore, a major objective of the thesis is to develop the necessary theoretical and practical tools for the estimation and control of rollover based on robust and adaptive techniques that are stable with respect to parameter variations.

Given this background, we first consider an implementation of the multiple model switching and tuning (MMST) algorithm for estimating the unknown parameters of automotive vehicles relevant to the roll and the lateral dynamics including the position of CG. This results in high performance estimation of the CG as well as other time varying parameters, which can be used in tuning of the active safety controllers in real time. We then look into automotive rollover prevention control based on a robust stable control design methodology. As part of this we introduce a dynamic version of the load transfer ratio (LTR) as a rollover detection criterion and then design robust controllers that take into account uncertainty in the CG position. As the next step we refine the controllers by integrating them with the multiple model switched CG position estimation algorithm. This results in adaptive controllers with higher performance than the robust counterparts.

In the second half of the thesis we analyze extensions of certain theoretical results with important implications for switched systems. First we obtain a non-Lyapunov stability result for a certain class of linear discrete time switched systems. Based on this result, we suggest switched controller synthesis procedures for two roll dynamics enhancement control applications. One control design approach is related to modifying the dynamical response characteristics of the automotive vehicle while guaranteeing the switching stability under

parametric variations. The other control synthesis method aims to obtain transient free reference tracking of vehicle roll dynamics subject to parametric switching. In a later discussion, we consider a particular decentralized control design procedure based on vector Lyapunov functions for simultaneous, and structurally robust model reference tracking of both the lateral and the roll dynamics of automotive vehicles. We show that this controller design approach guarantees the closed loop stability subject to certain types of structural uncertainty.

Finally, assuming a purely theoretical pitch, and motivated by the problems considered during the course of the thesis, we give new stability results on common Lyapunov solution (CLS) existence for two classes of switching linear systems; one is concerned with switching pair of systems in companion form and with interval uncertainty, and the other is concerned with switching pair of companion matrices with general inertia. For both problems we give easily verifiable spectral conditions that are sufficient for the CLS existence. For proving the second result we also obtain a certain generalization of the classical Kalman-Yacubovic-Popov lemma for matrices with general inertia.

Declaration

I hereby certify that this material, which I now submit for assessment on the programme of study leading to the award of Doctor of Philosophy from Hamilton Institute is entirely my own work and has not been taken from the work of others save and to the extent that such work has been cited and acknowledged within the text of my work.

Signed: _____ ID No. : 63125064

Date: 6 December 2007

Contents

List of Figures

Chapter 1

Introduction and Overview

In this chapter we first explain the motivation for the thesis and the problems considered in it, and then give a detailed literature review of the multiple model control literature, which is utilized extensively in this thesis. We provide a critical review of the recent literature in this area and also point out the open problems, some of which we consider in the later chapters. We conclude with a summary of the chapters and explain the contribution of this work.

1.1 Background and motivation

In this thesis, we are concerned with switched estimation and control problems that originate from and are motivated by automotive vehicles. The work of the thesis is also motivated by the practical importance of switched linear systems and the known fact that such systems can become unstable even when they are constructed by switching between individually stable constituent systems [89]. This requires easily verifiable and constructive methods for designing feedback systems that guarantee the stability of switched linear systems under arbitrary switching rules. While viewing automotive vehicles as time varying and switching

dynamical systems is not a traditional approach preferred by the industry due to complexity issues, it is possible to obtain sound control and estimation algorithms based on time varying principles and utilizing only the stock sensors and actuators, which can potentially improve the overall vehicle performance and safety. In this thesis we consider several such methods for a number of estimation and control problems.

An important motivation for this thesis is the problem of automotive vehicle rollover, which is, statistically, the most dangerous vehicle accident type. Rollover is a particularly important problem for vehicles with a high center of gravity, and its prevention is difficult due to the time varying nature of the parameters affecting it. Considering the fact that the composition of the current automotive fleet consists of nearly 36% light trucks, minivans and SUVs [22] along with the recent increase in the popularity of SUVs worldwide, makes the rollover an important safety problem, as these vehicles have unusually high center of gravity (CG) positions. While automotive manufacturers often provide the measurement of CG position and other vehicle parameters, this often pertains to an empty vehicle with known load distribution. Considering the fact that passenger, and/or load distribution in road vehicles can vary significantly, and sometimes even dangerously, it is difficult to overlook the change in the CG position and its influence on the rollover tendency of automotive vehicles. Given the importance of this problem, the automotive industry can greatly benefit from real-time CG position estimation capabilities. Such estimators can be used as a warning system to the driver or can conveniently be integrated into active road handling or rollover prevention controllers thus improving the overall vehicle and passenger safety. Motivated by these considerations, and inspired by the success of Multiple Model Switching & Tuning (MMST) methodology, we devote a significant portion of the thesis to implementing and analyzing the multiple model framework for the estimation and control of automotive rollover. Using the multiple model framework in conjunction with simple linear vehicle models we design real time estimator structures that infer vehicle parameters such as the CG height and the linear suspension parameters in relation to the rollover prevention prob-

lem. This information, when used in conjunction with active rollover prevention systems, can significantly improve the roll stability of road vehicles without sacrificing from the cornering performance. We give a detailed implementation and analysis of such an adaptive control structure as compared to alternative robust control designs in the following chapters.

There are two distinct types of vehicle rollover: tripped and un-tripped. Tripped rollover is usually caused by impact of the vehicle with something else, resulting in the rollover incident. For example, a tripped rollover commonly occurs when a vehicle slides sideways and digs its tires into soft soil or strikes an object such as a curb or guardrail. Driver induced un-tripped rollover can occur during typical driving situations and poses a real threat for top-heavy vehicles such as SUVs. It is however, possible to prevent such rollover accidents by monitoring the car dynamics and applying appropriate control effort ahead of time. In this context, an important consideration for active rollover mitigation system design is related to the assessment of the rollover risk. In this thesis we introduce a dynamical criterion that we name as "dynamic Load Transfer Ratio", to assess the rollover propensity of a vehicle; we utilize this criterion to trigger a range of active control mechanisms. In the following chapters we suggest several such control designs with a range of control objectives, and making use of a variety of control actuators that include active differential braking, active steering, and active suspension actuators, as well as their combinations. While most of the problems we tackle in this thesis relate directly to un-tripped rollover mitigation systems, many of our results can also be applied for tripped rollover mitigation.

In this thesis we also consider other alternative strategies based on certain Lyapunov and non-Lyapunov results for guaranteeing the stability of switched linear systems. In this context we consider the extensions of these results and implement them to automotive control problems related to roll and lateral dynamics control applications. Here the practical objective is the robust and transient free emulation of reference states, where the vehicle is subject to arbitrary parameter switches. The solution of this problem is complicated due to undesirable interactions between the vehicle's lateral and the roll dynamics. We also con-

sider control design methods that take these interactions into account, and are robust with respect to certain structural uncertainties in such applications.

Throughout this thesis at the beginning of each chapter there is a relevant literature review. For the literature on multiple model estimation and control, which is common to many chapters, a review follows.

1.2 Overview of Multiple Model Control and Estimation Methods

In this section we explain and motivate the need for the study of Multiple Model Control (henceforth MMC) to meet the challenge of real world time-varying control objectives for uncertain systems. This is followed by a review of the past and the current literature on the topic along with the description of the prominent approaches and their critical evaluations, thus presenting the state of the art in the area.

1.2.1 Motivation for MMC

Real world control problems of today's highly sophisticated technological society are difficult due to the four following reasons [83];

- computational complexity,
- nonlinearity,
- uncertainty,
- time-variations.

Computational complexity relates to the ever growing high dimensionality of the problem formulations, which require more calculations per solution. Nonlinearity of any form is a source of complexity as the general nonlinear analysis tools are still incomplete, while uncertainty is a measure of how well we know about the system at hand; the more we don't know the more difficult the control task will be. Finally, time variations may result due to changes in operating conditions, external disturbances or complete/partial failure in some of the subsystems of the plant, thus need to be compensated.

In the light of these challenges, adaptive and learning schemes were developed to tackle with the uncertainty problem, while in parallel neural network approaches were developed to cope with the complexity and the nonlinearity problems. However none of these methods can handle time variations properly [83]. Although the adaptive control theory has been developed with the objective of controlling uncertain and time varying problems, most of the results given in this field assume, since the very beginning, that the plant parameters vary very slowly compared to the dynamics of the system. This in theory can work given the model is accurate enough and the initial parameter errors are small. However this can not be guaranteed in all the real world applications, as in most cases models are poor and control designers have difficulty in finding a parametrization for the dynamical models such that they represent the systems under interest accurately.

As reported in various publications in the literature [14, 77, 78, 79, 84, 85, 87, 83], numerical studies as well real world experience suggest that the classical stable adaptive controllers suffer from lack of robustness. When the initial parameter errors are large, the adaptive controllers tend to perform poorly in their tracking task and usually result in oscillatory control errors along with unacceptably large amplitudes during the transient phase of their dynamics.

In order to achieve the ultimate objective of stable robust adaptive control, Narendra and Balakrishnan suggested in 1992 the use of the multiple models and switching control algorithm in the seminal technical report [77]. In this report as well as the follow-up papers

that appeared in the literature [78, 84] they elaborated the use of an indirect adaptive control approach and proposed the use of multiple identification models that are paired-up with corresponding controllers, which was derived as an extension to the explicit MRAC (Model Reference Adaptive Control [136], [135]) method. Their proposed algorithm drew serious attention as the improvement in the transient tracking performance of the controller was consequential, and as a result it inspired many researchers to work on the multiple model switching & tuning paradigm that developed into a whole methodology today. Before proceeding with the details of the prominent work in the literature related to MMC, we find it appropriate to list the specific reasons for using multiple models and switching control algorithms as described in [83], and [89].

(i) *Local dynamics:* A model is a mere representation of a dynamical process in a convenient form [83], which is usually based on the laws of physics under certain simplifying assumptions. While such simplifications (e.g. linearization) are usually required to assure mathematical tractability of the problem, the best choice of assumptions may change depending on the operating condition. This naturally calls for the use of multiple locally valid models and corresponding linear switched controllers [56].

(ii) *Multi-modal performance:* Many engineering systems are inherently multi-modal [89], meaning that their operation consists of different operating modes that result in different dynamical characteristics. Use of multiple model and switching controllers can yield better performance compared to traditional robust linear control design techniques based on a single model. The best application example for this is the longitudinal speed regulator [117] (cruise controller) of an automobile as formulated in [118]. In this problem, the car goes through different modes of operation dictated by each gear shift. A design based on switched controllers can perform significantly better compared to a single linear controller.

(iii) *Robustness and adaptation:* The requirements for a good control system are speed, accuracy and stability. The biggest interest for the need for supervisory switching

stems from the modern adaptive control problems, which aim for fast, precise and stable operation under uncertain and time-varying environments. Of special interest is the reconfigurable controller structure in the event of subsystem or component failure [56]. Such objectives can be archived using *multiple models switching & tuning* (MMST) controllers which can detect such changes rapidly and accurately and compensate accordingly [77, 78, 79, 84]. As mentioned earlier, classical stable adaptive controllers and robust control design methods can not achieve good performance under time varying and uncertain conditions.

(iv) *Decentralized design:* It is common practice to design complex engineering systems in a decentralized manner. Subsystems are designed in relative isolation and then the entire system is constructed by combining each component. The interaction of the subsystems are governed by a supervisory logic and such an application is ideally suitable for switched control systems [56].

(v) *Constrained control:* Practical control systems operate under sensor and actuator constraints. Switching between multiple control designs can provide satisfactory performance while still satisfying the constraints of the system [56, 89].

In the literature, control designs that possess the above qualities are often referred to as *intelligent control* systems [85, 31]. There are a number of approaches suggested to achieve these objectives, which are described in detail in the following section.

1.2.2 MMC Literature Review

Formally speaking *Multiple Model Control* (MMC) is a model based control strategy incorporating a set of model/controller pairs along with a logic-based supervisory switching rule rather than relying on a single robust controller to handle all operating conditions [105]. There are two prominent approaches to answering the question of how, when and to which

model/controller pair to switch. The first approach is the *indirect* MMC approach in which the switching is made in a discontinuous fashion as in the MMST algorithm [77, 78, 79, 84]. This requires multiple identification models, and a model is chosen to represent the plant based on minimizing a cost function of the identification error. The corresponding control input is used to control the plant. As opposed to the hard switching of MMST approach, the *direct* MMC approach uses a weighed sum of the multiple controllers such that the control action is performed in a continuous fashion as in [105, 12].

To the best of our knowledge, the first ideas on multiple model arrays and switching started to appear in the literature as early as mid 1960s in the PhD thesis of Magill that culminated in the paper [61]. In his paper Magill suggested an optimal (in the mean square sense) adaptive estimator for sampled Gauss-Markov random process with a certain structure of unknown parameters. He showed that the optimal adaptive estimate is an appropriately weighted sum of the conditional estimates of a set of elemental linear estimators. The calculation of the weighting factors required nonlinear probability calculations on the measured data. Also, the feasibility of his algorithm required that the unknown parameter vector must belong to a finite set of possibilities that are known a priori. He suggested that his algorithm may be implemented to time-varying problems but provided no analysis of it. Although Magill's work brought a new perspective into the optimal and adaptive control theory, the assumptions he made limited the use of his approach.

In the following decade the works of Lainiotis [52, 53], Athans et al. [12] and Baram et al. [15, 16] contributed to the development of the topic. In [52] and [53] Lainiotis defined his multiple model estimation and control method as the *Partitioning Algorithm*. He suggested the use of multiple Kalman filters with the same structure but different parameterizations, running in parallel to estimate the state of the plant. He used the residuals (innovations) of the Kalman filters to compute the posterior probabilities to decide which one of the Kalman filters is the correct one. Eventually the sum of the weighted estimates of the Kalman filters yields the state estimate along with the most likely parametrization. The approach required

only Gaussian white noise on the state and the measurement equations. In [52] he also tried to extend the same method to nonlinear plants with unknown parameters, which requires the use of nonlinear state estimators or extended Kalman filters. In [53] Lainiotis integrated his multiple model estimation algorithm with multiple *Linear Separation* controllers (an optimal quadratic-cost stochastic control design that assumes known model parameters) to obtain a closed loop estimator/controller structure that he named *Partitioning Adaptive Controller* shown in Figure 1.1. The nonlinear computation of the posterior probabilities pertaining to each model constitutes the adaptive part of the control algorithm, while the linear separation controller implementation is the non-adaptive linear part. It should be pointed out that the controller is suboptimal unless probability attached to the model with the correct parametrization is 1, because the eventual control effort is the weighted of sum of multiple controllers running in parallel. Also, given the difficulties of implementation of the Kalman filters, especially the extended Kalman filters, along with the assumption of white noise on the process and the measurement model (as it is required by the Kalman filter) renders this algorithm difficult to implement.

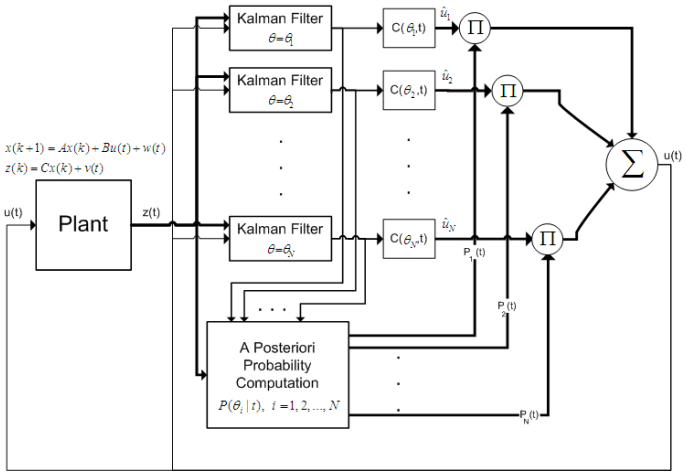

Figure 1.1: Partitioned adaptive controller.

An early real-life application of the MMC (which was missing in Lainoitis and Magill's previous publications) to our knowledge was the equilibrium flight controller implementation

for an F-8C supersonic jet fighter [12] published by Athans et al. of MIT Electronic Systems Laboratory. In this paper Athans et al. assessed the use of the MMC algorithm for the simple task of obtaining equilibrium-flight speed regulators at different flight regimes. They represented the highly nonlinear aircraft dynamics by a set of simple linear models that are valid within certain speed regimes. Here the problem was to get the best possible performance from the directional and the lateral control surfaces at different flight speeds ranging from subsonic flight dictated by laminar aerodynamic flow conditions to supersonic flight governed by shock waves, which has totally different dynamics compared to the former. As a consequence, a linear feedback controller optimized for one flight condition would not be suitable for another. Their controller concept was a complete Linear-Quadratic-Gaussian (LQG) design for each flight condition as shown in Figure 1.2, and every LQG consisted of a Kalman filter to process the noisy sensor data as well as to infer some state variables such as the angle of attack and the sideslip angle, which were assumed to be unmeasurable and were required to obtain the control command. The adaptive controller structure resembles to that of Lainiotis in [53] for the most part, only differing in the optimal stochastic controller design rule as well as in the use of steady state Kalman filters, in order to reduce the computational overhead. The LQG controllers, designed for N linear stochastic time-invariant

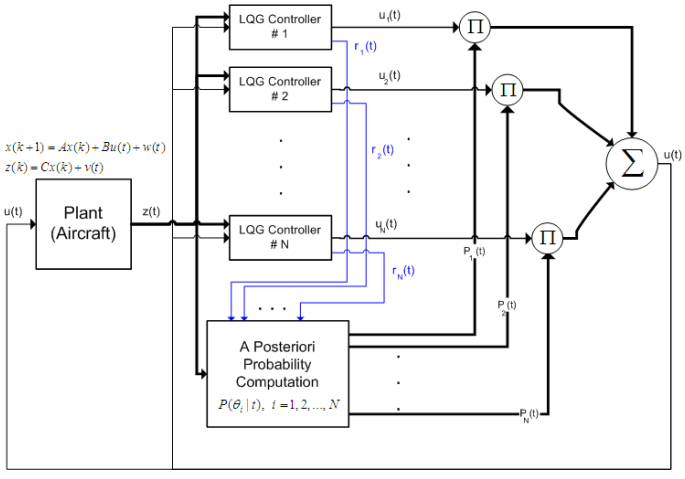

Figure 1.2: Multiple model adaptive controller implementation of Athans et al.

dynamic systems, generated two signals at each time step, which are;

(i) The control vector $u_i(t)$, which would be the optimal control if the aircraft was flying at the flight regime corresponding to i^{th} parametrization,

(ii) The residual innovations vector $r_i(t)$ generated by each Kalman filter (that is inside the i^{th} LQG compensator).

The residuals can be used to recursively calculate the conditional probabilities denoted by $P_i(t)$. In the paper they argue that since they used steady state Kalman filters, $P_i(t)$ for $i = 1,2,..N$ are not the exact conditional probabilities. Using the control vectors generated by each LQG controller $u_i(t)$, one can then compute the "adaptive" controller input as follows;

$$u(t) = \sum_{i=1}^{N} P_i(t)u_i(t).$$

They showed using real flight data that the suggested algorithm worked, however they did not present a comparison with alternative gain scheduling controllers. It is also pointed out in the paper that there is no rigorous proof of asymptotic convergence of the conditional probability $P_i(t)$ associated with the true model, to unity. This brings in the question of stability in the case when erroneous models are used to estimate the states due to mismatched or badly tuned Kalman filters. Such an implementation therefore would not be favorable in the case of time-varying parameters as the tuning of Kalman filters for time variations can pose to be a difficulty.

To the best of our knowledge, the first proof of stability for a multiple model estimation algorithm was shown by Baram et al. and was detailed in the papers [15] and [16]. They again used a Kalman filter based approach, where it was assumed that the identical models for the Kalman filters were linear, and dynamic equations as well as measurement relations were corrupted by uncorrelated white noise. The unknown parameters for the Kalman filters were assumed to belong to a finite set with arbitrary size. Their proof did not require the actual model parameter vector to be in the model set as this would be, in general, an unrealistic assumption. They further assumed that error covariances of all the Kalman filters

corresponding to the parameters in the set are positive definite, finite, and all the residuals (innovations) are ergodic. Under these assumptions they showed that the model in the nearest probabilistic neighborhood of the actual parameter vector will minimize the distance measure based on Kullback information metric. They also proved asymptotic convergence of the parameter vector under these assumptions. Although mathematically attractive, these results are difficult to implement in real life simply because the assumptions made for the proof were too limiting and hard to comply with.

In all the MMC publications that appeared since mid 1960s till late 1970s, only continuous control signals were considered which were composed of the convex combination of a set of linear optimal controllers. What's more, the stability analysis of the resulting controller was usually missing, or was proved only under very strict constraints, and most of the time the problem of using multiple models/controllers was considered only from the optimality perspective. In the context of stabilization of adaptive systems, switching schemes assumed importance towards the end of 1980s with a trend that was initiated with the PhD thesis of Bengt Mårtenson [63] which he later detailed in the papers [64], and [60]. In these publications he proved the stability of discontinuous switching (which occurs at increasing intervals i.e., switching gets slower in time) between a set of stabilizing adaptive controllers designed to stabilize a linear time invariant plant. He neither made stochastic assumptions on the system nor he assumed persistently exciting reference signals. The structure of Mårtenson's direct switched adaptive control implementation is shown in Figure 1.3, where K_i are operators each representing a finite set of stabilizing controllers that are known a priori. Also the direct controller parameter adaptation rule is a continuous increasing function and was based on the input and the output of the plant. The biggest achievement of Mårtensson's work was the relaxation of the common stochastic assumptions made in the previous publications on multiple switching models/controllers, up to that date. He also suggested the use of discontinuous switching between adaptive controllers to stabilize linear plants.

Following the trend started by Mårtensson, two kinds of switching algorithms were pro-

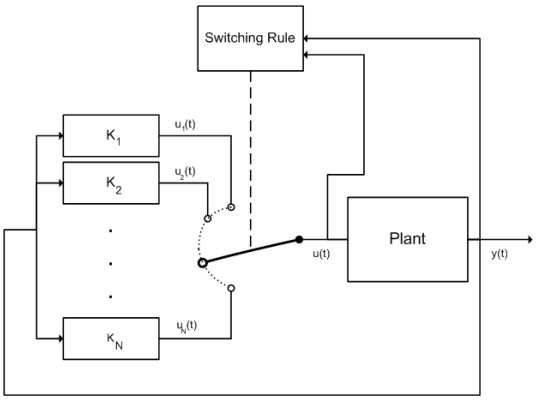

Figure 1.3: Mårtensson's switching function controller.

posed in the literature. The first of them was the direct switching approach as in Mårtensson's implementation, where the choice of when and to which controller to switch to is determined based on the output of the plant. Although this is a conceptually simple idea, it was reported to be impractical to utilize in complex systems [79, 31]. The second approach is the indirect approach that was initially suggested by Middleton et al. in [69] which involves using multiple identification models to estimate the unknown parameters of the plant based on a suitable performance index. Estimated plant parameters are then used to implement a controller based on the certainty equivalence principle. Their implementation required the assumption that the identified parameter belongs to a finite group of convex sets (not necessarily disjoint), where models corresponding to the parameters in each of these sets are uniformly stabilizable. In a separate paper, the same year, Middleton and Goodwin reported their findings on the adaptive control of time-varying linear systems in [68]. In this paper they proved that their adaptive algorithm achieved BIBS (Bounded Input Bounded State) stability without the persistency of excitation requirement, and robust with respect to unmodeled dynamics for the time varying linear system. They assumed parameter variations to be bounded yet slowly varying or have infrequent jumps. Although this method was designed for adaptive control based on a single model, it should be possible to extend the results to the multiple model case by dividing the arbitrarily large region of the

parameter space into multiple convex regions.

In the following years Morse [71] studied the use of multiple fixed models and optimization for robust set point control. He suggested the use of a supervisory "high-level" algorithm that is capable of switching to a sequence of linear positioning or set-point controllers from a set of candidates in order for the output of the process to approach and track a constant reference input for a single input single output (SISO) plant. The supervisor continuously evaluated each candidate controller using a performance criterion based on norm-squared estimation errors of the candidate nominal process identification models. He later detailed his method in the papers [72], and [73] and looked into the theoretical aspects of the robustness as well as the steady state tracking performance of the switching algorithm.

In the mean time, Narendra and Balakrishnan suggested in a 1992 technical report [77] that it is possible to improve the transient performance of adaptive controllers that operate in rapidly time varying environments, using both switching and tuning along with a multiple model structure. They developed and presented the idea during the 1990s in a series of papers [14, 77, 78, 79, 84, 85] and named the resulting algorithm multiple model switching & tuning (MMST) controller. They also referred to it as "intelligent control" to direct attention to its ability of recognizing the environment that it is operating and act accordingly in a fast, accurate manner while guaranteeing stability. They defined the intelligence of a controller as the speed and accuracy with which it responds to a sudden and large change [79]. In the papers [77] and [84] the MMST algorithm was considered as an extension to the indirect MRAC method, where multiple identification methods were used to identify an LTI plant with unknown and time varying parameters.

In the MMST algorithm each identification model is paired-up with an adaptive controller as seen in Figure 1.4, and based on a performance index of the identification error the model/controller pair is chosen to control the plant at every instant. The plant to be controlled has the input $u(t)$ and output $y(t)$. A reference model provides the desired output $y_{ref}(t)$ and the task is to drive the control error $e_c(t) = y(t) - y_{ref}(t)$ to within specified

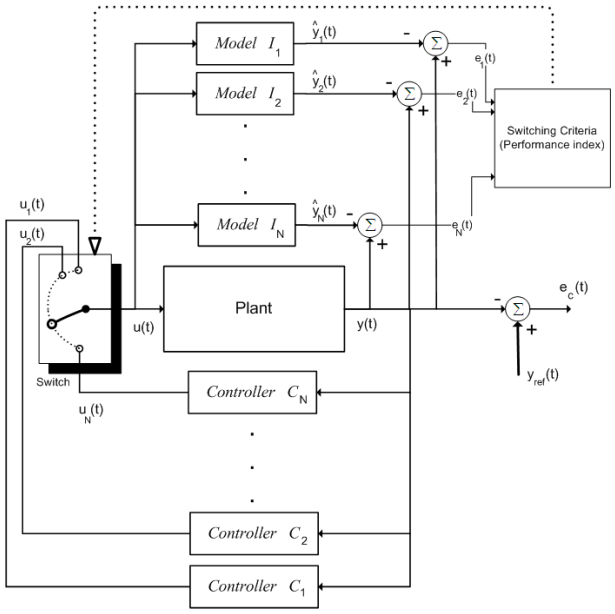

Figure 1.4: Multiple model switching & tuning Controller (MMST).

bounds or, if possible, to zero. N identification models $\{I_j\}_{j=1}^N$ with corresponding outputs $\{\hat{y}_j(t)\}_{j=1}^N$, where each one has identical structure but different parameterizations, are used in parallel to estimate the parameters of the plant. The identification error for each model is defined as $e_j(t) = y(t) - \hat{y}_j(t)$. Motivated by quadratic optimal control, the following performance criteria is used to select the model representing the plant at each instant;

$$J_j(t) = \alpha e_j^2(t) + \beta \int_0^t e^{-\lambda(t-\tau)} e_j^2(\tau) d\tau.$$

where $\alpha \geq 0$ is the weighting factor for the instantaneous changes, $\beta > 0$ is the weight for steady state error variations and $\lambda > 0$ is the forgetting factor. It is assumed that the model that minimizes this cost function is the closest model to the plant, and based on the certainty equivalence principle, the corresponding control input of the model is used to control the plant. Narendra and Balakrishnan explained the reason for using an indirect control method with the fact that stable control of identification error in real-time would lead to a stable control of the plant. This argument however is shadowed by the fact that there is no $1-1$ correspondence between the identification error and the control error based

on their switching criteria[1].

The global stability of the MMST algorithm applied to linear time invariant (LTI) plants was proved in [77] and [84] using candidate Lyapunov functions. The stability proof made no assumptions on the switching sequence given that there is a certain minimum dwell time between each switches (i.e., the controller is not allowed to switch too quickly). In later papers [78],[79] and [85] the algorithm was extended to include fixed (time invariant) models, adaptive models with fixed initial conditions, and adaptive models with re-initialized initial conditions, as well as various combinations of these. In these papers it was shown hypothetically as well as through numerical simulations that while the use of fixed models are computationally more efficient and they provide fast transient response, slow adaptive models are required to obtain zero steady state control error and long term improved performance.

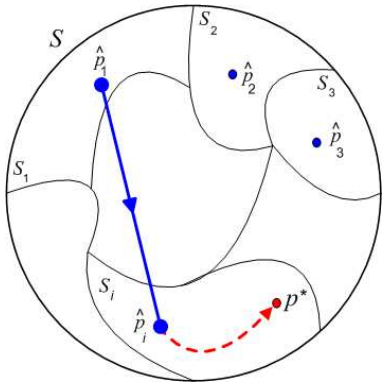

Figure 1.5: Switching between fixed models and tuning using adaptation.

The idea of using a combination of fixed and adaptive models can be illustrated with Figure 1.5, where S is a closed bounded set that symbolizes the finite parameter space, and S_i represents subsets of S each corresponding to a fixed model. $\hat{p}_i$ denotes the parametrization for the i^{th} fixed model which represents the plant in the subset S_i. We designate the actual plant parameters with p^*. Now assume that the algorithm is initialized at $\hat{p}_1$, at this point

[1]We shall explain this problem in detail later in Chapter 2.

the MMST algorithm will switch to $\hat{p}_i$ (perhaps after several switches) as it is the closest fixed model (based on the given performance criteria) to the actual plant parameters. At this point we can initialize the adaptive model from $\hat{p}_i$ an let it converge asymptotically to p^* (tuning). In [79] and [85] it has been shown that using multiple fixed models along with a free-running and a re-initialed adaptive model performs quite satisfactorily in the control of plants with rapidly time-varying environments.

The extension of the MMST algorithm to nonlinear plants was first suggested in [14] using neural networks, however stability proof was missing in this paper. In a more recent paper [87] however, stability of the MMST algorithm for a simple class of nonlinear systems was proved. Also, application of the MMST algorithm for adaptive stochastic control of discrete time systems was presented in the recent papers [82],[141],[86], and in the PhD thesis [31]. Summing up, MMST algorithm has theoretically, as well as through numerical simulations, been shown to be a high performance alternative way to tackle the adaptive control problem without the limitations of the previous approaches. However there are still questions that remains unanswered in the current literature on MMST, such as the previously mentioned 1-1 non-correspondence between the parameter space and the output space. This problem partly relates to the selection of the performance criteria to be minimized. The way the performance criteria was chosen seems to be heuristic and intuitive. The question to be asked is; what is the correct choice of the performance index as a function of the identification errors such that nearness in the parameter space uniquely correlates to nearness in the output space of the models? Another problem is related to the distribution of models in the parameter space, as having too many models for achieving sufficient accuracy may impose a computational overhead and limit the use of the algorithm in cost sensitive applications. Having too few models however, may limit the accuracy or the transient performance gained by the algorithm.

In parallel to the development of the MMST algorithm, a direct multiple model switching adaptive controller algorithm, advocated by Michael G. Safonov and Tung-Ching Tsao,

emerged in the late 1990s. Preliminary versions of the idea appeared in the mid 1990s however it made its debut in a 1997 paper [103]. They called it "Unfalsified Control" motivated from the scientific process of experimental validation, or unfalsification of experimental data against various parameterized classes of plausible models in search of one that has the best fit to the data according to some selected criteria. As it is a direct control approach, the algorithm does not require any identification models, which can exhibit only some aspects of the real plant. This prevents the designer from making crude and limiting assumptions on the plant structure or its stochastic characteristics. The idea is based on direct evaluation of the performance of all candidate controllers to identify and switch to the controller that will guarantee the specified performance criteria (by performance it is meant that how close the closed-loop plant would follow the reference signal had the candidate controller been in the feedback loop). This does not necessarily require the candidate controllers to be put into feedback-loop with the plant before they could be unfalsified, rather it can be done with stored input and output data. Through elimination (falsification) of the unsuitable controller structures, a data driven adaptive learning scheme is achieved. As pointed out in [103], the algorithm is a generalization of open loop model validation techniques to feedback systems.

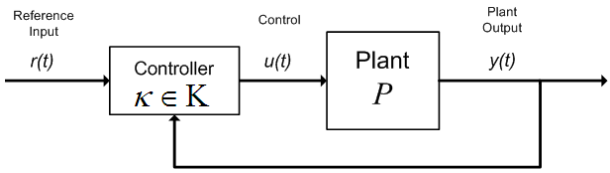

Figure 1.6: Unfalsified control concept.

Unfalsified control concept can be illustrated as in the Figure 1.6 where the goal is to use the controllers $\kappa \in \mathbf{K}$ to control the plant P to ensure a certain closed loop system response, which we denote with T_{spec}. Notice that any control law using any minimal representation can be chosen to design the candidate controller. Further, we can denote the space of inputs, outputs and reference inputs with U, Y and R respectively, such that $u(t) \in U$, $y(t) \in Y$ and

$r(t) \in R$. Now the unfalsified controller problem can formally be stated as follows [130]:

Given,

(i) Measurements of the plant input-output signals $(u_0, y_0) \in U \times Y$,

(ii) A candidate set of controllers $\kappa \in \mathbf{K} \subset R \times Y \times U$,

(iii) A closed loop performance criterion $T_{spec} \subset R \times Y \times U$,

then determine whether or not the control law satisfies the performance criterion.

In order to perform model free direct adaptive control one then starts with a candidate controller in the loop, where it remains till it is falsified by the data. In the case of falsification it is replaced by another candidate controller from the array of unfalsified controllers which manifests the inherent switching nature of the algorithm. Furthermore, the fact that controllers do not need to be inserted in the feedback loop to be falsified, guarantees fast response and improved transient performance compared to traditional adaptive controllers based on single models.

The questions regarding robustness, stability (whether the switching ceases at a point stabilizing the plant) and asymptotic convergence characteristics of the unfalsified direct adaptive control algorithm was addressed in the recent papers [129] and [45] by Safonov et al. They argued in a heuristic manner that from a practical point of view, the acquisition of an unfalsified controller is not asymptotic but rather immediate. This is due to the fact that the controller in the feedback loop is always the unfalsified one, which will guarantee the stability and convergence regardless of the plant being linear time-invariant or non-linear time-varying. Furthermore, they linked the robustness of the algorithm due to the following two facts;

(i) The set of controllers is monotone decreasing and bounded below by the empty set,

(ii) An unfalsified controller that is not stabilizing is unlikely to remain unfalsified for a long time.

In a recent paper, Paul and Safonov [94] compared the performance of the unfalsified adaptive control concept to that of Narendra's MMST algorithm for the MRAC problem. In terms of tracking performance both controllers obtained similar results. Several applications and theoretical extensions of the unfalsified control concept has been reported in the recent literature [13, 19, 21, 93]. Summing up, we believe that the simplicity of implementation of the unfalsified control algorithm has inspired many researches and engineers to implement the idea as evidenced by a high number of application papers in the recent years. Simplicity is partly due to the fact that the algorithm does not need identification models. However there are still questions regarding the choice of the candidate controllers, especially for complex systems. The size of the controller bank and the fact that the computational resources need to be facilitated to store and process the input output data in real time may come with computational overhead. Nevertheless, when the class of stabilizing controllers are known (say through experience or some nominal model) then unfalsified control algorithm offers quite good transient performance improvements without using complex models for the process. This algorithm can prove to be quite useful for widely used proportional-integral-derivative (PID) controller design and on-line tuning for improved performance as presented in [44].

Slight variations of the methods described thus far have also been published. In [5] ideas from MMST and unfalsified control approaches has been somewhat fused, where identification models as well as a falsification algorithm were employed. They suggested two different falsification criteria based on Lyapunov function variations and a statistical falsification based on closed loop variables. They named their approach Switching Supervisory Control (SSC), and demonstrated the improvement in the transient control performance of an uncertain linear time-varying plant through simulations. The algorithm has been extended for non-linear systems in [10].

A flashback to the Kalman filter based methods occurred recently with the papers [33], [34], and [35] by Fekri et al. The method is very similar to that implemented by Athans in the 1977 paper [12], where the fixed controller gains in the original paper were replaced with robust controllers designed with mixed-μ synthesis. They appropriately named the algorithm Robust-MMAC (Robust Multiple Model Adaptive Control or RMMAC).

Before finalizing this section we should mention that by no means this review is exhaustive, and there are many other authors publishing in the field of MMC. However we believe the methods reviewed so far covers the general trend in the area. In the next section we cite and briefly describe several applications of MMC.

1.2.3 Applications of MMC

The applications of MMC has been primarily focused on aircraft and missile autopilots and dynamics control, as well as chemical process control, while several applications including spacecraft attitude and structural control, air traffic control, drug delivery control, solar power plant control, robotic manipulator arm control, and automotive control has also been reported. The common divisor for all these applications is that they involve multiple operating modes and/or multiple operating environments.

Aerospace industry has been a constant driving factor for research in control theory. Without much surprise, the first implementation of MMC was for an aircraft control problem, as the need for the re-configurable, fast and accurate flight controllers are of cardinal importance for increasing aircraft safety and survivability in the presence of subsystem failure and structural damages [31]. As mentioned earlier, Athans et al. [12] did the first implementation of MMC in 1977 for the autopilot of the F-8C fighter aircraft, and for use in equilibrium flight control at different operating regimes. They used an indirect method based on multiple parallel-running Kalman filters that are connected in series to LQG controllers as seen in Figure 1.2. In the 1990s Maybeck continued the use of Kalman filter based MMAE (Multi-

ple Model Adaptive Estimation) and MMAC algorithms and implemented it in a F-15 STOL (Short Take Off and Landing) aircraft [65, 66]. Bošković implemented the MMST idea of Narendra et al. for detection of sensor failures in aircraft [17]. Unfalsified control algorithm found use in robust on-line PID parameter tuning of a missile autopilot [20]. Along these implementations, a somewhat related topic of multiple model air traffic control has been addressed by Bar-Shalom and Li in [57].

Multiple model control algorithms, in part due to their increasing popularity, started to appear in the space applications recently. A good example is the geostationary satellite attitude controller implementation reported in a recent paper by Safonov et al. [130] using the unfalsified control algorithm. In an earlier paper by Maybeck et al. [36] MMAE and MMAC algorithms that are based on the Kalman filter approach, were suggested for use in the control of structural vibrations of large flexible space structures.

Chemical process control is another area that can benefit from multiple model control applications as the problems in this field usually involve nonlinear dynamical characteristics and multiple operating environments. In [106] Schott and Bequette applied Kalman filter based MMAC algorithm for the control of Van de Vusse reactor and classic exothermic continuous stirred tank reactor. Same authors applied the MMAC method to the drug infusion control problem in [105], where infusion rate of nitroprusside is used to control the blood pressure in animal experiments. The same paper has a review of literature for the drug infusion control using multiple model approaches.

Robotic manipulator arm control using MMST approach has been reported by Narendra et al. in [14], while a similar implementation using the unfalsified control algorithm has been reported in [129] by Safonov et al. Safonov's implementation was nonlinear, and was shown to be robust with respect to load variations on the manipulator arm.

The adaptive control of a solar power plant is the subject matter of [96], where the power plant employs a distributed collector field to direct and collect the solar energy through a

heat exchanger. The heat energy is transferred to oil that circulates the system and is used to generate electric power. The electric power generator requires that the output temperature of the circulating oil needs to be kept constant under changing daily solar radiation cycle and atmospheric conditions. The paper concluded that multiple model switching controller implementation performed better than the traditional adaptive control designs.

Automotive applications of the multiple model estimation and control algorithms, which are addressed in this thesis, are quite new. A recent PhD thesis [23] used multiple model adaptive estimation and adaptive control for the adaptive cruise control (ACC) problem. In this thesis we tackle the problem of automotive rollover estimation and mitigation using the MMST framework. The summary of these and the other specific contributions of the current thesis follows next.

1.3 Thesis Overview and the Contributions

In Chapter 2 we introduce a real time parameter estimation algorithm based on the multiple model switching framework for inferring the unknown, and time varying parameters of automotive vehicles. Among the estimated parameters are the center of gravity (CG) position, which has primal importance for vehicle dynamics control applications. After explaining the estimation algorithm we give an analysis of the switching criterion of the multiple model switching algorithm with important conclusions. Based on these, we suggest a model space adaptation method in conjunction with the multiple switched estimator structure, for overcoming the limitations of the switching criteria and present the efficacy of the suggested technique with numerical examples.

In Chapter 3 we consider a novel approach for designing robust automotive rollover prevention controllers. As part of this analysis we introduce a dynamic version of the load transfer ratio (LTR) as a rollover detection criterion and then design robust controllers that take into

account uncertainty in the CG position. The control methodology we utilize is based on guaranteeing a set of linear matrix inequality (LMI) conditions, which result in controllers that are L_∞ stable. We also consider a controller mode switch to increase the performance of the resulting robust controllers, which does not affect the stability of the closed loop system. Again we present the resulting controllers with numerous numerical simulations.

In Chapter 4 we fuse the results of the previous two chapters to obtain a particular type of switched adaptive rollover mitigation control design. Based on the real time estimation of certain vehicle parameters, our controllers switch among a set of controllers, each of which guarantee robust L_∞ stability of the closed loop system. We also show numerically that this results in stable adaptive controllers with higher performance than the robust counterparts.

In Chapter 5 we consider a discrete time extension of a certain stability result for a class of switched discrete time linear systems and show that the stability result do not directly follow from the continuous time versions with this property. We obtain the conditions for stability of this system class by using a non-Lyapunov technique. This result also has an important interpretation for switched systems; the bilinear transform may not always preserve the stability properties between the continuous & discrete time counterparts of dynamical systems, and their stability properties need be analyzed separately. We then suggest two constructive pole-placement control design procedures based on the main results of the chapter; one is related to enhancement of driver experience subject to parameter switches and the second is related to transient free model reference tracking of vehicle roll motion regardless of arbitrary switches that can occur in the vehicle parameters.

In Chapter 6, we consider a particular decentralized control design procedure based on vector Lyapunov functions for simultaneous, and structurally robust model reference tracking of both the lateral and the roll dynamics of automotive vehicles. We show that this controller design approach guarantees the closed loop stability subject to certain types of structural uncertainty, which we demonstrate with detailed numerical simulations.

Finally, in Chapter 7 we extend certain theoretical results on the stability of switched linear systems. Particularly, we consider the problem of common Lyapunov solution (CLS) existence for two classes of switching linear systems; one is concerned with switching pair of systems in companion form subject to interval uncertainty, and the other is concerned with switching pair of companion matrices with a regular inertia. For both problems we give easily verifiable spectral conditions that are sufficient for the CLS existence. For proving the second result we also obtain a certain generalization of the classical Kalman-Yacubovic-Popov lemma for matrices with general regular inertia.

Chapter 2

Realtime Vehicle Parameter Estimation using Multiple Models and Switching

In this chapter we present an implementation of the multiple models and switching framework to the realtime parameter estimation in automotive vehicles. Among the estimated parameters, the center of gravity position is of primary importance, which directly affects the handling of the vehicle in extreme driving situations, and which can not be measured directly. The online estimation method utilizes well-known linear vehicle models for lateral and roll dynamics, and assumes the availability of standard automotive sensors. We illustrate the technique with numerical simulations as well as with off-line sensor data from a test vehicle; we also give comparisons to traditional estimation techniques. The chapter concludes with a brief theoretical analysis of the multiple model estimation algorithm, based on which we suggest a novel refinement of the estimation method in the form of adapting model spaces.

2.1 Chapter contributions

The scientific contribution of this chapter over the state of the art is twofold. Firstly, we successfully applied the multiple model switching framework for realtime parameter estimation in automotive vehicles. We showed through numerical simulations that the method provides fast and accurate estimations of unknown vehicle parameters. We also suggested a number of automotive applications for the suggested estimation technique. The second contribution of the chapter is a theoretical analysis of the MMST cost function (switching criteria) utilized in conjunction with the multiple model estimation algorithm. We proved that under certain conditions (e.g. a coarse model space), the algorithm can lead to wrong estimations. As a remedy and as a further contribution, we suggested a simple method for adapting the model space in conjunction with the multiple model estimation algorithm, while making use of the same cost function. We showed the benefits of this approach through numerical simulations.

The work in this chapter has culminated in the following publications:

(i) Solmaz S., Akar M., Shorten R., "*Method for Determining the Center of Gravity for an Automotive Vehicle*", Irish Patent Ref: (S2006/0162), March 2006. (PCT application filed in March 2007).

(ii) Solmaz S., Akar M., Shorten R., "*Online Center of Gravity Estimation in Automotive Vehicles using Multiple Models and Switching*", 9th IEEE International Conference on Control, Automation, Robotics and Vision, Singapore, Dec 5-8, 2006.

(iii) Solmaz S., Akar M., Shorten R., Kalkkuhl J. "*Realtime Multiple-Model Estimation of Center of Gravity Position in Automotive Vehicles*", Vehicle System Dynamics Journal. Accepted for publication, 2007.

2.2 Introduction

Vehicle center of gravity (CG) position and inertial properties are of primal importance in the assessment of vehicle handling and performance characteristics as well as its accident behavior. Although automotive manufacturers often provide the measurement of these parameters, such information often pertains to an empty vehicle with known load distribution. Considering the fact that passenger, and/or load distribution in road vehicles can vary significantly, and sometimes even dangerously, it is difficult to overlook the change in the CG position and its consequences. While the importance of this is known on the handling behavior, automotive manufacturers usually employ robust active road-handling control strategies to account for the unknown and changing CG position; they simply design for the worst case scenario. Another common approach in the case of Sport Utility Vehicles (SUVs) is to intentionally design the vehicle heavier than usual by adding ballast in the undercarriage, which aims to lower the CG position while reducing the percent margin of the load variation and thus constraining the variation of the CG location. While such approaches are successful up to certain extent, they also come with obvious drawbacks; performance loss under normal driving conditions and reduced efficiency due to added weight.

Analysis of recent car accident data indicates that vehicles with a high center of gravity such as vans, trucks and SUVs are more prone to rollover accidents than others [1]. Moreover it is known that rollover accidents alone constitute only a small percentage of all car accidents, while they cause disproportionately high rates of fatalities [38]. According to [1] rollover occurred in only 2.6% of all vehicle crashes during 2004 in the USA, while it was responsible for a massive 20.5% fatality rate, rendering it to be the most dangerous type of accident. Again according to the same data, light trucks (pickups, vans, SUVs) were involved in nearly 70% of all the rollover accidents, with SUVs alone responsible for almost 35% of this total. It has been also reported in the literature based on similar statistics, that rollover was involved in about 90% of the first harmful events of non-collision fatal accidents [25]. Considering the fact that the composition of the current automotive fleet

consists of nearly 36% light trucks, minivans and SUVs [22] along with the recent increase in the popularity of SUVs worldwide, makes the rollover an important safety problem. As CG height is the most prominent factor in un-tripped rollover occurrence, this problem can greatly benefit from real-time CG position estimation capabilities. Such estimators can be used as a warning system to the driver or can conveniently be integrated into active road handling or rollover prevention controllers thus improving the overall vehicle and passenger safety.

With this background in mind, and inspired by the success of Multiple Model Switching & Tuning (MMST) methodology suggested initially by Narendra et al. to improve the transient performance of adaptive controllers as described in [84, 78, 14], we present in this chapter multiple model and switching estimation approach based on simple linearized vehicle models and employing only standard stock automotive sensors [122]. The choice of the multiple model approach over the conventional methods (such as the least squares), is motivated by the fact that the method does not require the linearity of the parametric uncertainty. Also the method is ideally suited for automotive applications, where a rapid estimation of unknown parameters is required. Moreover, use of Kalman filter based methods for automotive parameter and state estimation applications are quite limited due to robustness limitations as well as computational resource requirements of such methods. Motivated by these considerations, we considered simplified linear vehicle models such as the single track model (i.e., linear bicycle model) and the second order roll plane model in conjunction with the multiple model switching framework. These models can only represent the respective vehicle behavior in a limited range of maneuvers and speeds, but it is possible to use a multitude of these simplistic models and switch between them in an intelligent way in real time, to track the vehicle behavior accurately over the complete operating conditions. Moreover, proper parametrization of these models gives way to the rapid estimation of unknown and time-varying vehicle parameters through the selected models. Using the described multi-model approach in conjunction with linear roll plane models, one can estimate parameters

such as the CG height and linear suspension parameters in relation to the rollover prevention problem. Through a similar implementation of multiple single track models one can also estimate parameters relevant to lateral dynamics control, such as the longitudinal CG position and linear tire stiffnesses. One of the benefits of this realtime estimation method is the fact that it is immune to the nonlinear dependance of unknown vehicle parameters in the models as shall be apparent in the Section 2.3. During the application of the method in Section 2.4 we make no assumptions about the parameter vector having a linear dependance on the states.

Recent publications related to automotive CG position measurement and estimation include that of Mango [62], where he described a method for accurately calculating the CG location based on portable wheel scales. His method requires external measurement equipment and is not intended for online measurement during regular driving conditions as it requires the vehicle to be stationary. In another recent article, Allen et al. [8] made a statistical analysis of vehicle inertial properties and CG positions as a function of weight, width, length and the height of the vehicle using the data for several existing stock cars. Although their analysis is useful in demonstrating the relationship between several physical parameters and vehicle's handling characteristics, their method can not be employed for realtime estimation purposes. There has been a number of recent publications about realtime estimation of vehicle parameters including the CG position. Vahidi et al. suggested a recursive linear least squares estimator with multiple forgetting factors in [131], for simultaneous estimation of the road grade and the vehicle mass in real time. Their algorithm took into account the different rates of change in both unknown parameters and incorporated different forgetting factors[1] into the cost function of the recursive least squares algorithm. Their results are promising as demonstrated with both numerical and measured data. However this method assumes that vehicle model is linear in the unknown parameters, which is not the case for

[1]The concept of forgetting implies that older measurement data is gradually discarded in favor of more recent sensor information [131].

the approach presented in the current chapter as shall be clear in the sequel. In a recent thesis [7], a model based estimation method for road bank angle and CG height was suggested using extended Kalman filters. The presented results showed slow convergence rates in the estimations and the accuracy was questionable. In a recent European patent EP 0918003*B*1 [55] an alternative method for estimating the height of the CG in real-time was described. The method utilizes an estimated drive/brake slip of at least one wheel using the wheel speed sensors, which is then used to compute the instantaneous radius of the corresponding wheel. Using this information, the angle of the corresponding wheel axle with respect to the ground is computed and then used in an equation related to the lateral dynamics of the car to compute the CG height. Since there are no other publications other then the cited patent, the details and the limitations of this method is not known to the authors. It should be noted that all the rollover prevention methods suggested to date assume known CG height [38, 25, 4, 88, 137, 138, 107, 22, 48]. However as we have explained, it is particularly unrealistic to assume the CG height to be known, and this parameter can vary significantly with changing passenger and loading conditions especially in large passenger vehicles such as SUVs.

2.3 Vehicle modelling

In this section we present three different models for the lateral motion and the roll plane dynamics of a car. While we use a 4-state vehicle model with a combined roll and lateral dynamics to represent the real vehicle behavior in our numerical simulations, we utilize two linear second-order models (i.e., the single track model, and the roll plane model) in conjunction with the multiple model switched parameter estimation algorithm that shall be introduced in the following section. We use the second-order linear models to simplify the implementation of the algorithm as well as to keep the required sensory information at a minimum level. All the models introduced here assume small angles and are valid when the

steering input is small. Also, in the second order linear single track model described below, a weak relationship between the lateral and the roll dynamics is assumed, which is the case when the steering angle is small [104]. Note that the choice of the models here is a trade off between complexity and sensitivity to different operating conditions. The assumption of linear models and small angles in the following discussion is indeed a restrictive argument as the linear models are not dependable during extreme driving situations, where the knowledge of the unknown vehicle parameters is required most (e.g., for the deployment of a suitable control action). However, the method described in the sequel is intended for estimating the unknown parameters during normal driving conditions and long before such extreme driving conditions occur.

Notation and definitions of the model parameters and variables are given in Table 2.1. In what follows we give three different dynamical equations of the motion of the car. For a through coverage of the derivations see [50], and [104]. Note that for simplicity, we assume in the following equations that, relative to the ground the sprung mass of the vehicle rolls about a horizontal axis along the centerline of the body.

2.3.1 Single track model

This two state linear model represents the lateral dynamics of a car in the horizontal plane. It is also referred to as “the 2-state single track model" or “the linear bicycle model" in the literature and is commonly used in automotive applications (see [132] for a good application example for vehicle lateral control).

For linearization, the model assumes that the motion of the vehicle is constrained to the horizontal plane at a constant speed such that the effects of heave, roll and pitch motions are all ignored [2]. It is also assumed that only the front tire is used for steering the vehicle, and the steering angle is small. Moreover, vehicle sideslip angle and the tire slip angles are assumed to be small as well. In the model, other sources of nonlinearities such as

Table 2.1: Model parameters and definitions

Parameter	Description	Unit
m	Vehicle mass	$[kg]$
g	Gravitational constant	$[m/s^2]$
v_x	Vehicle longitudinal speed	$[m/s]$
δ	Steering angle	$[rad]$
J_{xx}	Roll moment of inertia of the sprung mass measured at the CG	$[kg \cdot m^2]$
J_{zz}	Yaw moment of inertia of the chassis measured at the CG	$[kg \cdot m^2]$
L	Axle separation, such that $L = l_v + l_h$	$[m]$
T	Track width	$[m]$
l_v	longitudinal CG position measured w.r.t. the front axle	$[m]$
l_h	longitudinal CG position measured w.r.t. the rear axle	$[m]$
h	CG height measured over the ground	$[m]$
c	suspension damping coefficient	$[kg \cdot m^2/s]$
k	suspension spring stiffness	$[kg \cdot m^2/s^2]$
C_v	linear tire stiffness coefficient for the front tire	$[N/rad]$
C_h	linear tire stiffness coefficient for the rear tire	$[N/rad]$
β	Sideslip angle at vehicle CG	$[rad]$
α_v	Sideslip angles at the front tire	$[rad]$
α_h	Sideslip angles at the rear tire	$[rad]$
ϕ	Roll angle measured at the roll center	$[rad]$
$\dot{\phi}$	Roll rate measured at the roll center	$[rad]$

aerodynamic forces, tire nonlinearities and non-smooth road disturbances are all assumed to be negligible. See Figure 2.1 for the representation and notation of the model. Notice that in this model we lump left and right tires into a single one at the axle centerline, hence the name “Bicycle Model" or “Single Track Model".

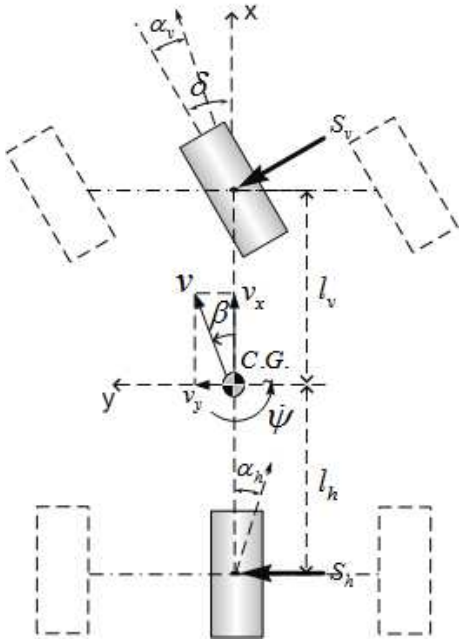

Figure 2.1: Linear bicycle model.

We represent the horizontal dynamics in terms of the state variables β and $\dot{\psi}$. The lateral tire forces S_v, S_h for front and rear tires respectively, are represented as linear functions of the tire slip angles such that $S_v = C_v\alpha_v$, and $S_h = C_h\alpha_h$, where for small angles tire slip angles are given as follows

$$\alpha_v = \delta - \beta - \frac{l_v}{v_x}\dot{\psi} \tag{2.1}$$

$$\alpha_h = -\beta + \frac{l_h}{v_x}\dot{\psi}. \tag{2.2}$$

Also notice that since we assume small angles and constant longitudinal velocity, sideslip angle β satisfies the following;

$$\beta \approx \frac{v_y}{v_x}, \qquad \dot{\beta} \approx \frac{\dot{v}_y}{v_x}. \tag{2.3}$$

Using the above relations and Newton's 2nd law of motion, one can get the following state space representation of the horizontal dynamics of the vehicle

$$\begin{bmatrix} \dot{\beta} \\ \ddot{\psi} \end{bmatrix} = \begin{bmatrix} -\frac{\sigma}{mv_x} & \frac{\rho}{mv_x^2} - 1 \\ \frac{\rho}{J_{zz}} & -\frac{\kappa}{J_{zz}v_x} \end{bmatrix} \cdot \begin{bmatrix} \beta \\ \dot{\psi} \end{bmatrix} + \begin{bmatrix} \frac{C_v}{mv_x} \\ \frac{C_v l_v}{J_{zz}} \end{bmatrix} \delta, \tag{2.4}$$

where the auxiliary parameters σ, ρ, and κ are defined as follows

$$\begin{aligned} \sigma &\triangleq C_v + C_h \\ \rho &\triangleq C_h l_h - C_v l_v \\ \kappa &\triangleq C_v l_v^2 + C_h l_h^2. \end{aligned} \tag{2.5}$$

For further details on the derivation of this model see [104] and [50].

We make use of this model mainly for the multiple model switched estimation of the uncertain tire stiffness parameters (i.e., C_v and C_h), and the uncertain longitudinal position of CG (i.e., l_v). Note that although (2.4) is linear in the state variables, it is nonlinear with respect to unknown parameter variations of C_v, C_h and l_v; this is a factor limiting the use of traditional recursive estimation methods such as the linear least squares for the estimation of unknown parameters, as shall be demonstrated in Section 2.4.3.

Comment: In the version of the linear second-order single track model introduced here, the effect of the variations in longitudinal CG position on the variations in the effective yaw moment of inertia J_{zz} were ignored on the grounds that such changes are insignificant for small vehicles, where loading options are limited and the resulting changes in the inertia are quite small. For the sake of simplicity, parameters for a compact class vehicle were used in the simulations in this chapter, and therefore this assumption makes sense. However for larger vehicles such as busses and trucks the changes in yaw moment of inertia with changing longitudinal CG position can be quite significant and thus can not be ignored in the analysis.

Comment: It is important to note here also that the single track model assumes a weak coupling from the vertical (i.e., roll) dynamics onto the lateral (see [2] for a thorough analysis

of the interactions between lateral and vertical vehicle dynamics). Therefore, there are no terms in (2.4) that reflect the effect of vertical dynamics, which is reasonable when the vehicle is operating in the linear regime at low levels of lateral acceleration [3]. However, the reverse argument is not true for the roll dynamics even under the small angles assumption, since the roll motion is heavily influenced by the lateral dynamics via lateral acceleration, as shall be clear in the next subsection.

2.3.2 Roll plane model

We use the 2-state roll plane model described here for the realtime estimation of CG height h as well as the parameters of the suspension system k, c based on the multiple model switching method. This is the simplest model that captures the roll dynamics of the car and it is free from the effects of uncertainties originating from unknown tire stiffness parameters, which in turn makes it suitable for the estimation task.

Assuming all vehicle mass is sprung, effective linear torques exerted by the suspension system about the roll center are defined as follows

$$T_{spring} = k\,\phi, \tag{2.6}$$

$$T_{damper} = c\,\dot{\phi}, \tag{2.7}$$

where k, c denote the linear spring stiffness and damping coefficients respectively. Using these one can then apply a torque balance in the roll plane of the vehicle in terms of the effective suspension torques (see Figure 2.2 for the notation of the roll plane model), and obtain the following relationship

$$J_{x_{eq}}\ddot{\phi} + c\dot{\phi} + k\phi = mh(a_y cos\phi + g sin\phi). \tag{2.8}$$

Note that for simplicity, it is assumed that, relative to the ground, the sprung mass rolls about a fixed horizontal roll axis which is along the centerline of the body and at ground level. In the last equation $J_{x_{eq}}$ denotes the equivalent roll moment of inertia derived using the

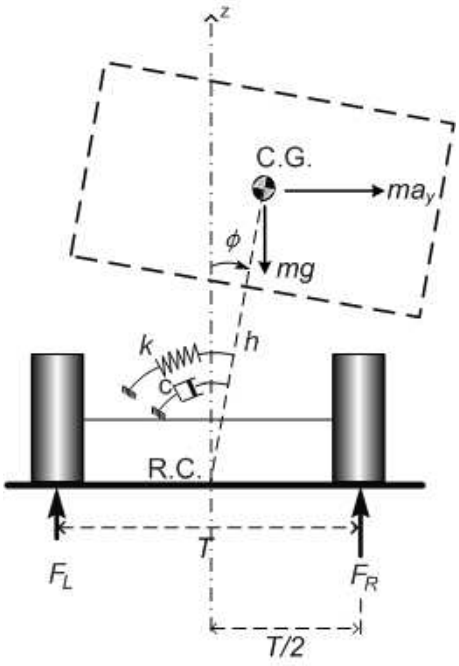

Figure 2.2: Second order roll plane model.

parallel axis theorem of mechanics taking into account the CG height variation as described below

$$J_{x_{eq}} \triangleq J_{xx} + mh^2. \tag{2.9}$$

For small ϕ, we can approximate the nonlinear terms in equation (2.8) as $cos\phi \approx 1$, $sin\phi \approx \phi$ and represent this equation as in the following state space form

$$\begin{bmatrix} \dot{\phi} \\ \ddot{\phi} \end{bmatrix} = \begin{bmatrix} 0 & 1 \\ -\frac{k-mgh}{J_{x_{eq}}} & -\frac{c}{J_{x_{eq}}} \end{bmatrix} \cdot \begin{bmatrix} \phi \\ \dot{\phi} \end{bmatrix} + \begin{bmatrix} 0 \\ \frac{mh}{J_{x_{eq}}} \end{bmatrix} a_y. \tag{2.10}$$

Note that at steady state one can calculate the CG height using a single model from the relationship

$$h = \frac{k\phi}{m(g\phi + a_y)}, \tag{2.11}$$

given that the roll angle ϕ, and the lateral acceleration a_y measurements as well as an accurate knowledge of the spring stiffness k are available. While the former can be measured

using suitable sensors, the spring stiffness k is unknown, which needs to be calculated depending on the specific maneuver and loading conditions; it is also affected by various other factors[2]. As will be explained in Section 2.4, using the multiple model switching method we neither need the exact knowledge of the suspension parameters, nor steady state type excitation to get an accurate estimation of the CG height. As a final remark we emphasize that although (2.10) is linear in the state variables, it is nonlinear with respect to unknown parameter variations of k, c and h.

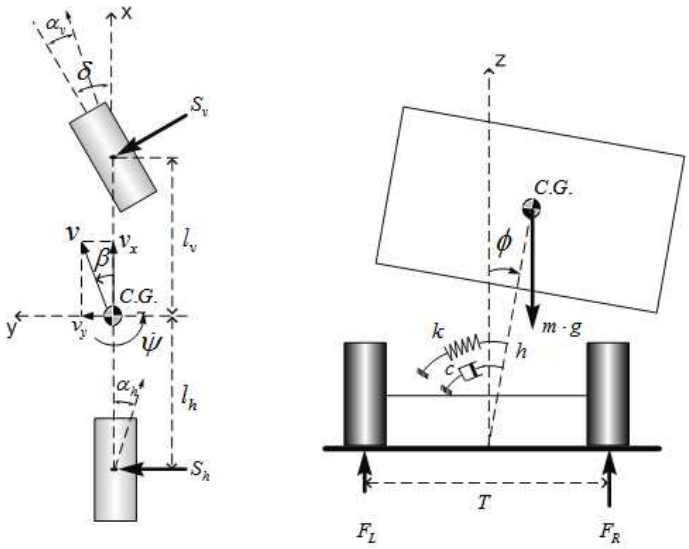

Figure 2.3: Linear bicycle model with roll degree of freedom.

2.3.3 Single track model with roll degree of freedom

While we utilize the previous two models for the estimation task of the unknown vehicle parameters, we employ the linear bicycle model with roll degree of freedom described here to generate the reference vehicle behavior. We shall also utilize variants of this model with different actuators for controller design in later chapters. The model as illustrated in Figure

[2] Aerodynamic forces, vertical tire loads, and variations in the roll center as a result of changes in the suspension geometry can affect the instantaneous value of k.

2.3 is the simplest model with coupled lateral and roll dynamics, which assumes that δ, ϕ, β are small and that all the vehicle mass is sprung. We can write the equations of motion for the single track model with the extended roll degree of freedom as follows

$$\dot{x} = \begin{bmatrix} -\frac{\sigma}{mv_x}\frac{J_{xeq}}{J_{xx}} & \frac{\rho}{mv_x^2}\frac{J_{xeq}}{J_{xx}} - 1 & -\frac{hc}{J_{xx}v_x} & \frac{h(mgh-k)}{J_{xx}v_x} \\ \frac{\rho}{J_{zz}} & -\frac{\kappa}{J_{zz}v_x} & 0 & 0 \\ -\frac{h\sigma}{J_{xx}} & \frac{h\rho}{v_x J_{xx}} & -\frac{c}{J_{xx}} & \frac{mgh-k}{J_{xx}} \\ 0 & 0 & 1 & 0 \end{bmatrix} x + \begin{bmatrix} \frac{C_v}{mv_x}\frac{J_{xeq}}{J_{xx}} \\ \frac{C_v l_v}{J_{zz}} \\ \frac{hC_v}{J_{xx}} \\ 0 \end{bmatrix} \delta, \tag{2.12}$$

where $x = \begin{bmatrix} \beta & \dot{\psi} & \dot{\phi} & \phi \end{bmatrix}^T$ is the state vector. Representative state responses of this model to a step steering input are shown in Figure 2.4 below, where the steering magnitude was 30° with a steering ratio of $1:18$, and the vehicle velocity during the simulation was $v_x = 30m/s$.

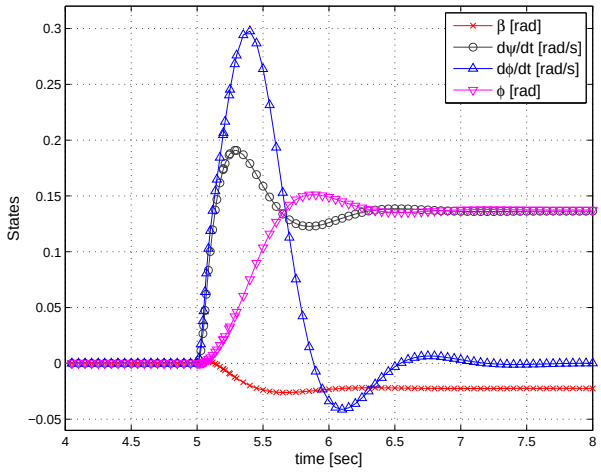

Figure 2.4: State responses of the single track model with roll degree of freedom to a step steering input ($v_x = 30m/s$, $\delta = \frac{30}{18}^\circ$.)

2.3.4 Load transfer ratio, LTR

In order to show the relationship between the roll dynamics and the vehicle CG height, we here define the lateral load transfer ratio (LTR) parameter based on a torque balance in the

roll plane of the vehicle model. Although this parameter is not utilized directly within the current chapter for the analysis, it is instrumental in understanding the dynamics of rollover. In later chapters we shall utilize this background to develop controllers to mitigate rollover. LTR appeared previously in the literature, most notably in [88] and [48] in order to assess the rollover threat.

The LTR can be defined simply as follows

$$LTR = \frac{\text{Load on Right Tires-Load on Left Tires}}{\text{Total Load on All Tires}}. \tag{2.13}$$

It is evident that this parameter varies in the interval $[-1,1]$, and during straight driving for a perfectly symmetric car it is 0. The extremum is reached in the case of a wheel lift-off of one side of the vehicle, in which case it becomes 1 or -1. Therefore, a direct measurement or an estimation of this parameter can be used as a rollover warning, or as a switch for a rollover controller. Indeed Kamnik et al. in [48] used wheel speeds measurements and Kalman filters to estimate LTR as a rollover controller activation switch for use in heavy trucks.

In Figure 2.3, the left and right wheel loads are shown with F_L and F_R respectively. Noticing that $F_L + F_R = mg$, we can express (2.13) as follows

$$LTR = \frac{F_R - F_L}{F_L + F_R} = \frac{2F_R - mg}{mg}. \tag{2.14}$$

We can obtain a simple steady state approximation of LTR in terms of a_y, and h as described in [88], which is given below

$$LTR \approx \frac{2a_y}{g}\frac{h}{T}. \tag{2.15}$$

From this approximation the dependence of LTR, thus the rollover threat, to the vehicle parameters a_y/g and h/T is clearly visible. Note that a_y is measurable via acceleration sensors whereas h is an unknown vehicle parameter that can not be measured directly. As apparent from this analysis, CG height is a prominent factor affecting rollover tendency of a vehicle, yet it is **not measurable**. Therefore any rollover mitigation controller can greatly benefit

from the estimation of this specific parameter by tuning of the control parameters based on the estimated CG height. This in turn can significantly improve the lateral and cornering performance of the vehicle in extreme driving situations without sacrificing vehicle safety and handling capability. In Chapter 3 we will utilize a dynamic version of the LTR in robust feedback control design for the rollover prevention problem, which we shall later in Chapter 4 integrate with the CG position estimation algorithm that we describe in the following sections.

2.3.5 Sensors and vehicle parameters

In this subsection we describe the configuration of sensors assumed in the automotive vehicle for use in conjunction with the multiple-model switching parameter estimation algorithm. Also we summarize the list of the assumptions on the known and estimated vehicle parameters that appear in the analysis that follows.

Sensors:

In the estimation algorithm we assume the availability of lateral acceleration a_y, yaw rate $\dot{\psi}$, velocity v_x and the steering angle δ measurements, which are available as part of the standard sensor packs found in modern cars that are commonly utilized for lateral and yaw dynamics control implementations such as the ESP (Electronic Stability Program) [132], [133]. Moreover, a measurement or an estimation of the vehicle roll angle is required for the implementation in this chapter, which can be obtained through spring displacement sensors (displacement transducers) found in vehicles with active suspension systems such as the ABC (Active Body Control).

Comment: The analysis given here does not necessarily require the use of a particular type of sensor to obtain the roll angle information: gyroscopic roll rate sensors, or any other suitable set of sensors can be utilized for computing the roll angle.

Parameters:

We assume that the vehicle mass m is known, which can be estimated as part of the braking system, yet this is outside scope of this thesis (see for example [131] for a realtime method for the estimation of vehicle mass). Furthermore C_v, C_h, l_v, k, c and h are all assumed to be **unknown** parameters of the vehicle and are estimated through the multiple model switching algorithm. We further assume that these parameters vary within certain closed intervals $C_v \in \mathscr{C}_v$, $C_h \in \mathscr{C}_h$, $l_v \in \mathscr{L}_v$, $c \in \mathscr{C}$, $k \in \mathscr{K}$ and $h \in \mathscr{H}$, and these intervals can be found via accurate numerical simulations as well as field tests. The number of models necessary to estimate these parameters relates to the size of the interval and the accuracy demand on the estimation, as shall be explained in the following section.

Comment: It is possible to extend the estimation scheme described in the next section to include the unknown and time-varying vehicle mass. However, as there are alternative and dependable methods for estimating the vehicle mass [131], as well as for the ease of exposition of the method described here, we omitted this parameter in the following discussion.

2.4 Vehicle parameter identification through multiple models & switching

While the conventional approach to parameter estimation is to employ a well-established linear least square type identification technique, such methods are susceptible to loss of identifiability due to feedback [120], [11] as is the case for the estimation problem described here. Also, the linear models introduced in Section 2.3 are nonlinear in the unknown vehicle parameters further complicating the formulation of the estimation problem using the traditional approaches. Although linear regression techniques typically converge quickly, they require measurement signals that are persistently exciting [120], [74]. For our problem this would impose some specific maneuver requirements on the driver input such that all

the modes of excitation are covered and a dependable estimation of the unknown parameters could be made. Such a demand on the driver input would not only be unrealistic but also unreliable. Thus there is a need for a different approach for the parameter identification task, which imposes no restrictions on the driver inputs, has fast convergence rates, and requires minimum additional output information (sensors). Here we introduce a multiple model switching algorithm [122] to identify unknown vehicle parameters rapidly in real-time. The method achieves this, in part, as a result of the fact that the model space representing the parameter uncertainty is bounded, and includes only the feasible parameters of the vehicle. This restricts infeasible estimations in cases when sensor signals are not persistently excited, and where the standard estimation methods such as the recursive linear least squares are destined to fail. Although we have no theoretical proof that the multiple model estimation algorithm is more immune to persistence of excitation issues, our numerical analysis shows that this is the case, at least as compared to the standard recursive least squares algorithm for this problem.

A natural approach here would be to setup the multiple estimation models using (2.12), which in this setup would imply that there is no modelling error. However in this case, the resulting parameter space would be too complex to handle. Instead we take a modular approach of decoupling the vehicle dynamics into subsystems by assuming a weak relationship from the roll dynamics onto the lateral. In the following two subsections we present our methodology and give numerical simulation results corresponding to the decoupled identification algorithms, which are then compared to recursive least squares based estimations.

Remark 2.4.1 As an alternative approach, the Extended Kalman Filter (EKF) can be utilized to tackle the nonlinear parameter estimation problem described in this chapter. We do not cover the EKF approach in the current thesis as the assumptions of the method are too restrictive, and there are known robustness issues of the algorithm due to linearization of the models, which can cause diverging estimations. While the EKF works well under certain conditions (e.g. process corrupted by white noise only, small nonlinearity, etc.), we

found the EKF to be difficult to tune and computationally complex to operate; a factor that prevents its use for automotive control applications. Regardless, a recent Master's thesis [7] looks into EKF based estimation of CG height for automotive vehicles. In the thesis an EKF implementation utilizing the measurements of lateral acceleration (a_y), yaw rate ($\dot{\psi}$), steering angle (δ), and roll rate ($\dot{\phi}$) based on the single track model with roll degree of freedom was suggested. Example CG height estimation results from this thesis corresponding to a step steer input is given in Figure 2.5. As can be observed from these results, the CG

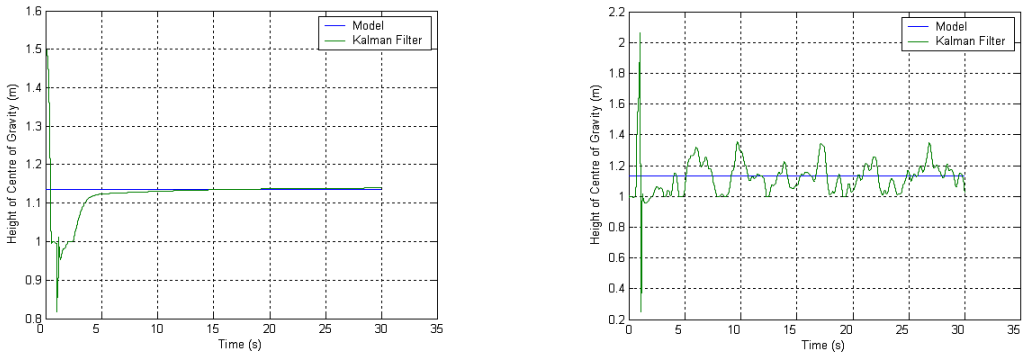

(a) **(b)**

Figure 2.5: CG height estimation results with Extended Kalman Filter (a) without sensor noise, (b) with gaussian white noise added on to the sensor signals [7] (Courtesy of Technische Universität Kaiserslautern).

height estimations based on this EKF implementation have large transients and very slow convergence rates. In the case of simulated sensor noise, where gaussian white noise is added on to the sensor signals, the estimation results have undesirable oscillatory behavior. These poor estimation results can be attributed, at large, to the modelling errors introduced by the single track model with roll degree of freedom. It is known that Kalman filters are sensitive to modelling errors [18]; the single track model utilized in [7] has fixed model parameters and thus it is only valid for a particular speed and steering input. Since the

measurement data used in the simulations pertain to real vehicles with a range of velocities and steering inputs, the model is not valid in all these operating conditions, which results in poor parameter estimations. While we utilize similar models in our multiple model vehicle parameter estimation technique, as shall be clear in the following sections, we allow for a finite range of vehicle parameters to be used at any given instant so that a set of single track (and roll plane) models track the real vehicle states accurately over a wide range of operating conditions.

2.4.1 Online identification of longitudinal CG location and tire stiffness parameters

The multiple model switching identification algorithm to estimate longitudinal CG location l_v and tire stiffness parameters C_v, C_h makes use of the lateral dynamics model given in (2.4). The method assumes that each unknown parameter belongs to a closed interval such that $C_v \in \mathscr{C}_v$, $C_h \in \mathscr{C}_h$, and $l_v \in \mathscr{L}_v$. These intervals are divided into certain number of grid points and they can be represented as $\{C_{v_1}, C_{v_2}, C_{v_3}, \ldots, C_{v_p}\} \subset \mathscr{C}_v$, $\{C_{h_1}, C_{h_2}, C_{h_3}, \ldots, C_{h_q}\} \subset \mathscr{C}_h$, and $\{l_{v_1}, l_{v_2}, l_{v_3}, \ldots, l_{v_r}\} \subset \mathscr{L}_v$ with dimensions p, q and r respectively.

Comment: There is a trade-off between the choice of the number of grid points in the parameter space and the numerical complexity, which is a design consideration depending on the accuracy demand from the estimation and the available computational resources for the specific problem under consideration.

With these in mind we form $n = p \times q \times r$ different models corresponding to the cross combinations of the grid points in the parameter space. Utilizing (2.4), the equations of motion corresponding to each model can be represented as

$$\begin{bmatrix} \dot{\beta}_i \\ \ddot{\psi}_i \end{bmatrix} = \begin{bmatrix} -\frac{\sigma_i}{mv_x} & \frac{\rho_i}{mv_x^2} - 1 \\ \frac{\rho_i}{J_{zz}} & -\frac{\kappa_i}{J_{zz}v_x} \end{bmatrix} \cdot \begin{bmatrix} \beta_i \\ \dot{\psi}_i \end{bmatrix} + \begin{bmatrix} \frac{(C_v)_i}{mv_x} \\ \frac{(C_v)_i l_{v_i}}{J_{zz}} \end{bmatrix} \delta, \tag{2.16}$$

where $i = 1, 2, \ldots, n$ denotes the model number. We assume that all models have zero initial conditions such that $\beta_i(0) = 0$, and $\dot{\psi}_i(0) = 0$, for $i = 1, 2, \ldots, n$. Furthermore, each model is driven by the same inputs δ and v_x as depicted in Figure 2.6, measurements of which are assumed to be provided by a suitable set of sensors.

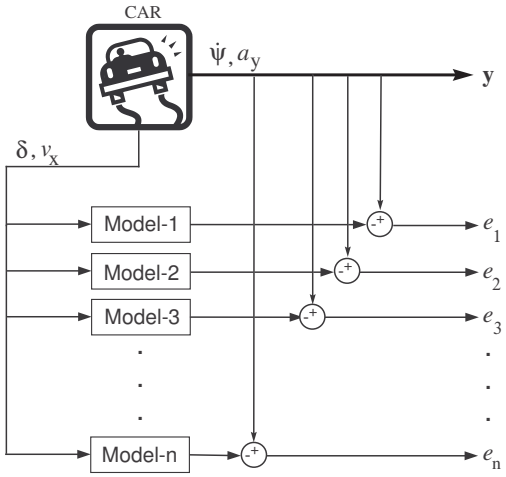

Figure 2.6: Multiple model system identification algorithm with single track models.

In order to select the model with the correct parametrization we look at the difference between the model and the plant outputs. The identification error e_i corresponding to the i^{th} model is defined as

$$e_i = y_{plant} - (y_{model})_i, \tag{2.17}$$

where y denotes the model or the plant output. In this implementation of the algorithm the output to be utilized is $y = [a_y, \dot{\psi}]$, and it is further assumed that the measurement of these variables are available for the vehicle. Thus we can represent the identification error for the i^{th} model as follows

$$e_i(t) = \begin{bmatrix} a_y(t) - a_{y,i}(t) \\ \dot{\psi}(t) - \dot{\psi}_i(t) \end{bmatrix}, \quad i = 1, 2, \ldots, n. \tag{2.18}$$

Note here that $a_y(t)$ and $\dot{\psi}(t)$ are the respective plant lateral acceleration and yaw rate output measurements obtained from the sensors, while $\dot{\psi}_i(t)$ is obtained from the second state of the i^{th} single track model given in (2.16), and corresponding $a_{y,i}(t)$ is calculated using the following function of the states at every instant

$$a_{y,i} = v_x(\dot{\psi}_i + \dot{\beta}_i) = -\frac{\sigma_i}{m}\beta_i + \frac{\rho_i}{mv_x}\dot{\psi}_i + \frac{(C_v)_i}{m}\delta. \tag{2.19}$$

By utilizing the identification errors it is possible to switch and choose a model that has the minimum distance to the plant outputs. Although control design is outside the scope of the current chapter, using a model that has the closest outputs to those of the plant is likely to yield the best feedback control performance. In other words a small identification error leads to a small tracking error [14], which, in the sense of adaptive control, is based on the principle of certainty equivalence from tuning to switching [79]. We will consider the control design implementation of the multiple model switched parameter estimation algorithm later in Chapter 4.

Based on empirical observations, the choice of the switching index should include both instantaneous and steady-state measures in order to reliably determine the identification models representing the plant at all instants. While there exist many such indices, we utilize the cost function J_i corresponding to the i^{th} identification error as given below, which is inspired by the quadratic cost optimization techniques and was originally suggested by Narendra et al. in [84, 78, 14] as a switching scheme

$$J_i(t) = \alpha||e_i(t)|| + \beta\int_0^t e^{-\lambda(t-\tau)}||e_i(\tau)||d\tau. \tag{2.20}$$

Comment: We emphasize that it is possible to choose alternative cost functions as the basis for model selection. The particular choice of (2.20) as the switching criterion in this thesis is motivated by the fact that this cost function is well established in the MMST literature.

In the expression for cost function (2.20), $\alpha \geq 0$ and $\beta \geq 0$ are the free design parameters controlling the relative weights given to transient and steady state measures respectively, whereas $\lambda \geq 0$ is the forgetting factor, which controls the rate of discarding the

past measurements in favor of the new information. As will be demonstrated in the sequel, switching based on (2.20) with nonzero combinations of α, β gives better results then using just the transient measures, e.g. $J_i(t) = e_i(t)^2$, or the steady-state measures, e.g. $J_i(t) = \int_0^t ||e_i(\tau)||d\tau$ alone. This is illustrated in Figure 2.7, where a comparison of the switching rule based on transient ($\alpha = 1, \beta = 0$), steady-state ($\alpha = 0, \beta = 1$) and combined ($\alpha = 0.2, \beta = 0.8$) output error dynamics is presented for the estimation of the longitudinal position of CG, where the true value of the reference vehicle is $1.2m$. It is obvious from the figure that the switching based on just the transient measures causes an undesirable chattering, while switching based only on the steady state measures has slower response in the estimations. For the details of the simulation see the following subsection on numerical analysis.

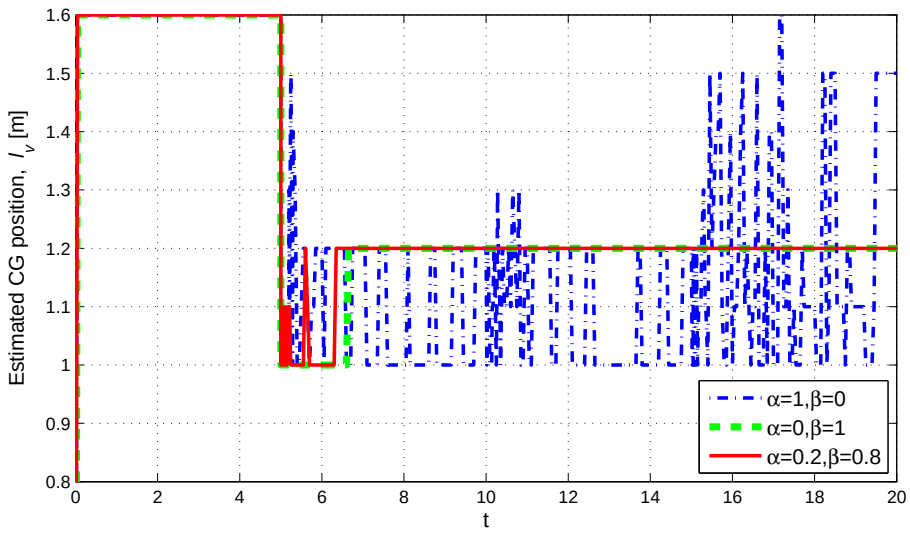

Figure 2.7: Comparison of switching based on transient, steady-state and combined output error dynamics.

Note that it is possible to use other type of cost functions depending on the specific estimation requirements from the problem at hand. Here we selected the model with the least

cumulative identification error according to (2.20) using

$$i^\star = \arg \min_{i=1,\ldots,n} J_i(t). \tag{2.21}$$

Within the parameter space described by a finite number of grid points in $\mathscr{C}_v, \mathscr{C}_h$ and $\mathscr{L}_v$, selected model $i^\star$ and the corresponding model parameters $C_v^\star, C_h^\star$ and $l_v^\star$ have the minimum cumulative distance[3] to the parameters of the plant.

Comment: As a rule of thumb based on our numerical experimentation, choosing $0.9 \leq \beta \leq 1$ and $0 < \alpha \leq 0.1$ for this problem gave the best estimation results in conjunction with the multiple model switched estimation algorithm. Also, the forgetting factor λ becomes important if the plant undergoes rapid switches; as this is not the case when CG position variation is considered, we set $\lambda = 0$ in the following discussion.

Numerical analysis:

In the following figures we present the estimation results for the algorithm based on simulated sensor signals generated by the vehicle model (2.12). The model parameters used are given in Table 2.2.

The maneuver was conducted at $108 km/h$, and as seen in Figure 2.8 the maneuver tested was an obstacle avoidance maneuver commonly known as the elk-test, with a peak magnitude of 30° at the steering wheel (the steering ratio is 1/18 between the tires and the steering wheel). The model space consisted of 140 models in total. The uniformly distributed parameter spaces were selected as $\mathscr{C}_v = [50000, 80000]$ with intervals of 10000, $\mathscr{C}_h = [60000, 100000]$ with intervals of 10000 corresponding to the range of tire stiffness parameters, and $\mathscr{L}_v = [1, 1.6]$ with intervals of 0.1 corresponding to the space of possible longitudinal CG positions. For this numerical example the free design parameters for the

[3]Cumulative distance here refers to the time variation of a measure of the parameter estimation error that is defined later in equation (2.22).

Table 2.2: Reference model parameters

parameter	value	unit
m	1300	$[kg]$
g	9.81	$[m/s^2]$
v_x	30	$[m/s]$
δ_{peak}	$30 \cdot \frac{1}{18}$	$[deg]$
J_{xx}	400	$[kg \cdot m^2]$
J_{zz}	1200	$[kg \cdot m^2]$
l_v	**1.2**	$[m]$
l_h	1.3	$[m]$
L	2.5	$[m]$
h	**0.7**	$[m]$
c	5000	$[kg \cdot m^2/s]$
k	36000	$[kg \cdot m^2/s^2]$
C_v	60000	$[N/rad]$
C_h	90000	$[N/rad]$

cost function were set as $\alpha = 0.05$ and $\beta = 1$, while the forgetting factor λ was chosen to be 0.

In Figure 2.9 the corresponding simulated sensor data and selected model outputs are compared. The discontinuous jumps in the model outputs are the result of the switching between the models. In Figure 2.10 the longitudinal CG position estimation is presented, where switching is more obvious. It is observed that based on the simulated measurement data, the multiple model switching algorithm successfully estimated the longitudinal CG

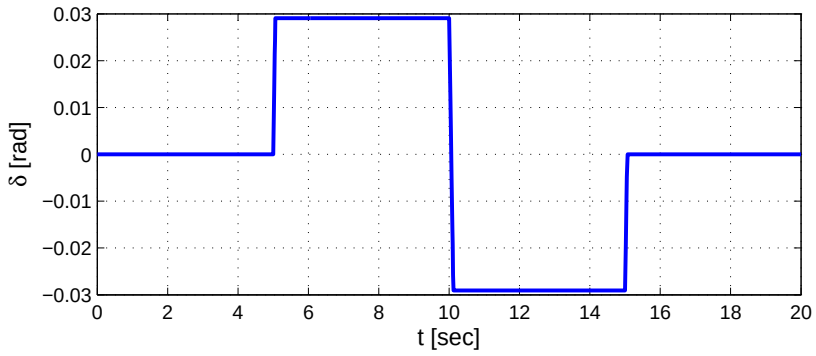

Figure 2.8: Steering input.

location to be $1.2m$, precisely matching the reference model. Similarly in Figure 2.11 the estimations for the front and rear tire stiffnesses with exact model match are presented. The algorithm successfully estimated the front tire stiffness C_v as 60000 and rear tire stiffness C_h as 90000, which are the exact parameters of the reference model. Finally in Figure 2.12 reference model sideslip angle β is compared with respect to that of the selected model which shows good agreement. For all practical means, the estimation result presented here is within sufficient tolerances for use in automotive control applications, particularly for adaptive lateral dynamics control problem.

Remark 2.4.2 Based on the numerical analysis above and as a motivation for further analysis, we wish to point a theoretical issue related to switching between the identification models based on the cost function (2.20). It is difficult to guarantee one-to-one correspondence between the distance (or error) in the output space and the distance in the parameter space at every instant based on the cost function (2.20) of identification errors. This can be demonstrated by defining a normalized parameter error corresponding to the i^{th} identification model as follows

$$\varepsilon_i = \sqrt{\left(1-\frac{(l_v)_i}{l_{v,p}}\right)^2+\left(1-\frac{(C_v)_i}{C_{v,p}}\right)^2+\left(1-\frac{(C_h)_i}{C_{h,p}}\right)^2}, \quad i=1,2,...,n, \tag{2.22}$$

where $l_{v,p}, C_{v,p}$, and $C_{h,p}$, denote the real parameters of the vehicle that we are trying to estimate. Note that for a given identification model, the normalized parameter error defined

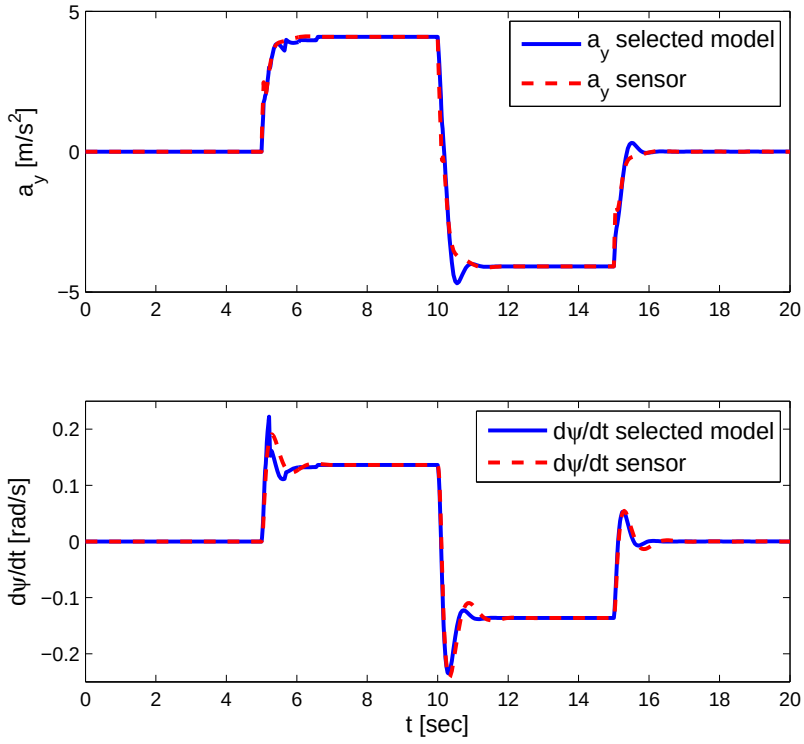

Figure 2.9: Sensor and the selected model output comparison for the longitudinal CG position estimation.

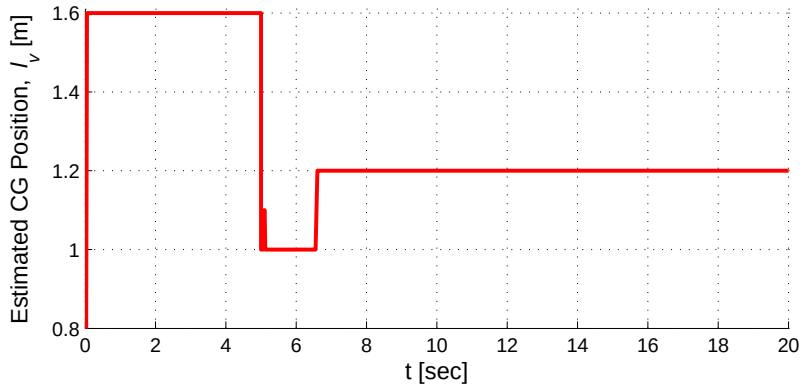

Figure 2.10: Longitudinal CG position estimation with exact match.

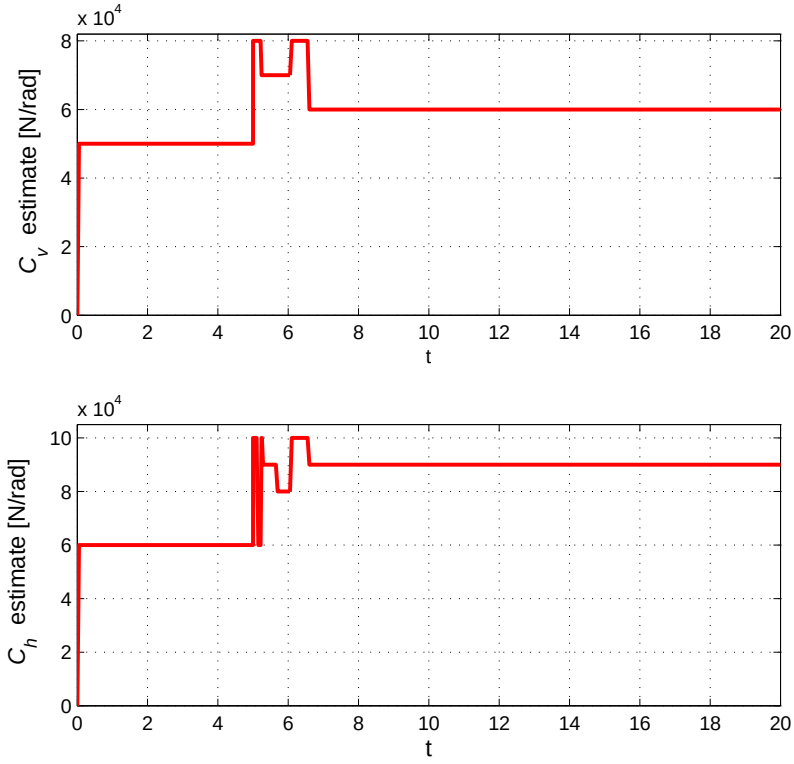

Figure 2.11: Estimation of the front and rear linear tire stiffness with exact model match.

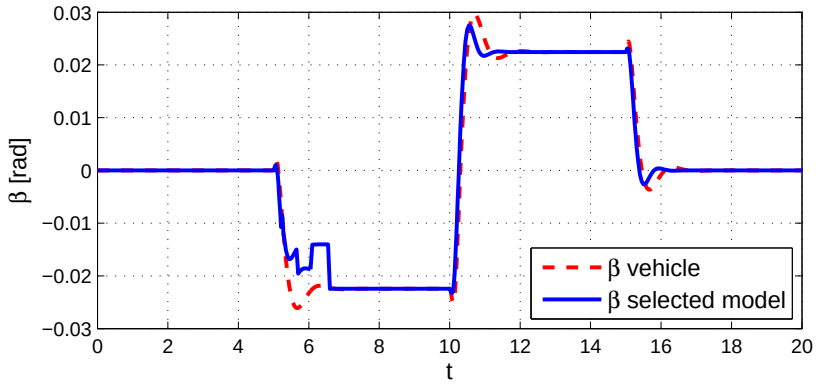

Figure 2.12: Comparison of the sideslip angles β for the vehicle and the selected models during the maneuver.

above is constant. At a given time instant t, the relationship between ε_i and $J_i(t)$ can be shown by comparing their variations across the model space (i.e., models corresponding to all combinations of the parameters). This is given in Figure 2.13 at an instant shortly after the initiation of the maneuver $(t = 5.25sec)$ for the 140 models used in the numerical simulation, and the result clearly demonstrates the problem with the lack of one-to-one correspondence between the output and the parameter spaces at this instant, where transient dynamics are dominant. In Figure 2.14 however, the time history of the normalized parameter error corresponding to the selected model at each instant during the estimation is shown, where it is observed that the parameter error goes to zero. This can be attributed to the fact that as the steady-state dynamics start to dominate, the cost functions $J_i(t)$ corresponding to models with large parameter errors grow much faster than those with small parameter errors, yielding the desired estimation result. To the best of our knowledge, determination of a cost function of the output errors that has a one-to-one correspondence in the parameter space at every instant, is still an open question in this framework.

Remark 2.4.3 It is relevant here to note also that when the model space does not contain the exact parameters of the plant, that is when there is no exact model match in the parameter space, a small offset is expected due to the unique shape of the selected cost function (2.20) in the parameter space, which for this simulation is shown in Figure 2.13 (note here that the cost function is plotted against increasing model indices) shortly after the initiation of the maneuver. It is obvious from the figure that cost function is non-symmetric about its minimum point at any given instant and in any given parameter space; this will be proven in detail later in Section 2.7.1 for a simpler problem. When the parameter space of the candidate models is too coarse (i.e., when there is insufficient number of grid points) about the minimum of the cost function, the estimation error can be significant. Inclusion of sufficient number of grid points and/or redistribution (adaptation) of model space however, can alleviate this problem to yield the closest parameter match.

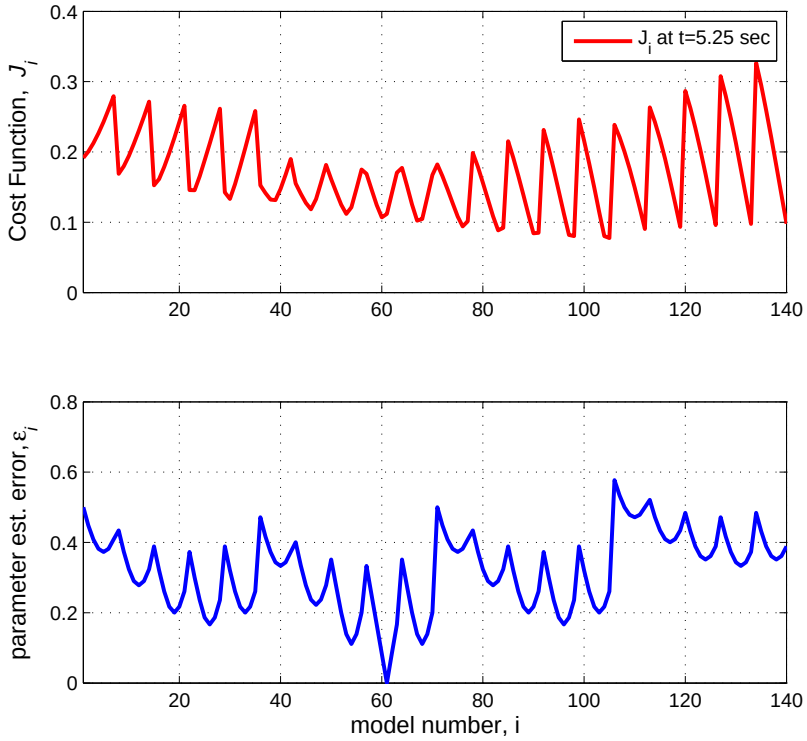

Figure 2.13: Variation of the cost functions J_i across the model space at an instant $(t = 5.25sec)$ shortly after the initiation of the maneuver and compared to the normalized parameter error ε_i for the numerical example.

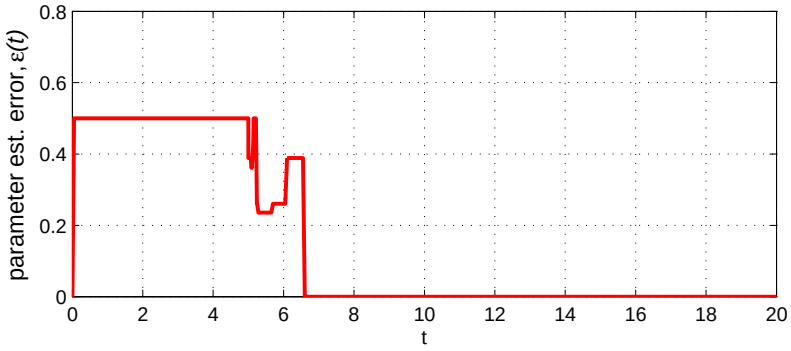

Figure 2.14: Time history of the normalized parameter error $\varepsilon(t)$ of the selected model during the simulation.

2.4.2 Online identification of CG height and suspension system parameters

In this subsection we present the multiple model switching algorithm to estimate CG height h along with the linear suspension parameters k, c based on the roll-plane model (2.10). Similarly, we assume that each unknown parameter belongs to a closed interval such that $h \in \mathscr{H}$, $k \in \mathscr{K}$, and $c \in \mathscr{C}$. These intervals are divided into a finite number of grid points and they can be represented as $\{h_1, h_2, h_3, \ldots, h_p\} \subset \mathscr{H}$, $\{k_1, k_2, k_3, \ldots, k_q\} \subset \mathscr{K}$, and $\{c_1, c_2, c_3, \ldots, c_r\} \subset \mathscr{C}$ with dimensions p, q and r respectively. We then form $n = p \times q \times r$ different models corresponding to the cross combinations of the grid points in the parameter space. Utilizing (2.10) the equations of motion corresponding to each model can be represented as

$$\begin{bmatrix} \dot{\phi}_i \\ \ddot{\phi}_i \end{bmatrix} = \begin{bmatrix} 0 & 1 \\ -\frac{k_i - mgh_i}{J_{xeq,i}} & -\frac{c_i}{J_{xeq,i}} \end{bmatrix} \cdot \begin{bmatrix} \phi_i \\ \dot{\phi}_i \end{bmatrix} + \begin{bmatrix} 0 \\ \frac{mh_i}{J_{xeq,i}} \end{bmatrix} a_y, \tag{2.23}$$

where $i = 1, 2, \ldots, n$ denotes the model number. We assume that all models have zero initial conditions such that $\phi_i(0) = 0$, and $\dot{\phi}_i(0) = 0$, for $i = 1, 2, \ldots, n$. Similar to what is shown in Figure 2.15, every model is driven by the same input a_y, which is measured.

According to (2.17) we again calculate identification errors e_i, however this time the plant and model outputs to compare are the roll angles, as follows

$$e_i(t) = \phi(t) - \phi_i(t), \quad i = 1, 2, \ldots, n. \tag{2.24}$$

Note that one can also include the roll rate $\dot{\phi}$ measurement, if available, in the output vector. However, for the specific maneuver chosen for the numerical tests, the influence of $\dot{\phi}$ on the estimation results for the CG height was relatively insignificant as compared to the roll angle ϕ measurements. Thus, the roll rate estimation error was omitted in the identification error definition (2.24). This is also in accordance with our assumption of no additional sensors to the available ones.

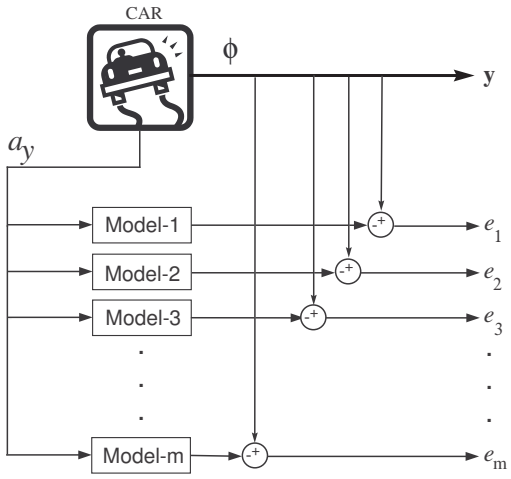

Figure 2.15: Multiple model system identification algorithm with roll plane models.

Now one can compute cost functions (2.20) corresponding to each identification error. Switching among the models based on (2.21) yields the one with the minimum cumulative identification error and the selected $k^\star, c^\star$ and $h^\star$ represent the plant in the parameter space described by a finite number of grid points in the intervals $\mathscr{K}$, $\mathscr{C}$ and $\mathscr{H}$ respectively.

Numerical analysis:

Here we present the CG height estimation results for the simulated measurement data described in the previous subsection. The model space consisted of 240 models in total. The uniformly distributed parameter space were selected as $\mathscr{K} = [30000, 40000]$ with intervals of 2000, $\mathscr{C} = [4000, 6000]$ with intervals of 500 corresponding to the parameter space for suspension parameters, and $\mathscr{H} = [0.5, 0.85]$ with intervals of 0.05 corresponding to the range of possible CG heights. For this numerical example the free design parameters for the cost function were set as $\alpha = 0.01$ and $\beta = 1$, while the forgetting factor λ was chosen to be 0.

In Figure 2.16 sensor and the switched model outputs are compared whereas in Figure 2.17

the CG height estimation results are shown. Based on the results, we again observe that the multiple model switching algorithm successfully estimated the CG height to be 0.7 m, precisely matching the reference vehicle data. Finally in Figure 2.18 the corresponding estimations of the suspension parameters are presented. The linear torsional spring stiffness k was estimated as 36000 exactly matching that of the reference vehicle model, while the roll damping coefficient c was estimated to be 6000 with a 20% estimation error.

Comment: The 20% estimation error in the damping coefficient can be attributed to the specific expression chosen for the model identification errors $e_i(t)$ given in (2.24), which is based on the roll angle measurements alone. As apparent from the expression for roll dynamics as described by (2.8), the damping coefficient c relates to the roll rate of the vehicle. Since we do not consider the roll rate estimation error in (2.24), this results in some expected estimation offset in c.

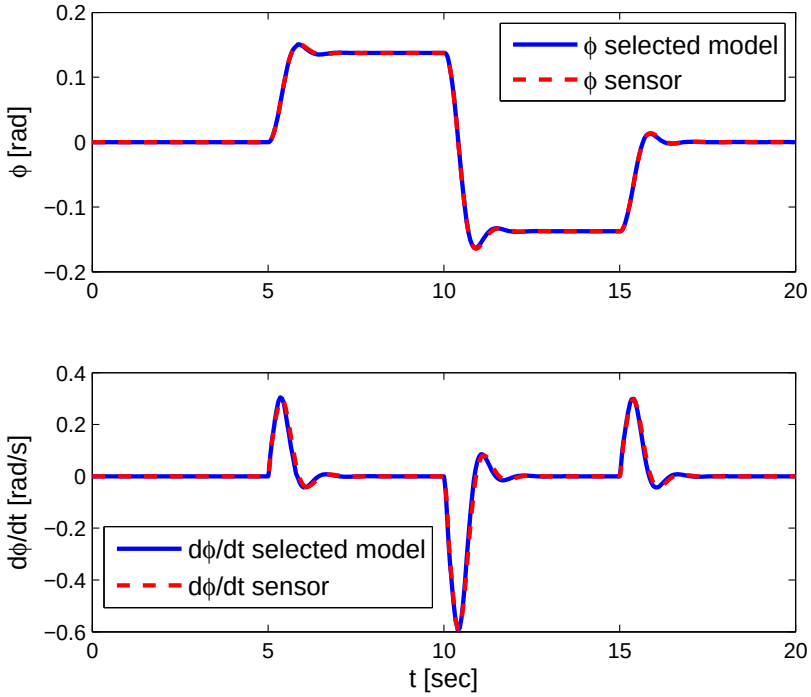

Figure 2.16: Sensor and the selected model output comparison for the CG height estimation.

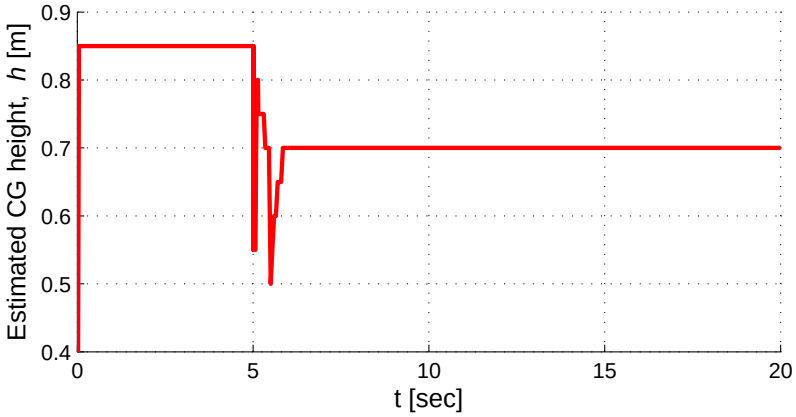

Figure 2.17: CG height estimation with exact match.

Despite the estimation offset in the roll damping coefficient, the suggested algorithm was successful in providing a fast and accurate estimation of the CG height, which is the main concern in this discussion. Therefore, for all practical means, the method described here is suitable for use in active automotive handling control systems, particularly in rollover mitigation control applications.

Remark 2.4.4 For the CG height estimation algorithm, the road bank angle (road superelevation) was not considered. When a measurement or an estimation of this parameter is provided, (where there is vast number of literature on this topic), the analysis presented in this section can be extended and applied without much modification.

Remark 2.4.5 In the numerical simulations presented in Sections 2.4.1 and 2.4.2, the parameter sets $\mathscr{C}_v, \mathscr{C}_h, \mathscr{L}, \mathscr{K}, \mathscr{C}, \mathscr{H}$ representing the uncertainty in the system were constructed such that the grid points include the unknown vehicle parameters of the reference model. When the parameter sets do not contain the exact model parametrization, then the method can only guarantee that the selected model outputs match the sensor measurements, yet the selected model may not necessarily have the closest distance in the parameter space to the plant. It is however possible to include a vast amount of grid points to resolve this

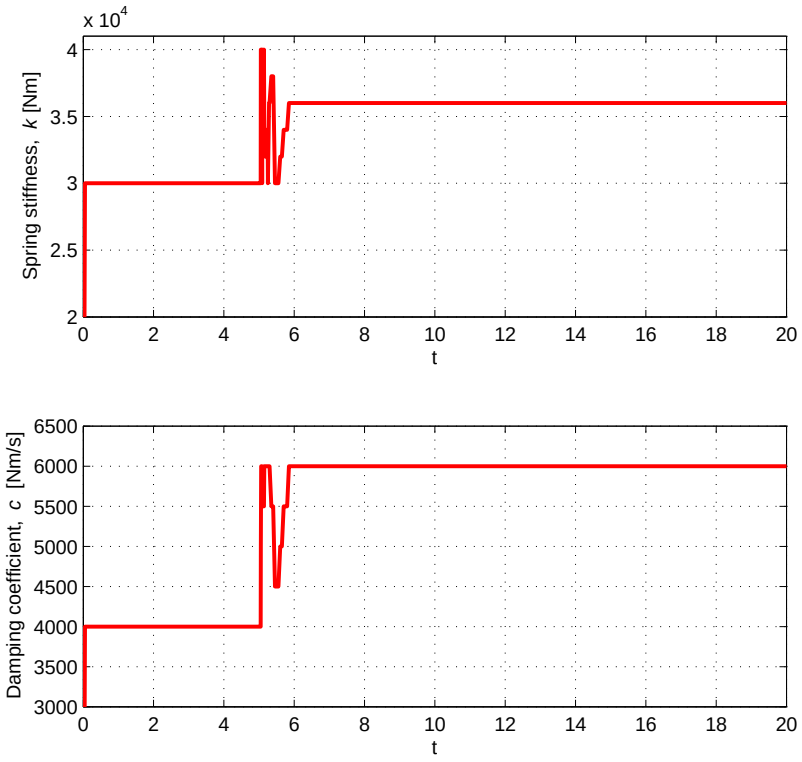

Figure 2.18: Estimation of the suspension parameters k, and c.

issue, which may be computationally difficult to implement in automotive applications. Alternatively, parameter adaptation rules or redistribution of the parameter space can be implemented to provide the exact model match with a limited number of models. We describe such an adaptive variation of the multiple model estimation method in Section 2.7.2 and implement it to the parameter estimation problem described in the current section.

2.4.3 Estimation of CG position using recursive least squares

In order to compare the quality of estimations described in the preceding subsections thus far, we now introduce a conventional method for estimating the CG position based on recursive linear least squares method. Although there exist other, perhaps more suitable methods,

we chose this one as it is a convenient benchmark for our application, and it is easier to implement than the alternatives. We first define the estimation method for a generic scalar system given by

$$y(t) = \xi^T(t)\theta + \varepsilon(t), \tag{2.25}$$

where $y(t)$ is the measurement corrupted by noise, $\varepsilon(t)$ is the measurement error, $\theta = [\theta_1, \theta_2, ..., \theta_N]^T$ is the unknown parameter vector, and $\xi = [\xi_1, \xi_2, ..., \xi_N]^T$ is the known regression vector. Using this system and denoting $\hat{\theta}(t)$ as the estimation of the unknown parameter vector θ at time t, we can give the recursive least squares method as follows

$$\begin{aligned} \kappa(t) &= P(t-1)\xi(t)[1+\xi(t)^T P(t-1)\xi(t)]^{-1} \\ P(t) &= [I-\kappa(t)\xi(t)^T]P(t-1) \\ \hat{\theta}(t) &= \hat{\theta}(t-1) + \kappa(t)[y(t) - \xi(t)^T\hat{\theta}(t-1)], \end{aligned} \tag{2.26}$$

where $P(t)$ is error the covariance matrix, and $\kappa(t)$ is the gain vector. Initial value for the covariance matrix is selected as $P(0) = \alpha I$, where I is the identity matrix and α is a large scalar constant. Notice that the estimation $\hat{\theta}(t)$ is calculated based on the previous estimation $\hat{\theta}(t-1)$ and the current measurements only. For a detailed derivation of these equations see [11].

We give the implementation of CG height estimation based on this method and making use of (2.8). In this implementation we assumed availability of the measurements for ϕ,$\dot{\phi}$,$\ddot{\phi}$ as well as a_y, where the simulated sensor signals are generated by the single track model with roll degree of freedom given in (2.12). We first denote the measurement vector as follows

$$a_y^{meas} = a_y cos\phi + gsin\phi. \tag{2.27}$$

As our reference model (2.12) is linear in the states as a result of the small angles assumption, for consistency, we can also express the measurement vector a_y^{meas} using the same assumption as follows

$$a_y^{meas} = a_y + g\phi. \tag{2.28}$$

Making use of (2.28) therefore, one can express the equation for roll dynamics (2.8) as

$$y(t) = a_y^{meas} = \frac{1}{mh}[J_{x_{eq}}\ddot{\phi} + c\dot{\phi} + k\phi]. \tag{2.29}$$

Notice here that there is a nonlinear coupling between the measurement variable $y(t)$ and the state variables $\dot{\phi}$ and ϕ, which is likely to induce errors in estimations as the linearity assumption of the least squares method does not hold. For this type of coupled estimation problems more complicated instrumental-variable type methods can be employed [120]. For demonstration purposes however, we proceed with the recursive least squares method to present the shortcomings of this method as compared to ours. Keeping these in mind, we further denote the regression and the unknown parameter vectors respectively as follows

$$\xi = \begin{bmatrix} \ddot{\phi} & \dot{\phi} & \phi \end{bmatrix}^T, \tag{2.30}$$

$$\theta = \begin{bmatrix} \theta_1 & \theta_2 & \theta_3 \end{bmatrix}^T, \tag{2.31}$$

where $\theta_1 = \frac{J_{x_{eq}}}{mh}$, $\theta_2 = \frac{c}{mh}$, and $\theta_3 = \frac{k}{mh}$. One can now use the recursive formulas (2.26) to compute $\hat{\theta}$ that minimizes the square of the cumulative measurement error. Based on the estimated parameters $\hat{\theta}$, the CG height can then be calculated from the roots of the polynomial below

$$mh^2 - m\theta_1 h + J_{xx} = 0. \tag{2.32}$$

As there are two roots of this polynomial, it is uncertain which one is closer to the real unknown parameter. In order to be conservative we always selected the larger root in the computations; this choice is motivated by the fact that an underestimation of CG height can cause an underestimation of the rollover threat. As the vehicle's safety is more important than its performance, a conservative estimation of the CG height can only cause loss of vehicle's performance in the context of rollover mitigation systems. We shall study these concepts in detail later in Chapters 3 and 4.

The CG height estimation results using the recursive least squares algorithm, and employing the reference vehicle data introduced in the preceding section, is given in Figure 2.19

as compared to the multiple model based estimation. As it is apparent from the figure, even though least squares method utilized a vast amount of sensory information (some of which are unmeasurable using the standard vehicle sensor equipment), the corresponding estimation has an undesirable bias and its convergence rate is slower than the multi-model based estimation. This clearly demonstrates the efficacy of our estimation technique over the traditional least squares approach for this specific problem. Finally, we note that there are more sophisticated, and perhaps more suitable, recursive estimation methods such as the instrumental-variable predictors or the least squares algorithm with multiple resetting as described in [131], both of which can be considered for the CG estimation problem described in the current Chapter. Investigation and comparison of these methods shall be considered as a future direction.

Comment: One of the advantages of the multiple model based estimation over the recursive least squares method is due to the fact that the former limits the possible set of solutions of the estimation problem by using a finite number of models and performs, basically, hypothesis testing. This inherently eliminates infeasible solutions. Also, when using recursive least squares method, it is possible to get numerical problems due to dynamics that are not stimulated persistently, which result in degraded estimations with large transient oscillations. For examples of this see [118] Appendix A, where an analysis of robustness of the standard least squares algorithm with respect to persistency of excitation is reported also. In the context of automotive parameter estimation, Section 7.2 of [50] contains an example representing the effects of non-persistent excitations.

Comment: The number of grid points required in the model space of the multiple model estimator is a function of the type of excitation to the system; in this case the vehicle maneuver. In general, if the sensor signals are persistently exciting one can expect better performance in terms of speed and accuracy and may not need a large number of models.

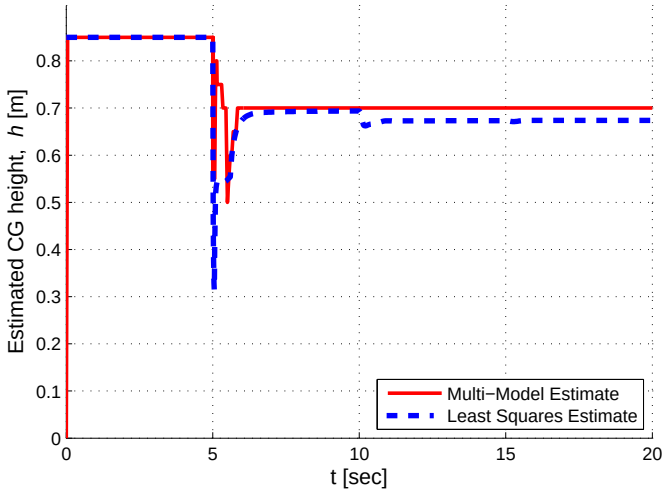

Figure 2.19: CG height estimation based on recursive least squares method as compared to the multiple model switching approach.

2.5 Preliminary evaluation of the realtime CG position estimation algorithm with off-line sensor measurements

In this section we present the results of preliminary tests conducted with sensor measurement data obtained from an industrial partner without disclosing the type and make of the test vehicle. The mass and inertia properties of the vehicle were specified as $m = 3062kg$, $J_{zz} = 4892kg/m^2$, and $J_{xx} = 1174kg/m^2$. The velocity and steering angle corresponding to the measurement are shown in Figure 2.20. It is important to note here that no feedback control systems were active during the measurements.

For the estimation of the longitudinal CG position, the parameter space consisted 180 models with the grid points selected as $\{1.3, 1.4, 1.425, 1.45, 1.475, 1.5, 1.525, 1.55, 1.6\} \subset \mathscr{L}_v$, $\{80000, 100000, 120000, 140000\} \subset \mathscr{C}_v$, and $\{120000, 140000, 160000, 180000, 200000\} \subset \mathscr{C}_h$. For this numerical example the free design parameters for the cost function were set as

$\alpha = 0.01$ and $\beta = 0.99$, while the forgetting factor λ was chosen to be 0 (we emphasize that the choice of $\lambda = 0$ is motivated due to the fact that the estimated parameters do not change during the course of the estimation). Comparison of the measured lateral acceleration and yaw rate of the vehicle to that of the multiple model algorithm is shown in Figure 2.21. Note here that there is a noticeable bias in the yaw rate measurement. Corresponding unknown parameter estimates of l_v, C_v and C_h are shown in Figure 2.22.

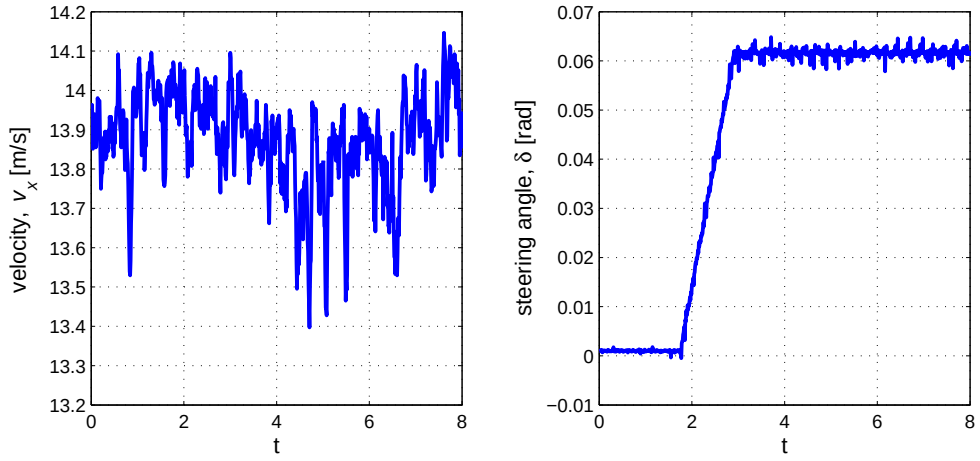

Figure 2.20: Velocity and steering angle inputs.

The results of the estimation of CG height using multiple roll plane models using the measurement data are shown in Figure 2.23 and Figure 2.24. In this estimation, the model space consisted of 275 models in total with parameter grid points set as $\{190000, 195000, 200000, 205000, 210000\} \subset \mathscr{K}$, $\{3000, 4000, 5000, 6000, 7000\} \in \mathscr{C}$, and $\{0.55, 0.6, 0.65, 0.675, 0.7, 0.725, 0.75, 0.775, 0.8, 0.825, 0.85\} \subset \mathscr{H}$. For this numerical example the free design parameters for the cost function were set as $\alpha = 0.01$ and $\beta = 0.99$, while the forgetting factor λ was chosen to be 0. In this measurement data, the roll angle was obtained from spring displacement sensors, which measure the vertical travel of the suspensions. Despite the significant offset in roll angle measurement as noticeable from Figure 2.23, the estimation results were successful.

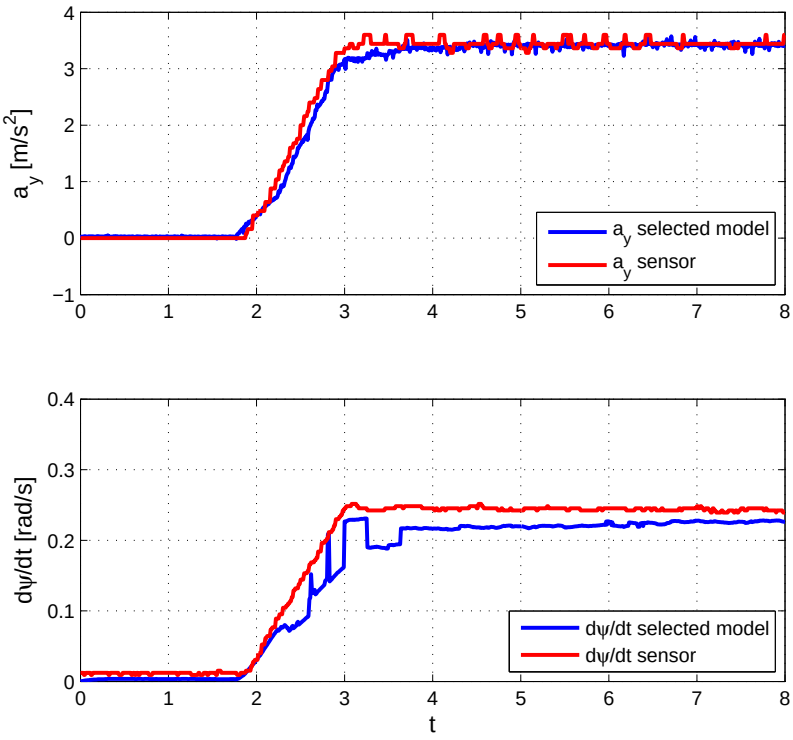

Figure 2.21: Comparison of the estimated and measured lateral acceleration and yaw rate.

Comment: It is important to note here that the specific problem at hand is about the estimation of unknown vehicle parameters in real-time rather than the control of specific vehicle states. Therefore, the abrupt switching between models and the corresponding “chattering" behavior in the estimations during the transient phase of the maneuvers is acceptable.

2.6 Application example: load condition estimator

In this section we introduce a problem related to rollover prevention for implementing our estimation technique. The problem originates from a particular robust rollover controller design in an SUV class vehicle such that when the vehicle is empty excluding the weight of driver, there is no risk of un-tripped rollover. In this case, a possible intervention of the

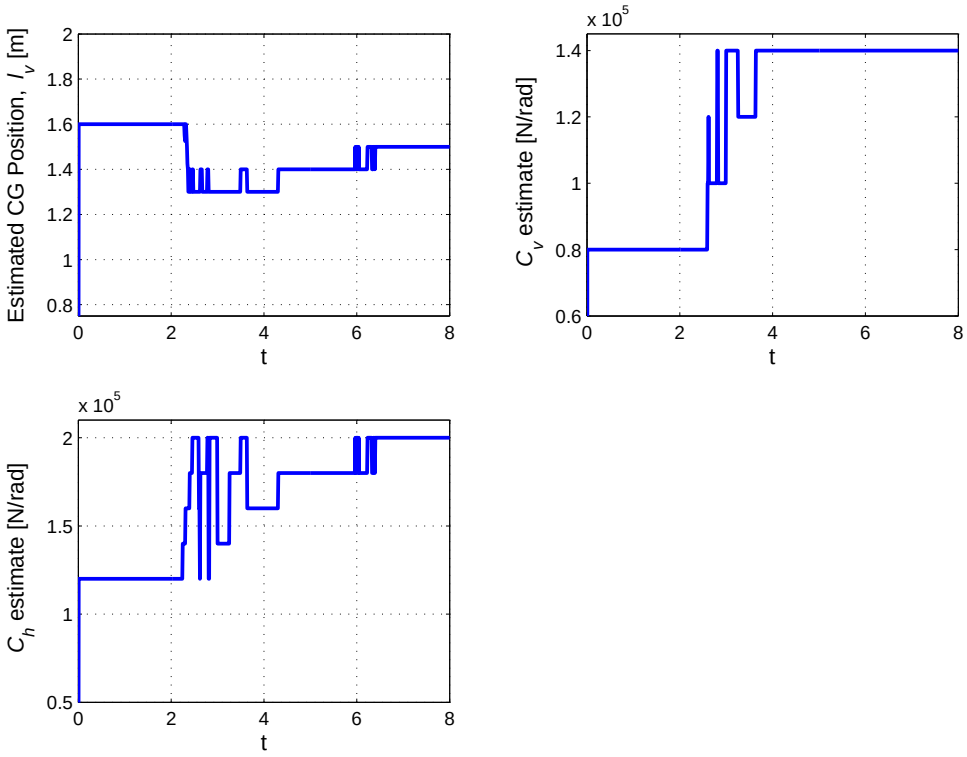

Figure 2.22: Estimations of longitudinal CG position and the linear tire stifnesses.

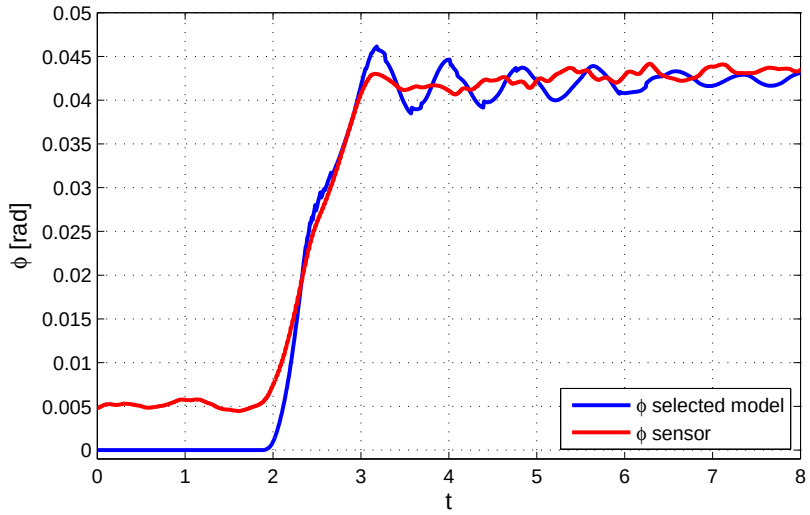

Figure 2.23: Roll angle measurement compared to the corresponding multiple model output.

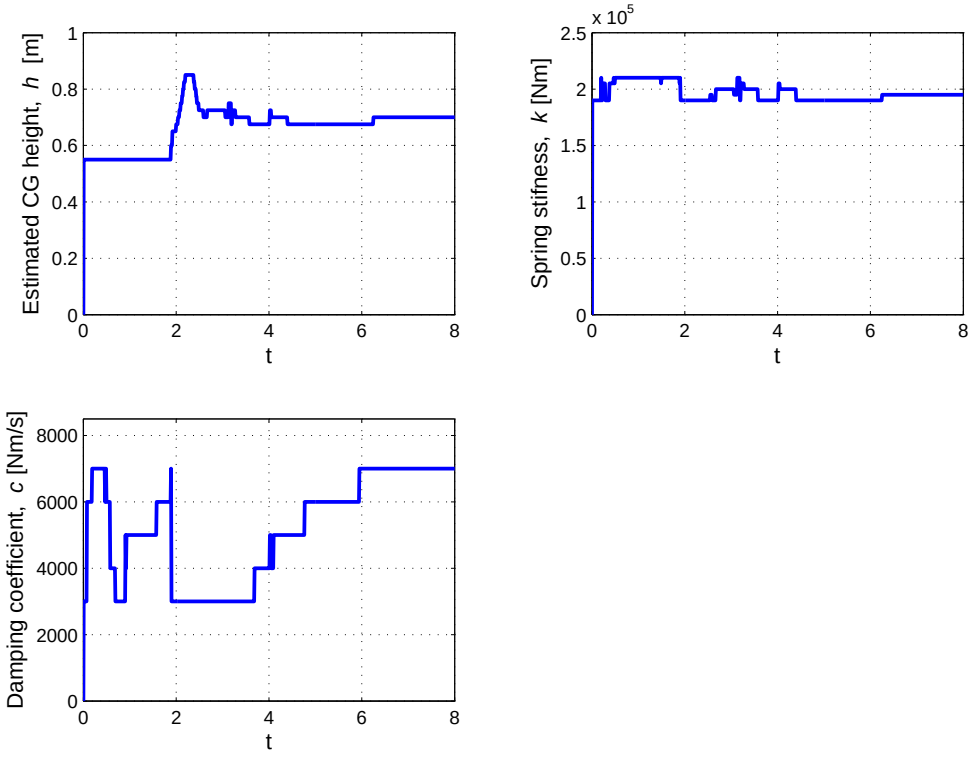

Figure 2.24: Estimations of CG height and the suspension parameters.

controller results in a loss of performance and must be avoided. In what follows, we give a version of the multiple model & switching algorithm to estimate whether the load condition of the vehicle is above the threshold weight. The threshold weight here is defined by the total weight of the empty vehicle and the driver. For this problem we employed the roll plane model (2.10) and further assumed the availability of the set of the roll angle (ϕ), and the lateral acceleration (a_y) sensors. We also assumed that we know the parameters of the vehicle corresponding to the threshold loading condition.

For the multiple model switching algorithm we set the known mass m, CG height h, damping coefficient c, and roll moment of inertia J_{xx} corresponding to the threshold loading condition to be the same in every model, where the models are parameterized with different spring stiffnesses. We assumed that spring stiffness belongs to a closed interval such that

$k \in \mathscr{K}$, where the interval is divided into n grid points such that $\{k_1, k_2, k_3, \ldots, k_n\} \subset \mathscr{K}$. In other words we have n different models corresponding to the different k values. The equations of motion for the models with zero initial conditions can be expressed with (2.23). While each model is driven by the same input a_y, the corresponding identification errors e_i are calculated according to (2.24). Given this setup, one can compute cost functions (2.20) corresponding to each identification error and switching among the models based on (2.21) yields the one with the minimum cumulative identification error. The selected $k^\star$ represents the plant in the parameter space described by a finite number of grid points in $\mathscr{K}$, and if it is different than that of the vehicle with threshold load condition then we can conclude that there is more load on the vehicle than the threshold value.

Numerical analysis:

In our simulations we chose the parameters given in Table 2.2 to represent the threshold loading of the vehicle. We also used the same obstacle avoidance maneuver introduced in the preceding section, at the speed of $108 km/h$ and with a steering profile as shown in Figure 2.8. We tested 9 different loading scenarios as described in Table 2.3, where the first case corresponds to the threshold loading condition. The model space consisted of 11 models in total, where the uniformly distributed parameter space was chosen as $\mathscr{K} = [30000, 40000]$ with intervals of 1000. Based on the described algorithm, only the first case was recognized as the threshold loading condition, and the recognition took less then 1.5 seconds into the maneuver in all the cases.

Based on the results, we conclude that this version of the multiple model & switching algorithm can be used to rapidly recognize a specific loading condition of a vehicle, based on the dynamics of the car alone, and utilizing only a small number of models.

Table 2.3: Loading scenarios

Case	Weight [kg]	CG height [m]	Threshold Loading?
1	**1300**	**0.70**	**yes**
2	1350	0.70	no
3	1400	0.70	no
4	1450	0.70	no
5	1500	0.70	no
6	1300	0.75	no
7	1300	0.80	no
8	1300	0.85	no
9	1300	0.90	no

2.7 Analysis of the switching criteria & adaptation

In this section we give a brief analysis of the cost function (2.20) of the multiple model switching algorithm described in the preceding section by utilizing a simple estimation problem. The addition of a multiple estimator structure, in compliance with the MMST framework, into a feedback control loop introduces the problem of switching stability. It is therefore important that the criteria used for switching between the identification models do not introduce unwanted instabilities to the controlled system. As we described in the previous section, the switching is performed based on the minimization of a cost function of the identification errors. The output (i.e., identification) error is defined as $e_i(t) = y_{plant} - (y_{model})_i$, where y_{plant} denotes the plant output while $(y_{model})_i$ is the corresponding output of the i^{th} identification model. In [78], motivated by quadratic optimal control techniques Narendra and Balakrishnan rather intuitively suggested the following cost function as the

switching criterion between the models;

$$J_i(t) = \alpha e_i^2(t) + \beta \int_0^t e_i^2(\tau) d\tau, \quad i = 1,2,...,n \tag{2.33}$$

where $\alpha \geq 0$ and $\beta \geq 0$ are scalar design parameters controlling the weights on the transient and steady state error dynamics, respectively. Note here that this cost function is in essence the same as (2.20) without the forgetting factor; as we are interested in the estimation of slowly varying and/or constant parameters we assumed the forgetting factor to be 0, thus resulting in the cost function (2.33). In MMST framework this cost function is computed for each model and the one minimizing it is selected at every instant. In what follows we present an analysis of this cost function candidate using a simple discrete time plant. We show analytically and numerically that this selection of the cost function may point to a wrong model when the exact plant parameter is not in the set of candidate models. This problem is related to the lack of one-to-one correspondence between the parameter space of the models and the output identification errors, which implies that the model with the smallest parameter error may not necessarily have the smallest cost. This is mainly due to the fact that the cost function (2.33) in any given parameter space is non-symmetric about its minimum point, and in some cases it is even non-convex. As a remedy to this problem, we suggest a simple adaptation algorithm, which modifies the distribution of models, yet uses equation (2.33) to minimize the cost. The suggested adaptation method helps to achieve better estimation accuracy while still using a small number of identification models.

2.7.1 An analysis of the MMST cost function

Here we introduce a simple estimation problem in conjunction with the multiple model estimation algorithm and obtain an analytic expression for the cost function given with (2.33). In order to simplify the analysis, we chose the following simple first order discrete time system for the estimation problem

$$x(k+1) = bx(k), \tag{2.34}$$

where k is the discrete time instant, and b represents an unknown positive scalar constant in the unit circle such that the plant is stable. We want to find b using the multiple model estimation approach and utilizing a finite number of models. Also we are interested in the behavior of the estimation algorithm when the parameter set of the identification models does not contain the exact plant parameter. Ideally, we expect the algorithm to choose the closest parameter from the set to that of the plant. We assume that we have a finite number of identification models of the form below

$$\hat{x}_i(k+1) = a_i\hat{x}(k), \quad a_i \in \{a_1, \ldots, a_N\}. \tag{2.35}$$

Note here that we assumed no modelling error for the sake of simplicity. Also, without loss of generality, we further assume that $0 < a_1 < a_2 < \ldots < a_N$. We can express the identification error corresponding to each model as follows

$$e_i(k) = x(k) - \hat{x}_i(k), \quad for \quad i \in \{1, \ldots, N\}. \tag{2.36}$$

Also, since we assumed a discrete time system, we can express the discrete time analog of the cost function (2.33), which is given below

$$J_i(k) = \alpha e_i^2(k) + \beta \sum_{\tau=0}^{k} e_i^2(\tau)\triangle t, \quad for \quad i \in \{1, \ldots, N\}, \tag{2.37}$$

where $\triangle t$ is the discrete time step (which can be fixed or variable) and $\alpha, \beta \geq 0$ are non-negative scalars. Now we have the following theorem that gives the main result of this subsection.

Theorem 2.7.1 *Suppose that the discrete time system (2.34) and N identification models described in (2.35) are given such that they all have identical initial conditions x_0. Also assume that $b \neq a_i$ for all $i \in \{1, \ldots, N\}$, and that $0 < a_1 < a_2 < \ldots < a_N$. Further, we denote ξ as the index for which (2.37) is minimum at the time instant k, i.e.,*

$$\xi = \arg \min_{i=1,\ldots,N} J_i(k). \tag{2.38}$$

Then the cost function (2.37) has the following properties:

(a) For each k, (2.37) is a monotonically decreasing function in $[a_1, a_\xi]$*, and a monotonically increasing function in* $[a_\xi, a_N]$.

(b) For each k, (2.37) is non-symmetric about its minimum point $J_\xi(k)$*, and thus there is no one-to-one correspondence between the parameter error and the identification error.*

(c) For some fixed k, (2.37) is non-convex on the interval $[a_1, a_N]$.

Proof of Theorem 2.7.1: For identical initial conditions x_0 for the plant and N identification models, we can express the corresponding plant and model trajectories as follows

$$x(k) = b^k x_0, \qquad \textit{and} \qquad \hat{x}_i(k) = a_i^k x_0 \;\; \textit{for} \;\; i \in \{1, \ldots, N\}. \tag{2.39}$$

Utilizing these relations the cost function (2.37) can be expressed as below

$$J(k, a_i) = \alpha (b^k - a_i^k)^2 x_0^2 + \beta \sum_{\tau=0}^{k} (b^\tau - a_i^\tau)^2 x_0^2 \triangle t, \tag{2.40}$$

for each $i \in \{1, \ldots, N\}$. Arranging and factoring the like-terms in the equation yields

$$J(k, a_i) = x_0^2 \triangle t [\beta (b - a_i)^2 + \beta (b^2 - a_i^2)^2 + \ldots + \beta (b^{k-1} - a_i^{k-1})^2 + (\beta + \frac{\alpha}{\triangle t})(b^k - a_i^k)^2]$$

We can further arrange this expression by noting that

$$\begin{aligned}
(b - a_i)^2 &= (b - a_i)^2, \\
(b^2 - a_i^2)^2 &= (b - a_i)^2 (b + a_i)^2, \\
(b^3 - a_i^3)^2 &= (b - a_i)^2 (b^2 + b a_i + b^2)^2, \\
&\vdots \\
(b^k - a_i^k)^2 &= (b - a_i)^2 (b^{k-1} + b^{k-2} a_i + \ldots + b a_i^{k-2} + a_i^{k-1})^2.
\end{aligned}$$

and substituting these relations back in the last expression results in the following function

$$\begin{aligned}
J(k, a_i) &= x_0^2 \triangle t (b - a_i)^2 [\beta + \beta (b + a_i)^2 + \beta (b^2 + b a_i + a_i^2)^2 + \ldots \\
&+ \beta (b^{k-2} + b^{k-3} a_i + \ldots + b a_i^{k-3} + a_i^{k-2})^2 \\
&+ (\beta + \frac{\alpha}{\triangle t})(b^{k-1} + b^{k-2} a_i + \ldots + b a_i^{k-2} + a_i^{k-1})^2],
\end{aligned} \tag{2.41}$$

where $i \in \{1,\ldots,N\}$. Based on equation (2.41) we can draw some conclusions about this cost function. But before we do so, we give the following definition of monotonic functions that is useful in proving the property (a).

Definition 2.7.1 *[101] Let $f(\cdot)$ be a real valued function on the interval $[\,\underline{y},\bar{y}\,]$. Then $f(\cdot)$ is said to be monotonically increasing on $[\,\underline{y},\bar{y}\,]$ if $\underline{y} < y_1 < y_2 < \bar{y}$ implies $f(y_1) \leq f(y_2)$. If instead it implies $f(y_1) \geq f(y_2)$, then $f(\cdot)$ is said to be a monotonically decreasing function.*

Now for a given k discrete time instant, there exist $\xi \in \{1,\ldots,N\}$ satisfying (2.38) such that $J(k,a_\xi) < J(k,a_i)$ for all $i \neq \xi$, that is $J(k,a_\xi) = \min\{J(k,a_1),\ldots,J(k,a_N)\}$. Recall the assumption that $a_1 < \ldots < a_N$ are an ordered set of scalars all of which have the same (positive) sign as the plant parameter b. Then based on equation (2.41) and the definition of monotonicity given above, it is straightforward to show that $J(k,a_i)$ is a monotonically increasing function for varying a_i within the interval $[a_\xi, a_N]$; this follows from the fact that for a given pair $a_{y_1} < a_{y_2}$ with $a_{y_1}, a_{y_2} \in [a_\xi, a_N]$ results in $J(k,a_{y_1}) < J(k,a_{y_2})$ in this interval. However, based on the expression (2.41) for the cost function, it is not straightforward to show that $J(k,a_i)$ is monotonically decreasing for each $a_i \in [a_\xi, a_{\xi+1},\ldots,a_N]$. In order to do so we will express the cost function as a continuous function in the parameter space. We denote η as the independent variable of the function such that $\eta \in [a_1, a_N]$, and based on (2.40) the cost function can be expressed as

$$J(k,\eta) = \alpha(b^k - \eta^k)^2 x_0^2 + \beta \sum_{\tau=0}^{k} (b^\tau - \eta^\tau)^2 x_0^2 \triangle t. \tag{2.42}$$

Note that at a given discrete time step k, the global minimum of this non-negative function is at $\eta = b$, with $J(k,b) = 0$. It is sufficient to show that $J(k,\eta)$ decreases for all $\eta \in [a_1, a_\xi]$. To do so, we look at the first derivative of $J(k,\eta)$ with respect to η, which is

$$\frac{dJ(k,\eta)}{d\eta} = -2\alpha x_0^2 k(b^k - \eta^k)\eta^{k-1} - 2\beta x_0^2 \triangle t \sum_{\tau=0}^{k} (b^\tau - \eta^\tau)\eta^{k-1}. \tag{2.43}$$

Obviously, for each $\eta < b$, the above expression is negative, which implies that for a given pair $a_{y_3} < a_{y_4}$ with $a_{y_3}, a_{y_4} \in [a_1, a_\xi]$ results in $J(k,a_{y_3}) > J(k,a_{y_4})$ in this interval, which

concludes the proof of the property (a). We note that (2.43) can also be used to show increasing monotonicity of $J(k,\eta)$ for all $\eta \in [a_\xi, a_N]$, which is in agreement with the result based on (2.41).

Another obvious conclusion based on (2.41) is that this function is not symmetric in the parameter space for changing a_i. In order to understand this, we consider three adjacent and equidistant nodes with a separation distance d in the parameter space, which is depicted schematically in Figure 2.25. We denote these adjacent nodes as $a_{\xi-1}, a_\xi, a_{\xi+1}$ such that

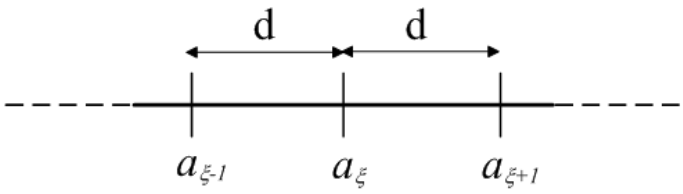

Figure 2.25: Three equidistant nodes in the parameter space.

$a_{\xi-1}, a_\xi, a_{\xi+1} \in \{a_1, \ldots, a_N\}$. We assume without loss of generality that these parameters all have the same sign as b. Further suppose that the cost function is minimum for the center node a_ξ at a particular discrete time instant k, i.e.,

$$J(k,a_\xi) < J(k,a_i), \;\; i = 1,2,...,N, \;\; i \neq \xi \tag{2.44}$$

At this instant one would expect to find the two neighboring, equidistant nodes $a_{\xi-1}$ and $a_{\xi+1}$ to have the same cost values. However if we look at the equation (2.41) more closely, we observe that while the first term is the same for both neighboring nodes i.e., $(b - a_{\xi-1})^2 = (b - a_{\xi+1})^2 = d^2$, the term in the square brackets is smaller for the node $a_{\xi-1}$ (remember the assumption that $0 < a_{\xi-1} < a_{\xi+1}$). We conclude that the cost functions $J_{\xi-1}(k)$ and $J_{\xi+1}(k)$ for the two respective equidistant neighboring nodes $a_{\xi-1}$ and $a_{\xi+1}$ have the property that

$$J(k,a_{\xi-1}) < J(k,a_{\xi+1}). \tag{2.45}$$

Having proved the property (b), this result clearly indicates that even for the simple discrete system (2.34), there is no one-to-one correspondence between the parameter error and the identification error based on the cost function (2.37).

A final observation based on (2.41) is is related to convexity. In order for a real valued function $f(\cdot)$ to be convex, which is defined over a convex subset C of a linear vector space, it needs satisfy

$$f(\gamma y_1 + (1-\gamma)y_2) \leqslant \gamma f(y_1) + (1-\gamma) f(y_2) \tag{2.46}$$

for all $y_1, y_2 \in C$ and all γ, where $0 < \gamma < 1$. However, it is not straightforward to do this check on the cost function given with (2.41). Instead, one can alternatively check a necessary condition for convexity, which requires that there should be no inflection points to have strict convexity, that is $\frac{d^2 f(y)}{dy^2} > 0$ for all $y \in C$. To test this we observe from (2.41) that for k=2 the cost function is

$$J(2, a_i) = x_0^2 \triangle t[\beta(b-a_i)^2 + (\beta + \frac{\alpha}{\triangle t})(b^2 - a_i^2)^2]. \tag{2.47}$$

Taking the second derivative of $J(2, a_i)$ with respect to a_i then yields

$$\frac{J^2(2, a_i)}{da_i^2} = -2x_0^2 \triangle t[-\beta + 2(\beta + \frac{\alpha}{\triangle t})(b^2 - a_i^2) - 4(\beta + \frac{\alpha}{\triangle t})a_i^2]. \tag{2.48}$$

It is possible choose a set of numbers a_i, b and $\alpha, \beta, \triangle t$ to make the last equation negative, which would make the cost function a non-convex function for the time instant $k = 2$. Thus for some k, $J(k, a_i)$ can be non-convex, which proves the property (c).

Q.E.D.

The result of the Theorem 2.7.1 can be verified numerically as well. Variation of the cost function in the parameter space is not symmetric as shown in Figure 2.26 for a numerical example. This curve shows the variation of the cost function given in equation (2.37) with respect to models distributed evenly at 0.05 intervals within [-1,1]. The plant dynamics are governed by the equation $x_p(k+1) = 0.5251 x_p(k)$. As claimed the shape of the function is

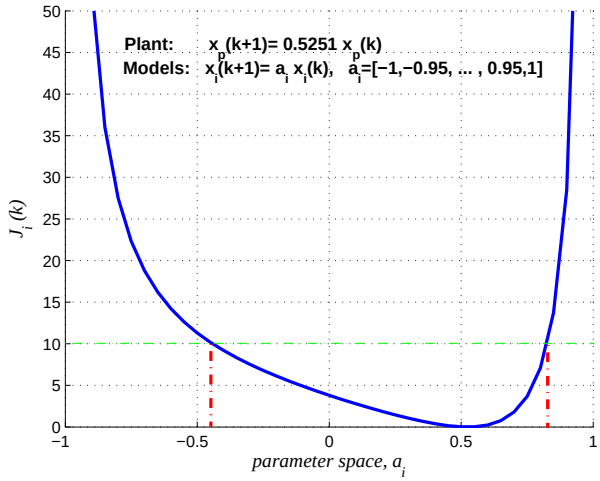

Figure 2.26: Cost function variation in parameter space.

not symmetric, and due to this reason if one is not careful about choosing the location of the models, the algorithm may end up choosing a model that is not the closest in the parameter space. This problem is depicted in Figure 2.26 by the two vertical dashed lines, which represent two hypothetical models with the same cost function values. As can be easily seen from the figure, if there are no models in between these two, the algorithm may end up choosing the wrong model. In order to prevent this one needs to have a dense number of models, which may come with a computational overhead for complex estimation and control problems.

Comment: A final observation based on the equation (2.37) is that when $b \notin \{a_1, \ldots, a_N\}$, the interval containing the unknown parameter b in the parameter space is ambiguous. Theorem 2.7.1 verifies that the minimum cost function may not always point to the closest model in the parameter space, which necessitates the analysis of the variation of the cost function in the neighborhood of the selected minimum point $J(k, \xi)$. This problem is illustrated in Figure 2.27, where b can be contained in either of the intervals $[a_{\xi-1}, a_\xi]$ and $[a_\xi, a_{\xi+1}]$. In Section 2.7.2 we will address this problem with an adaptive estimation algorithm that does not require a dense multiple model structure.

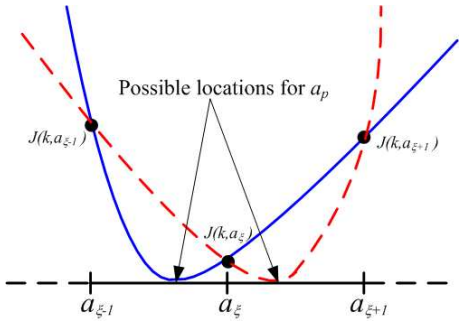

Figure 2.27: Ambiguity in the interval containing the minimum point.

Remark 2.7.1 (**Comments on extension to finite dimensional systems**) The results we obtained so far are based on a scalar discrete time system, and the implications of these results for higher dimensional dynamical systems is unclear. While it is, at present, difficult to directly generalize these analytical results to generic finite dimensional systems, under certain conditions this can be achieved. In analogy to Theorem 2.7.1, it is possible to extend the conclusions for the MMST cost function

$$J_i(k) = \alpha||e_i(k)|| + \beta \sum_{\tau=0}^{k} ||e_i(\tau)||\triangle t, \quad for \quad i \in \{1,\ldots,N\}, \tag{2.49}$$

to certain classes of finite dimensional discrete time systems. The following comment gives a trivial extension to a class of finite dimensional systems, which follows directly from Theorem 2.7.1.

Comment: Suppose that a discrete-time linear system in $\mathbb{R}^m$ with a diagonal system matrix is given as below

$$x(k+1) = Bx(k) \quad with \quad B = diag(b_1, b_2, \ldots, b_m), \tag{2.50}$$

where $diag(b_1, b_2, \ldots, b_m)$ denotes the matrix in $\mathbb{R}^{m\times m}$ with scalars $b_1, b_2, \ldots, b_m$ as the diagonal elements. Suppose further that we have N identification models that are given as

$$\hat{x}(k+1) = A_i\hat{x}(k) \quad with \quad A_i = diag(a_i, b_2, \ldots, b_m), \tag{2.51}$$

where $i \in \{1,2,\ldots,N\}$. We assume that the plant (2.50) and the identification models (2.51) have identical initial conditions $x_0 \in \mathbb{R}^m$.

We are interested in estimating b_1 with the N candidate models. We assume that $b_1 \neq a_i$ for all $i \in \{1,\ldots,N\}$, and also that $0 < a_1 < a_2 < \ldots < a_N$. Further, we denote ξ as the index for which the cost function (2.49) is minimum at the time instant k, i.e.,

$$\xi = \arg \min_{i=1,\ldots,N} J_i(k).$$

Then the cost function (2.49) with the identification error $e_i(k) = [x(k) - \hat{x}(k)]$ for $i \in \{1,\ldots,N\}$, has the following properties:

(a) For each k, (2.49) is a monotonically decreasing function in $[a_1, a_\xi]$, and a monotonically increasing function in $[a_\xi, a_N]$.

(b) For each k, (2.49) is non-symmetric about its minimum point $J_\xi(k)$, and thus there is no one-to-one correspondence between the parameter error and the identification error.

(c) For some k, (2.49) is non-convex in the parameter space $[a_1, a_2 \ldots, a_N]$.

The proof of properties (a), (b), and (c) directly follow from Theorem 2.7.1. The last comment achieves a trivial extension for the conclusions about the MMST cost function to finite dimensional systems with a diagonal system matrix and with uncertainty in the first element. It is trivial to show that the results also extend to the case when there is uncertainty in multiple elements of the diagonal system matrix B given in (2.50). In this case, it can be shown based on the last comment that the cost function (2.49) becomes a multi-variable function of, at most, m uncertain parameters, i.e., $J(k, a_i, b_i, \ldots, m_i)$, and that this function can be written as a summation of m decoupled functions

$$J(k, a_i, b_i, \ldots, m_i) = J_1(k, a_i) + J_1(k, a_i) + \ldots + J_N(k, m_i) \tag{2.52}$$

where each of the decoupled functions $J_1(k, a_i), J_1(k, a_i), \ldots, J_N(k, m_i)$ are of the form (2.40), and each are non-convex and non-symmetric in their respective bounded parameter spaces $\{a_1,\ldots,a_N\}, \{b_1,\ldots,b_N\}, \ldots, \{m_1,\ldots,m_N\}$.

Comment: While it is difficult to analyze the properties of the cost function (2.49) for generic finite dimensional systems analytically, a similar conclusion obtained in Theorem 2.7.1 can be conjectured numerically for such systems. Here we give a simple example of this, where we estimate 2 unknown parameters a,b of a second order plant with a companion system matrix, in conjunction with the multiple model switching framework. We emphasize that the choice of second order companion systems in this numerical example is motivated by the ease of exposition. Suppose that the plant and the identification models with companion systems matrices are specified as follows

$$x(k+1) = \begin{bmatrix} 0 & 1 \\ a & b \end{bmatrix} x(k), \qquad \hat{x}(k+1) = \begin{bmatrix} 0 & 1 \\ a_i & b_i \end{bmatrix} \hat{x}(k),$$

The parameter space of the identification models are chosen such that $a_i \in \{-1, -0.95, \ldots, 0.95, 1\}$ and $b_i \in \{-1, -0.95, \ldots, 0.95, 1\}$. We want to estimate the scalars a,b using the measurements of the state $x(k)$ alone, and based on the MMST approach. For this example we assume the initial conditions for the plant and the identification models to be $x_0^T = [5\ 20]$. The variation of the cost function (2.49) in the parameter space is shown in Figure 2.28 as a 3D surface at a randomly selected time instant of $t = 1$ second, where the reference plant parameters were selected to be $a = 0.9$ and $b = -0.2$. In the figure, the vertical axis represents the value of the cost function corresponding to all possible combinations of the grid points of the parameter space in the horizontal plane (the plot on the right is the top view). As observed from the figure, the cost function is monotonic about its minimum point $J(1, 0.9, -0.2)$. Furthermore, a further observation is that for any given fixed values of $b_i \in [-1, 1]$ the cost function is not symmetric in the parameter space $a_i \in [-1, 1]$, and for any given fixed values of $a_i \in [-1, 1]$ the cost function is not symmetric in the parameter space $b_i \in [-1, 1]$.

In Figure 2.29, the result of the numerical simulation for a different reference plant with parameters $a = -0.5$, $b = 0.1$ is shown. Again, based on the plots we can draw the same conclusion as above regarding the MMST cost function.

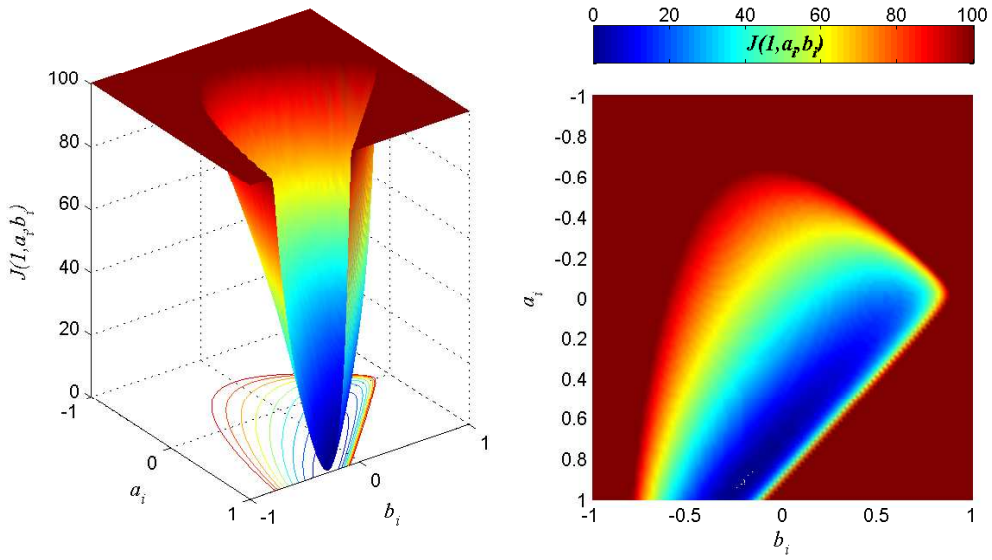

Figure 2.28: Cost function variation in parameter space for a second order estimation problem with plant parameters $a = 0.9$, $b = -0.2$.

The above numerical examples support the claim that the shape of the cost function is not symmetric for higher dimensional systems also, which necessitates a careful selection and structuring of the model space for any given multiple model switched estimation problem based on fixed models. We emphasize that a rigorous theoretical analysis of the properties of the MMST cost function for finite dimensional systems will be part of the future work based on this section.

The analysis given in this subsection using a simple discrete time system (2.34) in conjunction with the cost function (2.37) reveals the two undesirable characteristics of the function, which are the lack of one-to-one correspondence between the output and parameter spaces, and the non-convexity. Also, we have showed hypothetically that when the identification models do not contain the exact plant parametrization, there is an ambiguity in the minimum point of the cost function, as it can be contained in the either side of the current selected minimum point. Finally, we gave an extension of these conclusions for a class of finite dimensional discrete-time dynamical systems with a diagonal structure. In what follows, we

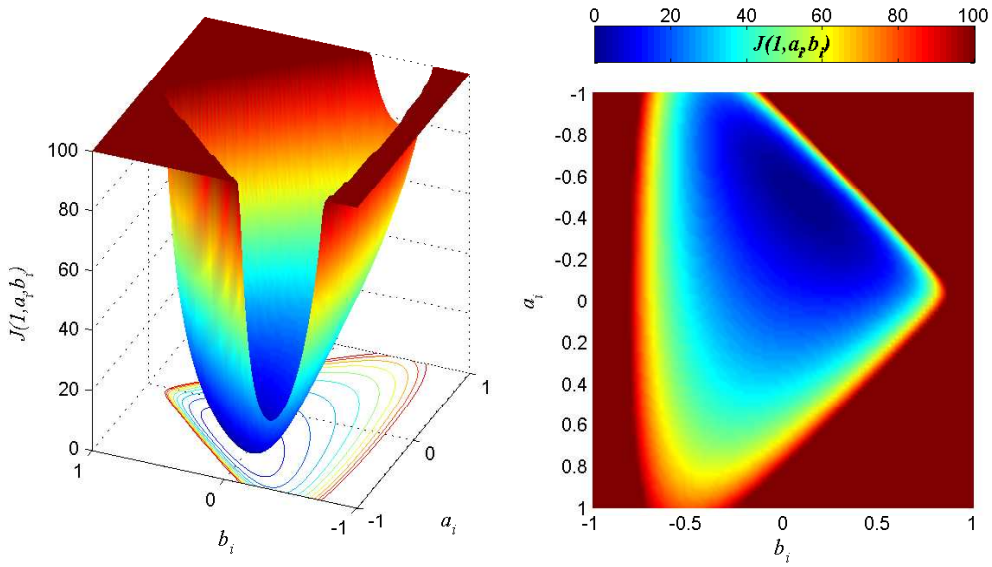

Figure 2.29: Cost function variation in parameter space for a second order estimation problem with plant parameters $a = -0.5$, $b = 0.1$.

describe a model space adaptation method that can alleviate the problems described thus far without using a dense number of models, and still utilizing (2.33) as the cost function.

2.7.2 An adaptive model distribution algorithm

In this subsection we introduce a model distribution scheme to improve the accuracy of estimation in conjunction with the multiple model estimation algorithm, with a sparse number of models and making use of the cost function (2.33). As mentioned before, it is difficult to find a general form of a cost function that would provide a one-to-one correspondence between parameter error and identification error spaces. However, the modification suggested here makes use of (2.33) and refines the distribution of the models within the interval that is likely to contain the minimum point of the function.

In order to explain how the modified algorithm works, we refer to the Figure 2.30. The multiple model estimation algorithm is initiated with a small number of grid points, and

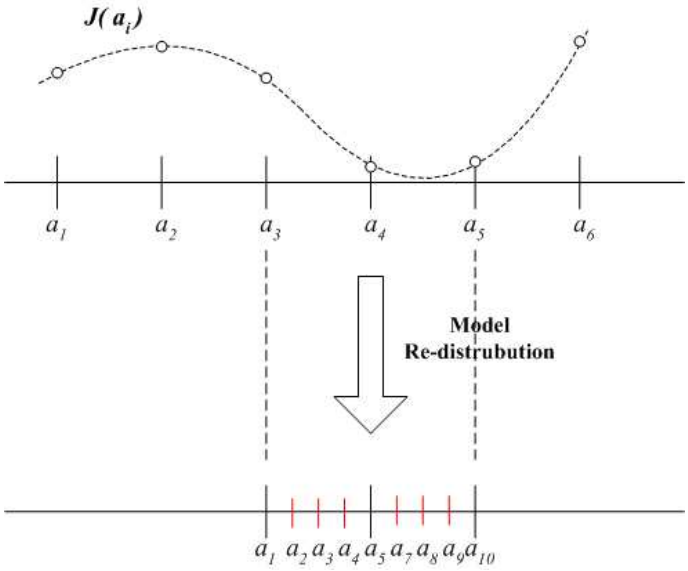

Figure 2.30: Model re-distribution algorithm.

based on (2.33) the minimum is selected, which as explained in the preceding section, is not guaranteed to give the smallest parameter estimation error. As a remedy, we suggest a re-distribution of the models in the parameter space over the immediate neighborhood of the selected minimum model after a finite time horizon. After the new parameterizations and the corresponding models are defined, we run the estimation algorithm again on the same data. Assuming that a_i is selected as the model minimizing the cost function after a finite time horizon, both a_{i-1} and a_{i+1} needs to be included in the redistributed model space due to the ambiguity in the interval containing the minimum, explained earlier. In the hypothetical example depicted in Figure 2.30, 4^{th} model minimizes the cost function although the real parameter is closer to the 5^{th} model. Therefore, it is possible to capture the minimum point in this example by redistributing the models between parameter grid points a_3 and a_5 of the original parameter space, by the suggested algorithm. It is noted here again that it is a design choice between accuracy and numerical complexity to decide how many models to have in the initial models space and how many to include in the redistribution.

Next we give numerical example of how the algorithm works. It is the same multiple model

estimation problem we described earlier, i.e., where the plant dynamics are governed with

$$x_p(k+1) = 0.5251 x_p(k). \tag{2.53}$$

Estimation models are of the same form of (2.53) with the models located at 0.05 intervals within $[-1,1]$ with a total of 41 models. Estimation results based on the standard multiple model estimation scheme is shown in Figure 2.31, where it can be observed that although the closest model is at 0.55 in the parameter space, the algorithm converged to 0.5.

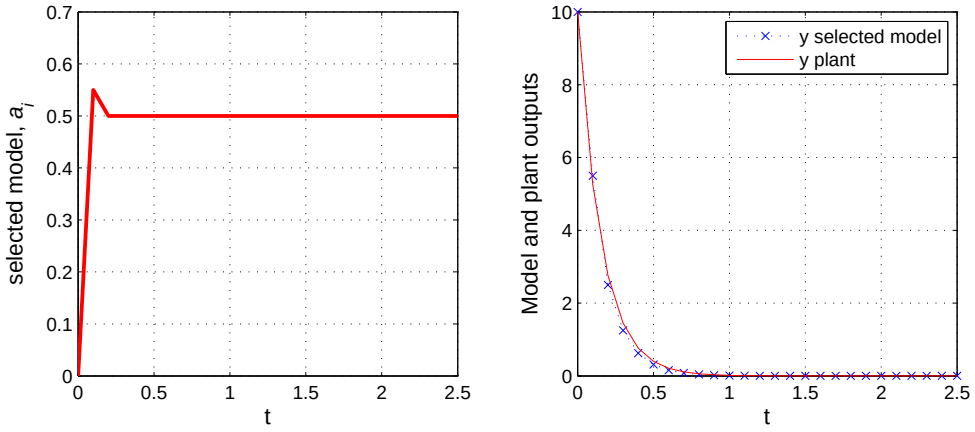

Figure 2.31: Standard multiple model estimation results with fixed model space.

When we implemented the described adaptive estimation algorithm with a single step refinement (i.e., models redistributed once), we obtained the result shown in Figure 2.32. Initial parameter space consisted of a very coarse grid with 0.25 intervals between $[-1,1]$, resulting in a total 9 identification models. In the redistribution step we used 20 models and repeated the standard multiple model estimation algorithm on the same data. In total we employed 29 models after a single iteration of the model space, and as observed from the Figure 2.32 we obtained the parameter estimation result of $a = 0.525$. In the same figure we also show the variation of the cost function $J(a_i)$ in the parameter space before and after the model redistribution step , where the effect of iteration is clearly seen. Numerical simulation results show the efficacy of the suggested adapted algorithm, which achieves better

accuracy using a smaller number of models as compared to the multiple model estimation with fixed models. Even better accuracy can be obtained with more redistributions (i.e., more iterations) and/or including more number of models in the iteration steps.

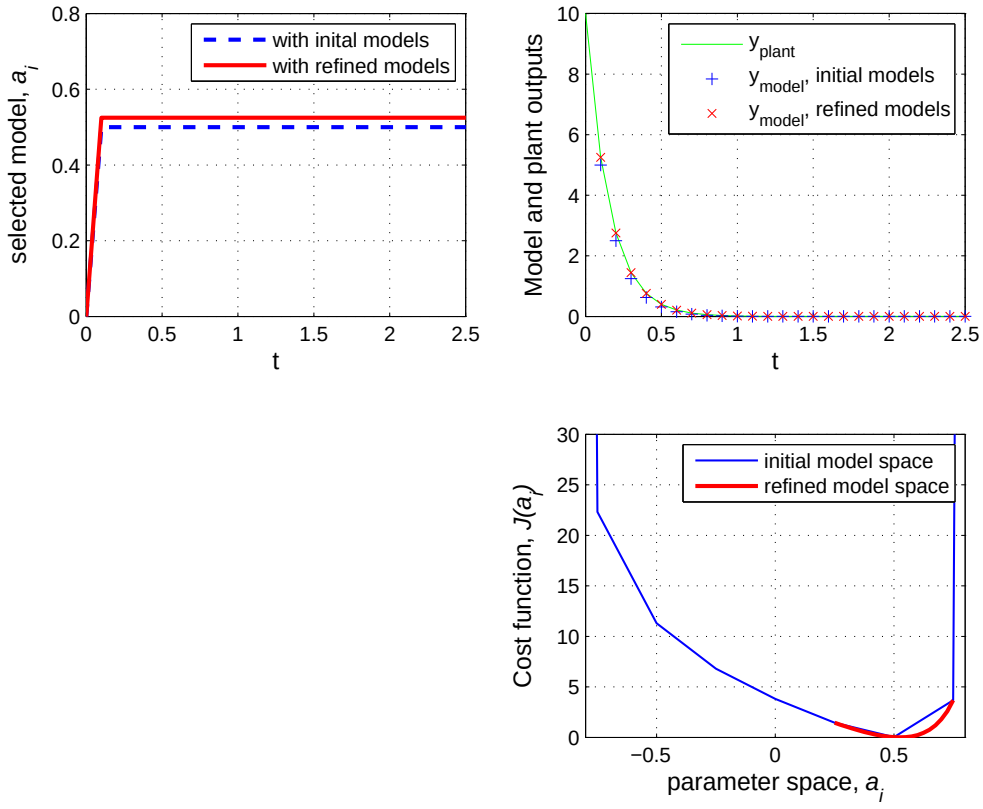

Figure 2.32: Multiple model estimation results with an adaptive model distribution.

In this subsection we introduced an adaptation scheme in order to improve the estimation accuracy of the standard multiple model estimation algorithm with fixed models, without increasing its numerical complexity. The suggested adaptive model distribution algorithm employs the same cost function as the original scheme, yet it iterates on the distribution of the models in the parameter space. Our numerical results with the adaptive algorithm show that one can obtain more accurate estimations using less number of models as compared to the standard multiple model estimation with only fixed models, achieving the goal set

forth at the start of the subsection. The only drawback of this simple adaptive estimation scheme is the fact that the iterative distribution of models can not be done in real time, and the algorithm has to run on stored data. Therefore this adaptive scheme is more suitable for applications, where the need for accuracy in estimation is more important than the real time performance. Next we look into the extension of the adaptive model distribution algorithm for the estimation of switching system parameters.

2.7.3 Adaptive multiple model estimation of switching unknown parameters

In Section 2.7.1 we made an analysis of the cost function of the multiple model switching algorithm and showed that the identification models need to distributed carefully in the parameter space as the cost function (2.33) can lead to a wrong model selection. We emphasize that this problem is related to the lack of one-to-one correspondence between the parameter space of the models and the output identification errors, which is a very important observation. Consequently the closest model in the parameter space may not always be chosen due to the non-convex or non-symmetric properties of the cost function. As a remedy we suggested an adaptive algorithm in the preceding subsection, which addresses this problem by iterating on the distribution of models, while still choosing the best model based on the minimization of the cost function (2.33). In this subsection we look at an extension of this adaptive algorithm for estimating switching and unknown parameters of dynamical systems.

In the literature, an analysis of the estimation of rapidly switching parameters in conjunction with the multiple model switching framework was made in a recent paper by Narendra et al. [80] as well as in the PhD thesis by Feiler [32]. In this recent thesis the algorithm was named as self-organization method. It was suggested in these publications that, a set of candidate models with arbitrary locations in the parameter space are adapted simultaneously based

on a time varying gain (that is a function of identification errors of each model) and with respect to the plant operating point in existence. The convergence logic they employed for parameter adaptation resembles to that of winner-takes-all methods. They assumed for the effective operation of the self-organization algorithm that the set of all operating points to be in existence (and in some cases periodic) in a finite time interval such that all candidate models converge to the set of operating points. Furthermore, the number of switches in the system parameters were assumed to be precisely known. In order to relax some of the restrictions of the self-organization method, we describe an alternative approach in the sequel for the estimation of rapidly switching system parameters, which is based on the adaptive model distribution method developed in the preceding subsection. We first start with the formal statement of the problem.

Problem Definition

Let the parameter vector $\theta(t)$ of a dynamical system to be switching randomly (not necessarily slowly) between a set of operating points denoted by $\mathbf{S} = \{\theta_1, \theta_2, ..., \theta_N\}$, where $\theta_j,\ j \in \{1, 2, ..., N\}$ are unknown. This is depicted hypothetically in Figure 2.33. Also, the instants of switching is assumed to be unknown. Furthermore, the total number of possible operating points N is assumed known, but this requirement can be relaxed. We would like to have minimum number of candidate models in conjunction with the multiple model estimation framework, to estimate the unknown operating points $\theta_j,\ j \in \{1, 2, ..., N\}$ quickly and with sufficient accuracy, where the dynamical system is subject to changes in the operating conditions.

In order to motivate the need to study this problem, we can give real-life examples where such problems arise naturally. In general, any engineering system that operates in a multitude of environments such as cars and airplanes have suitable applications in the scope of this problem. A good application example to such a problem is the adaptive cruise control in cars, where sudden gear shifts of the car can be represented as a new operating condition

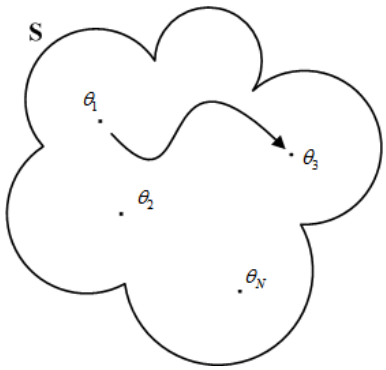

Figure 2.33: Switching operating conditions (or parameters) of the plant.

θ. The speed controller needs to incorporate the engaged gear information for high performance, i.e. for tracking the desired speed smoothly, quickly and with minimum error. Another automotive related problem is the shifting of loads in large road vehicles such as trucks or vans, which can happen as result of inertial forces acting on the vehicle during high speed cornering maneuvers. Naturally, active safety control systems should take the change in CG position into account, as this change may affect the vehicle response significantly. Next we describe our adaptive estimation method.

Adaptive Estimation Algorithm

The adaptive estimation method given here is an extension of the adaptive model distribution method given in Section 2.7.2. The algorithm uses the same model distribution scheme, however the adaptation is restarted every time a (detectable) change in the dynamics, or the operating condition occurs. Information on the change of the operating condition can be explicitly available, as in the case of the adaptive cruise control problem, where the information of gear position is known at all times. However, in general, if such information is not explicitly available it needs to be inferred. For the sake of simplicity, we assume that the instant of change in the plant parameters is known.

In order to explain how the algorithm works, we refer to figure 2.34, which depicts a hypo-

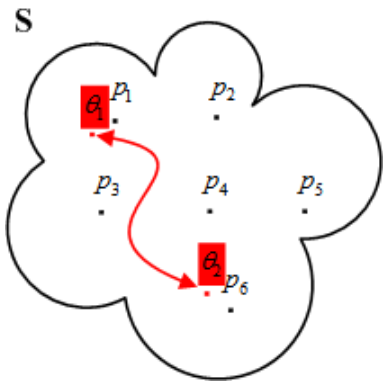

Figure 2.34: Switching parameters and candidate models.

thetical plant operating on the parameter space **S** and switches between two operating points represented with the two parameterizations θ_1 and θ_2. The parameterizations $p_1, p_2, \ldots, p_6$ correspond to the 6 different candidate models for use in conjunction with the adaptive model distribution algorithm. Suppose that the plant operates at the point denoted with θ_1 initially. In order to get an estimate of this parameter we can use the model distribution algorithm described in Section 2.7.2. As shown in Figure 2.35 the algorithm will choose the neighborhood of p_1 as the place where the parameter is most likely to be present. Accordingly new models will be placed around the close vicinity of p_1 and the model minimizing the cost function will be selected. This adaptation step can be repeated multiple times to get a very good estimate θ_1^* of the unknown parameter θ_1. So far the problem was the estimation of the unknown plant parameter θ_1. Now suppose that there happens to be a switch in the plant parameters to θ_2 as depicted on the right-hand side of Figure 2.35. When the switch is detected, the identification models are re-initialized with the parameter sets $p_1, p_2, \ldots, p_6$. Consequently the same model distribution algorithm is employed to estimate the unknown parameter θ_2, which will distribute the new models around p_6 until the desired accuracy is achieved and a suitable model θ_2^* is selected. We emphasize that the algorithm does not explicitly make use the information on the number of switches (i.e., parameterizations) and it can easily be generalized to plants with high number of switches; this can be accommo-

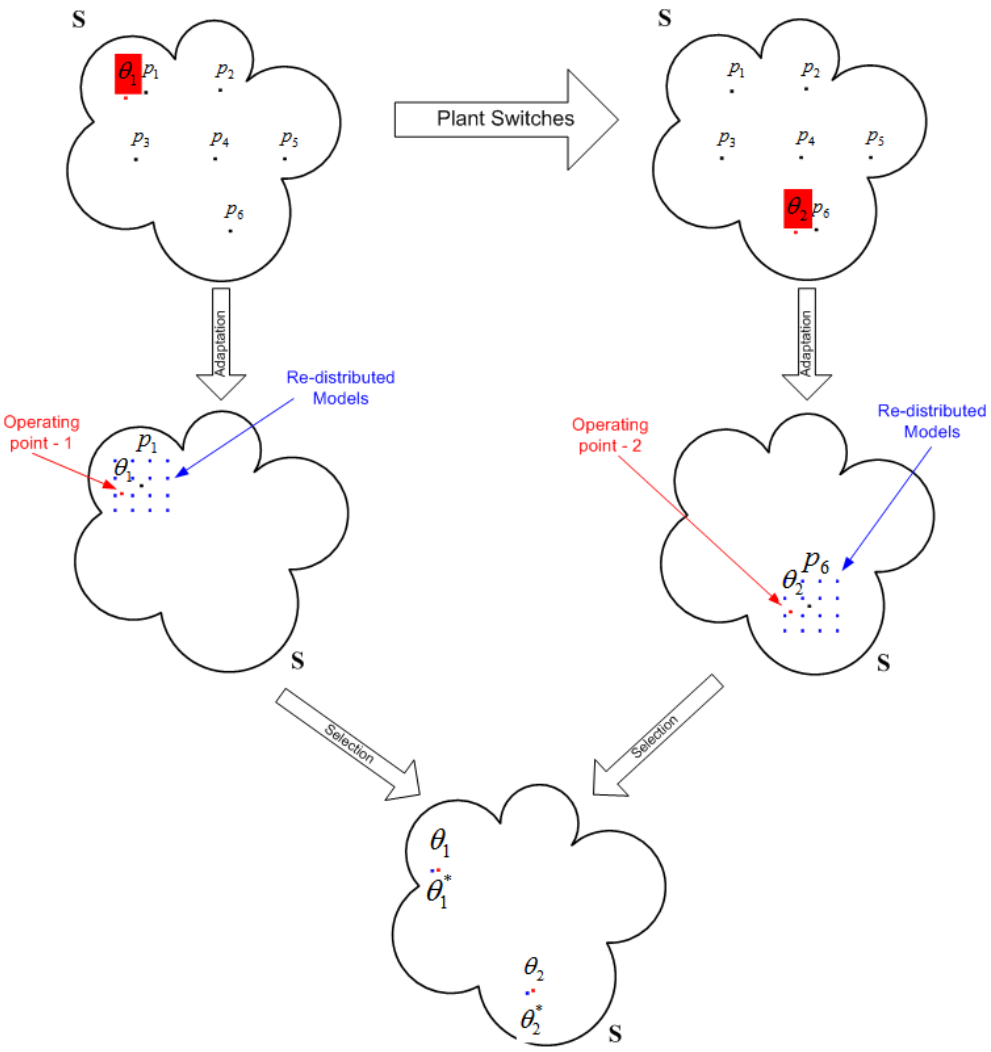

Figure 2.35: Schematic representation of the adaptive estimation method.

dated by changing the initial candidate model space. In what follows, we implement this algorithm to a simple estimation problem and give the corresponding numerical results.

Numerical Analysis

For the sake of exposition we consider the following simple discrete time system as the plant model

$$x(k+1) = \theta(k)x(k), \qquad \theta(k) \in \{\theta_1, \theta_2\} \tag{2.54}$$

where θ_1, and θ_2 represent distinct unknown scalar constants in the unit circle such that the plant dynamics corresponding to either parameter is stable. Furthermore the parameter $\theta(k)$ is assumed to switch at an unknown instant during the evolution of the dynamics of the plant (2.54). We want to estimate the parameters θ_1 and θ_2 with sufficient accuracy, and using only a small number of models. We assume that the distinct identification models are of the following form

$$\hat{x}_i(k+1) = p_i\hat{x}(k), \tag{2.55}$$

which are parameterized at N grid points in the parameter space where $i = 1, 2, ..., N$. Notice here that we assumed neither modelling errors nor process noise. Further assuming identical initial conditions x_0 for the plant and all the identification models, we can express the corresponding trajectory of the plant and the identification models as follows

$$x(k) = \theta^k(k)x_0, \tag{2.56}$$

$$\hat{x}_i(k) = p_i^k x_0, \tag{2.57}$$

where $i = 1, 2, ..., N$ are the model indices. Also, the discrete time version of the cost function (2.33) that is to be used for this problem and is given as

$$J_i(k) = \alpha e_i^2(k) + \beta \sum_{\tau=0}^{k} e_i^2(\tau)\triangle t, \tag{2.58}$$

where $\triangle t$ is the discrete time step (which can be fixed or variable).

For the numerical simulations we used the following plant parameters and the switching instant

$$\theta \in [0.9251, 0.2615], \quad t_{switch} = 2.2 \ \ sec..$$

Also, the initial candidate models were chosen to be symmetrically distributed between $[-1,1]$ with 0.1 intervals. i.e.,

$$p_i = -1 + 0.1 * (i-1), \qquad i = 1,2,...,21 \tag{2.59}$$

with a total of 21 models. Further, the initial conditions for the plant (2.54), and all of the models (2.55) were chosen to be $x_0 = 10$. The parameter switching sequence and corresponding plant trajectory for $t \in [0,5]$ is shown in figure 2.36.

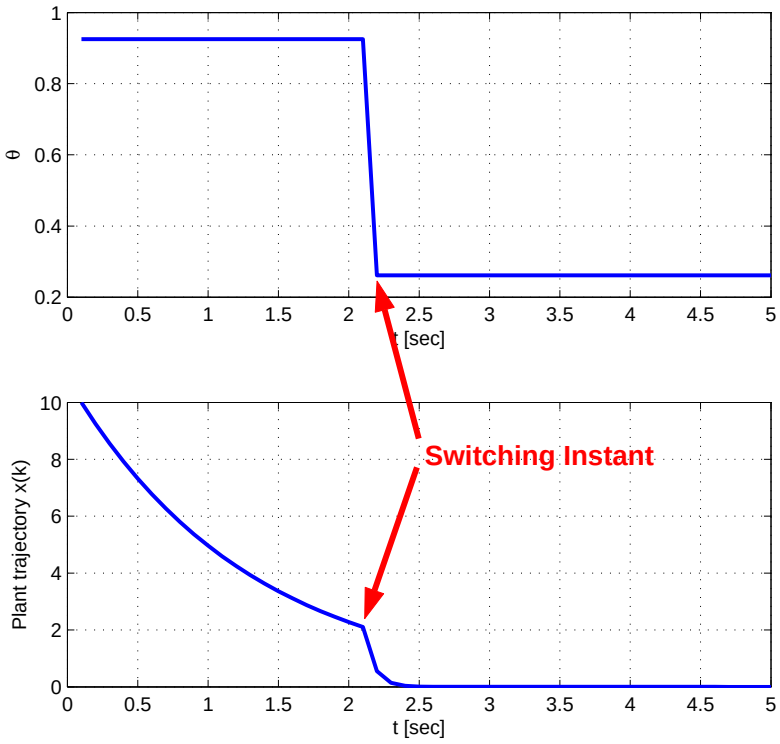

Figure 2.36: Plant trajectory for the example.

For the redistribution of the models we chose to insert 40 equidistant models in a single iteration step around the neighborhood of the selected initial candidate model for each detected operating point. Notice that processing the same data and applying further adaptation steps, a better accuracy can be achieved. Also note that in the statement of the problem we

assumed no explicit knowledge of the the switching instant, which necessitates a separate estimation of the switching in the dynamics. For this simple problem, an ad hoc solution to detect the switching position was achieved by looking at the left-hand and right-hand derivatives of the trajectory at each instant; the point where there is a drastic gradient was classified as a switching point. In other words, the check for the switching of the piecewise continuous trajectory $x(t)$ was made using the following binary criterion

$$switch = \begin{cases} \text{Yes} , & \text{if } |\dot{x}_+(k) - \dot{x}_-(k)| > \kappa_T, \\ \text{No} , & \text{if } |\dot{x}_+(k) - \dot{x}_-(k)| \leq \kappa_T \end{cases}, \tag{2.60}$$

where $\dot{x}_+(k)$ and $\dot{x}_-(k)$ are the left hand and right hand derivatives at k^{th} instant. Also, κ_T is a positive scalar, which defines the maximum difference allowed between the left and right hand derivatives of the plant trajectory $x(k)$. Note that since this is a discrete time plant κ_T is nonzero, whereas for a continuous time version of this problem the switching criterion would be the same as (2.60) but with $\kappa_T = 0$ imposing identical left and right hand derivatives for no switching. For our simulations we set the $\kappa_T = 5$ as the threshold slope difference. Next we present our estimation results for this problem.

The suggested algorithm used 21 initial candidate models, both before and after the switching instant. Once the algorithm is started, 40 models were used at each of the two adaptation steps. Therefore, a total 122 models were employed for the overall algorithm, and its accuracy is equivalent to 401 fixed models distributed evenly between $[-1,1]$. The algorithm successfully estimated θ to be switching between the following two parameters

$$\theta^* \quad \in \quad [0.925, 0.26].$$

Estimated plant parameters are shown in Figure 2.37 before (left hand side) and after (right hand side) the switching, where the dashed lines correspond to the rough estimates by the initial candidate models, while the solid lines were obtained by adaptation based on the model distribution technique.

In Figure 2.38 the plant and the selected model trajectories obtained during the estimation

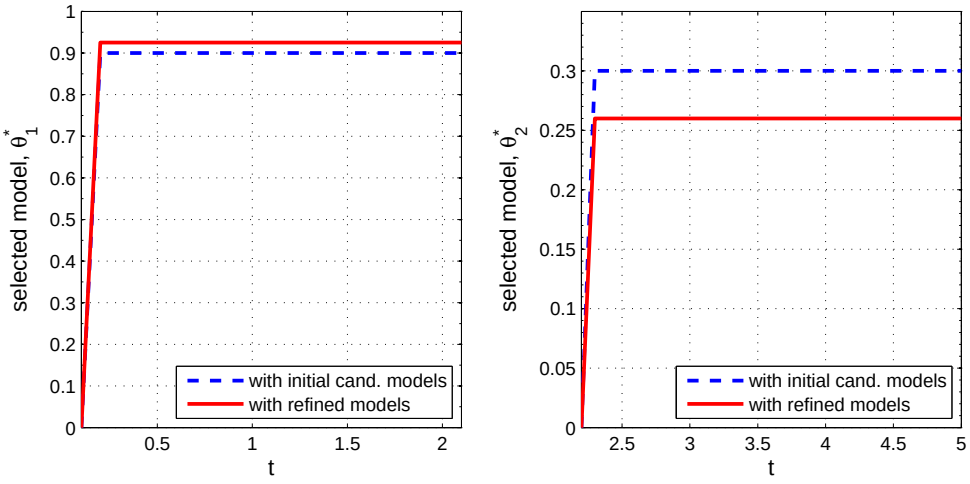

Figure 2.37: Estimated plant parameters.

are presented, both before (left hand side) and after (right hand side) the switching. The

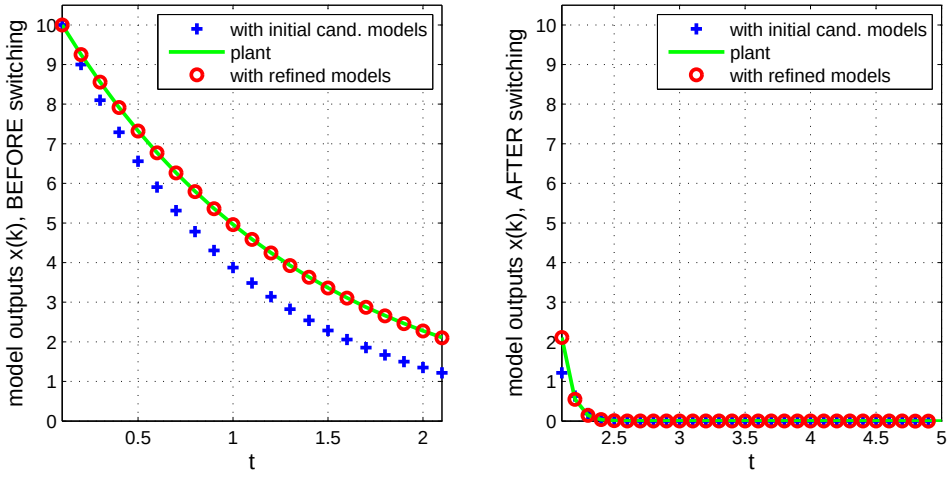

Figure 2.38: Comparison of the plant trajectory with respect to the selected candidate models.

corresponding variation of the cost functions in the parameter space, before and after the switch is shown in Figure 2.39, where the dashed line corresponds to the initial candidate models and the solid line represents variation after the distribution of models around the selected minimum candidate model. Insets are provided to show the effectiveness and detail

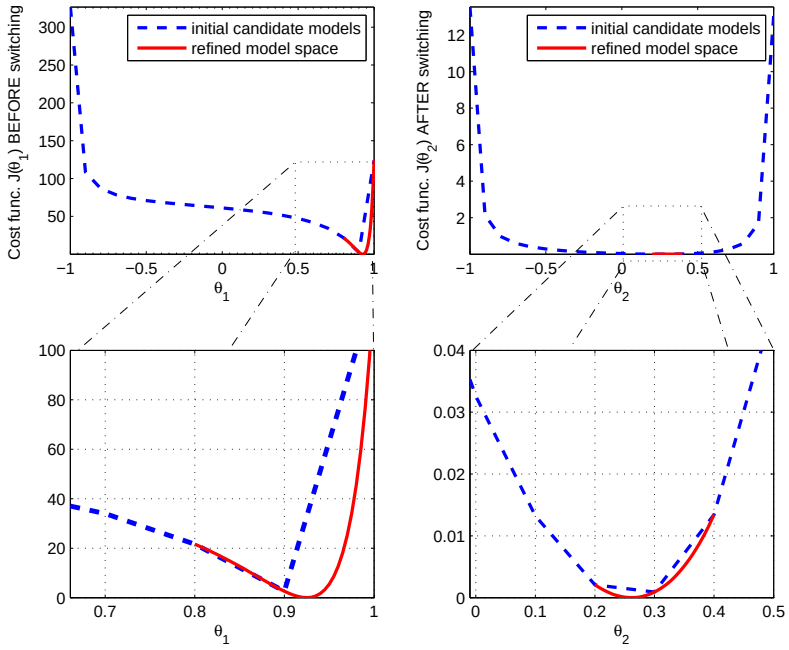

Figure 2.39: Variation of the cost function in the parameter space before and after the switching.

obtained as a result of the adaptation algorithm for this specific problem.

2.7.4 Adaptive multiple model estimation of CG position

In this subsection we present the implementation of the adaptive multiple model estimation method described in Section 2.7.2 to the problem of CG height estimation. In doing so, the main goal of this exercise is to reduce the model space used for the estimation with the multiple model framework, and obtain comparable estimation accuracy to that of Section 2.4.2, where we used a dense number of grid points to get a good estimation of the CG height. Note here that we are concerned with the estimation of the unknown parameters related to the roll dynamics of a vehicle, which are assumed to stay constant in a short time horizon (as opposed to the preceding subsection where the parameters could switch instantaneously).

The multiple model switching algorithm described here is the same as in Section 2.4.2 for the most part, except for a single adaptation step of the model space. The algorithm estimates the CG height h along with the linear suspension parameters k, and c based on the roll-plane model (2.10). We assume that each unknown parameter belongs to a closed interval such that $h \in \mathscr{H}$, $k \in \mathscr{K}$, and $c \in \mathscr{C}$, which are divided into a small number of initial candidate grid points such that $\{h_1, h_2, h_3, \ldots, h_p\} \subset \mathscr{H}$, $\{k_1, k_2, k_3, \ldots, k_q\} \subset \mathscr{K}$, and $\{c_1, c_2, c_3, \ldots, c_r\} \subset \mathscr{C}$ with dimensions p, q and r respectively. We then form $n = p \times q \times r$ different models corresponding to the cross combinations of the grid points in the parameter space. The equations of motion corresponding to each of the n models (with zero initial conditions) can be represented with (2.23). Also as shown in Figure 2.15, every model is driven by the same input a_y, which is measured. According to (2.24) identification errors e_i are calculated for each model and then corresponding cost functions (2.20) are computed. Switching among the models based on (2.21) yields the one with the minimum cumulative identification error, and the selected k_{i^*}, c_{j^*} and h_{l^*} represent the plant in the parameter space described by a finite number of grid points in $\mathscr{K}$, $\mathscr{C}$ and $\mathscr{H}$ respectively. Note here that the indices i^*, j^*, l^* satisfy $i^* \in \{1, 2, ..., p\}$, $j^* \in \{1, 2, ..., q\}$ and $l^* \in \{1, 2, ..., r\}$.

Adaptation is achieved by re-distributing models in the immediate neighborhood of the selected initial grid points k_{i^*}, c_{j^*} and h_{l^*} as a result of the initial iteration. That is, for the adaptation step, the grid points are chosen such that $\{h_{l^*-1}, ..., h_{l^*}, ..., h_{l^*+1}\} \subset \mathscr{H}^*$, $\{k_{i^*-1}, ..., k_{i^*}, ..., k_{i^*+1}\} \subset \mathscr{K}^*$, and $\{c_{j^*-1}, ..., c_{j^*}, ..., c_{j^*+1}\} \subset \mathscr{C}^*$ with dimensions p^*, q^* and r^* respectively. Then the same multiple model estimation procedure described above is repeated for $n^* = p^* \times q^* \times r^*$ number of models, and switching among these based on (2.21) yields a new estimate that minimizes the cost function (2.20). The corresponding parameters of the selected model, that is $k^\star, c^\star$ and $h^\star$ represent the plant in the parameter space described by $\mathscr{K}^*$, $\mathscr{C}^*$ and $\mathscr{H}^*$ respectively. Note that, the total number of models utilized after a single adaptation step is $n + n^*$. Next we present the results of a numerical implementation of this adaptive estimation method.

Numerical Analysis

Here we present the CG height estimation results for the simulated measurement data described in Subsection 2.4.1. The initial candidate model space consisted of 24 models, where grid points belong to the sets $\{32000, 36500, 38000\} \subset \mathscr{K}$, $\{4500, 5500\} \subset \mathscr{C}$, and $\{0.56, 0.64,\ 0.72, 0.8\} \subset \mathscr{H}$. Note that the exact plant parameters $h_{plant} = 0.7$, $c_{plant} = 5000$, and $k_{plant} = 36000$ are not part of the initial grid points. For this numerical example the free design parameters for the cost function were set as $\alpha = 0.1$ and $\beta = 0.9$, while the forgetting factor λ was chosen to be 0. For the adaptation step we chose to insert $6, 4$, and 3 models in the immediate neighborhood the selected minimum of the initial parameter space, which yielded adapted model grid points given below

$$\{\ 0.8,\ 0.768,\ 0.736,\ 0.704\ 0.672,\ ,0.64\} \subset \mathscr{H}^*$$

$$\{\ 32000,\ 34000,\ 36000,\ 38000\} \subset \mathscr{K}^*$$

$$\{\ 4500,\ 5000,\ 5500\} \subset \mathscr{C}^*$$

As a result of the single adaptation step, 72 new models have been utilized, which eventually caused the total number of models utilized to be 96 during the course of the estimation.

In Figure 2.40 the resulting sensor and the switched model outputs of the plant, initial models, and the adapted models are compared whereas in Figure 2.41 the CG height estimation results are shown for the initial grid and the adapted models. Based on the estimation results, we observe that the multiple model switching algorithm successfully estimated the CG height to be 0.704 *m*. Also in Figure 2.42 the corresponding estimations of the suspension parameters are presented. Linear torsional spring stiffness *k* was estimated as 36000 exactly matching that of reference vehicle model, while roll damping coefficient *c* was estimated to be 5500 slightly different then that of the reference vehicle model which was 5000.

We observe from the numerical results that the adaptive estimation achieved similar estimations to that of Section 2.4.2 while utilizing only 96 models (as opposed to 240 models used there). Thus this adaptation scheme can be employed when large number of models can not

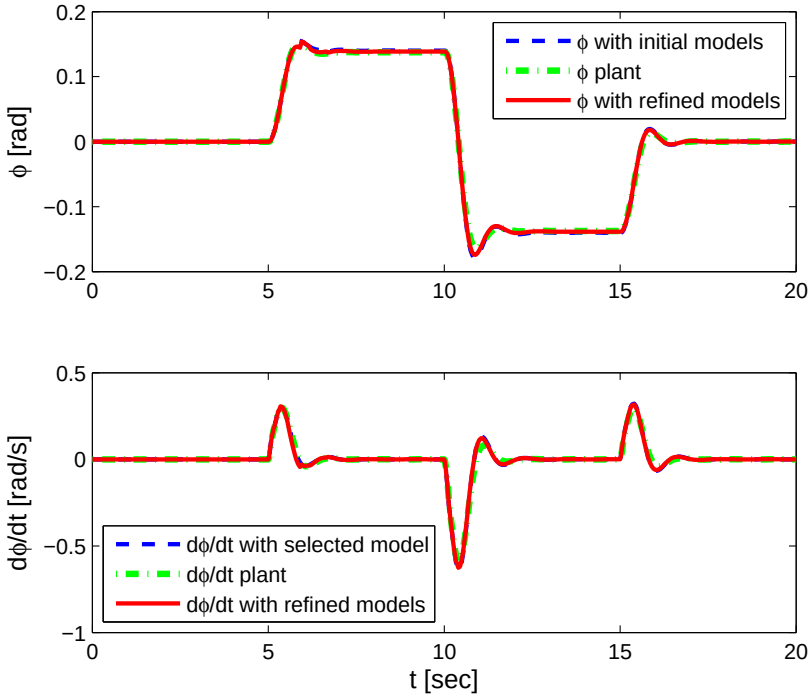

Figure 2.40: Sensor and the selected model output comparison for the adaptive CG height estimation.

be utilized due to computational constraints.

2.8 Conclusions and possible future directions

In this chapter we have presented a realtime parameter estimation algorithm using a multiple model switching approach incorporating simple linear models. Based on the simulation results, we demonstrated the accuracy of the suggested technique as compared to the traditional least squares identification approach, which shows significant benefits. We also presented preliminary tests of the algorithm with off-line measurement data taken from an undisclosed test vehicle, and results were promising. The results showed that the algorithm can also work in cases where the signals are corrupted by noise and bias. Moreover, the load

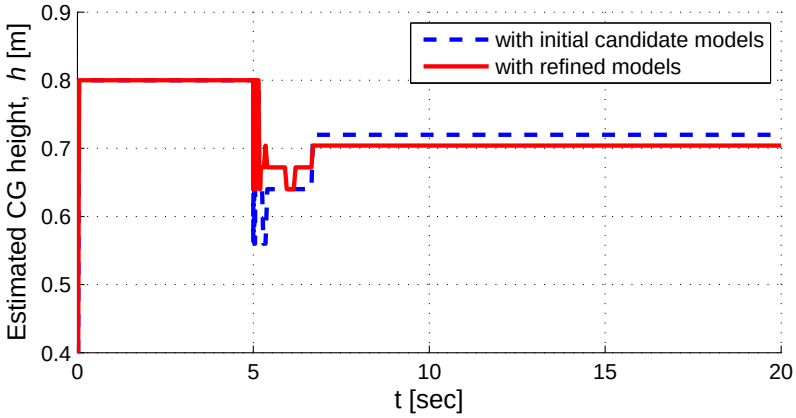

Figure 2.41: Adaptive CG height estimation.

condition estimator example demonstrated that a simple version of the suggested algorithm can easily be integrated into current rollover or lateral dynamics controllers to enhance their performance. In the last part of the chapter we conducted an analysis of the cost function, and also introduced a simple adaptation scheme to improve estimations based on multiple model estimation method. With simple numerical examples we showed that the suggested adaptation method can provide good estimation results while utilizing a smaller number of identification models as compared to estimations with fixed models alone. One important observation in our analysis was that the multiple model algorithm employing only fixed models required too many models to produce the desired estimation accuracy and performance (as apparent from numerical simulations, where we had 240 models for CG height estimation based on roll dynamics). Our adaptation scheme can be used to circumvent this problem, which employs only a small number of models initially and are updated and re-parameterized in fixed time intervals. In our numerical simulations we managed to get a good CG height estimation using only 96 models in conjunction with the adaptive estimation method, which shows efficacy of the suggested algorithm.

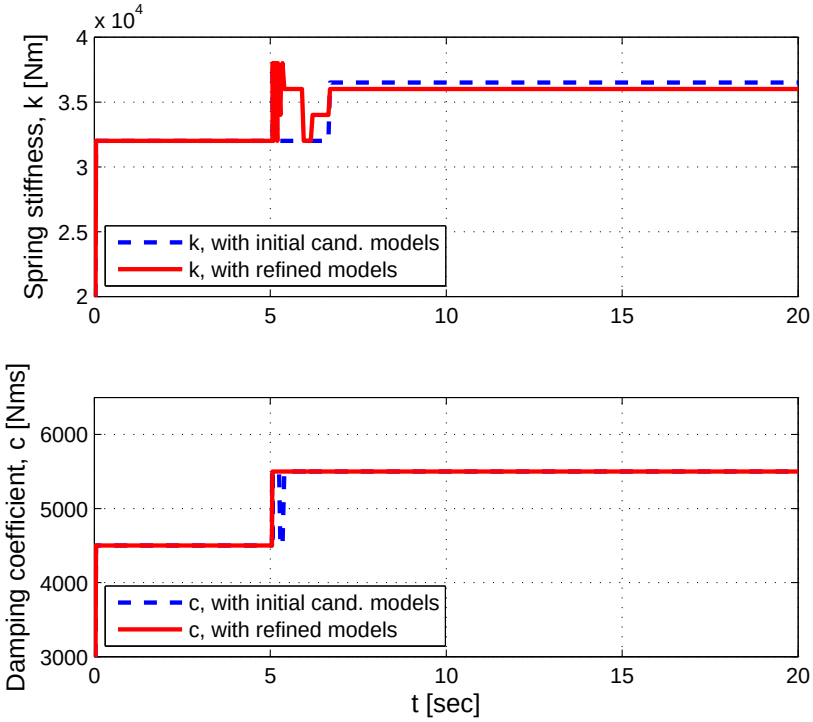

Figure 2.42: Adaptive estimation of the suspension parameters k, and c.

Chapter 3

A Methodology for the Design of Robust Rollover Prevention Controllers for Automotive Vehicles

In this chapter we present a robust controller design methodology for vehicle rollover prevention utilizing active steering and differential braking actuators. Control design is based on keeping the magnitude of the vehicle performance outputs, including load transfer ratio (LTR), below a certain level in the presence of driver steering inputs; we also develop an exact expression for calculating LTR. The proposed controllers have a proportional-integral structure whose gain matrices are obtained by solving a set of LMIs, which provide controllers to robustly guarantee that the peak magnitudes of the performance outputs do not exceed certain values. We show that using the design method the controllers can be designed to be robust with respect to unknown vehicle parameters such as speed and center of gravity height. We also provide a switching rule for controller activation based on the potential for rollover.

3.1 Chapter contributions

The scientific contribution of this chapter over the literature is mainly in the area of vehicle dynamics control; particularly in the area of automotive rollover prevention. Our control design was formulated as a bounded input bounded output (BIBO) disturbance rejection problem. We viewed the automotive vehicle as an uncertain dynamical system with disturbance inputs, and our controllers guarantee that the performance outputs of the system relevant to rollover are bounded. In doing so, we suggested using a dynamic version of the load transfer ratio (LTR) as a criterion for rollover occurrence. Our suggested robust control design method is unique in the sense that it gives way to a quantification of robustness of the controllers. We also considered vehicle parameter uncertainty in our control designs given that the uncertainty satisfies certain conditions.

The work contained in this chapter has resulted in the following publications:

(i) Solmaz S., Corless M., Shorten R., "*A methodology for the design of robust rollover prevention controllers for automotive vehicles: Part 1-Differential Braking*", 45th IEEE Conference on Decision and Control, San Diego, Dec 13-15, 2006.

(ii) Solmaz S., Corless M., Shorten R., "*A methodology for the design of robust rollover prevention controllers for automotive vehicles: Part 2-Active steering*", HYCON-CEMaCS Joint Workshop on Automotive Systems & Control, Lund, June 1-2, 2006.

(iii) Solmaz S., Corless M., Shorten R., "*A methodology for the design of robust rollover prevention controllers for automotive vehicles: Part 2-Active steering*", American Control Conference, New York, July 11-13, 2007.

(iv) Solmaz S., Corless M., Shorten R., "*A methodology for the design of robust rollover prevention controllers for automotive vehicles with active steering*", International Journal of Control, Special Issue on Automotive Systems and Control, Vol. 80, No. 11, pages 1763-1779, November 2007.

3.2 Introduction

It should be clear from the preceding chapter that the vehicle center of gravity position directly affects vehicle accident behavior. Particularly, it is well known that vehicles with a high center of gravity such as vans, trucks and the highly popular SUVs (Sport Utility Vehicles) are more prone to rollover accidents, which are, by far, the most dangerous type of accidents. As evident from to the 2004 accident data [1] compiled in the USA, light trucks (pickups, vans and SUVs) were involved in nearly 70% of all the rollover accidents, with SUVs alone responsible for almost 35% of this total. The fact that the composition of the current automotive fleet in the U.S. consists of nearly 36% pickups, vans and SUVs [22], along with the recent increase in the popularity of SUVs worldwide, makes rollover an important vehicle safety problem.

There are two distinct types of vehicle rollover: tripped and un-tripped. Tripped rollover is usually caused by impact of the vehicle with something else (e.g. obstacles, curb etc.) resulting in the rollover incident. For example, a tripped rollover commonly occurs when a vehicle slides sideways and digs its tires into soft soil or strikes an object such as a curb or guardrail. Driver induced un-tripped rollover can occur during typical driving situations and poses a real threat for top-heavy vehicles. Examples are excessive speed during cornering, obstacle avoidance and severe lane change maneuvers, where rollover occurs as a direct result of the wheel forces induced during these maneuvers. In recent years, rollover has been the subject of intensive research, especially by the major automobile manufacturers; see, for example, [28, 27]. That research is geared towards the development of rollover prediction schemes and occupant protection devices. It is however, possible to prevent such a rollover incident by monitoring the car dynamics and applying appropriate control effort ahead of time. Therefore there is a need to develop driver assistance technologies which would be transparent to the driver during normal driving conditions, but which act when needed to recover handling of the vehicle during extreme maneuvers [22].

In this chapter we present a robust rollover prevention controller design methodology, which represents the first of the two available approaches (i.e., robust and adaptive) towards the feedback design for systems with parameter uncertainties. Although most of the controller designs for automotive applications are in this category, our robust design method is unique in the sense that, unlike the traditional approaches, it quantifies the robustness of the attenuation from the actuator inputs to the performance outputs, which can be used as structured way of tuning the controllers. The robust controller design described in the sequel is based on two separate type of actuators: active steering and differential braking. Also, as an accurate indicator of performance related to rollover, we consider the vehicle Load Transfer Ratio (LTR) in the feedback design. This measure of performance is related to tire lift-off and it can be considered as an early indicator of impending vehicle rollover. Vehicle wheel lift off occurs when the magnitude of this variable reaches one. We develop an exact expression for this variable taking the vehicle roll dynamics fully into account. To distinguish our expression from previous (static) approximations of LTR in the literature, we denote it by LTR_d. We emphasize that although vehicle rollover is a dynamical process, the static approximations of LTR ignore the roll dynamics; thus, they are not fully capable of determining the onset of rollover.

Our proposed controllers based on differential braking have a P (proportional) structure with a fixed gain matrix K_P, while active steering based controllers have a PI (proportional-integral) structure with two fixed gain matrices K_P and K_I. By utilizing the integral action in the latter, we ensure that the steady state steering response of the vehicle is as expected by the driver. The gain matrices are chosen to reduce the magnitude of LTR_d during transient behavior.

The design of the controller gain matrices is based on recent results in [92] where they consider uncertain systems with performance outputs and subject to a bounded disturbance input. For each performance output z_j they introduce a performance measure γ_j which guarantees that the magnitude of the output is less than or equal to γ_j times the peak value of

the magnitude of the disturbance. They present a controller design procedure which can be used to minimize the performance level for one main output while keeping the performance levels for the other outputs below some prespecified levels. In addition, the controllers in [92] are robust in the sense that they ensure performance in the presence of any allowable uncertainty which was taken into account in the control design. In applying these results to rollover problem, we consider the driver steering input as a disturbance input. Since we wish to keep the magnitude of LTR_d less than one, we view this as the main performance output. To limit the amount of control effort and to accommodate actuator constraints, we choose the control input as an additional performance output in the feedback design. We note that many robust control designs in the literature are based on keeping the root mean square (or Euclidian norm[1]) of a performance output (i.e., $\|z_j(t)\|_2$) small. However, for this problem we consider it to be more important to utilize a controller which is designed to keep the peak magnitude (infinity norm or maximum norm[2]) of outputs (i.e., $\|z_j(t)\|_\infty$) to be small rather than their rms value; this choice is motivated by the fact that $\|LTR_d\| \geq 1$ implies rollover, where LTR_d is the main performance output for this problem.

We initially consider control design for fixed vehicle parameters and illustrate the efficacy of our approach with some numerical simulations using typical data for a compact car. We then design a fixed robust controller which is effective for a range of vehicle speeds and vehicle CG (center of gravity) heights. The efficacy of this controller is illustrated by simulating the vehicle with different CG heights and with varying speeds. Finally, we propose a modification to our controllers so that they only activate when the potential for rollover is significant. This modification prevents the controllers from activating in non-critical situations and possibly annoying the driver.

[1] for a vector $y \in \mathbb{R}^n$ with $y = (y_1, \ldots, y_n)^T$, the Euclidian norm is given by $\|y\|_2 = \sqrt{y_1^2 + \ldots + y_n^2}$.
[2] for a vector $y \in \mathbb{R}^n$, the infinity (or maximum) norm is given by $\|y\|_\infty = max\{|y_1|, \ldots, |y_n|\}$.

3.3 Related work

Rollover prevention is a topical area of research in the automotive industry and several studies have recently been published. Relevant publications include that of Palkovics et al. [107], where they proposed the ROP (Roll-Over Prevention) system for use in commercial trucks making use of lateral acceleration measurement as well as the wheel slip difference on the two sides of the axles to predict tire lift-off prior to rollover. They utilized full braking action through EBS (Electronic Brake System) in the event that tire lift-off is detected, which in turn reduces vehicle speed to eliminate the rollover threat. In a similar implementation, Wielenga [137] suggested the ARB (Anti Roll Braking) system utilizing braking of the individual front wheel outside the turn or the full front axle instead of the full braking action. The suggested control system is based on lateral acceleration thresholds and/or tire lift-off sensors in the form of simple contact switches. Again making use of differential braking actuators, Chen et al. in [25] suggested utilization of an estimated TTR (Time To Rollover) metric as an early indicator for the rollover threat. When TTR is less than a certain preset threshold value for the particular vehicle under interest, they utilized differential breaking to prevent rollover. Ackermann et al. and Odenthal et al. [4], and [88] proposed a robust active steering controller, as well as a combination of active steering and emergency braking controllers. They utilized an active steering controller based on roll rate measurement. They also suggested the use of a static Load Transfer Ratio (LTR_s) which is based on lateral acceleration measurement; this was utilized as a criterion to activate the emergency steering and braking controllers. In [22] Carlson et al. made use of sideslip, yaw rate, roll angle and roll rate measurements based on GPS aided INS (Inertial Navigation System) along with steer by wire and differential braking actuators to limit excessive roll angle during dangerous maneuvers. They based their controller design on MPC (Model Predictive Control).

3.4 Vehicle modelling and LTR_d

In this section we introduce the models that we use for controller design. We also define the rollover detection criterion LTR_d and present the assumptions on the sensors and actuators used in the design.

3.4.1 Vehicle model

In order to capture the salient features of vehicle rollover and for controller design purposes, we utilize the well known linearized vehicle model commonly referred as the single-track model (or bicycle model) with roll degree of freedom, which was introduced in the preceding chapter; this is illustrated in Figure 3.1 for convenience. This specific model or its variations are widely used in vehicle dynamics control applications (see for example [22], [128], [4], [88], [25], [38], [50]). In this linear model the steering angle δ, the roll angle ϕ, and the vehicle sideslip angle β are all assumed to be small. We further assume that all the vehicle mass is sprung, which implies insignificant wheel and suspension weights. Also the

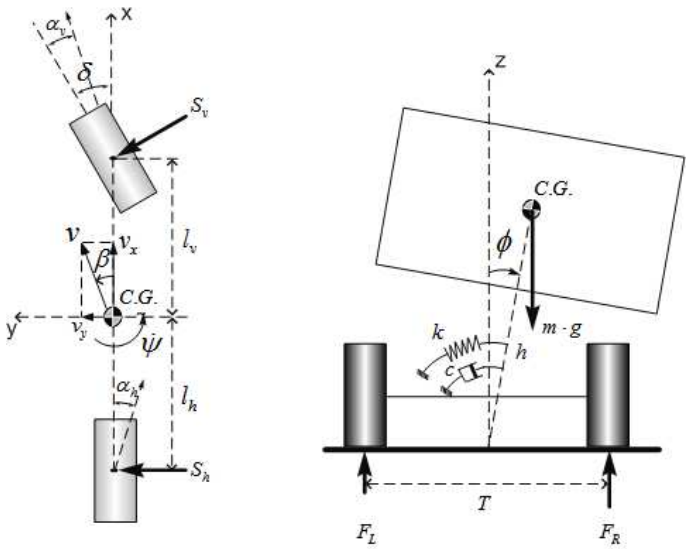

Figure 3.1: Single track model with roll degree of freedom.

lateral forces on the front and rear tires, denoted by S_v and S_h, respectively, are represented as linear functions of the tire slip angles α_v and α_h, that is, $S_v = C_v\alpha_v$ and $S_h = C_h\alpha_h$, where C_v and C_h are the front and rear tire stiffness parameters respectively. The assumptions of small angles and linear tire forces provide a good balance between capturing the salient features of vehicle behavior while keeping the complexity at a manageable level. We further define the following auxiliary variables

$$\begin{aligned} \sigma &\triangleq C_v + C_h\,, \\ \rho &\triangleq C_h l_h - C_v l_v\,, \\ \kappa &\triangleq C_v l_v^2 + C_h l_h^2\,, \end{aligned} \tag{3.1}$$

where the lengths l_v and l_h are defined in Figure 3.1. It is assumed that the sprung mass rolls about a horizontal roll axis which is along the centerline of the track and at ground level. Using the parallel axis theorem , the moment of inertia of the vehicle about the assumed roll axis, denoted $J_{x_{eq}}$, is given by

$$J_{x_{eq}} = J_{xx} + mh^2, \tag{3.2}$$

where h is the distance between the center of gravity (CG) and the assumed roll axis and J_{xx} is the moment of inertia of the vehicle about the roll axis through the CG.

Single track model with active steering input

For use with the control design based on the active steering actuator we introduce the state vector $\xi = \begin{bmatrix} v_y & \dot{\psi} & \dot{\phi} & \phi \end{bmatrix}^T$, where

- v_y : lateral velocity of the vehicle,
- $\dot{\psi}$: yaw rate of the undercarriage,
- $\dot{\phi}$: roll rate of the sprung mass about the roll axis,
- ϕ : roll angle of the sprung mass about the roll axis.

Then the linearized equations of motion corresponding to this model are as follows

$$\dot{\xi} = \tilde{A}\xi + \tilde{B}\delta + \tilde{B}u \quad \text{with} \tag{3.3}$$

$$\tilde{A} = \begin{bmatrix} -\frac{\sigma J_{xeq}}{mvJ_{xx}} & \frac{\rho J_{xeq}}{mvJ_{xx}} - v & -\frac{hc}{J_{xx}} & \frac{h(mgh-k)}{J_{xx}} \\ \frac{\rho}{J_{zz}v} & -\frac{\kappa}{J_{zz}v} & 0 & 0 \\ -\frac{h\sigma}{vJ_{xx}} & \frac{h\rho}{vJ_{xx}} & -\frac{c}{J_{xx}} & \frac{mgh-k}{J_{xx}} \\ 0 & 0 & 1 & 0 \end{bmatrix}, \quad \tilde{B} = \begin{bmatrix} \frac{C_v J_{xeq}}{mJ_{xx}} \\ \frac{C_v l_v}{J_{zz}} \\ \frac{hC_v}{J_{xx}} \\ 0 \end{bmatrix}, \tag{3.4}$$

where δ is the driver steering command, which we will view as the disturbance input for the control design, and u is the steering command from the actuator; these are illustrated in Figure 3.2 below. Further definitions of the parameters appearing in (3.4) are given in Table 3.1.

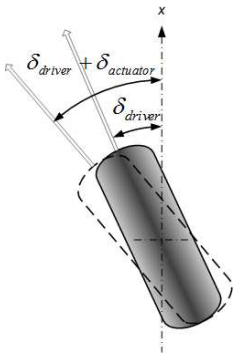

Figure 3.2: Active steering as control input.

Single track model with differential braking input

For use with the control design based on the active differential braking actuator we introduce the state $x = \begin{bmatrix} \beta & \dot{\psi} & \dot{\phi} & \phi \end{bmatrix}^T$, where β is the sideslip angle of the vehicle. Then the

linearized equations of motion corresponding to this model are as follows

$$\dot{x} = Ax + B_\delta \delta + B_u u \quad with \tag{3.5}$$

$$A = \begin{bmatrix} -\frac{\sigma J_{x_{eq}}}{m J_{xx} v} & \frac{\rho J_{x_{eq}}}{m J_{xx} v^2} - 1 & -\frac{hc}{J_{xx} v} & \frac{h(mgh-k)}{J_{xx} v} \\ \frac{\rho}{J_{zz}} & -\frac{\kappa}{J_{zz} v} & 0 & 0 \\ -\frac{h\sigma}{J_{xx}} & \frac{h\rho}{J_{xx} v} & -\frac{c}{J_{xx}} & \frac{mgh-k}{J_{xx}} \\ 0 & 0 & 1 & 0 \end{bmatrix}, \tag{3.6}$$

$$B_\delta = \begin{bmatrix} \frac{C_v J_{x_{eq}}}{m J_{xx} v} & \frac{C_v l_v}{J_{zz}} & \frac{hC_v}{J_{xx}} & 0 \end{bmatrix}^T, \quad B_u = \begin{bmatrix} 0 & -\frac{T}{2J_{zz}} & 0 & 0 \end{bmatrix}^T, \tag{3.7}$$

where u represents the differential braking force on the wheels; it is positive if braking is on the right wheels and negative if braking is on the left wheels. Differential braking force as the control input is depicted in Figure 3.3 below. Note that we can brake either front, rear or both of the wheels on each side of the vehicle depending on the maneuver and u is the total effective braking force acting on either side as illustrated in the Figure 3.3. Further

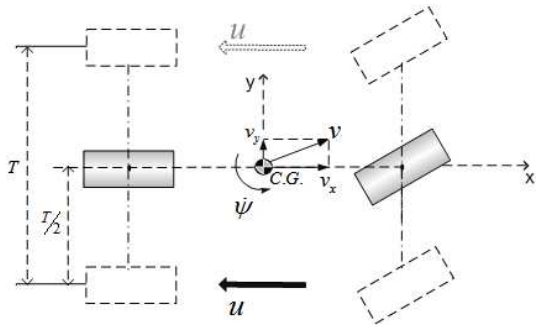

Figure 3.3: Differential braking force as control input.

definitions for all the parameters in (3.6) and (3.7) are given in Table 3.1. Also see [50] for a detailed derivation of these vehicle models.

In order to model the change in the vehicle speed v as a simple function of the braking force, we assume in this version of the model that the longitudinal wheel forces generated by the engine counteract the rolling resistance and the aerodynamic drag at all times. Under this

Table 3.1: Model Parameters and their definitions

Parameter	Description	Unit
m	vehicle mass	$[kg]$
v	vehicle speed	$[m/s]$
δ	steering angle	$[rad]$
J_{xx}	roll moment of inertia of the sprung mass measured at the CG	$[kg \cdot m^2]$
J_{zz}	yaw moment of inertia of the chassis measured at the CG	$[kg \cdot m^2]$
l_v	longitudinal CG position measured w.r.t. the front axle	$[m]$
l_h	longitudinal CG position measured w.r.t. the rear axle	$[m]$
h	CG height measured over the ground	$[m]$
c	suspension damping coefficient	$[kg \cdot m^2/s]$
k	suspension spring stiffness	$[kg \cdot m^2/s^2]$
C_v	linear tire stiffness coefficient for the front tire	$[N/rad]$
C_h	linear tire stiffness coefficient for the rear tire	$[N/rad]$

assumption, the vehicle speed is approximately governed by

$$\dot{v} = -\frac{|u|}{m}. \tag{3.8}$$

In the following subsection we give the description of the dynamic LTR that we utilize in the robust control design.

3.4.2 The dynamic load transfer ratio, LTR_d

Traditionally, as discussed in the related work section, some estimate of the vehicle load transfer ratio has been used as a basis for the design of rollover prevention systems. The

load transfer ratio [88, 48] can be simply defined as the load (i.e., vertical force) difference between the right and left wheels of the vehicle, normalized by the total load (i.e., the weight of the car). In other words,

$$\text{Load transfer ratio} = \frac{\text{Load on right tires} - \text{Load on left tires}}{\text{Total weight}}. \tag{3.9}$$

Clearly, this quantity varies between -1 and 1, and for a perfectly symmetric vehicle that is driving in a straight line, it is zero. The extrema are reached in the case of a wheel lift-off on one side of the vehicle, in which case the load transfer ratio is 1 or -1 depending on the side that lifts off. If roll dynamics are ignored, it is easily shown in [88] that the corresponding load transfer ratio (which we denote by LTR_s) is approximated by

$$LTR_s = \frac{2a_y h}{gT}, \tag{3.10}$$

where a_y is the lateral acceleration of the CG and T is the vehicle track width.

Note that rollover estimation based upon (3.10) is not sufficient to detect the transient phase of rollover (due to the fact that it is derived ignoring roll dynamics). Here we obtain an exact expression for the vehicle load transfer ratio which does not ignore roll dynamics; we denote this by LTR_d. This was initially suggested by us in [124], and to aid exposition we repeat the derivation here. Recall that we assumed the unsprung mass weight to be insignificant and the main body of the vehicle rolls about an axis along the centerline of the track at the ground level. We can write a torque balance for the unsprung mass about the assumed roll axis in terms of the suspension torques and the vertical wheel forces as follows:

$$-F_R\frac{T}{2} + F_L\frac{T}{2} + k\phi + c\dot{\phi} = 0. \tag{3.11}$$

Now substituting the definition of load transfer from (3.9) and rearranging yields the following expression for LTR_d:

$$LTR_d \;=\; \frac{2}{mgT}\left(c\dot{\phi} + k\phi\right). \tag{3.12}$$

In terms of the state, LTR_d can be represented by the following relationship

$$LTR_d \;=\; \tilde{C}\xi \qquad \text{where} \qquad \tilde{C} = \begin{bmatrix} 0 & 0 & \frac{2c}{mgT} & \frac{2k}{mgT} \end{bmatrix}. \tag{3.13}$$

We now provide a brief description of the actuators to be used in implementing our proposed controllers based on active steering and differential braking. In what follows, we also give the assumptions regarding the known and unknown vehicle parameters, as well as the sensory information that we utilize in our controller design.

3.4.3 Actuators, sensors and parameters

We are interested in control design based on two type of actuators: active differential braking and active steering actuators. Active braking actuators are already found in many stock production cars that are equipped with active safety systems such as ABS (Anti-lock Braking System) and EBS (Electronic Brake System) or similar such systems, which are capable of selectively braking each of the wheels. These systems are becoming more popular and have been accepted as an industry standard in most of the vehicle segments. Using these actuators, a yaw moment can be induced during a turn by braking combination of the four wheels, which can impose increased oversteer or understeer depending on the application. In the context of rollover prevention, the active braking can be used, for example, to reduce the lateral acceleration or any other suitable measure of rollover potential such as the LTR_d. Braking actuators also have the side effect of reducing the forward velocity, which has positive influence on the rollover threat. The fact that control designs using these actuators can be commissioned without much financial overhead makes them the preferred actuator candidates in the literature. Therefore, in one of the implementations of the robust design methodology explained in this chapter, we assume active differential braking actuators with access to full state information.

As an alternative to the active differential braking, we are also interested in robust control design based on active steering actuators. There are two types of active steering meth-

ods: full steer-by-wire and mechatronic-angle-superposition types. Steer-by-wire actuators do not contain a physical steering column between the steering wheel and the wheels; the steering torque is generated by a servo motor based on the driver steering command. This enables steer-by-wire actuators to be flexible and suitable for various vehicle dynamics control applications. However, stringent safety requirements on such systems prevent them from entering today's series-production vehicles. Mechatronic-angle-superposition type active steering actuators however have been recently introduced to the market. They contain a physical steering column and act cooperatively with the driver, while they permit various functions such as speed dependent steering ratio modification, and active response to mild environmental disturbances. It is plausible that active steering actuators will become an industry standard in the near future, due to their capability of directly and most efficiently (in the sense that they do not cause any speed loss) affecting the lateral dynamics of the car. Active steering based lateral control methods can be perfectly transparent to the driver and they are likely to cause the least interference with the driver intent unlike the control approaches based on differential braking and active suspension. Moreover, the use of active steering actuators do not result in a significant velocity loss, therefore they are likely to enter the market initially for the high performance vehicle segment. Therefore as an alternative implementation of the design methodology we describe in this chapter, we utilize mechatronic-angle-superposition type steering actuators with access to full state information. Although such active steering actuators require torque inputs from the driver, initially we assume no internal actuator dynamics or delays that might arise from driver interactions. It is however possible to account for the effects of these in the controller design. Also, our results can easily be extended to the case of steer-by-wire actuators where driver interactions are of less importance.

In the discussion that follows, we assume that all the model parameters $m, J_{xx}, J_{zz}, l_v, l_h$, C_v, C_h, k, h, and c are known to demonstrate the method. However, our control design is easily extended to account for uncertainty in these parameters, which we demonstrate by

designing our controllers to be robust with respect to uncertainties in vehicle speed v and center of gravity height h. As a side note, although we assumed all the vehicle model parameters to be known, it is possible to estimate some of these that are fixed (but unknown) using the sensor information available for the control design suggested here; we have analyzed this in detail in the preceding chapter and examples of it can also be found in the literature [122], [131].

3.5 State feedback controllers for robust disturbance attenuation

We are interested in designing a controller to prevent rollover that is robust with respect to parameter uncertainty, and in doing so we consider the vehicle models both of the form (3.5), and (3.3). Our starting point is in results obtained by Pancake, Corless and Brockman in [92, 91] for uncertain systems of the form

$$\dot{x} = A(\theta)x + B(\theta)\omega + B_u(\theta)u \tag{3.14}$$

$$z_j = C_j(\theta)x + D_j(\theta)\omega + D_{ju}(\theta)u\,, \quad j = 1,\ldots,r\ , \tag{3.15}$$

where θ is some parameter vector that captures the plant nonlinearity/uncertainty, which can depend on t, x, ω and u. The vector $x(t) \in \mathbb{R}^n$ is the state at time $t \in [0,\infty)$ and $\omega(t) \in \mathbb{R}^m$ is a bounded disturbance input. Also $u(t) \in \mathbb{R}^{u_m}$ is the control input and $z_j(t) \in \mathbb{R}^{p_j}$ are the performance outputs. We wish to synthesize a stabilizing controller which prevents the peak values of the performance outputs exceeding certain values. In doing so, for each output z_j we introduce a measure of performance γ_j which guarantees that the magnitude of that output is less than or equal to γ_j times the peak value of the magnitude of the disturbance. We describe here a controller design strategy which can be used to minimize the performance level for one main output while keeping the performance levels for the other outputs below some prespecified levels. In addition the controllers are robust in the sense that they

ensure performance in the presence of any allowable uncertainty which was taken into account in the control design. In other words, our feedback controllers guarantee a bounded performance output given a bounded uncertain disturbance, that is, $||\omega(t)|| \leq \omega_{max}$.

We consider linear state feedback controllers of the form

$$u = Kx, \tag{3.16}$$

where K is a constant state feedback gain matrix. This results in a closed loop system described by

$$\dot{x} = [A(\theta) + B_u(\theta)K]x + B(\theta)\omega \tag{3.17}$$

$$z_j = [C_j(\theta) + D_{ju}(\theta)K]x + D_j(\theta)\omega, \qquad j = 1,\ldots,r. \tag{3.18}$$

The uncertainty in the plant is required to satisfy the following condition.

Assumption 3.5.1 *For each θ and $j = 1,\ldots,r$, the matrix*

$$\begin{bmatrix} A(\theta) & B(\theta) & B_u(\theta) & C_j(\theta) & D_j(\theta) & D_{ju}(\theta) \end{bmatrix} \tag{3.19}$$

can be written as a convex combination of a finite number of matrices (called vertex matrices)

$$\begin{bmatrix} A_1 & B_1 & B_{u_1} & C_{j_1} & D_{j_1} & D_{ju_1} \end{bmatrix}, \cdots, \begin{bmatrix} A_N & B_N & B_{u_N} & C_{j_N} & D_{j_N} & D_{ju_N} \end{bmatrix}.$$

Remark 3.5.1 Suppose that each of the matrices $A(\theta), B(\theta), B_u(\theta), C_j(\theta), D_j(\theta), D_{ju}(\theta)$ depend in a multi-affine fashion on the components of the M-vector θ and each element of θ is bounded, that is,

$$\underline{\theta}_k \leq \theta_k \leq \overline{\theta}_k \qquad \text{for} \qquad k = 1,\ldots,M.$$

Then, for all θ, the matrix in (3.19) can be expressed as a convex combination of the 2^M matrices corresponding to the extreme values of the components of θ; these vertex matrices

are given by

$$[A(\theta)\ B(\theta)\ B_u(\theta)\ C_j(\theta)\ D_j(\theta)\ D_{ju}(\theta)] \quad \textit{where} \quad \theta_k = \underline{\theta}_k \text{ or } \overline{\theta}_k \tag{3.20}$$

for $k = 1, \ldots, M$.

Remark 3.5.2 One can easily show that when the uncertain system (3.14)-(3.15) satisfies Assumption 3.5.1 then, for each θ, and $j = 1, \ldots, r$, the matrix quadruple

$$(A_{cl}(\theta), B(\theta), C_{cl}(\theta), D(\theta))$$

can be written as a convex combination of the matrix quadruples

$$(A_{cl_1}, B_1, C_{cl_1}, D_1), \ldots, (A_{cl_N}, B_N, C_{cl_N}, D_N),$$

where

$$A_{cl_i} = A_i + B_{u_i}K \quad \text{and} \quad C_{cl_i} = C_{j_i} + D_{ju_i}K, \quad for \quad i = 1, \ldots, N. \tag{3.21}$$

The following result from [92, 91] is useful in designing our rollover prevention controllers.

Theorem 3.5.1 *Consider a nonlinear/uncertain system described by (3.14)-(3.15) and satisfying Assumption 3.5.1. Suppose that there exist a matrix $S = S^T > 0$, a matrix L and scalars $\beta_1, \ldots \beta_N > 0$ and $\mu_0, \mu_{1j}, \mu_{2j} \geq 0$, $j = 1, \ldots, r$, such that the following matrix inequalities hold*

$$\begin{bmatrix} \beta_i(SA_i^T + A_iS + L^TB_{u_i}^T + B_{u_i}L) + S & \beta_iB_i \\ \beta_iB_i^T & -\mu_0 I \end{bmatrix} \leq 0, \tag{3.22}$$

$$\begin{bmatrix} -\mu_{1j}S & 0 & SC_{j_i}^T + L^TD_{ju_i}^T \\ 0 & -\mu_{2j}I & D_{j_i}^T \\ C_{j_i}S + D_{ju_i}L & D_{j_i} & -I \end{bmatrix} \leq 0, \tag{3.23}$$

for all $i = 1,\ldots,N$ and $j = 1,\ldots,r$. Then the controller

$$u = Kx \qquad with \qquad K = LS^{-1} \tag{3.24}$$

results in a closed loop nonlinear/uncertain system which has the following properties.

(a) The undisturbed system ($\omega = 0$) is globally exponentially stable, that is, all state trajectories decay exponentially.

(b) If the disturbance input is bounded, that is, $\|\omega(t)\| \leq \rho_\omega$ for all t then, for zero initial state, the performance outputs $z_1,\ldots,z_r$ of the closed loop system are bounded and satisfy

$$\|z_j(t)\| \leq \gamma_j \rho_\omega \tag{3.25}$$

for all t where

$$\gamma_j = \sqrt{\mu_0 \mu_{1j} + \mu_{2j}}. \tag{3.26}$$

The scalars $\gamma_1,\ldots.\gamma_r$ are called **levels of performance** and can be regarded as measures of the ability of the closed loop system to attenuate the effect of the disturbance input on the performance outputs; a smaller γ_j means better performance in the sense of increased attenuation. For a proof of the theorem, see Appendix A.

Comment: In Appendix B we give an iterative LMI solution algorithm to find control gains that satisfy the hypotheses of Theorem 3.5.1 for the rollover control design problem. This numerical algorithm attempts to minimize γ_1 for the specified values of γ_2 (where we consider only two performance outputs) in every iterative solution step. Unfortunately, our solution method does not permit external specification of both performance levels γ_1, γ_2, but rather we specify one of them and then try to minimize the other. In future extensions we shall investigate convergence and feasibility conditions to determine the existence of control gains guaranteeing pre-specified performance levels γ_j.

Remark 3.5.3 It is straightforward to show that the inequality (3.22) can be expressed as follows

$$\begin{bmatrix} A_iS+SA_i^T+B_{ui}L+L^TB_{ui}^T+\alpha_iS & B_i \\ B_i^T & -\alpha_iI \end{bmatrix} \leq 0, \tag{3.27}$$

for $i = 1,\ldots,N$, where $\alpha_1,\ldots,\alpha_N > 0$ are scalars.

Remark 3.5.4 Consider the situation in which the matrices $D_{j_1},\ldots,D_{j_N}$ are all zero for some performance output z_j. Then, for each i, inequality (3.23) is satisfied for some $\mu_{2j} \geq 0$ if and only if it is satisfied with $\mu_{2j} = 0$. Hence, if $D_{j_1},\ldots,D_{j_N}$ are all zero, inequality (3.23) can be replaced with

$$\begin{bmatrix} -\mu_{1j}S & SC_{j_i}^T+L^TD_{ju_i}^T \\ C_{j_i}S+D_{ju_i}L & -I \end{bmatrix} \leq 0\,. \tag{3.28}$$

In this case,

$$\gamma_j = \sqrt{\mu_0\mu_{1j}}\,. \tag{3.29}$$

Also, using Schur complements, one can show that the above inequality is equivalent to the following inequality which is linear in the variables S and μ_{1j}.

$$\begin{bmatrix} -S & SC_{j_i}^T+L^TD_{ju_i}^T \\ C_{j_i}S+D_{ju_i}L & -\mu_{1j}I \end{bmatrix} \leq 0\,. \tag{3.30}$$

Remark 3.5.5 Consider the closed loop system subject to a fixed bounded disturbance ω which satisfies $\|\omega(t)\| \leq \rho_\omega$. Let

$$V(x) = x^TPx \tag{3.31}$$

and consider the bounded ellipsoid in state space defined by

$$\mathscr{E}(\rho_\omega) = \left\{x \in \mathbb{R}^n : V(x) \leq \mu_0\rho_\omega^2\right\}. \tag{3.32}$$

The inequalities in (3.22) guarantee that whenever a state trajectory is outside of the ellipsoid the time rate change of the Lyapunov function V is negative. From this one can show

that the ellipsoid is both invariant and attractive. Attractive means that all state trajectories converge to the ellipsoid with increasing time. Invariance means that if a state trajectory starts in the ellipsoid, it remains there forever; in particular, if a trajectory starts at the origin, it will always be contained in the ellipsoid.

The inequalities in (3.23) guarantee that each performance output z_j satisfies

$$\|z_j(t)\|^2 \leq \mu_{1j} V(x(t)) + \mu_{2j} \omega(t)^2 . \tag{3.33}$$

Hence, if a trajectory starts within the ellipsoid, it must satisfy $\|z_j(t)\| \leq \gamma_j \rho_\omega$ for all t. Otherwise, $\|z_j(t)\|$ is "eventually bounded" by $\gamma_j \rho_\omega$.

3.5.1 Rollover prevention controllers with differential braking

Here we use the above results to obtain rollover prevention controllers using differential braking as the sole control input. The vehicle model utilized is the single track model given in (3.5) along with systems matrices (3.6), and (3.7). We consider the driver's steering wheel angle in degrees as the disturbance input ω; this is related to the steering angle δ by

$$\delta = \frac{\pi}{180\,\lambda}\omega \tag{3.34}$$

where λ is the steering ratio between the steering wheel and the wheels and is taken to be 18.

For reasons discussed earlier, we choose $z_1 = LTR_d$ given by (3.12) as one performance output; we want to keep $\|z_1\| \leq 1$ for the largest possible steering inputs. We consider the magnitude of the braking force u to be limited by the weight mg of the vehicle; so we choose $z_2 = u$ as a second performance output. The resulting system with two performance outputs can be described by

$$\begin{aligned} \dot{x} &= Ax + B\omega + B_u u \\ z_1 &= C_1 x \\ z_2 &= u\,, \end{aligned} \tag{3.35}$$

where

$$B = \frac{\pi}{180\lambda} B_\delta \,. \tag{3.36}$$

The parameters of the above model were tuned against the dynamics of a compact passenger vehicle such that there is a close match between the model and the measured vehicle states. The tuning was performed at $v = 40m/s$ and with a step steering input of magnitude 30°. The corresponding tuned vehicle parameters are given in Table 3.2.

First we obtain a control design which is based on the model (3.5) with a fixed speed; we call this the fixed model controller. We then consider the effect of varying speed in our control design and we obtain a control design assuming that the speed varies over some prespecified range; we call this the robust controller.

(a) Controller Based on Fixed Speed

Here we base controller design on model (3.35) in which all matrices are constant and correspond to a fixed vehicle speed of $v = 40m/s$. To obtain a state feedback controller, we applied Theorem 3.5.1. Since we desire that $\|z_1\| \leq 1$ and $\|z_2\| \leq mg$ for the largest possible steering inputs, we considered $\gamma_2 = mg\gamma_1$. We used a simplified version of the iterative solution algorithm described in Appendix B with $N = 1$, and utilized with it the alternative form of the inequalities given in (3.27) and (3.30). By performing a linear line search with respect to the scalar α_1 we obtained a minimum value of 0.0089 for γ_1. The corresponding control gain matrix is

$$K = mg \cdot \begin{bmatrix} -7.1287 & 0.9842 & 0.3271 & -0.0944 \end{bmatrix} \cdot$$

Remark 3.5.6 *Consider the constant speed model subject to the above control gain matrix. According to (3.25), the constraints on the outputs will not be violated for this constant speed closed loop system if the maximum magnitude ω_{max} of the driver steering disturbance input satisfies $\omega_{max} \leq 1/\gamma_1 \approx 112.97^\circ$. However application of the braking controller re-*

Table 3.2: Fixed model parameters

parameter	value	unit
m	1224.1	$[kg]$
J_{xx}	362	$[kg \cdot m^2]$
J_{zz}	1279	$[kg \cdot m^2]$
l_v	1.102	$[m]$
l_h	1.254	$[m]$
T	1.51	$[m]$
h	0.375	$[m]$
c	4000	$[kg \cdot m^2/s]$
k	36075	$[kg \cdot m^2/s^2]$
C_v	90240	$[N/rad]$
C_h	180000	$[N/rad]$

duces vehicle speed. As the vehicle speed reduces, its tendency to rollover decreases and the vehicle can actually tolerate disturbances inputs with magnitude considerably larger than $1/\gamma_1$. *In simulations where the speed varies according to (3.8), the above controller gain matrix was able to maintain* $|LTR_d| \leq 1$ *and* $\|u\| \leq mg$ *for steering input magnitudes up to* $\omega_{max} = 130^\circ$.

For numerical simulations we chose a driver steering input corresponding to an obstacle avoidance maneuver that is known as the elk-test; we chose an initial speed of $v = 40m/s$ and a peak steering magnitude of $\omega_{\max} = 130^\circ$. The steering profile corresponding to this maneuver and a comparison of speed histories for the controlled and uncontrolled vehicles are shown in Figure 3.4. Notice that, the dramatic speed drop of the controlled vehicle is a direct consequence of the braking action. In Figure 3.5 we further observe that $|LTR_d| > 1$

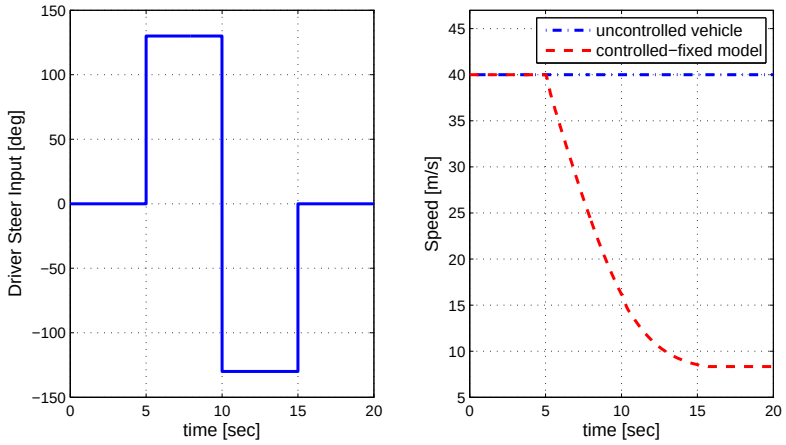

Figure 3.4: Steering and speed histories.

for the uncontrolled vehicle throughout the manoeuver indicating possible rollover, whereas the vehicle with the proposed controller satisfies $|LTR_d| < 1$ achieving the intended design goal and demonstrating the effectiveness of the proposed controller. Also for this maneuver, the peak value of the control force generated was about 80% of the total weight of the vehicle (i.e., $|u| < mg$), thus achieving the other design goal.

In the next subsection we demonstrate how our control design method can be extended to account for varying parameter uncertainties.

(b) Controller Based on Variable Speed Model

Here we present a rollover controller design which takes into account varying vehicle speed; it assumes constant model parameters given in Table 3.2. We assume that the speed is bounded above and below by $\bar{v}$ and $\underline{v}$, respectively, that is, $\underline{v} \leq v \leq \bar{v}$. In order to represent typical freeway driving conditions for a compact passenger vehicle we chose $\underline{v} = 25m/s$, and $\bar{v} = 40m/s$ as the extremum design speeds. Again, we used the model (3.35) for controller design, where the matrices A, B, B_u and C_1 are given in equations (3.6), (3.7) and (3.12). System matrices B_u and C_1 are independent of speed. The matrices A and B can be expressed

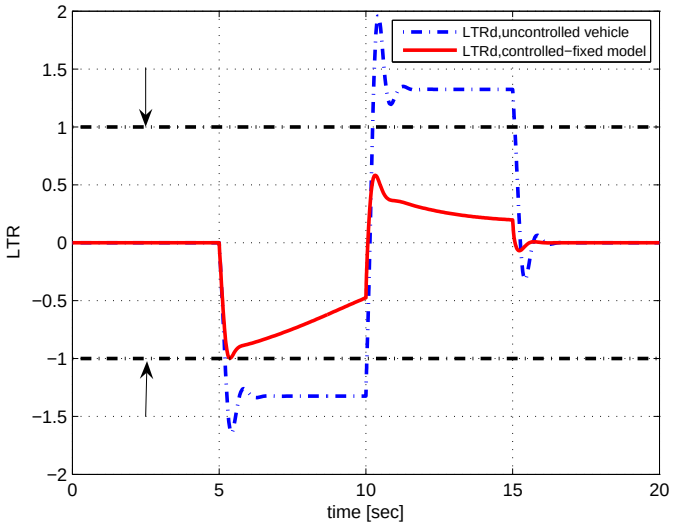

Figure 3.5: Comparison of LTR_d for the uncontrolled vehicle and the controlled vehicle with the fixed model.

as affine linear functions of the time-varying parameters $\theta_1 := 1/v$ and $\theta_2 := 1/v^2$. These parameters are bounded as follows:

$$\underline{\theta}_1 \leq \theta_1 \leq \overline{\theta}_1\,, \qquad \underline{\theta}_2 \leq \theta_2 \leq \overline{\theta}_2 \tag{3.37}$$

where

$$\underline{\theta}_1 = \frac{1}{\overline{v}}\,, \quad \overline{\theta}_1 = \frac{1}{\underline{v}}\,, \quad \underline{\theta}_2 = \frac{1}{\overline{v}^2}\,, \quad \overline{\theta}_2 = \frac{1}{\underline{v}^2}\,.$$

Hence our system description satisfies Assumption 3.5.1 with the following vertex matrices

$$\begin{aligned}
A_1 &= \overline{\theta}_1 Y_1 + \overline{\theta}_2 Y_2 + Y_3\,, \qquad A_2 = \overline{\theta}_1 Y_1 + \underline{\theta}_2 Y_2 + Y_3\,,\\
A_3 &= \underline{\theta}_1 Y_1 + \overline{\theta}_2 Y_2 + Y_3\,, \qquad A_4 = \underline{\theta}_1 Y_1 + \underline{\theta}_2 Y_2 + Y_3\,,\\
B_1 &= B_2 = \frac{\pi}{180\,\lambda}\begin{bmatrix} \frac{C_v J_{x_{eq}}}{m J_{xx}}\overline{\theta}_1 & \frac{C_v l_v}{J_{zz}} & \frac{h C_v}{J_{xx}} & 0 \end{bmatrix}^T,\\
B_3 &= B_4 = \frac{\pi}{180\,\lambda}\begin{bmatrix} \frac{C_v J_{x_{eq}}}{m J_{xx}}\underline{\theta}_1 & \frac{C_v l_v}{J_{zz}} & \frac{h C_v}{J_{xx}} & 0 \end{bmatrix}^T,
\end{aligned}$$

where

$$Y_1 = \begin{bmatrix} -\frac{\sigma J_{xeq}}{mJ_{xx}} & 0 & -\frac{hc}{J_{xx}} & \frac{h(mgh-k)}{J_{xx}} \\ 0 & -\frac{\kappa}{J_{zz}} & 0 & 0 \\ 0 & \frac{h\rho}{J_{xx}} & 0 & 0 \\ 0 & 0 & 0 & 0 \end{bmatrix}, \quad Y_2 = \begin{bmatrix} 0 & \frac{\rho J_{xeq}}{mJ_{xx}} & 0 & 0 \\ 0 & 0 & 0 & 0 \\ 0 & 0 & 0 & 0 \\ 0 & 0 & 0 & 0 \end{bmatrix},$$

$$Y_3 = \begin{bmatrix} 0 & -1 & 0 & 0 \\ \frac{\rho}{J_{zz}} & 0 & 0 & 0 \\ -\frac{h\sigma}{J_{xx}} & 0 & -\frac{c}{J_{xx}} & \frac{mgh-k}{J_{xx}} \\ 0 & 0 & 1 & 0 \end{bmatrix}.$$

We used Theorem 3.5.1 to design a controller which guarantees performance levels γ_1 and $\gamma_2 = mg\gamma_1$, in presence of the any variations in speed satisfying $\underline{v} \leq v \leq \bar{v}$. We again used the iterative solution algorithm described in Appendix B with $N = 4$, and in conjunction with the inequalities (3.27) and (3.30). As a results, we achieved $\gamma_1 = 0.009$, and the corresponding control gain matrix

$$K = mg \cdot [\ -7.5858 \quad 1.1995 \quad 0.3508 \quad -0.1478\ ] \cdot$$

Note that, according to (3.25) the maximum theoretical driver steering disturbance input permitted is, $\omega_{max} = 1/\gamma_1 \approx 111.36^\circ$. In our simulations however, for the reasons explained in Remark 3.5.6, the robust controller was able to keep $|LTR_d| \leq 1$ for driver steering inputs with magnitudes up to $\omega_{max} = 136.5^\circ$.

For numerical simulations, we used the same obstacle avoidance (elk test) scenario as before, however with a peak driver steering input of magnitude $\omega_{max} = 136.5^\circ$ and an initial speed of $v = 40m/s$. The steering profile corresponding to this maneuver and a comparison of speed histories for the uncontrolled vehicle as well as the controlled vehicles with the two suggested control designs are shown in Figure 3.6. Notice here again that, the dramatic speed drop in the controlled vehicles is a direct consequence of the braking action. Also

we observe that the speed loss due to the robust controller is slightly more than that due to the fixed-model controller. Further results are presented in Figures 3.7 and 3.8, where we compare the performances of both the robust and the fixed-model controller designs. We observe in Figure 3.7 that, the LTR_d due to the fixed-model controller slightly exceeds the lower boundary -1 at the initiation of the steering maneuver, while the robust controller results in $|LTR_d| \leq 1$ throughout the maneuver. In Figure 3.8 we compare the normalized control force histories for both of the controllers and observe that they are close and both result in $|u| \leq mg$ as desired.

It is of particular interest for us to see how the suggested controllers affect the vehicle path. To do this, we note that the coordinates (x, y) of the vehicle CG relative to the road satisfy

$$\dot{x} = v\cos(\beta + \psi), \tag{3.38}$$

$$\dot{y} = v\sin(\beta + \psi), \tag{3.39}$$

where we choose the initial coordinates $(x(0), y(0))$ to be zero. In Figure 3.9 the CG trajectories of the controlled and the uncontrolled vehicles are compared. Notice here that the shorter paths of the controlled vehicles are due to slowing down as a result of braking. We observe in Figure 3.9 that both controllers cause a small divergence from the intended vehicle path during the first half of the maneuver; in a real driving situation, the driver would time the second half of the maneuver based on the speed and location of the vehicle. Hence the second part of the maneuver would occur later for the controlled vehicles.

Comment : From the simulation results for the fixed model and the robust controllers, we observe that both controllers are effective in reducing the vehicle load transfer ratio LTR_d, and thus preventing rollover.

Comment : Our design is easily extended to incorporate other sources of parameter uncertainty such as the vehicle parameters, mass and center of gravity height.

In this subsection we have presented a methodology for the design of vehicle rollover prevention systems using differential braking. Next we consider the design method in conjunc-

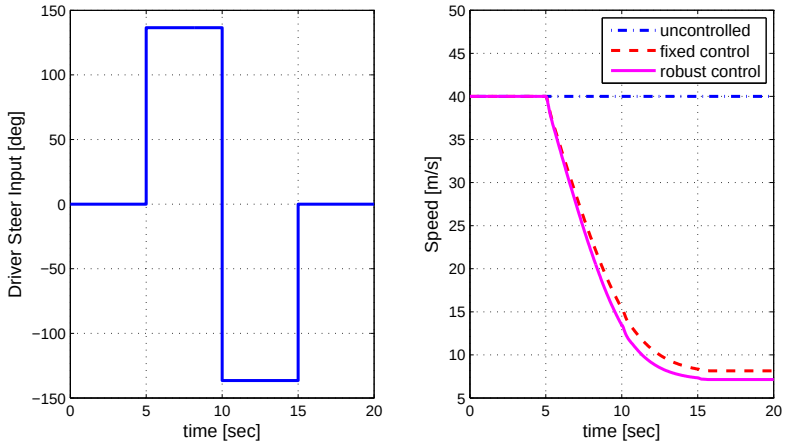

Figure 3.6: Steering profile and a comparison of speed histories.

tion with the active steering actuators.

3.5.2 Rollover prevention controllers with active steering

As an alternative to the rollover control design described in the preceding subsection, here we apply the control design methodology discussed earlier for the design of rollover prevention controllers utilizing active steering actuators. We first present a design under the assumption that the plant parameters are known and fixed (Part a). We then extend our design to cope with plant parameter uncertainties (Part b). Finally, we further refine our design to incorporate a mode switch to deactivate the controller in situations when there is no rollover danger (Part c).

(a) Active steering PI controller with known plant parameters

Our objective here is to superimpose an active steering control input $u = \delta_c$ on the driver steering input δ_d to prevent rollover. Thus, the total steering input δ to the vehicle consists

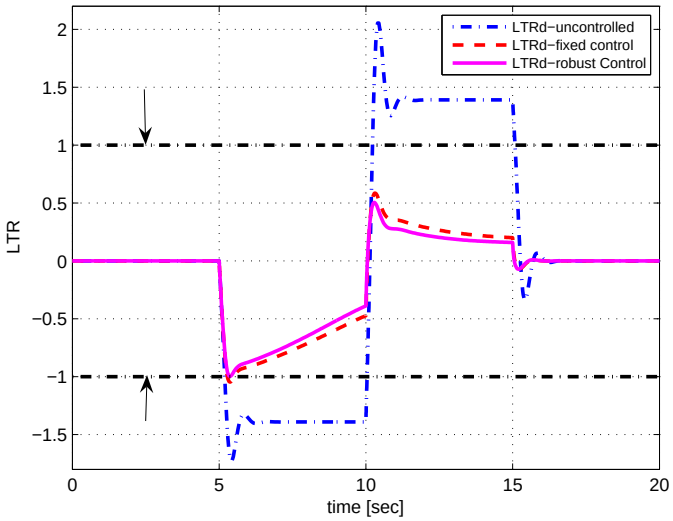

Figure 3.7: Comparison of LTR_d for the uncontrolled and controlled vehicles with differential braking.

of two parts and is given by

$$\delta = \delta_d + u\,. \tag{3.40}$$

The driver input δ_d will be regarded as a disturbance input ω. Recalling model (3.3), our system is now described by

$$\dot{\xi} = \tilde{A}\xi + \tilde{B}\omega + \tilde{B}u, \tag{3.41}$$

where $\xi(t) \in \mathbb{R}^4$ is the state at time $t \in \mathbb{R}$, $u(t)$ is a scalar control input and $\omega(t)$ is a scalar disturbance input. The matrices $\tilde{A}$ and $\tilde{B}$ are fixed and are as described as in (3.4).

We propose a proportional-integral (PI) type state feedback controller of the form

$$u = K_P\xi + K_I\xi_I, \tag{3.42}$$

where the integrator state ξ_I is the integral of the yaw rate tracking error:

$$\dot{\xi}_I = \dot{\psi} - \dot{\psi}_d\,, \qquad \xi_I(0) = 0\,. \tag{3.43}$$

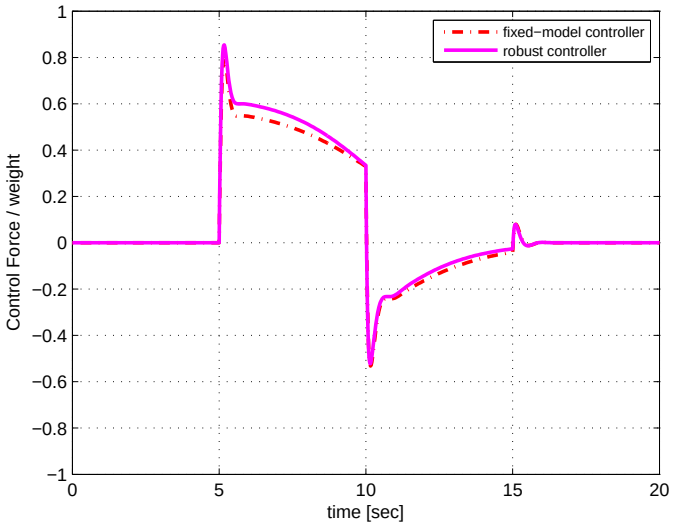

Figure 3.8: Normalized control history comparisons for vehicles with differential braking.

The reference yaw rate $\dot{\psi}_d$ is given by

$$\dot{\psi}_d = \alpha \delta_d, \tag{3.44}$$

for a constant gain α. Although this is a major simplification of the reference driver intent, we chose this linear expression for the sake of simplicity. The resulting control structure is depicted in Figure 3.10 below.

Comment : The purpose of utilizing the integral action in the controller is to guarantee that when driver input δ_d is constant, the corresponding steady state yaw rate is given by $\dot{\psi} = \dot{\psi}_d = \alpha \delta_d$. This yaw rate will be large for large δ_d and will result in a large steady state value of LTR_d. To avoid this one could saturate $\dot{\psi}_d$ at a certain value such that, in steady state, $||LTR||$ stays below 1, regardless of the driver input.

We want the controller to keep the magnitude of LTR_d small during transients with reasonable control effort. In view of this, we introduce the following two performance outputs:

$$z_1 = LTR_d = \tilde{C}\xi \tag{3.45}$$

$$z_2 = u, \tag{3.46}$$

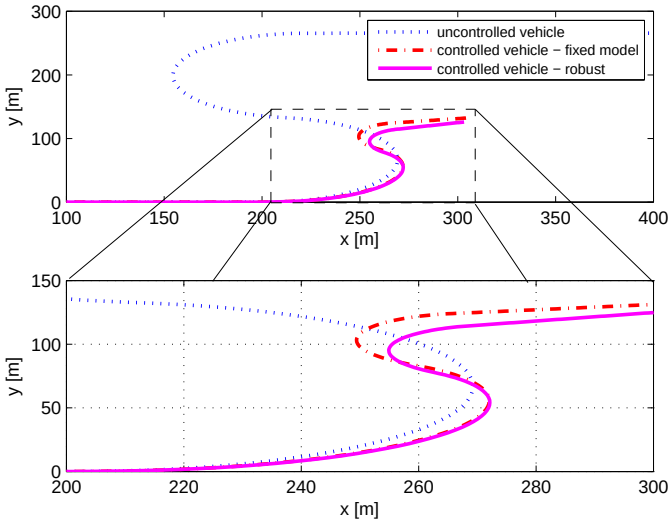

Figure 3.9: Comparison of CG trajectories for the uncontrolled and controlled vehicles with differential braking.

where $\tilde{C}$ is given in (3.12). Augmenting the vehicle dynamics with the integrator dynamics and introducing the augmented state $x = [\xi^T \quad \xi_I]^T$ results in the following system description:

$$\begin{aligned} \dot{x} &= Ax + B\omega + B_u u \\ z_1 &= C_1 x \\ z_2 &= D_{2u} u, \end{aligned} \tag{3.47}$$

where

$$A = \begin{bmatrix} \tilde{A} & 0 \\ c_{\dot{\psi}} & 0 \end{bmatrix}, B = \begin{bmatrix} \tilde{B} \\ -\alpha \end{bmatrix}, B_u = \begin{bmatrix} \tilde{B} \\ 0 \end{bmatrix}, C_1 = \begin{bmatrix} \tilde{C} & 0 \end{bmatrix}, D_{2u} = 1 \tag{3.48}$$

and $c_{\dot{\psi}} = \begin{bmatrix} 0 & 1 & 0 & 0 \end{bmatrix}$.

Also, a proposed controller (3.42) can be described by $u = Kx$ where

$$K = \begin{bmatrix} K_P & K_I \end{bmatrix}. \tag{3.49}$$

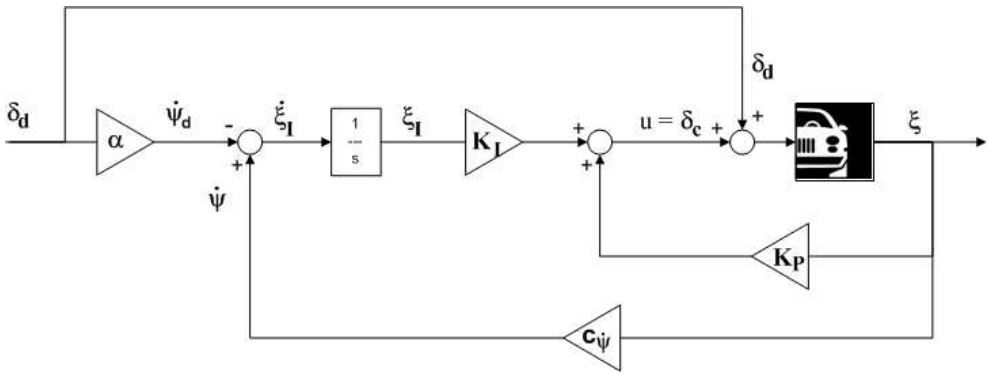

Figure 3.10: Flow diagram of the PI active steering controller.

In view of our original control objectives, we will use the results of Theorem 3.5.1 to obtain a gain matrix K which minimizes the level of performance γ_1 for z_1 while keeping the level of performance γ_2 for z_2 below some prespecified level $\overline{\gamma}_2$.

Simulations

The model parameters used here are given in Table 3.2. They are typical for a compact car. The steering ratio was assumed to be 1:18. In using Theorem 3.5.1 to obtain a gain matrix K which minimizes the level of performance γ_1 for z_1 subject to a specified level of performance γ_2 for z_2, we used a simplified version of the iterative solution algorithm described in Appendix B with $N = 1$.

In the numerical simulations presented here, we again simulated an obstacle avoidance maneuver that is commonly known as the elk-test. The maneuver takes place at a speed of $v = 140$ km/h and with a peak steering magnitude of 100°. The results of the simulations are presented in Figure 3.11, which demonstrates the effectiveness of the controller in preventing rollover in this dangerous maneuver by keeping the magnitude of LTR_d less than one. Notice that driver intervention of the controller as measured by the difference in roll angles of the controlled and uncontrolled vehicles show a slight difference, implying that the control action would probably be undiscernible by the driver, which is favorable and

was one of our aims.

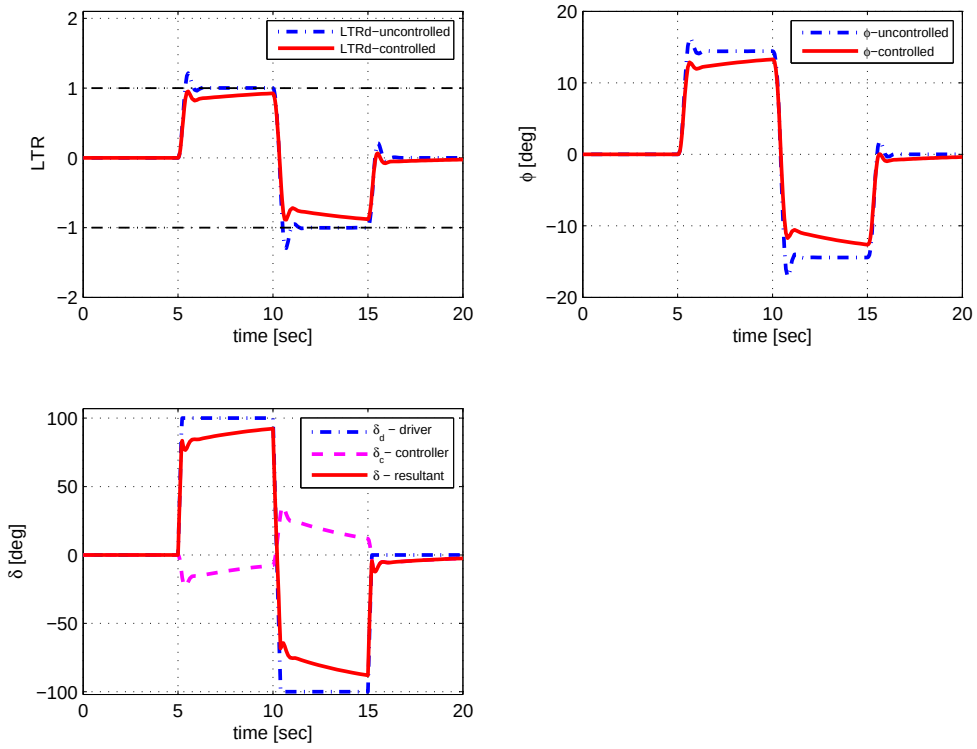

Figure 3.11: Comparison of the uncontrolled and controlled vehicles with active steering (fixed model).

It is interesting to see how the suggested controllers affect the vehicle path. To do this, we note that the coordinates (x, y) of the vehicle CG relative to the road satisfy the equations (3.38) and (3.39), where the initial coordinates $(x(0), y(0))$ are assumed to be zero. In Figure 3.12 the CG trajectories of the controlled and the uncontrolled vehicles are compared along with the remaining states. We observe from trajectory plots that control action causes a small divergence from the uncontrolled vehicle path during the first half of the maneuver while preventing rollover; in a real driving situation, the driver would time the second half of the maneuver based on the speed and location of the vehicle. Also similar to the roll angle variation, the remaining state plots of the controlled vehicle are close to those of the

uncontrolled vehicle during the maneuver.

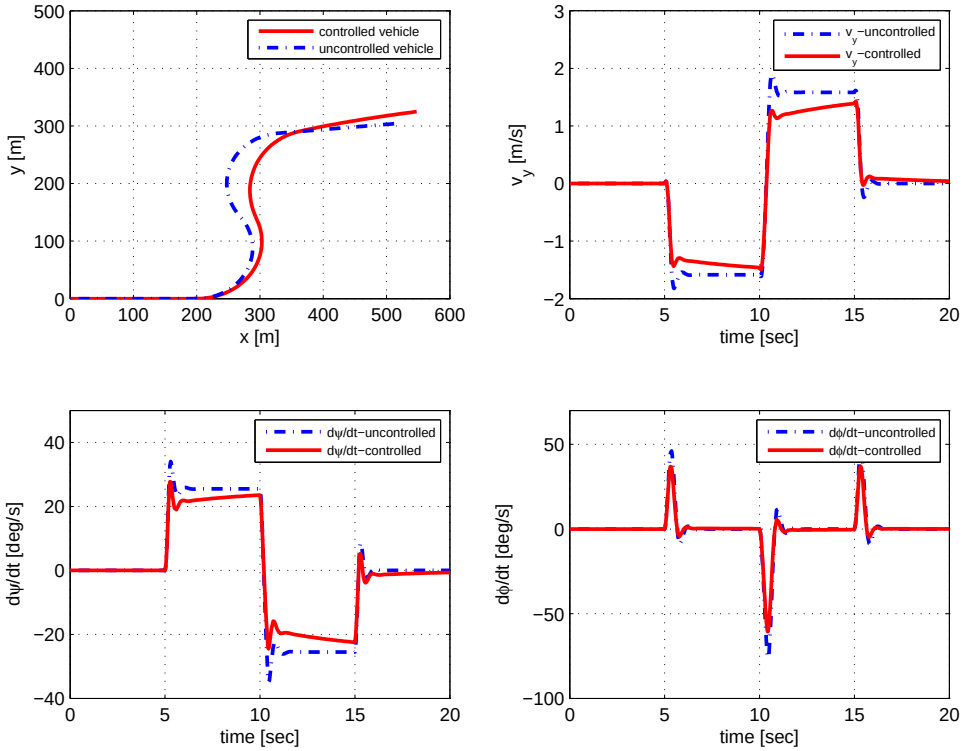

Figure 3.12: Comparison of the states and trajectories of the uncontrolled and the controlled vehicles with active steering (fixed model).

(b) Robust control design

We now extend the suggested design based on active steering to cope with parameter uncertainty. Specifically, we now redesign the controller to take into account the parameter uncertainties resulting from bounded vehicle speed variations as well as CG height uncertainties by utilizing Assumption 3.5.1 and using Theorem 3.5.1.

In what follows we shall assume that the vehicle speed v is bounded, that is, $\underline{v} \leq v \leq \bar{v}$, where $\underline{v}$ and $\bar{v}$ denote the lower and upper bounds on the speed, respectively. In order to

represent typical freeway driving conditions we chose the speed extrema as $\underline{v} = 20m/s$ and $\overline{v} = 40m/s$ in the numerical simulations below. We further assume that uncertain CG height h belongs to the interval $[\underline{h}, \overline{h}]$, where $\underline{h} = 0.2[m]$, and $\overline{h} = 0.5[m]$ denote the lower and upper bounds of the uncertain CG height, respectively.

We proceed as in the previous subsection, where we used (3.41) as the vehicle model for our control design and the matrices $\tilde{A}$ and $\tilde{B}$ are described in (3.4). Note that these matrices depend in a multi-affine fashion on the parameters

$$\theta_1 := 1/v, \quad \theta_2 := v, \qquad \theta_3 := h, \qquad \theta_4 := h^2. \tag{3.50}$$

Hence, as our model for robust control design, we consider

$$\dot{\xi} = \tilde{A}(\theta)\xi + \tilde{B}(\theta)\omega + \tilde{B}(\theta)u \tag{3.51}$$

where

$$\tilde{A}(\theta) = \begin{bmatrix} -\frac{\sigma}{m}\theta_1 - \frac{\sigma}{J_{xx}}\theta_1\theta_4 & \frac{\rho}{m}\theta_1 + \frac{\rho}{J_{xx}}\theta_1\theta_4 - \theta_2 & -\frac{c}{J_{xx}}\theta_3 & -\frac{k}{J_{xx}}\theta_3 + \frac{mg}{J_{xx}}\theta_4 \\ \frac{\rho}{J_{zz}}\theta_1 & -\frac{\kappa}{J_{zz}}\theta_1 & 0 & 0 \\ -\frac{\sigma}{J_{xx}}\theta_1\theta_3 & \frac{\rho}{J_{xx}}\theta_1\theta_3 & -\frac{c}{J_{xx}} & -\frac{k}{J_{xx}} + \frac{mg}{J_{xx}}\theta_3 \\ 0 & 0 & 1 & 0 \end{bmatrix}, \tag{3.52}$$

$$\tilde{B}(\theta) = \begin{bmatrix} \frac{C_v}{m} + \frac{C_v}{J_{xx}}\theta_4 & \frac{C_v l_v}{J_{zz}} & \frac{C_v}{J_{xx}}\theta_3 & 0 \end{bmatrix}^T \tag{3.53}$$

and

$$\frac{1}{\overline{v}} \leq \theta_1 \leq \frac{1}{\underline{v}}, \qquad \underline{v} \leq \theta_2 \leq \overline{v}, \qquad \underline{h} \leq \theta_3 \leq \overline{h}, \qquad \underline{h}^2 \leq \theta_4 \leq \overline{h}^2. \tag{3.54}$$

As before, we consider PI controllers of the form

$$\begin{aligned} u &= K_P\xi + K_I\xi_I, \\ \dot{\xi}_I &= \dot{\psi} - \alpha\delta_d \qquad \xi_I(0) = 0. \end{aligned} \tag{3.55}$$

Recall the performance outputs z_1 and z_2 described in (3.45) and (3.46). Again, we are interested in synthesizing a stabilizing controller which minimizes the level of performance γ_1 for z_1 while keeping the level of performance γ_2 for z_2 below some prespecified level $\overline{\gamma}_2$. With the augmented state $x = [\xi^T \;\; \xi_I]^T$, the proposed controller structure can be simply described by $u = Kx$ where

$$K = \left[\begin{array}{cc} K_P & K_I \end{array} \right], \tag{3.56}$$

and the behavior of x and the performance outputs can be described by

$$\begin{aligned} \dot{x} &= A(\theta)x + B(\theta)\omega + B_u(\theta)u \\ z_1 &= C_1 x \\ z_2 &= D_{2u}u, \end{aligned} \tag{3.57}$$

with matrices

$$A(\theta) = \left[\begin{array}{cc} \tilde{A}(\theta) & 0 \\ c_{\dot{\psi}} & 0 \end{array} \right], \; B(\theta) = \left[\begin{array}{c} \tilde{B}(\theta) \\ -\alpha \end{array} \right], \; B_u(\theta) = \left[\begin{array}{c} \tilde{B}(\theta) \\ 0 \end{array} \right], \; C_1 = \left[\begin{array}{cc} \tilde{C} & 0 \end{array} \right], \tag{3.58}$$

where $c_{\dot{\psi}} = [\,0 \;\; 1 \;\; 0 \;\; 0\,]$, and $D_{2u} = 1$. Since the matrices $A(\theta), B(\theta), B_u(\theta)$ depend in a multi-affine fashion on θ and each component of θ is bounded, it follows that the matrix $[A(\theta) \;\; B(\theta) \;\; B_u(\theta)]$ can always be expressed as a convex combination of the following 16 matrices

$$\left[\begin{array}{ccc} A(\theta) & B(\theta) & B_u(\theta) \end{array} \right] \quad \textit{where} \quad \theta_k = \underline{\theta}_k \text{ or } \overline{\theta}_k \tag{3.59}$$

that is θ_k equals its minimum or maximum value for $k = 1, \ldots, 4$. Note here that θ_k denotes the k^{th} element of the 4-vector θ. Hence the augmented plant satisfies Assumption 3.5.1.

Now one can use Theorem 3.5.1 to design a controller which guarantees desirable output performance which is robust with respect to variations of speed and CG height which satisfy $\underline{v} \le v \le \overline{v}$ and $\underline{h} \le h \le \overline{h}$. In using Theorem 3.5.1 to obtain a controller which minimizes the level of performance γ_1 for z_1 subject to a specified level of performance γ_2 for z_2, we used an iterative solution algorithm similar to the one described in Appendix B.

Simulations

Here we present three sets of numerical simulations. The first one is the identical obstacle avoidance (elk test) scenario as in the fixed parameter case. Thus, the peak value of the driver steering input was $\delta_p = 100^\circ$ and constant speed was set to be $v = 140km/h$. The results are presented in Figures 3.13 and 3.14, which demonstrate the effectiveness of the controller.

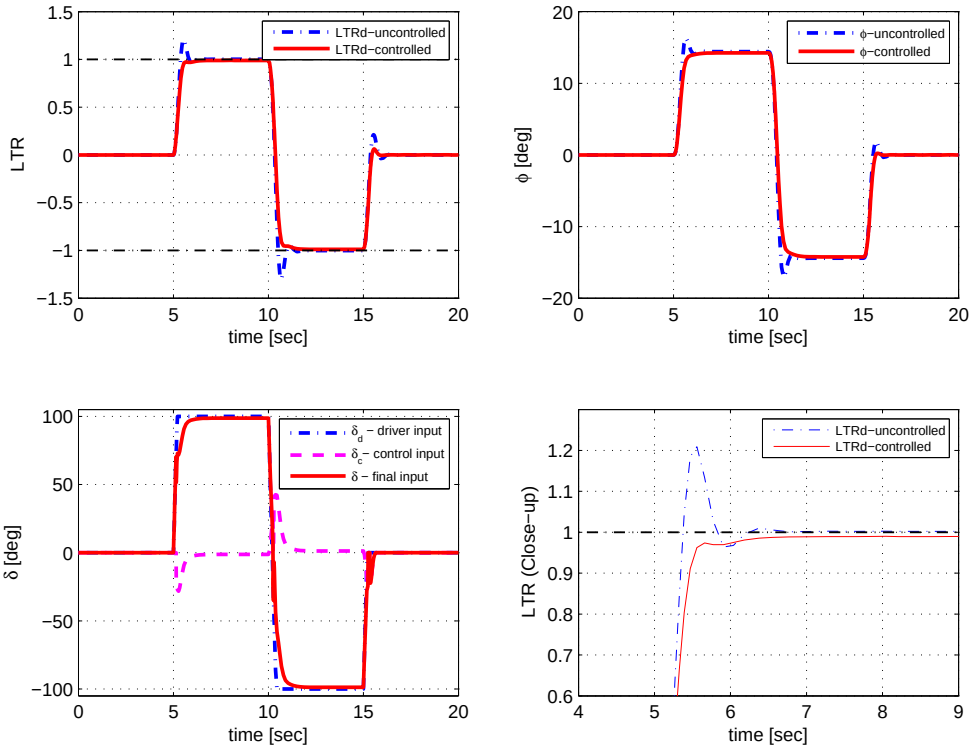

Figure 3.13: Comparison of the robustly controlled (with active steering) and the uncontrolled vehicles ($v = 140km/h$, $\delta_{peak} = 100^\circ$, and $h = 0.375m$).

Comment : From the simulation results of the fixed and the robust controllers for the same maneuver, we observe that both methods are effective in reducing the load transfer ratio LTR_d, and thus preventing rollover. However the robust controller performance is far less

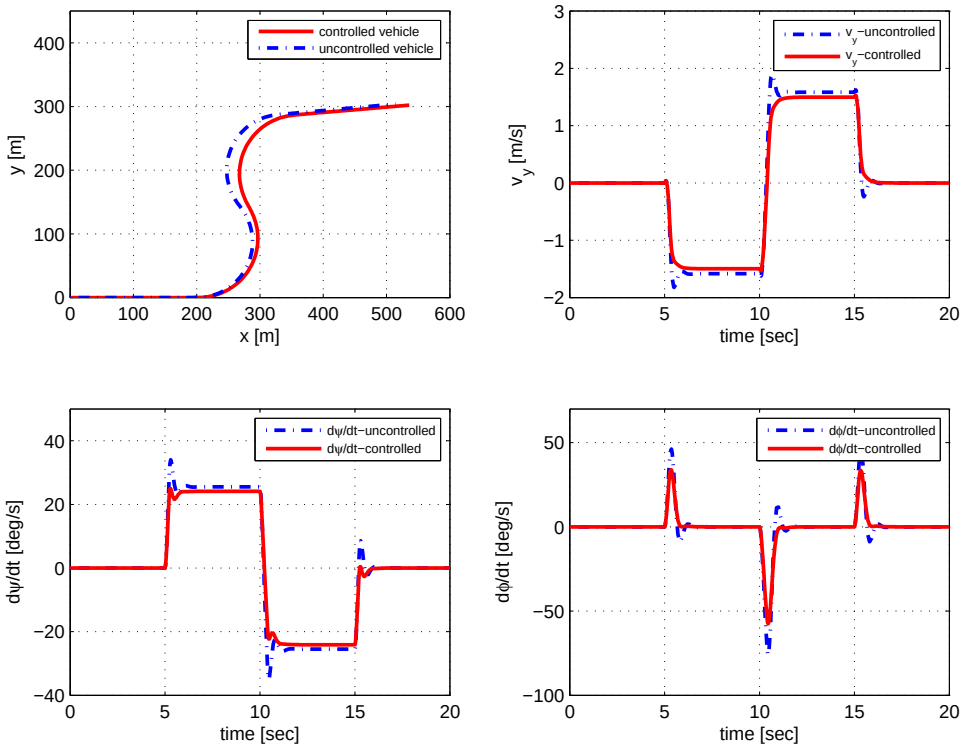

Figure 3.14: Comparison of the trajectories and states of robustly controlled (with active steering) and the uncontrolled vehicles ($v = 140km/h$, $\delta_{peak} = 100^\circ$, and $h = 0.375m$).

conservative. Also notice that driver intervention of the controller by any chosen measure is practically undiscernible by the driver, which is favorable and was one of our aims.

In the second set of numerical simulations, we again tested a similar obstacle avoidance maneuver (elk test) however, this time we set the peak value of the driver steering input as $\delta_p = 150^\circ$ and constant speed was fixed as $v = 70km/h$. Moreover the CG height was selected as $h = 0.45m$. The corresponding simulation results are presented in Figures 3.15 and 3.16, which demonstrate the effectiveness of the controller for varying CG height.

In the third set of numerical simulations, we performed an obstacle avoidance maneuver with a peak driver steering input of $\delta_p = 120^\circ$. Also this time we implemented a rapid

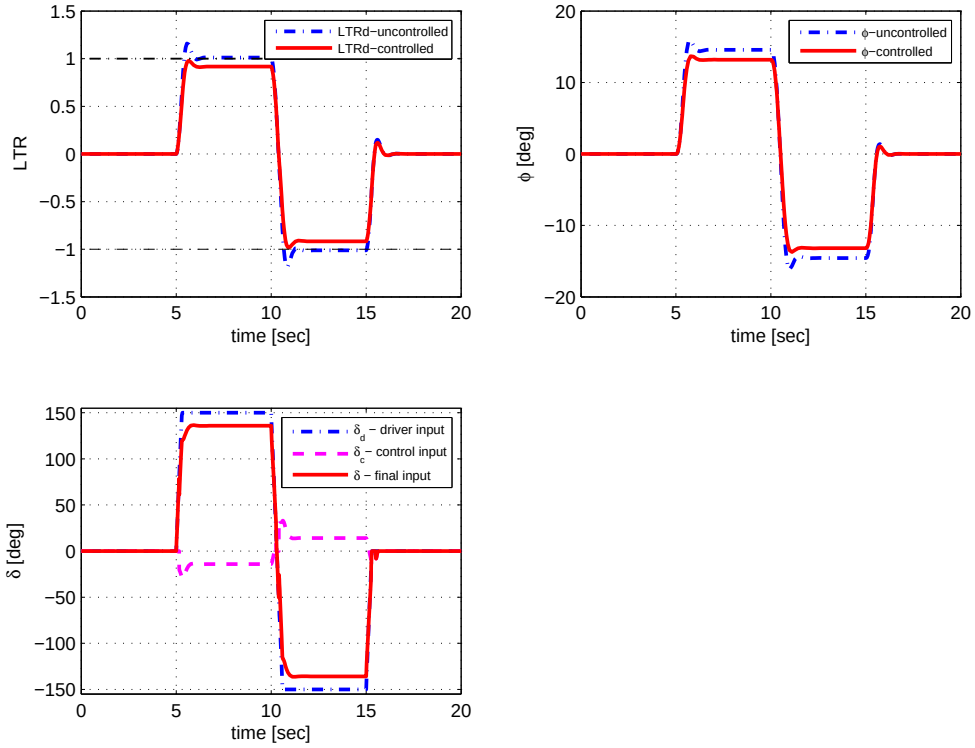

Figure 3.15: Comparison of the robustly controlled (with active steering) and the uncontrolled vehicles ($v = 70km/h$, $\delta_{peak} = 150^{\circ}$, and $h = 0.45m$).

change in velocity from the initial value of $v = 140km/h$, which simulates braking action during the maneuver. In this simulation CG height was fixed to be $h = 0.375m$. The corresponding simulation results are presented in Figure 3.17 and Figure 3.18 demonstrating the effectiveness of the controller design for varying CG height and speed.

Comment : In all the simulation examples we observe that the robust controller is quite effective in reducing the load transfer ratio LTR_d below the safety limits while keeping the controlled states to be sufficiently close to the reference vehicle states. Also notice that driver intervention of the controller is insignificant, which was one of the intended design goals.

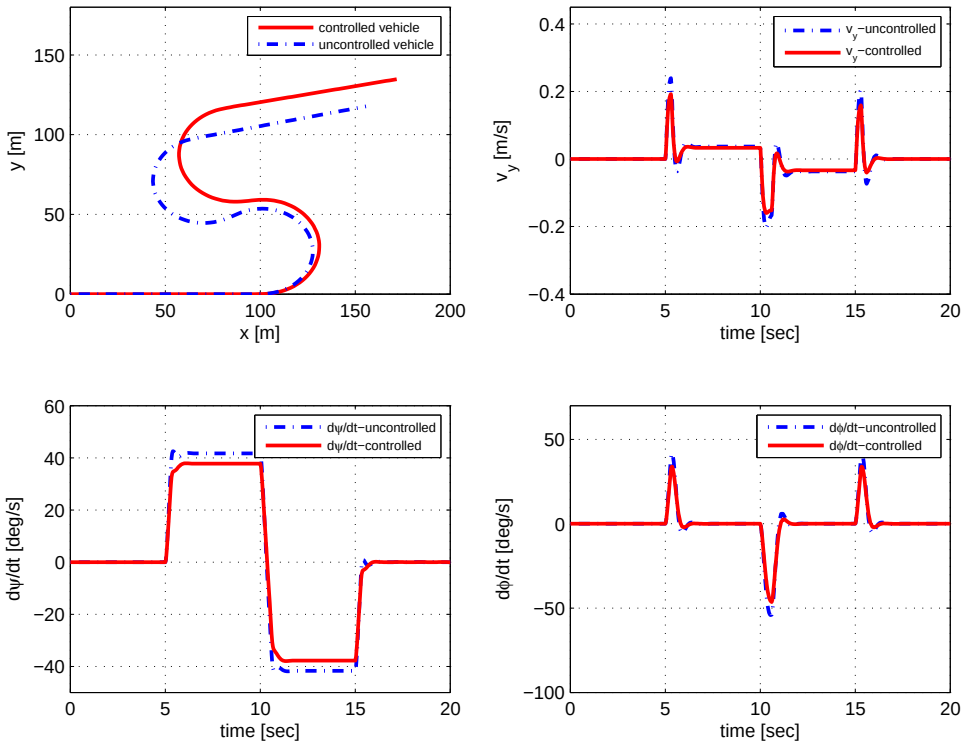

Figure 3.16: Comparison of trajectories and states for robustly controlled (with active steering) and uncontrolled vehicles ($v = 70km/h$, $\delta_{peak} = 150°$, $h = 0.45m$).

3.5.3 Controller mode switch

A basic problem with the aforementioned controllers is that they are always active. That is, they are always attempting to limit the LTR, even in non-critical situations, thus potentially interfering with, and annoying the vehicle driver. It therefore makes sense only to activate the controller in situations where the potential for rollover is significant. Here we introduce one such criterion for controller activation.

The switching method introduced here is based on the Lyapunov function $V(x) = x^T Px$, where the positive definite symmetric matrix P is given by $P = S^{-1}$ and S is obtained when solving the LMIs in the controller design. Ideally, the controller is only activated when

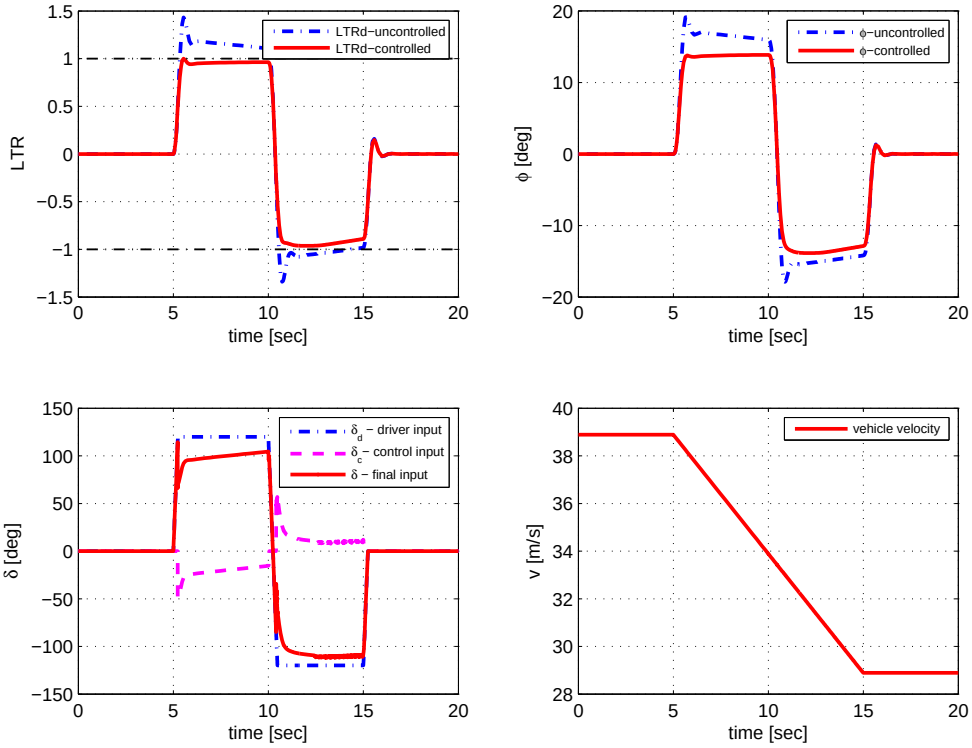

Figure 3.17: Comparison of the robustly controlled (with active steering) and the uncontrolled vehicles ($v_0 = 140km/h$, $\delta_{peak} = 120^\circ$, and $h = 0.375m$).

$V(x)$ reaches some critical value V_{crit}. The critical value is chosen so that $|LTR_d| < 1$ when $V(x) \leq V_{crit}$. In particular, we regulate the controller input according to

$$u = \begin{cases} 0 & \text{if} \quad V(x) \leq V_{crit} - \varepsilon \\ Kx & \text{if} \quad V(x) \geq V_{crit} \end{cases}$$

with V_{crit} chosen to guarantee that the LTR_d is close to one when the controller is activated.

The reasoning behind the above strategy is as follows. Recall from Remark 3.5.5 that our original controller design guarantees that $\dot{V}$, the time rate of change of V along a solution, is negative outside the ellipsoid $\mathscr{E}(\rho_\omega)$ defined in (3.32) where ρ_ω is a bound on the magnitude of the disturbance input. Suppose now that the controller is not activated until $V(x) > V_{crit}$.

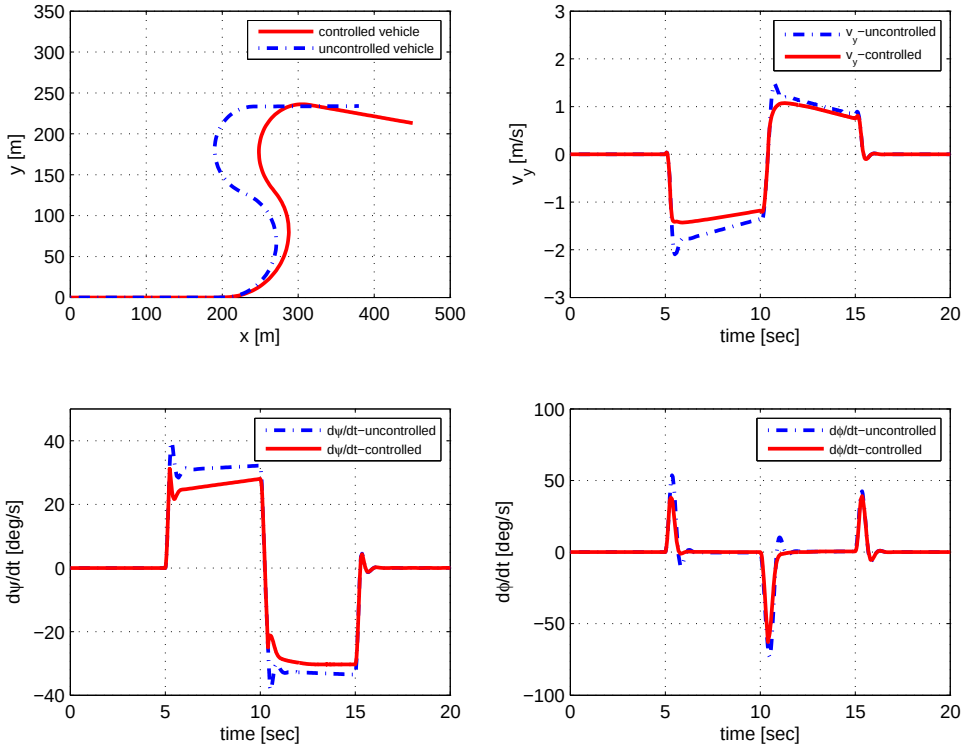

Figure 3.18: Comparison of trajectories and states for robustly controlled (with active steering) and uncontrolled vehicles ($v_0 = 140km/h$, $\delta_{peak} = 120°$,$h = 0.375m$).

Then for driver inputs ω which satisfy $\mu_0\|\omega(t)\|^2 \leq V_{crit}$, the switching controller will guarantee that $\dot{V}$ is negative outside the ellipsoid

$$\mathscr{E}_{crit} := \{x \in \mathbb{R}^n : V(x) \leq V_{crit}\} . \tag{3.60}$$

This in turn guarantees that the ellipsoid is invariant and attractive. In particular, if a state trajectory starts at zero and $\mu_0\|\omega(t)\|^2 \leq V_{crit}$ then, the state trajectory remains within this ellipsoid. Recall also that $\|z_1\| \leq \mu_{11}V(x)$ and $z_1 = LTR_d$; hence, whenever a state trajectory starts at zero and $\mu_0\|\omega(t)\|^2 \leq V_{crit}$, we have that $|LTR_d| \leq \mu_{11}V_{crit}$. By choosing

$$V_{crit} < 1/\mu_{11} , \tag{3.61}$$

we guarantee that the controller turns on before $|LTR_d|$ reaches one, but, the controller does

not switch on for small driver steering inputs. In accordance with standard practice we propose the following continuous switching-type controller to avoid chattering action:

$$u = \zeta(V(x))Kx \qquad \text{where} \qquad V(x) = x^T S^{-1} x \tag{3.62}$$

and

$$\zeta(V) = \frac{1}{2} + \frac{1}{2} sat\left[\frac{2}{\varepsilon}(V - V_{crit}) + 1\right]; \tag{3.63}$$

here *sat* denotes the saturation function and ε is a small positive number. The graph of ζ is depicted in Figure 3.19.

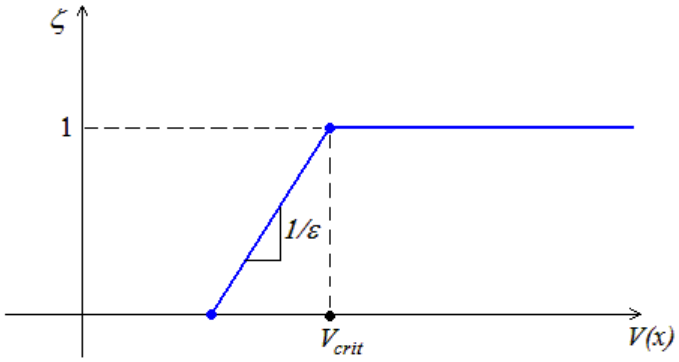

Figure 3.19: Graph of the function ζ.

We demonstrate the performance of the above switching controller with further simulations whose results are illustrated in Figure 3.20. These correspond to an obstacle avoidance maneuver where the peak value of the driver steering input is $\delta_p = 50^\circ$ and the vehicle speed was fixed at $v = 140 km/h$. Notice that although there is no rollover threat in this maneuver, the original linear robust controller was trying to compensate by a very small amount as seen from the actuator input plot. Whereas the robust controller with the suggested switching produces no input and the LTR_d corresponding to the switching controller is identical to that of the uncontrolled vehicle, demonstrating the efficacy of the suggested method.

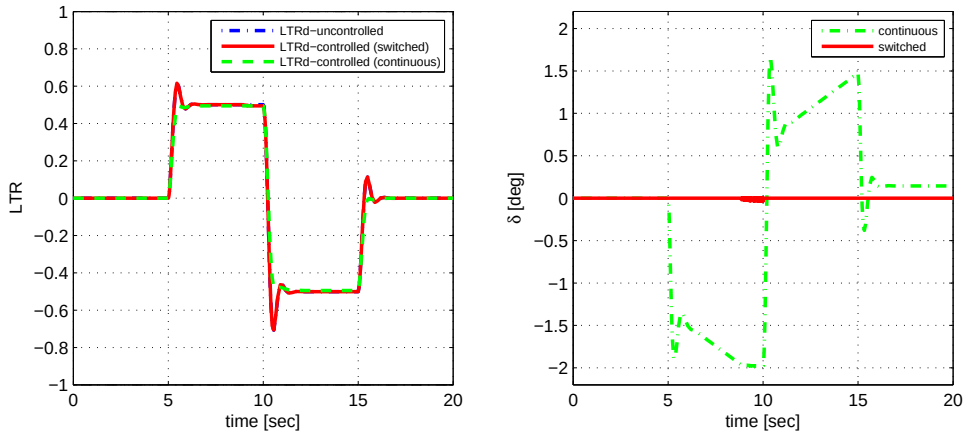

Figure 3.20: Comparison of continuous and switched robust controllers with active steering at a non critical maneuver ($v = 140km/h$, $\delta_{peak} = 50^{\circ}$, and $h = 0.375m$).

3.6 Conclusions and possible future directions

In this chapter, we have presented a methodology for the design of robust vehicle rollover prevention systems using differential braking and active steering actuators. By introducing the load transfer ratio LTR_d, we obtained a system performance output whose value provides an accurate measure for determining the onset of rollover. Our rollover prevention controllers are robust in the sense that they guarantee the peak values of the performance outputs of an uncertain system do not exceed certain values. Simulation results demonstrate the benefits of the proposed approach in a real-life problem. In the case of control design based on differential braking actuators, the results can easily be tested and implemented without much financial overhead, since these actuators already exist in most stock passenger vehicles.

Future work will proceed in several directions. We shall extend the methodology to include active suspension and combinations thereof to refine our rollover prevention strategy, and analyze the resulting control allocation problem. We shall also examine the efficacy of our controllers in the presence of conditions which can result in a tripped rollover. Also, we are

looking into extending these ideas to railroad vehicles. Applications of control strategies with several actuators is not only limited to road and railroad vehicle roll stabilization, but can also be used to make the dynamics of a vehicle emulate those of another vehicle (e.g. having an SUV behave like a sports car), which shall be future direction for this research.

Another strand of work will investigate refinement of the synthesis procedure. In particular, we shall also investigate a gain scheduled control approach based on locally valid fixed models and LMI based controllers as described in this chapter. We shall also investigate whether convergence and feasibility conditions can be developed to determine the existence of control gains to achieve certain pre-specified performance parameters γ_j.

On the practical side of this work, we have scheduled with our industrial partners an evaluation of our control design in real production vehicles.

Comment : A straightforward refinement of the rollover controller synthesis procedure introduced in this chapter can be obtained by utilizing more complex vehicle models such as the 2-track (i.e., 4 wheel) vehicle model [50] and/or nonlinear tire models (e.g., HSRI [22]) in conjunction with the LMI algorithm. We shall consider this extension in the near future.

Chapter 4

A Methodology for Adaptive Rollover Prevention Control Design for Automotive Vehicles

In an attempt to refine the rollover prevention systems introduced in the last chapter, we suggest here an adaptive controller synthesis procedure based on multiple models and switching. We utilize the estimation techniques developed in Chapter 2 to infer the unknown CG height and suspension parameters of the vehicle, which is then used to switch among a paired set of robust controllers. Controller adaptation is a byproduct of the switching action, and it results in higher performance as compared to fixed controllers. Our controllers are based on differential braking, and each one is designed to be robust with respect to varying velocity.

4.1 Chapter contributions

The contribution of this chapter is in implementing the rollover mitigation methodology given in the preceding chapter in conjunction with the MMST framework. This was achieved by combining the vehicle parameter estimation technique introduced Chapter 2, and the robust rollover mitigation methodology introduced in the preceding chapter with a switched estimator-corrector structure. To do this, we formulated the rollover mitigation problem as a bounded input bounded output (BIBO) disturbance rejection problem with switched matrices. In doing so, we viewed the automotive vehicle as an uncertain dynamical system with disturbance inputs, and our controllers guarantee that the performance outputs of the system relevant to rollover are bounded regardless of the parametric switching. As was the case in the preceding chapter, our suggested robust control design method allows vehicle parameter uncertainty to be taken into account in our designs, given that the uncertainty belongs to convex hull.

The work contained in this chapter has resulted in the following publication:

(i) Solmaz S., Akar M., Shorten R., "*Adaptive Rollover Prevention for Automotive Vehicles with Differential Braking*", Under review for 17th IFAC World Congress, Seoul Korea, 2008.

4.2 Introduction

It has been emphasized several times in the preceding chapters that the vehicle CG position plays an important role for the vehicle dynamics and the vehicle road handling behavior. Therefore, the effects of changes in the CG position, or the uncertainty in the knowledge of it, have to be considered for analyzing vehicle dynamics, and must be accounted for in designing active control systems for accident mitigation. However, the difficulty is that this

unknown parameter is not directly measurable and it can vary significantly with changing passenger and loading configurations; such changes are the most severe in large passenger vehicles such as SUVs, which statistically have the highest rate of rollover accidents. With these in mind, we suggested in Chapter 2 a method inspired by the MMST paradigm, for estimating the unknown and unmeasurable parameters of the vehicle including the CG position, and then in Chapter 3, we proposed a robust controller synthesis method that accounts for the parametric uncertainties for the specific problem of automotive rollover prevention. In order to further refine the control design methodology developed in the preceding chapter, we fuse in the current chapter the parameter estimation technique of Chapter 2, and the locally robust rollover prevention design method of the last chapter in a unified switched feedback control implementation for the rollover prevention problem.

As explained in detail in Section 2.3.4, the height of CG along with the lateral acceleration are the most important parameters affecting the rollover propensity of an automotive vehicle; while the vehicle lateral acceleration can be measured directly by sensors, the CG height can not be measured and it needs to be estimated indirectly. One such method for inferring CG height was suggested in Chapter 2. Therefore, we utilize this result for the control strategy advocated in the current chapter with the aim to improve the performance of our active rollover mitigation systems. Specifically, we use multiple identification models for inferring the unknown vehicle CG height developed in Chapter 2, which is then used to switch among a paired set of locally robust rollover prevention controllers that are designed based on the results of Chapter 3. Due to this structure of multiple indirect estimation models and the paired controllers, the suggested feedback implementation is an adaptive control approach for the problem of mitigation of rollover, which involves inherent parametric uncertainties due to the unknown or time varying vehicle parameters.

Our motivation for considering an adaptive controller implementation for the rollover mitigation problem is twofold. Firstly, adaptive controllers are the alternative option to the robust ones and they can potentially provide higher performance. As we have seen in the ro-

bust rollover controller implementation example in the preceding chapter, robust controllers have fixed gains that are chosen considering the worst-case that the plant undergoes; for the rollover problem the worst operating condition translates to operating the vehicle with the highest possible CG position. While choosing the controller gains for the worst-case guarantees the performance (i.e., safety) under the designed extreme operating condition, the feedback performance of the robustly controlled systems under less severe or even normal operating conditions are suboptimal. This is evident from our robust control implementations of the last chapter in that, the suggested controllers were still trying to compensate even when the rollover potential as measured by the "dynamic load transfer ratio" (LTR_d) was insignificant; this is why we considered the switching rule given in Section 3.5.3 to switch the controllers on and off depending on the Lyapunov functions. Although such an on-off switch solution was effective in retaining the expected performance of the vehicle under normal operating conditions (i.e., when the rollover risk is small), the suboptimal performance of the controllers for varying rollover accident scenarios was still an issue, which can potentially be addressed by adaptation. The second motivation for considering the adaptive feedback design for the rollover prevention problem is related to the time constant of rollover accidents, which is on the order of seconds (sometimes even a fraction of a second) and is usually accepted to be quite small (see for example [25] for a discussion of this). While conventional adaptive controllers are known to have slow convergence rates and large transient control errors when the initial parameter errors are large [77], [78] (a factor that renders these control approaches unsuited for use in rollover mitigation applications), utilization of MMST type algorithms [14] may overcome these problems and provide high performance adaptive controllers. Therefore, when improving the controller performance and speed for the rollover problem is considered, MMST framework becomes an ideal choice as it can provide a rapid identification of the unknown parameters as part of the closed loop implementation. In this respect, we consider the vehicle parameter estimation methods developed in Chapter 2 in conjunction with a multiple model switched controller implementation. This way we can rapidly switch to a controller that is optimal

for the maneuver and the vehicle operating conditions, thus improving the overall safety of the vehicle without sacrificing its performance.

The robust controller design described in the sequel is based on differential braking actuators only, where each of the n proposed switched controllers based on differential braking actuator has a linear feedback structure with a fixed gain matrix K_η, where $\eta \in \{1,2,...,n\}$. The choice of the control actuator is motivated by the desire to aid the exposition of the multiple model switched control implementation, as the resulting controllers are of simple proportional type. However, the extension of the results of this chapter to the proportional-integral type active steering actuator based rollover prevention controller suggested in Chapter 3 as well as other alternative control approaches is a straightforward practice.

Similar to the analysis in Chapter 3, we view the automotive vehicle as an uncertain system with a number of performance outputs and subject to a bounded disturbance input. For each performance output z_j, a performance measure γ_{η_j} guarantees that the magnitude of the output is less than or equal to the maximum of γ_{η_j} times the peak value of the magnitude of the disturbance, for all $\eta \in \{1,2,...,n\}$. For each of the switched controllers we utilize a controller design procedure, similar to the one introduced in the preceding chapter, to minimize the performance level for one main output while keeping the performance levels for the other outputs below some prespecified levels. Each of the switched controllers is robust in the sense that it ensures performance in the presence of any allowable uncertainty which was taken into account in the control design. In applying these results to the rollover problem, we consider the driver steering input as a disturbance input. Since we wish to keep the magnitude of LTR_d less than one, we view this as the main performance output. To limit the amount of control effort and to accommodate actuator constraints, we choose the control input as an additional performance output in the feedback design. Also, we design each of the switched controller gains to be robust with respect to changing velocity, which is motivated by the fact that the differential braking actuators reduce the vehicle velocity. This change should be taken into account in the control design as the vehicle velocity directly

affects the vehicle dynamics; this is why we consider incorporating a robustness criteria with respect to changing velocity, which was possible with the aid of the design methodology developed in Chapter 3. Eventually, our controllers are designed to keep the peak magnitude of LTR_d less than one, which is the criterion for preventing rollover occurrence as it is equivalent to preventing one-side wheel lift off. Also, as compared to the control designs of the preceding chapter we can do this in a less conservative fashion with the help of the switching among a set of locally robust controllers, which we demonstrate by a numerical example.

4.3 Vehicle modelling

For the multiple model switched controller design that shall be described in the following sections, we utilize two separate vehicle models that we have already developed in the preceding chapters; these are the second order roll plane model, and the single track model with roll degree of freedom and with differential brake input. While we use the roll plane models for estimating the unknown CG height of the vehicle in real time, we utilize the single track model with roll degree of freedom for designing switched and locally robust control gain matrices for use with the state feedback controllers based on the differential braking actuator. As both of these models have been described in detail in the preceding chapters, we just give the resulting models in the following discussion along with references to earlier sections.

Roll plane model

We use the roll plane model given here and derived in Section 2.3.2 for the realtime estimation of CG height based on the multiple model switching framework, details of which were described in Chapter 2. The 2-state roll plane model is the simplest model capturing the roll

dynamics of an automotive vehicle and it is free from the effects of uncertainties originating from unknown tire stiffness parameters; we emphasize that this a factor that makes the roll plane model suitable for the real time estimation of unknown CG position.

Under the small angles assumption, and with reference to Figure 2.2, the equations of motion describing the roll plane dynamics can be expressed in the following 2^{nd} order state space form

$$\begin{bmatrix} \dot{\phi} \\ \ddot{\phi} \end{bmatrix} = \begin{bmatrix} 0 & 1 \\ -\frac{k-mgh}{J_{x_{eq}}} & -\frac{c}{J_{x_{eq}}} \end{bmatrix} \cdot \begin{bmatrix} \phi \\ \dot{\phi} \end{bmatrix} + \begin{bmatrix} 0 \\ \frac{mh}{J_{x_{eq}}} \end{bmatrix} a_y, \tag{4.1}$$

where a_y is the lateral acceleration and g is the gravitational acceleration. As a simplifying assumption for the derivation of the model, it was assumed that relative to the ground, the sprung mass rolls about a fixed horizontal roll axis along the centerline of the vehicle body at the ground level. For further description of the parameters appearing in the equation refer to Table 3.1. Also, $J_{x_{eq}}$ above denotes the equivalent roll moment of inertia as described in (2.9).

Single track model with roll degree of freedom and differential brake input

We use this model with the active differential braking input to design locally robust state feedback controllers. Denoting β as the sideslip angle of the vehicle, and with reference to Figure 3.1, the equations of motion corresponding to this model are given as follows

$$\dot{x} = Ax + B_\delta \delta + B_u u \quad \text{with} \tag{4.2}$$

$$A = \begin{bmatrix} -\frac{\sigma J_{xeq}}{m J_{xx} v} & \frac{\rho J_{xeq}}{m J_{xx} v^2} - 1 & -\frac{hc}{J_{xx} v} & \frac{h(mgh-k)}{J_{xx} v} \\ \frac{\rho}{J_{zz}} & -\frac{\kappa}{J_{zz} v} & 0 & 0 \\ -\frac{h\sigma}{J_{xx}} & \frac{h\rho}{J_{xx} v} & -\frac{c}{J_{xx}} & \frac{mgh-k}{J_{xx}} \\ 0 & 0 & 1 & 0 \end{bmatrix}, \tag{4.3}$$

$$B_\delta = \begin{bmatrix} \frac{C_v J_{xeq}}{m J_{xx} v} & \frac{C_v l_v}{J_{zz}} & \frac{h C_v}{J_{xx}} & 0 \end{bmatrix}^T, \quad B_u = \begin{bmatrix} 0 & -\frac{T}{2J_{zz}} & 0 & 0 \end{bmatrix}^T, \tag{4.4}$$

where $x = \begin{bmatrix} \beta & \dot{\psi} & \dot{\phi} & \phi \end{bmatrix}^T$ is the state, and u represents the total effective differential braking force acting on the wheels; it is positive if braking is on the right wheels and negative if braking is on the left wheels. Differential braking force as the control input is depicted in Figure 3.3. Further notations and parameters appearing in (4.3) and (4.4) are described in Table 3.1. Also, for further details of the derivation of this model refer to Section 3.4.1.

In order to model the change in the vehicle longitudinal speed as a result of the braking force, we assume that the longitudinal wheel forces generated by the engine counteract the rolling resistance and the aerodynamic drag at all times. Under this assumption, the vehicle speed is approximately governed by

$$\dot{v} = -\frac{|u|}{m}. \tag{4.5}$$

Comment: A detailed discussion of the rationale for using differential braking actuators for the rollover mitigation problem was given in Section 3.4.3. In the same section, further assumptions on the known and unknown vehicle parameters appearing in the models above have been discussed. Also it has been mentioned earlier that the potential of rollover occurrence is measured by LTR_d, which was derived and explained in detail in Section 3.4.2. As it will be utilized in the following discussion, we give here the resultant expression for LTR_d in terms of the states of the single track model with roll degree of freedom, which is

$$LTR_d \quad = \quad Cx \qquad \text{where} \qquad C = \begin{bmatrix} 0 & 0 & \frac{2c}{mgT} & \frac{2k}{mgT} \end{bmatrix}. \tag{4.6}$$

4.4 Adaptive rollover control design with multiple models & switching based on differential braking actuators

In this section we describe an approach for combining the CG estimation method given in Chapter 2 with the robust state feedback rollover prevention control design methodology

developed in Chapter 3. We note that the adaptive control implementation given here is inspired, at large, by the MMST control framework developed by Narendra et al. in a series of publications [77, 84, 78, 85, 79, 14]. In the MMST control framework, each identification model is paired-up with a controller as shown in Figure 1.4, and based on a performance index of the identification errors a model/controller pair is chosen to control the plant at every instant. In this chapter we consider a version of this control strategy for obtaining high performance rollover prevention controllers.

Our LMI based multiple switched controller design methodology is unique in the sense that it enables us to synthesize locally robust controllers to account for the changing vehicle speed as described in detail in Section 3.5.1. In doing so, we utilize a variation of the iterative numerical procedure given in Appendix B to guarantee the robustness of the switched controllers. Also, in order to improve the overall controller performance, we switch among multiple fixed controllers (where each is locally robust with respect to changing velocity) based on the real time estimation of the CG height and the suspension parameters. We emphasize that in this controller implementation, adaptation is a byproduct of the switching itself.

4.4.1 Switched state feedback control

We utilize a variation on the LMI based design methodology developed in Chapter 3 to obtain a set of robust rollover prevention controllers using the differential braking as the sole control input. In order to explain this in detail, we shall first express our control design procedure in terms of a generic switching state space system given, which is parameterized in terms of a parameter vector θ

$$\dot{x} = A_\eta(\theta)x + B_\eta(\theta)\omega + B_{u,\eta}(\theta)u \tag{4.7}$$

$$z_j = C_{j,\eta}(\theta)x + D_{j,\eta}(\theta)\omega + D_{ju,\eta}(\theta)u, \quad j = 1,\ldots,r\ , \tag{4.8}$$

where the vector $x(t) \in \mathbb{R}^{n_x}$ is the state at time $t \in [0,\infty)$ and $\omega(t) \in \mathbb{R}^{n_\omega}$ is a bounded disturbance input. Also $u(t) \in \mathbb{R}^{n_u}$ is the control input and $z_j(t) \in \mathbb{R}^{p_j}$ are the performance outputs. The index $\eta \in \{1,2,\ldots,n\}$ represents discrete switches in the system matrices. We assume that parameter vector θ captures the plant parametric uncertainty, which can depend on t, x, ω and u. Moreover, we have the following assumption that is required by the plant uncertainty θ to be satisfied.

Assumption 4.4.1 *For each $\eta \in \{1,2,\ldots,n\}$, and $j \in \{1,2,\ldots,r\}$ the matrix sextuple*

$$\begin{bmatrix} A_\eta(\theta) & B_\eta(\theta) & B_{u,\eta}(\theta) & C_{j,\eta}(\theta) & D_{j,\eta}(\theta) & D_{ju,\eta}(\theta) \end{bmatrix}$$

belongs to the convex hull of a finite number of N matrix sextuples below

$$\begin{bmatrix} A_{1,\eta} & B_{1,\eta} & B_{u_1,\eta} & C_{j_1,\eta} & D_{j_1,\eta} & D_{ju_1,\eta} \end{bmatrix}, \ldots$$
$$\ldots, \begin{bmatrix} A_{N,\eta} & B_{N,\eta} & B_{u_N,\eta} & C_{j_N,\eta} & D_{j_N,\eta} & D_{ju_N,\eta} \end{bmatrix}.$$

This implies that for each $\eta \in \{1,2,\ldots,n\}$, and $j \in \{1,2,\ldots,r\}$, there exists non-negative scalars $\xi_1,\ldots,\xi_N$ such that $\sum_{i=1}^N \xi_i = 1$ and

$$A_\eta(\theta) = \sum_{i=1}^N \xi_i A_{i,\eta}, \qquad B_\eta(\theta) = \sum_{i=1}^N \xi_i B_{i,\eta}, \qquad B_{u,\eta}(\theta) = \sum_{i=1}^N \xi_i B_{u_i,\eta},$$
$$C_{j,\eta}(\theta) = \sum_{i=1}^N \xi_i C_{j_i,\eta}, \quad D_{j,\eta}(\theta) = \sum_{i=1}^N \xi_i D_{j_i,\eta}, \quad D_{ju,\eta}(\theta) = \sum_{i=1}^N \xi_i B_{ju_i,\eta}.$$

Note that for each $\eta \in \{1,2,\ldots,n\}$ this assumption is the analogue of Assumption 3.5.1.

Now, we wish to synthesize stabilizing switching state feedback controllers, which prevent the peak values of the performance outputs exceeding certain values. In doing so, for each output z_j we introduce a measure of performance γ_{η_j}, which guarantees that the magnitude of that output is less than or equal to γ_{η_j} times the peak value of the magnitude of the disturbance. In order to achieve this, we base our controller on the following theorem that is analogous to Theorem 3.5.1 and is the main result of this chapter.

Theorem 4.4.1 *Consider the system described by (4.7)-(4.8) and satisfying Assumption 4.4.1. Suppose that there exist an invertible matrix $S = S^T > 0$ (with $P = S^{-1}$), matrices L_η, scalars $\beta_{\eta_1}, \ldots, \beta_{\eta_N} > 0$ and $\mu_{\eta_0}, \mu_{\eta_{1j}}, \mu_{\eta_{2j}} \geq 0$, for all $j = 1, \ldots, r$ and $\eta \in \{1, 2, \ldots, n\}$, such that the following matrix inequalities hold*

$$\begin{bmatrix} \beta_{\eta_i}(SA_{i,\eta}^T + A_{i,\eta}S + L_\eta^T B_{u_i,\eta}^T + B_{u_i,\eta}L_\eta) + S & \beta_{\eta_i}B_{i,\eta} \\ \beta_{\eta_i}B_{i,\eta}^T & -\mu_{\eta_0}I \end{bmatrix} \leq 0, \tag{4.9}$$

$$\begin{bmatrix} -\mu_{\eta_{1j}}S & 0 & SC_{ji,\eta}^T + L_\eta^T D_{ju_i,\eta}^T \\ 0 & -\mu_{\eta_{2j}}I & D_{ji,\eta}^T \\ C_{ji,\eta}S + D_{ju_i,\eta}L_\eta & D_{ji,\eta} & -I \end{bmatrix} \leq 0, \tag{4.10}$$

for all $i = 1, \ldots, N$, $j = 1, \ldots, r$ and $\eta \in \{1, 2, \ldots, n\}$. Then the switched state feedback controllers

$$u_\eta = K_\eta x \qquad with \qquad K_\eta = L_\eta S^{-1} \tag{4.11}$$

result in a switched nonlinear/uncertain closed loop system, which has the following properties.

(a) For each $\eta \in \{1, 2, \ldots, n\}$, the undisturbed system (4.7) with $\omega = 0$, is globally exponentially stable. That is, all state trajectories decay exponentially.

(b) The undisturbed closed loop switching system $\dot{x} = A_\eta(\theta)x + B_{u,\eta}(\theta)u$ is quadratically stabilizable with switched controllers $u(t) \in \{u_1, u_2, \ldots, u_n\}$.

(c) If the disturbance input is bounded, that is, $\|\omega(t)\| \leq \rho_\omega$ for all $t \geq 0$ then, for zero initial state, the performance outputs $z_1, \ldots, z_r$ of the closed loop system are bounded and satisfy

$$\|z_j(t)\| \leq \left[\arg \max_{\eta=1,\ldots,n} \gamma_{\eta_j}\right] \rho_\omega \tag{4.12}$$

for all $t \geq 0$ where

$$\gamma_{\eta_j} = \sqrt{\mu_{\eta_0}\mu_{\eta_{1j}} + \mu_{\eta_{2j}}}, \quad for \quad \eta \in \{1, 2, \ldots, n\} \tag{4.13}$$

which implies the L_∞ stability of the closed loop switched system (4.7)-(4.8).

Proof of Theorem 4.4.1: As a first observation, we note that for each $\eta \in \{1,2,\ldots,n\}$ this theorem analogous to Theorem 3.5.1. Thus for the constituent systems the result is given by Theorem 3.5.1. Accordingly, properties (a) and (c) above, directly follow from Appendix A. Specifically inequality (4.12) results from the fact that the maximum element of $\{\gamma_{1_j}, \gamma_{2_j}, \ldots, \gamma_{n_j}\}$ determines the upper bound on the performance outputs $\|z_j(t)\|$ for each $j = 1,\ldots,r$. Next we show that property (b) holds.

The undisturbed system associated with (4.7) can be expressed by

$$\dot{x} \quad = \quad A_\eta(\theta)x + B_{u,\eta}(\theta)u \tag{4.14}$$

for each $\eta \in \{1,2,\ldots,n\}$. This undisturbed feedback system is said to be quadratically stabilizable via linear state feedback [91] if a Lyapunov solution (or Lyapunov matrix) $P = P^T > 0$ and controller $u_\eta = K_\eta x$ exist along with a positive definite and symmetric matrix $Q = Q^T > 0$ such that

$$2x^T P(A_\eta(\theta) + B_{u,\eta}(\theta)K_\eta)x \leq -x^T Qx \tag{4.15}$$

for all $t \in \mathbb{R}$, $x \in \mathbb{R}^{n_x}$ and $\eta \in \{1,2,\ldots,n\}$. From Assumption 4.4.1, for each $t \in \mathbb{R}$ and θ we can express each of the matrices $A_\eta(\theta)$, and $B_{u,\eta}(\theta)$ as a convex combination of N matrices as follows

$$A_\eta(\theta) = \sum_{i=1}^{N} \xi_i A_{i,\eta}, \qquad B_{u,\eta}(\theta) = \sum_{i=1}^{N} \xi_i B_{u_i,\eta}, \tag{4.16}$$

where $\xi_1, \xi_2, \ldots, \xi_N$ are scalars such that $\Sigma_{i=1}^{N} \xi_i = 1$. Based on this observation, quadratic stabilizability condition (4.15) can be expressed as

$$A_{i,\eta}^T P + PA_{i,\eta} + K_\eta^T B_{u_i,\eta}^T P + PB_{u_i,\eta}K_\eta < 0 \quad for \quad i = 1,2,\ldots,N \tag{4.17}$$

where $\eta \in \{1,2,\ldots,n\}$. Pre and post multiplying this inequality by $S = P^{-1}$ and substituting $L_\eta = K_\eta S$ then yields the following quadratic stabilizability condition in terms of S and L_η

$$SA_{i,\eta}^T + A_{i,\eta}S + L_\eta^T B_{u_i,\eta}^T + B_{u_i,\eta}L_\eta < 0 \quad for \quad i = 1,2,\ldots,N \tag{4.18}$$

where $\eta \in \{1,2,\ldots,n\}$. We note that this last condition is a necessary condition for inequality (4.9) of the theorem. This establishes the quadratic stability of the undisturbed system (4.14) for each $\eta \in \{1,2,\ldots,n\}$. We emphasize that the quadratic stability of the undisturbed system (4.14) implies the *Bounded-Input, Bounded-Output* (BIBO) stability of the system with bounded disturbance inputs [102].

Therefore the nonlinear/uncertain system given with equations (4.7)-(4.8) in compliance with Assumption 4.4.1 is L_∞ stable[1] by Theorem A.0.1 of Appendix A.

Q.E.D.

In the sequel we give the implementation of Theorem 4.4.1 to the switched adaptive rollover controller design based on differential braking actuators.

4.4.2 Adaptive rollover control design

In applying the Theorem 4.4.1 to the rollover prevention problem, we utilize both the simple roll plane model and the single track model with roll degree of freedom with differential brake input, as described in Section 4.3. We consider the driver steering input as a disturbance input. Also, since we wish to prevent rollover of the vehicle, our switched controllers are designed to keep the peak magnitude of the load transfer ratio less than one, which implies preventing one-side wheel lift-off, and thus avoiding rollover. Therefore, we view the dynamic load transfer ratio LTR_d given in (4.6) as the main performance output. Also, in order to limit the amount of control effort as well as to accommodate actuator constraints, we choose the control input as a secondary performance output in the feedback design. Moreover, as an integral part of our design, we consider the switched controller gains to be robust with respect to changing velocity, which is motivated by the fact that the differential

[1] this is similar to the definition of input/output stability (IOS) in [126], with the exception that it takes into account the initial state. See Appendix A for the precise definition of L_∞ stability.

braking actuators reduce the vehicle velocity. This change should be taken into account in the control design as the vehicle velocity directly affects the vehicle dynamics; this is why we consider incorporating a robustness criterion in the controller design for changing velocity, which is possible with the aid of the Theorem 4.4.1.

The switched multiple model control structure is schematically shown in Figure 4.1, where there are n identification models driven by the same plant output, which are paired up with n locally robust state feedback controllers. In what follows, we first describe the switched identification algorithm as a control switching criterion, and then give the implementation of the stable switched adaptive rollover controller design utilizing differential braking actuators and making use of Theorem 4.4.1.

(a) Controller switching criteria

As explained in detail in the preceding chapters, the height of CG along with the lateral acceleration are the most important parameters affecting the rollover propensity of an automotive vehicle; while the vehicle lateral acceleration can be measured directly by sensors, the CG height can not be measured and it needs to be estimated indirectly. Here we use multiple identification models for inferring the unknown vehicle CG height along with the relevant suspension parameters in real time, as developed in Chapter 2, which is then used as a criterion to switch among a paired set of locally robust rollover prevention controllers. We emphasize that due to this structure of multiple indirect estimation models and the paired controllers, the suggested feedback implementation is an adaptive control approach for the problem of mitigation of rollover, which involves inherent parametric uncertainties due to the unknown and/or time varying vehicle parameters.

The identification models are based on the 2^{nd} order roll plane model (4.1) and are mainly used to determine the unknown CG height of the vehicle. The estimation models are obtained by varying the uncertain model parameters within bounded intervals and at a finite

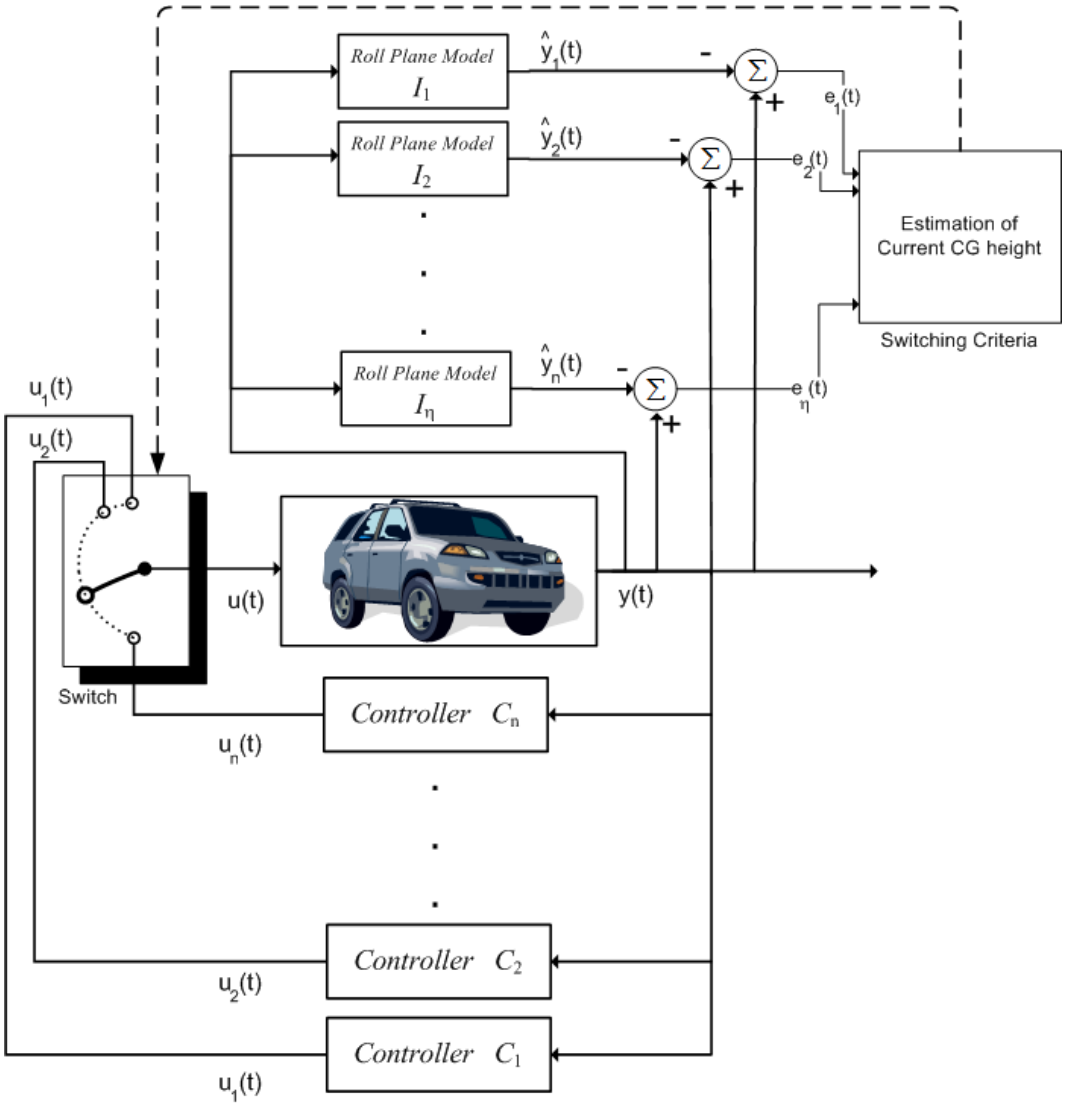

Figure 4.1: Multiple model switched adaptive control structure.

number of grid points, where the uncertain parameters are the CG height h, linear roll spring stiffness k, and the roll damping coefficient c. Specifically, each of the unknown parameters is assumed to belong to a closed uncertainty interval such that $h \in \mathscr{H}$, $k \in \mathscr{K}$, and $c \in \mathscr{C}$, where each interval contains a finite number of grid points so that they can be represented as $\{h_1, h_2, h_3, \ldots, h_p\} \subset \mathscr{H}$, $\{k_1, k_2, k_3, \ldots, k_q\} \subset \mathscr{K}$, and $\{c_1, c_2, c_3, \ldots, c_d\} \subset \mathscr{C}$ with dimensions p, q and d respectively. Then $n = p \times q \times d$ different identification models are formed

corresponding to the cross combinations of the grid points in the parameter space. Utilizing (4.1) the equations of motion corresponding to each model I_ζ can be represented as below

$$I_\zeta : \quad \begin{bmatrix} \dot{\phi}_\zeta \\ \ddot{\phi}_\zeta \end{bmatrix} = \begin{bmatrix} 0 & 1 \\ -\frac{k_\zeta - mgh_\zeta}{J^\zeta_{x_{eq}}} & -\frac{c_\zeta}{J^\zeta_{x_{eq}}} \end{bmatrix} \cdot \begin{bmatrix} \phi_\zeta \\ \dot{\phi}_\zeta \end{bmatrix} + \begin{bmatrix} 0 \\ \frac{mh_\zeta}{J^\zeta_{x_{eq}}} \end{bmatrix} a_y, \tag{4.19}$$

where $\zeta = 1,2,\ldots,n$ denotes the identification model number and

$$J^\zeta_{x_{eq}} = J_{xx} + mh^2_\zeta$$

is the equivalent roll moment of inertia. We assume that all models have zero initial conditions such that $\phi_\zeta(0) = 0$, and $\dot{\phi}_\zeta(0) = 0$, for $\zeta = 1,2,\ldots,n$. Note that the zero initial conditions physically correspond to starting the identification algorithm at a straight driving state, where the roll angle ϕ, and the roll rate $\dot{\phi}$ of the vehicle are both zero. Also note that every model is driven by the same input a_y (lateral acceleration), which is a measured sensor quantity of the vehicle.

Since we are interested in designing state feedback controllers, the state $x = \begin{bmatrix} \beta & \dot{\psi} & \dot{\phi} & \phi \end{bmatrix}^T$ defined earlier, is assumed to be available at all times. Consequently the roll angle ϕ of the vehicle is a measurable quantity. We can then define the identification error for the ζ^{th} roll plane model as the difference between the vehicle's measured roll angle and the corresponding model output; we denote this by e_ζ and compute it from

$$e_\zeta = \phi - \phi_\zeta, \quad for \quad \zeta = 1,2,\ldots,n. \tag{4.20}$$

Next we compute the MMST cost function (a function of the identification error for each model) described in detail in Section 2.4.1, and repeated below

$$J_\zeta(t) = \alpha||e_\zeta(t)|| + \beta \int_0^t e^{-\lambda_f(t-\tau)}||e_\zeta(\tau)||d\tau, \tag{4.21}$$

where $\zeta = 1,2,\ldots,n$ and $\alpha,\beta \geq 0$ are scalars controlling the relative weights on instantaneous and cumulative identification error measures. Also λ_f denotes the forgetting factor.

Switching among the models and choosing the one with the minimum cost based on the criterion below

$$\eta(t) = \arg \min_{\zeta=1,\ldots,n} J_\zeta(t), \tag{4.22}$$

yields the model with the minimum cumulative error; we denote the minimum cumulative error by $J_\eta(t)$, and the corresponding selected model parameters by k_η, c_η and h_η, which represent the vehicle in the parameter space described by $\mathscr{K}$, $\mathscr{C}$ and $\mathscr{H}$, respectively. Based on the certainty equivalence principle[2], the selected model with the estimated CG height h_η, and linear suspension parameters k_η, c_η is then used to switch to a paired locally robust linear state feedback controller $\mathbf{C}_\eta \in \{\mathbf{C_1}, \mathbf{C_2}, \ldots, \mathbf{C_n}\}$, where

$$\mathbf{C}_\eta : \qquad u_\eta = K_\eta x, \quad \eta \in \{1, 2, \ldots, n\}. \tag{4.23}$$

Having described the controller switching criteria, we next give the procedure for designing individual robust rollover prevention controllers $\mathbf{C}_\eta$, for the switched controller implementation shown in Figure 4.1. We utilize a control design methodology based on Theorem 4.4.1 to obtain a switched set of locally robust rollover prevention controllers using the differential braking as the sole control input.

(b) Adaptive rollover control implementation based on differential braking

The vehicle model utilized is the single track model with roll degree of freedom and with differential brake input given in (4.2) along with systems matrices (4.3), and (4.4). We consider the driver's steering wheel angle in degrees as the disturbance input ω; this is related to the steering angle δ by

$$\delta = \frac{\pi}{180\,\lambda}\omega \tag{4.24}$$

[2]in the sense of adaptive control, the principle of certainty equivalence from tuning to switching is based on the hypothesis that a small identification error leads to a small tracking error [14],[79]. Therefore using a model that has the closest outputs to those of the plant is likely to yield the best feedback control performance.

where λ is the steering ratio between the steering wheel and the wheels. We wish to synthesize a stabilizing controller corresponding to each CG height setting, which prevents the peak values of the performance outputs exceeding certain values. Our LMI based controller design strategy is used to minimize the performance level for one main output (LTR_d), while keeping the performance level for another output (control input, u) below some prespecified levels. In addition, our controllers are locally robust in the sense that they ensure performance in the presence of any allowable uncertainty in the vehicle speed, which results from the differential braking based controller intervention. Thus, we consider the effect of varying speed in our control design assuming that the speed varies over some prespecified range; we call this the locally robust controller corresponding to each combination of CG height and suspension parameter configurations within the parameter space defined by a finite number of grid points in $\mathscr{K}$, $\mathscr{C}$, $\mathscr{H}$, and is denoted by the index $\eta \in \{1,2,\ldots,n\}$.

As the load transfer ratio is a metric directly related to rollover occurrence (see Section 3.4.2 for the significance of LTR_d in terms of rollover), we set this parameter as the first performance output, that is $z_1 = LTR_d$, where LTR_d is defined as a function of the vehicle states in (4.6). We want to keep $\|z_1\| \leq 1$ for the largest possible steering inputs (i.e., the disturbance inputs), which is equivalent to keeping all the 4 wheels in contact with the road and thus preventing rollover. Also, we consider the magnitude of the braking force u to be limited by the weight mg of the vehicle; so we choose $z_2 = u$ as a second performance output. Note that this is a simple approach for imposing hard actuator constraints in the control design based on differential braking. The resulting system with two performance outputs can be described as follows

$$\begin{aligned} \dot{x} &= A_\eta(t)x + B_\eta(t)\omega + B_u u \\ z_1 &= C_\eta x \\ z_2 &= u, \end{aligned} \tag{4.25}$$

where the switching uncertain system matrices $A_\eta(t)$, $B_\eta(t)$, and switching matrix C_η are

given by

$$A_\eta(t) = \begin{bmatrix} -\frac{\sigma J^\eta_{x_{eq}}}{mJ_{xx}v} & \frac{\rho J^\eta_{x_{eq}}}{mJ_{xx}v^2} - 1 & -\frac{h_\eta c_\eta}{J_{xx}v} & \frac{h_\eta(mgh_\eta - k)}{J_{xx}v} \\ \frac{\rho}{J_{zz}} & -\frac{\kappa}{J_{zz}v} & 0 & 0 \\ -\frac{h_\eta \sigma}{J_{xx}} & \frac{h_\eta \rho}{J_{xx}v} & -\frac{c_\eta}{J_{xx}} & \frac{mgh_\eta - k_\eta}{J_{xx}} \\ 0 & 0 & 1 & 0 \end{bmatrix}, \; B_\eta(t) = \frac{\pi}{180\lambda} \begin{bmatrix} \frac{C_v J^\eta_{x_{eq}}}{mJ_{xx}v} \\ \frac{C_v l_v}{J_{zz}} \\ \frac{hC_v}{J_{xx}} \\ 0 \end{bmatrix} \tag{4.26}$$

and

$$C_\eta \;=\; \begin{bmatrix} 0 & 0 & \frac{2c_\eta}{mgT} & \frac{2k_\eta}{mgT} \end{bmatrix}, \tag{4.27}$$

for each $\eta \in \{1,2,\ldots,n\}$. In order to consider uncertainty arising from changing vehicle velocity in the control design, we assume that the speed is bounded above and below by $\overline{v}$ and $\underline{v}$, respectively, that is, $\underline{v} \le v \le \overline{v}$. Note that the matrices B_u and C_η are independent of vehicle speed whereas the system matrices $A_\eta(t)$ and $B_\eta(t)$ can be expressed as affine linear functions of the time-varying parameters $\theta_1 := 1/v$ and $\theta_2 := 1/v^2$. These parameters are bounded as follows:

$$\underline{\theta}_1 \le \theta_1 \le \overline{\theta}_1, \qquad \underline{\theta}_2 \le \theta_2 \le \overline{\theta}_2 \tag{4.28}$$

where

$$\underline{\theta}_1 = \frac{1}{\overline{v}}, \quad \overline{\theta}_1 = \frac{1}{\underline{v}}, \quad \underline{\theta}_2 = \frac{1}{\overline{v}^2}, \quad \overline{\theta}_2 = \frac{1}{\underline{v}^2}. \tag{4.29}$$

We can also define $\theta = [\ \theta_1,\ \theta_2\ ]^T$ as a 2-vector representing the parameter uncertainty resulting from changing velocity.

$$\begin{aligned} A_{1,\eta} &= \overline{\theta}_1 Y_{1,\eta} + \overline{\theta}_2 Y_{2,\eta} + Y_{3,\eta}, \qquad A_{2,\eta} = \overline{\theta}_1 Y_{1,\eta} + \underline{\theta}_2 Y_{2,\eta} + Y_{3,\eta}, \\ A_{3,\eta} &= \underline{\theta}_1 Y_{1,\eta} + \overline{\theta}_2 Y_{2,\eta} + Y_{3,\eta}, \qquad A_{4,\eta} = \underline{\theta}_1 Y_{1,\eta} + \underline{\theta}_2 Y_{2,\eta} + Y_{3,\eta}, \end{aligned} \tag{4.30}$$

$$\begin{aligned} B_{1,\eta} = B_{2,\eta} &= \tfrac{\pi}{180\lambda} \begin{bmatrix} \frac{C_v J^\eta_{x_{eq}}}{mJ_{xx}} \overline{\theta}_1 & \frac{C_v l_v}{J_{zz}} & \frac{h_\eta C_v}{J_{xx}} & 0 \end{bmatrix}^T, \\ B_{3,\eta} = B_{4,\eta} &= \tfrac{\pi}{180\lambda} \begin{bmatrix} \frac{C_v J^\eta_{x_{eq}}}{mJ_{xx}} \underline{\theta}_1 & \frac{C_v l_v}{J_{zz}} & \frac{h_\eta C_v}{J_{xx}} & 0 \end{bmatrix}^T, \end{aligned} \tag{4.31}$$

where

$$Y_{1,\eta} = \begin{bmatrix} -\frac{\sigma J_{xeq}^{\eta}}{mJ_{xx}} & 0 & -\frac{h_\eta c_\eta}{J_{xx}} & \frac{h_\eta(mgh_\eta - k_\eta)}{J_{xx}} \\ 0 & -\frac{\kappa}{J_{zz}} & 0 & 0 \\ 0 & \frac{h_\eta \rho}{J_{xx}} & 0 & 0 \\ 0 & 0 & 0 & 0 \end{bmatrix}, \quad Y_{2,\eta} = \begin{bmatrix} 0 & \frac{\rho J_{xeq}^{\eta}}{mJ_{xx}} & 0 & 0 \\ 0 & 0 & 0 & 0 \\ 0 & 0 & 0 & 0 \\ 0 & 0 & 0 & 0 \end{bmatrix},$$
$$Y_{3,\eta} = \begin{bmatrix} 0 & -1 & 0 & 0 \\ \frac{\rho}{J_{zz}} & 0 & 0 & 0 \\ -\frac{h_\eta \sigma}{J_{xx}} & 0 & -\frac{c_\eta}{J_{xx}} & \frac{mgh_\eta - k_\eta}{J_{xx}} \\ 0 & 0 & 1 & 0 \end{bmatrix}. \tag{4.32}$$

for each $\eta \in \{1,2,\ldots,n\}$. Note that for each η, it is possible to express both of the uncertain matrices $A_\eta(t)$ and $B_\eta(t)$ as a convex combination of the 4 distinct vertex matrices defined above, i.e.,

$$A_\eta(t) = \sum_{i=1}^{4} \xi_i A_{i,\eta}, \qquad B_\eta(t) = \sum_{i=1}^{4} \xi_i B_{i,\eta},$$

where $\xi_1, \xi_2, \xi_3, \xi_4$ are positive scalars such that $\Sigma_{i=1}^{4} \xi_i = 1$. Thus our system description satisfies Assumption 4.4.1, and therefore we can employ Theorem 4.4.1 to design the switched rollover prevention controllers.

Numerical implementation

Here we present the implementation of the adaptive switching rollover controller design as depicted in Figure 4.1, which takes into account robustness with respect to varying vehicle speed as well as the switches in the CG height of the vehicle. We used the model parameters given in Table 4.1 for the model representing the simulated vehicle dynamics based on the single track model with roll degree of freedom. For the ease of exposition, we considered only the switching in the CG height (h) in our simulations, which can occur as a result of rapid vertical motion of passengers and loads (e.g, loads falling vertically due the inertial

forces exerted during a cornering maneuver). Note that we considered the linear suspension parameters c, and k to be fixed and known parameters in conjunction with the CG height estimation algorithm (i.e., the controller switching logic). For the controller switching algorithm (CG height estimating algorithm) we considered CG height uncertainty to be such that $\{0.5, 0.55, \ldots, 0.85\} \subset \mathscr{H}$, comprising of 8 possible CG height configurations in total. Also we set the free design parameters for the cost function (4.21) as $\alpha = 0.2$ and $\beta = 0.8$, while the forgetting factor λ_f was chosen to be 0. We emphasize that the forgetting factor becomes important if the plant undergoes rapid switches; this is not the case for the CG height uncertainty considered here (where we assume that CG height is unknown and not changing in a finite time horizon), thus we set $\lambda_f = 0$ in the following discussion.

For the design of corresponding velocity-robustified controllers, we assumed that the speed is bounded above and below by $\underline{v} = 20m/s$, and $\overline{v} = 40m/s$, which represents typical freeway driving conditions for a compact passenger vehicle. Then we employed Theorem 3.5.1 based on the system description (4.25) along with the vertex matrices (4.30) and (4.32) to design 8 switched controllers based on switching CG height configurations, denoted by $\eta \in \{1, 2, \ldots, 8\}$, where each locally robust controller guarantees performance levels γ_{η_1} and $\gamma_{\eta_2} = mg\gamma_{\eta_1}$, in the presence of any variations in speed satisfying $\underline{v} \leq v \leq \overline{v}$.

In order to choose the switched controller gains based on Theorem 3.5.1, we utilized a variation of the iterative LMI solution algorithm described in Appendix B with $N = 4$. The algorithm was modified such that it calculates controller gains for the 8 CG height configurations, all of which conform to Theorem 3.5.1 and also share a common Lyapunov solution (CLS) $P = P^T > 0$. In order to obtain the common P matrix, the same LMI algorithm was used for the worst case CG height (i.e., $h_{max} = 0.85$ [m]) as described in the appendix. Then obtained Lyapunov solution P was fixed for the other CG configurations and the iterative LMI algorithm was repeated. As a result we obtained the following 8 controller gain

Table 4.1: Simulation model parameters

parameter	value	unit
m	1300	$[kg]$
g	9.81	$[m/s^2]$
δ_{peak}	150	$[deg]$
λ	18	non-dimensional
J_{xx}	400	$[kg \cdot m^2]$
J_{zz}	1200	$[kg \cdot m^2]$
l_v	1.2	$[m]$
l_h	1.3	$[m]$
L	2.5	$[m]$
T	1.5	$[m]$
h	**0.5**	$[m]$
c	5000	$[kg \cdot m^2/s]$
k	36000	$[kg \cdot m^2/s^2]$
C_v	60000	$[N/rad]$
C_h	90000	$[N/rad]$

matrices

$$
\begin{aligned}
K_{h=0.85} &= [\ -5.9767 \quad 0.9345 \quad 0.2430 \quad 0.4289\ ] \cdot 10^4 \\
K_{h=0.80} &= [\ -6.0000 \quad 1.0179 \quad 0.2078 \quad 0.3171\ ] \cdot 10^4 \\
K_{h=0.75} &= [\ -7.4097 \quad 1.1068 \quad 0.1630 \quad 0.0803\ ] \cdot 10^4 \\
K_{h=0.70} &= [\ -7.6453 \quad 1.1675 \quad 0.1307 \quad 0.0003\ ] \cdot 10^4 \\
K_{h=0.65} &= [\ -7.8537 \quad 1.2186 \quad 0.1009 \quad -0.0565\ ] \cdot 10^4 \\
K_{h=0.60} &= [\ -8.0653 \quad 1.2632 \quad 0.0727 \quad -0.0988\ ] \cdot 10^4 \\
K_{h=0.55} &= [\ -8.2826 \quad 1.3029 \quad 0.0452 \quad -0.1308\ ] \cdot 10^4 \\
K_{h=0.50} &= [\ -8.5039 \quad 1.3384 \quad 0.0182 \quad -0.1554\ ] \cdot 10^4
\end{aligned}
$$

In what follows, we present the simulation results corresponding to the switched control structure shown in Figure 4.1 which utilize the above control gains based on varying CG configurations. In our plots we provide a comparisons of the switched adaptive control with a fixed robust controller, where the robust controller has the fixed gain $K_{h=0.85}$ assuming the worst case CG height of $h = 0.85m$. We also compare the results with uncontrolled single track model with roll degree of freedom.

For the numerical simulations, we used the obstacle avoidance maneuver (elk test) scenario described in Chapter 3 with a peak driver steering input of magnitude $\omega_{max} = 150^\circ$ and with an initial speed of $v = 120km/h$. The steering profile corresponding to this maneuver and the resulting CG height estimation are shown in Figure 4.2. In this figure we note that the CG height estimation does not start until the maneuver is initiated at $t = 5sec$, and till this point (where no maneuver takes place), the worst case CG configuration (i.e., the maximum CG height, $h = 0.85m$) is assumed for safety considerations.

In Figure 4.3 we give the comparison of the vehicle speed and the control force histories

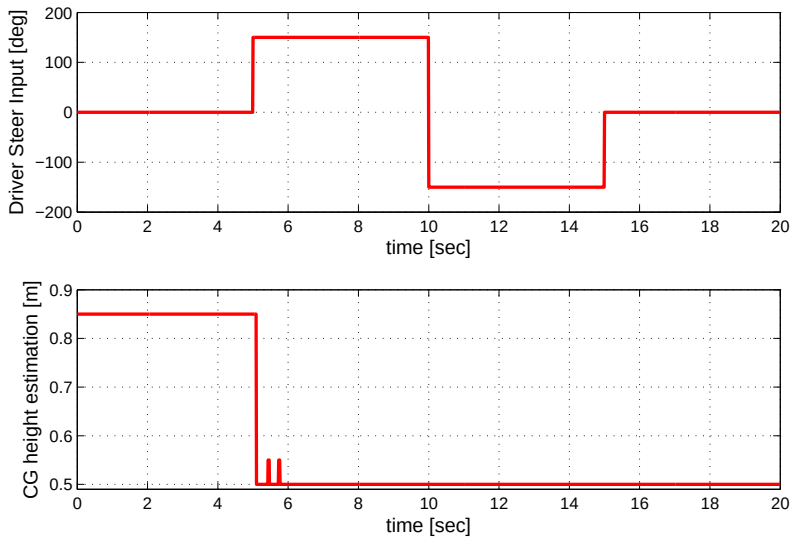

Figure 4.2: Driver steering input and the corresponding real-time estimation of CG height.

corresponding to the switched adaptive controller and the robust controller. Note that the positive control effort indicates a clockwise effective braking torque and the negative one indicates the anti-clockwise, as depicted in Figure 3.3. Also, both the adaptive and the robust controllers result in $|u| \leq mg$ as desired as seen in in Figure 4.3. The dramatic speed drop observed in the controlled vehicles is a direct consequence of the controller braking action. Also notice in the figure that the resulting control actuation profile for the adaptive controller is smaller, which causes a less speed drop of the vehicle compared to the robustly controlled vehicle; this is an indication of the effectiveness of our adaptive control approach.

The corresponding LTR_d plots for both of the robust and the adaptive switched controllers are presented in Figure 4.4. We observe in the figure that, while both of the controllers achieve $|LTR_d| \leq 1$ throughout the maneuver, the LTR_d due to the switched adaptive controller is less conservative than the robust one, which indicates higher performance. Note that this observation is in agreement with the conclusions derived from Figure 4.3. Also notice in this figure that the LTR_d corresponding to the uncontrolled vehicle is close to 2, which is well above the vehicle rollover limit.

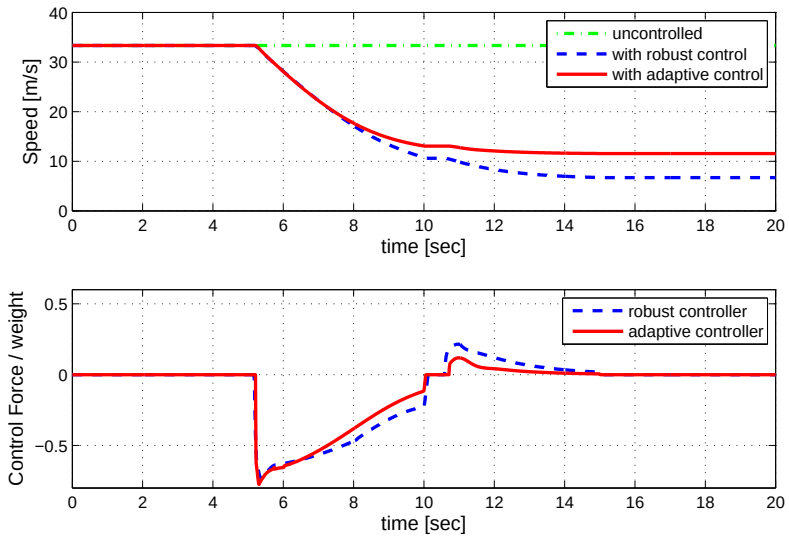

Figure 4.3: Vehicle speed variation and normalized control force history.

In Figure 4.5 we give a further comparison of all the vehicle states corresponding to uncontrolled, robustly controlled and adaptively controlled vehicles.

As a final comparison we look at how the suggested controllers affect the vehicle path. To do this, we note that the coordinates (x, y) of the vehicle CG relative to the road satisfy

$$\dot{x} = v\cos(\beta + \psi), \tag{4.33}$$

$$\dot{y} = v\sin(\beta + \psi), \tag{4.34}$$

where we choose the initial coordinates $(x(0), y(0))$ to be zero. In Figure 4.6 the CG trajectories over the horizontal plane (representing the road plane) for the controlled and the uncontrolled vehicles are compared. Notice here that the shorter paths of the controlled vehicles are due to slowing down as a result of braking.

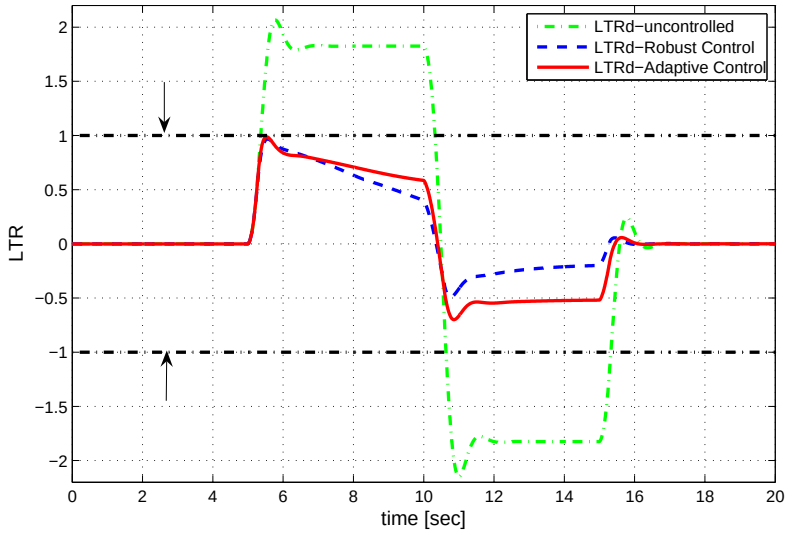

Figure 4.4: Comparison of LTR_d for the controlled and uncontrolled vehicles.

4.5 Conclusions and possible future directions

In this chapter, we have presented a methodology for the design of switched adaptive vehicle rollover prevention control systems using differential braking actuators. We suggested using real time estimation of CG height as well as suspension parameters as a controller switching criteria. We designed our rollover prevention controllers to be locally robust in the sense that they guarantee the peak values of the performance outputs to be bounded in the presence of parametric uncertainties in the system. We demonstrated our control designs with numerical simulations and compared them with fixed robust controllers. The results indicate performance gains with the proposed adaptive switched control approach over the robust controller alternative. We emphasize that due to the chosen control actuator (i.e., differential braking), our suggested control designs can easily be implemented and tested without much financial overhead, since these actuators already exist in most stock passenger vehicles.

Future work will proceed in several directions. We shall extend the methodology to include

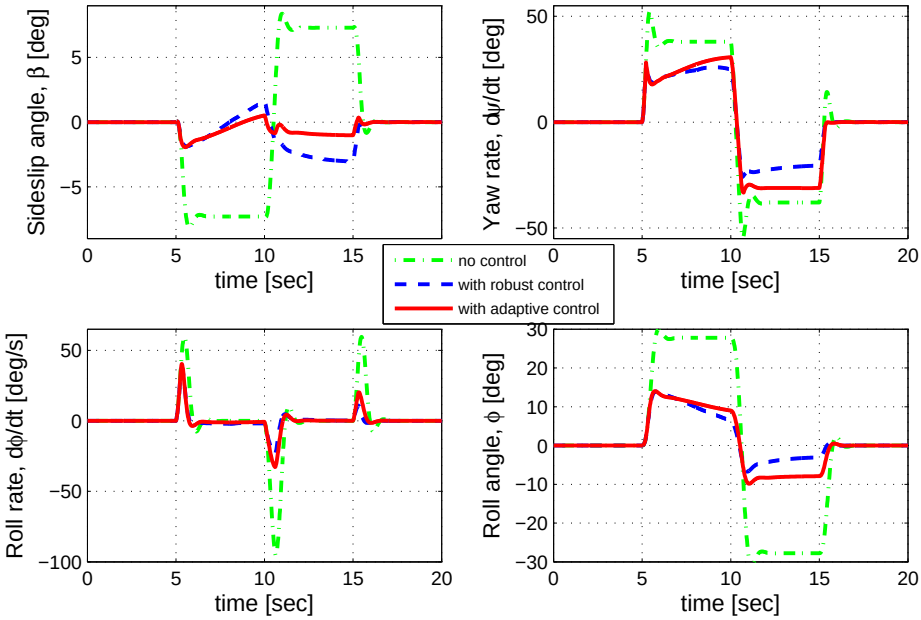

Figure 4.5: Comparison of the controlled and uncontrolled vehicle states.

active steering, active suspension, and combinations thereof to refine our rollover prevention strategy, and analyze the resulting control allocation problem. Applications of such a control strategy with several actuators are not limited to road vehicle stabilization, but it can also be used to make the dynamics of a vehicle emulate those of another vehicle (e.g. having an SUV behave like a sports car), which shall be future direction for this research.

On the practical side of this work, we are planning to evaluate the suggested switched controller design in real production vehicles.

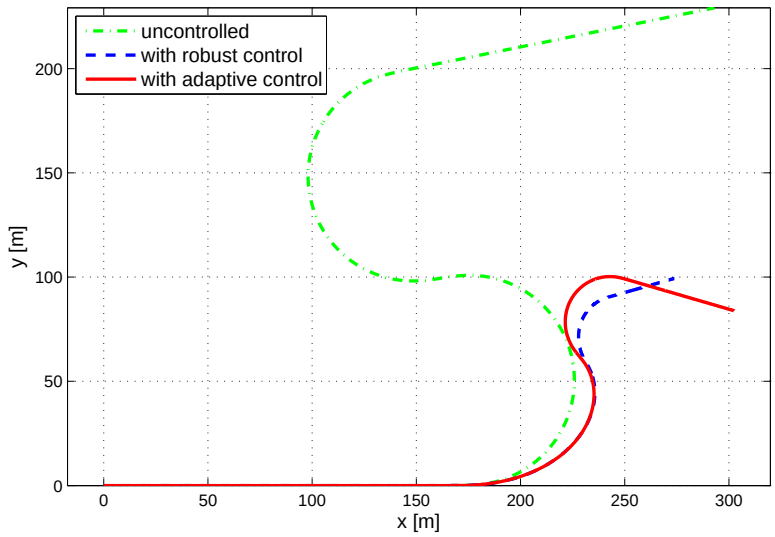

Figure 4.6: Comparison of the controlled and uncontrolled vehicle trajectories over the horizontal plane.

Chapter 5

A Pole Placement Design Methodology for Switched Discrete Time Linear Systems with Applications to Automotive Roll Dynamics Control

In this chapter we consider the asymptotic stability of a class of discrete-time switching linear systems, where each of the constituent subsystem is Schur stable. We first present an example to motivate our study, which illustrates that the bilinear transform does not preserve the stability of a class of discrete time switched linear systems. Consequently, continuous time stability results cannot be transformed to discrete time analogs using this transformation. We then present a subclass of discrete-time switching systems, that arise frequently in practical applications, with globally asymptotic origin. We show that global

attractivity can be established without requiring the existence of a common quadratic Lyapunov function (CQLF). Utilizing this result we present synthesis procedures to construct switching stabilizing controllers for two separate problems in automotive control; the first problem is related to the stabilization of road vehicle roll dynamics subject to changes in the center of gravity (CG) height. The second problem concerns the design of PID tracking controllers for emulating reference roll dynamics while guaranteeing transient free switching as well as stability due to varying CG height. The efficacy of our designs is demonstrated by numerical simulations.

5.1 Chapter contributions

The scientific contribution of this chapter over the state of the art is threefold. Firstly, we showed by means of a simple example that the bilinear transform does not preserve the stability properties of linear time-varying systems. This implies that the asymptotic stability of certain type of switching discrete time systems does not necessarily follow from the continuous time systems with this property, and that their stability must be investigated using a 'first principles approach'. Based on this conclusion, the second contribution of the chapter is the extension of a recent stability result for a class of continuous time switched systems to discrete time. We provided a rigorous proof of this using a non-Lyapunov approach and showed that the conditions for stability of this specific system class do not simply follow from the existing continuous time results in the literature. The final major contribution of this chapter is the application of these theoretical results for practical control design laws for switched systems. In particular, we formulated the motion of the automotive roll dynamics as a switched dynamical system, where the switching was assumed to be caused by changing CG height. Then we utilized active suspension actuators to design controllers for two separate problems for this dynamical system: driver experience enhancement and the

roll dynamics emulation (i.e., reference trajectory following). We showed that for both of these problems, our synthesis procedures guarantee that the switched closed loop system is stable under arbitrary switching.

The work contained in this chapter has resulted in the following publications:

(i) Solmaz S., Shorten R., O'Cairbre F., "*A global attractivity result for a class of switching discrete-time systems*", American Control Conference, July 11-13, 2007.

(ii) Solmaz S., Shorten R., Wulf K., O'Cairbre F., "*A design methodology for switched discrete time linear systems with applications to automotive roll dynamics control*", Automatica, Accepted for Publication, November 2007.

(iii) Solmaz S., Shorten R., "*A discrete time stable switched control design methodology for automotive roll dynamics tracking based on pole placement*", Under Review for American Control Conference, Seattle, Washington, 2008.

5.2 Introduction

Many control problems that arise in automotive engineering lead naturally to solutions that involve switching between a set of stabilizing controllers. Examples include ABS control [95], speed control systems [118], and robust rollover systems [124], [125]. In this chapter we consider two such problems, where switching arises naturally due to changes in the vehicle parameters. Both problems are related to the design of feedback controllers to regulate the roll degree of freedom of an automotive vehicle making use of active suspension actuators. In one implementation we look into design of robust switched controllers that prevent instabilities due to abrupt changes in the center of gravity position. In a second implementation we consider tracking of a reference state related to roll dynamics, and in doing so we again design our controllers to guarantee that possible changes in center of gravity position do not cause any instabilities.

Typically, switched linear controllers are designed using linear matrix inequalities (LMIs); for example see Chapter 3 as well as [124], and [125] for examples of such designs for automotive rollover prevention control applications. More often than not, LMI based control system design is based on quadratic Lyapunov functions, and is iterative in nature, requiring multiple searches before a controller satisfying certain performance criteria is found, as should be clear from Chapter 3. It is known that the existence of a common quadratic Lyapunov function (CQLF) is sufficient, but not necessary, to guarantee the exponential stability of the linear discrete-time switching system of the form

$$x(k+1) = A_i x(k),\ A_i \in \mathscr{A}, \tag{5.1}$$

where $\mathscr{A} \triangleq \{A_1, ..., A_m\}$ with Schur stable constituent matrices $A_i \in \mathbb{R}^{n\times n}$ for $i \in \{1, ..., m\}$, and $x(k) \in \mathbb{R}^n$. Design methods that are constructive, in the manner of pole placement, say, for linear systems, are generally not available for the design of switched systems. One such method was however initially proposed in [112]. Here, for continuous time systems, the authors prove that sets of system matrices that are Hurwitz stable, for which every matrix pair is simultaneously triangularizable, and which have real eigenvalues amongst other conditions, result in linear switched systems that are globally uniformly exponentially stable.

The basic problem addressed here is to study the discrete time analog of this system class. To show that this is not a trivial exercise we present the following example.

Example 5.2.1 Consider the following stable LTI systems,

$$\Sigma_{A_i} : \dot{x} = A_i x, \quad A_i \in \mathbb{R}^{3\times 3}, \tag{5.2}$$

with, matrices

$$A_1 = \begin{bmatrix} -19 & 0 & 0 \\ 0 & -9 & 0 \\ 0 & 0 & -0.25 \end{bmatrix}, \qquad A_2 = \begin{bmatrix} -19 & 0 & 0 \\ -10 & -9 & 0 \\ -18.75 & 0 & -0.25 \end{bmatrix},$$

$$A_3 = \begin{bmatrix} -19 & 0 & 18.75 \\ 0 & -9 & 8.75 \\ 0 & 0 & -0.25 \end{bmatrix}.$$

These three matrices all share the same eigenvalues, and they satisfy the conditions of the Theorem given in [112]. Therefore, one can conclude that the continuous time switched system (5.2) is stable. Now consider the bilinear mapping [70] (or “Tustin" transform) below

$$A_{d,i} = (A_i - I)^{-1}(A_i + I), \qquad i \in \{1,2,3\},$$

where $I \in \mathbb{R}^{3\times 3}$ is the identity matrix. The resulting discrete time matrices are

$$A_{d,1} = \begin{bmatrix} 0.9 & 0 & 0 \\ 0 & 0.8 & 0 \\ 0 & 0 & -0.6 \end{bmatrix}, \qquad A_{d,2} = \begin{bmatrix} 0.9 & 0 & 0 \\ 0.1 & 0.8 & 0 \\ 1.5 & 0 & -0.6 \end{bmatrix},$$

$$A_{d,3} = \begin{bmatrix} 0.9 & 0 & -1.5 \\ 0 & 0.8 & -1.4 \\ 0 & 0 & -0.6 \end{bmatrix}.$$

It is sufficient to show that there exists a switching sequence between the matrices $\{A_{d,1}, A_{d,2}, A_{d,3}\}$ such that the resulting system

$$\Sigma_{A_{d,i}} : x(k+1) = A(k)x(k) \quad \text{for} \quad A(k) \in \{A_{d,1}, A_{d,2}, A_{d,3}\},$$

has eigenvalues outside the unit circle. We simply consider the incremental switching sequence $A_{d,1} \to A_{d,2} \to A_{d,3}$; then the dynamics of the system evolve according to the matrix

product

$$A_d = A_{d,1}A_{d,2}A_{d,3}.$$

Since the eigenvalues of A_d are $\{0.512, -0.081, 1.944\}$, then with one eigenvalue outside the unit circle, this switching sequence is unstable.

Remark 5.2.1 This example shows that, unlike LTI systems, the Bilinear (i.e., Tustin) transform does not, in general, preserve the stability of linear time-varying systems.

This example and the resulting observation has profound implications for control system design. Traditionally, the approach to relate continuous-time linear time invariant (LTI) Hurwitz stability results to discrete-time LTI Schur stability counterparts requires the use of the bilinear transform. However, the above example illustrates that this approach is flawed for designing switched systems. Our example is consistent with the results reported in a recent paper [70]. Here, it is known that while quadratic Lyapunov functions are preserved under the Bilinear transform, other non-quadratic Lyapunov functions are not [70]. Unfortunately, the example demonstrates that matters are much worse than reported in this paper; namely, that **not only are non-quadratic functions not preserved under Bilinear mapping, but also that stability need not be either**.

Fortunately, it is possible to modify the proof in [111] to place additional discrete time conditions on the system matrices to guarantee the global attractivity, and hence the exponential stability [102] of the origin for this system class. This is one of the principal contributions of this chapter. With this background in mind, and making use of the main results given in Section 5.4, we give two distinct examples of stabilizing controller design as applied to aforementioned automotive control problems; this is another major contribution of the current chapter, where we consider switching stability as well as transient free switching (i.e., bumpless transfer) as a design criteria for problems related to roll dynamics control. Specifically, the first problem that is the main motivation for the study in the current chapter, is related to stabilization of the roll motion in automotive vehicles, which can be

modelled with discrete-time switching dynamical modes; this is introduced in Section 5.5. The switching in roll dynamics occurs as a result of changes in the center of gravity (CG) height during fast cornering maneuvers, which can happen as a result of vertical load shifts (i.e. loads falling and/or moving vertically). The second problem introduced in Section 5.6 is about reference tracking controller design for the switched roll dynamics problem, which can be used to emulate the roll behavior of a given reference vehicle while guaranteeing switching stability. We give a proportional-integral-derivative (PID) controller synthesis procedure for this problem. We also give numerical simulations for both of the applications that demonstrate the efficacy of our controller synthesis procedures.

5.3 Definitions

In this section we give simple concepts and definitions, which are useful in the remainder of the chapter. Although some of these concepts have been utilized in previous chapters, we state them here for added convenience.

(i) ***The switching system*** : Consider the discrete time linear time-varying system

$$x(k+1) = A(k)x(k), \tag{5.3}$$

where $x(k) \in \mathbb{R}^n$, and where the system matrix $A(k)$ is such that it switches between the matrices $A_i \in \mathbb{R}^{n\times n}$ belonging to the set $\mathscr{A} = \{A_1, ..., A_m\}$. We shall refer to this as *the switching system*. The time-invariant discrete time linear system $x(k+1) = A_i x(k)$, denoted Σ_{A_i} is referred to as the i^{th} *constituent system*.

Suppose the dynamics of the discrete-time switched system (5.3) is described by the α^{th} constituent linear time invariant system starting at the discrete time step k_α, where $1 \leq \alpha \leq m$ such that $x(k+1) = A_\alpha x(k)$ over the discrete time interval $[k_\alpha, k_\alpha + s]$. By definition, the next system that we switch to, say the γ^{th} system ($1 \leq \gamma \leq m$) starts at the end of s number of discrete time steps, that is at $k_\alpha + s$, with initial

conditions equal to the terminal conditions of the α^{th} system at the discrete time step $k_\alpha + s$.

(ii) ***(Uniform) Stability of the origin*** : The origin of the discrete-time system (5.3) is an equilibrium state. The equilibrium state (origin) is said to be stable if for every $\varepsilon > 0$ and $k_0 \geq 0$, there exists a $\delta(\varepsilon, k_0) > 0$ such that $\| x_0 \| < \delta(\varepsilon, k_0)$ implies that $\| x(k; x_0, k_0) \| < \varepsilon$, $\forall\, k \geq k_0$.

(iii) ***Attractivity of the origin*** : The equilibrium state (origin) of (5.3) is said to be attractive if for some $\rho > 0$, and for every $\theta > 0$ and k_0, there exists a number $T(\theta, x_0, k_0)$ such that $\| x_0 \| < \rho$ implies that $\| x(k; x_0, k_0) \| < \theta$, $\forall\, k \geq k_0 + T$.

(iv) ***Global attractivity of the origin*** : The equilibrium state (origin) of (5.3) is said to be globally attractive if $\lim_{k\to\infty} x(k; x_0, k_0) = 0$, for all initial conditions x_0 and for all $k_0 \geq 0$. Global attractivity of the origin implies that all trajectories starting in any given neighborhood of the origin will eventually approach the origin.

(v) ***(Uniform) Asymptotic stability*** : The equilibrium state of (5.3) is said to be asymptotically stable if it is both stable and attractive.

(vi) ***(Uniform) Exponential stability*** [102]: The equilibrium state of Equation (5.3) is said to be exponentially stable if there exists a finite positive constant $\gamma > 1$ and a constant $0 \leq \lambda < 1$, such that

$$\| x(k; x_0, k_0) \| < \gamma \lambda^{k - k_0} \| x_0 \|, \tag{5.4}$$

for all $k \geq k_0$. Note that “uniformity" here means that γ and λ are independent of k_0.

In the study of switching systems it is often of interest to establish stability under arbitrary switching. For this case uniformity requires that the parameters $\varepsilon, \delta, \gamma, \lambda$ are independent of the switching signal.

A useful technique for establishing the exponential stability of the system (5.3) is to look for the existence of a Lyapunov function.

(vii) ***Common quadratic Lyapunov function (CQLF)*** [112]: Consider the switching system defined in (5.3) where all the elements of $\mathscr{A}$ are Schur stable. The quadratic function

$$V(x) = x^T P x, \;\; P = P^T > 0, \;\; P \in \mathbb{R}^{n \times n}, \tag{5.5}$$

is said to be a CQLF for each of the constituent subsystems Σ_{A_i}, $i \in \{1, ..., m\}$, if the symmetric positive matrix P is a solution for the Stein inequality

$$A_i^T P A_i - P < 0. \tag{5.6}$$

The existence of a common quadratic Lyapunov function implies the exponential stability of the switching system (5.3).

(viii) ***Pairwise Triangularizability*** [112]: We will refer to pairwise triangularizable matrices later in the chapter. Let a switching system described by (5.3) be given. Suppose that a number of non-singular matrices T_{ij} exist, such that for each pair of matrices $\{A_i, A_j\}$ in $\mathscr{A}$, where $i, j \in \{1, ..., m\}$ and $i \neq j$, the pair of matrices $\{T_{ij} A_i T_{ij}^{-1}, T_{ij} A_j T_{ij}^{-1}\}$ are upper triangular. Then every distinct pair of matrices $\{A_i, A_j\}$ in $\mathscr{A}$ are called pairwise triangularizable. In general, pairwise triangularizability is not sufficient for the existence of a CQLF for the switched system (5.3).

(ix) ***Linear Systems***: It is well known for continuous and discrete time linear systems that global uniform attractivity (GUA) of the origin implies global uniform exponential stability (GUES) [40]. Thus establishing GUA of the origin is enough to establish GUES.

5.4 Stability of a class of discrete-time linear switched systems

While the ultimate objective of this chapter is to obtain the conditions for the global attractivity and stability of the origin of a class of systems defined with (5.1) (where any two A_i matrices can be simultaneously triangularized), for the purpose of exposition we consider a subclass of such systems, where amongst other conditions, the A_i matrices in $\mathscr{A}$ are diagonalizable, and where any two of the A_i matrices share at least $n-1$ real linearly independent eigenvectors. Note here that the assumption of diagonalizability is motivated by the examples that we wish to consider in sections 5.5 and 5.6. Under these conditions, the origin of the switching system is globally attractive as verified in the following theorem.

Theorem 5.4.1 *Let $\mathscr{V} = \{v_1, \ldots, v_{n+1}\}$ be a set of real vectors, where each $v_i \in \mathbb{R}^n$ for $i = \{1,2,...,n+1\}$. Suppose any choice of n vectors in $\mathscr{V}$ are linearly independent. For each $i \in \{1,2,\ldots,n+1\}$, we construct $M_i \in \mathbb{R}^{n\times n}$ matrices as follows*

$$M_i = \begin{cases} [v_1, v_2, \ \ldots \ , v_{n-1}, v_n] & for \qquad i = 1 \\ [v_1, ..., v_{n+1}, v_i, ..., v_n] & for \quad 2 \leq i \leq n+1 \end{cases}, \tag{5.7}$$

i.e., M_i is obtained by replacing the $(i-1)^{th}$ column in M_1 with the vector v_{n+1}. Suppose we also have p different diagonal matrices $D_1, D_2, \ldots, D_p$ in $\mathbb{R}^{n\times n}$ with all diagonal entries in the right half of the unit circle, i.e., for every diagonal entry $\lambda_{h,j}$ of D_h, we can write

$$0 < \lambda_{h,j} < 1, \quad for \quad 1 \leq h \leq p, \ \ 1 \leq j \leq n. \tag{5.8}$$

We now define the matrices $A_{h,i} \in \mathbb{R}^{n\times n}$ as follows

$$A_{h,i} = M_i D_h M_i^{-1}, \tag{5.9}$$

and let $\mathscr{A}$ be the set of all $A_{h,i}$ for $h \in \{1,2,...,p\}$ and $i \in \{1,2,...,n+1\}$. Then for the switching system (5.1) with the set $\mathscr{A}$ defined as above, the origin is globally attractive.

Proof of Theorem 5.4.1: As a first observation, we note that the set $\mathscr{A}$ with elements as defined in (5.9) consists of m different diagonalizable matrices $A_{h,i}$, where $m = p(n+1)$. Also note that the eigenvalues of $A_{h,i} \in \mathscr{A}$ are the diagonal entries of D_h, which were all assumed to be in the right half of the unit circle, while the eigenvectors of $A_{h,i}$ are the linearly independent columns of $M_i \in \mathbb{R}^{n\times n}$. A further observation is that M_i matrices as defined in (5.7) are formed by n distinct linearly independent elements of the set $\mathscr{V}$, which consists of a total $n+1$ real n-vectors, i.e., $v_i \in \mathbb{R}^n$ for $i \in \{1,2,...,n+1\}$. Then any choice of two matrices in $\mathscr{A}$ will share at least $n-1$, and at most n common linearly independent real eigenvectors. For ease of exposition we divide the proof that follows into three distinct steps to arrive at the global attractivity result of the origin for (5.1).

Step-1 : In this step we replace the $n \times n$ matrices M_j and $A_{h,i} \in \mathscr{A}$ by $(n+1)\times(n+1)$ matrices $\bar{M}_j$ and $\bar{A}_{h,i}$, respectively. The matrices $\bar{A}_{h,i} \in \bar{\mathscr{A}} \triangleq \{\bar{A}_{h,i} : A_{h,i} \in \mathscr{A}\}$ are chosen such that there is at least one common eigenvector $\tau \triangleq (\ 1 \quad 0 \quad \dots \quad 0\ )^T$ for all the matrices in $\bar{\mathscr{A}}$, and also such that the properties of the solutions of the dynamic system

$$\bar{x}(k+1) = \bar{A}(k)\bar{x}(k), \quad \bar{A}(k) \in \bar{\mathscr{A}}, \tag{5.10}$$

will ultimately imply the global attractivity of the origin of the system (5.1), where $x(k) = (x_1(k),...,x_n(k))$ and $\bar{x}(k) = (x_{n+1}(k),x_1(k),...,x_n(k))$. In what follows, we first give a technical lemma which helps us construct the augmented matrices $\bar{M}_j \in \mathbb{R}^{(n+1)\times(n+1)}$ in the higher dimensional state space.

Lemma 5.4.1 [112]: *Let $\mathscr{V} = \{v_1,\dots,v_{n+1}\}$ be a set of real vectors with each $v_i \in \mathbb{R}^n$ for $i = \{1,2,...,n+1\}$. Suppose any choice of n vectors in $\mathscr{V}$ are linearly independent. Then there exists a positive number "a" such that the set $W = \{(a,v_1),(1,v_2),(1,v_3),\dots,(1,v_{n+1})\}$ is linearly independent in $\mathbb{R}^{n+1}$. Here (a,v_1) is the vector with $n+1$ coordinates, whose first coordinate is "a" and remaining n coordinates are the n coordinates of v_1.*

See [112] for a proof of this lemma. Making use of this lemma we now define matrices $\bar{M}_i \in \mathbb{R}^{(n+1)\times(n+1)}$ with a special structure such that they embed the $M_i \in \mathbb{R}^{n\times n}$ matrices

defined in (5.7) as follows

$$\bar{M}_i = \begin{bmatrix} 1 & b & 1 & 1 & \dots & 1 \\ 0 & & & & & \\ 0 & & & & & \\ 0 & & & M_i & & \\ \vdots & & & & & \\ 0 & & & & & \end{bmatrix}, \quad b = \begin{cases} 1 & if \quad i = 2 \\ a & if \quad i \neq 2 \end{cases}, \tag{5.11}$$

where $i \in \{1, 2, \dots, n+1\}$, and "$a$" is a scalar as defined in Lemma 5.4.1. This structure for $\bar{M}_i$ was used to ensure that its columns are linearly independent for each i. Note that the change in the value of b is necessary as the vector v_1 does not appear in M_i when $i = 2$. Also notice that the columns of $\bar{M}_i$, apart from the first column, are the vector elements of the set W defined in Lemma 5.4.1 and thus they are linearly independent.

We shall use $\bar{M}_i^{-1}$ in the following discussion, and given (5.11) it can be expressed as

$$\bar{M}_i^{-1} = \begin{bmatrix} 1 & s_{i,1} & s_{i,2} & \dots & s_{i,n} \\ 0 & & & & \\ 0 & & M_i^{-1} & & \\ \vdots & & & & \\ 0 & & & & \end{bmatrix}, \tag{5.12}$$

for some real numbers $s_{i,1}, s_{i,2}, \dots, s_{i,n}$ that depend on i.

We further define matrices $\bar{D}_h \in \mathbb{R}^{(n+1)\times(n+1)}$, which embed the diagonal matrices $D_h \in \mathbb{R}^{n\times n}$ satisfying (5.8), to be the following set of matrices

$$\bar{D}_h = \begin{bmatrix} 0 & \dots & 0 \\ \vdots & D_h & \\ 0 & & \end{bmatrix}. \tag{5.13}$$

Making use of these newly defined matrices in $n+1$ dimensional real vector space, we now consider an analogue of the expression (5.9) to construct the matrices $\bar{A}_{h,i}$ and the set $\bar{\mathscr{A}}$, which are defined as follows

$$\bar{A}_{h,i} \in \bar{\mathscr{A}} \triangleq \{\bar{A}_{h,i} : A_{h,i} \in \mathscr{A}\}, \quad \textit{where} \tag{5.14}$$

$$\bar{A}_{h,i} \triangleq \bar{M}_i \bar{D}_h \bar{M}_i^{-1} = \begin{bmatrix} 0 & c_{hi,1} & c_{hi,2} & \dots & c_{hi,n} \\ 0 & & & & \\ 0 & & A_{h,i} & & \\ \vdots & & & & \\ 0 & & & & \end{bmatrix}, \tag{5.15}$$

for some real numbers $c_{hi,1}, c_{hi,2}, \dots, c_{hi,n}$ that depend on h and i. Note here that $\tau = \begin{pmatrix} 1 & 0 & \dots & 0 \end{pmatrix}^T$ is a common eigenvector for all the $m = p(n+1)$ number of matrices $\bar{A}_{h,i}$ in $\bar{\mathscr{A}}$. We can now express the $(n+1)^{th}$ order state space system with the augmented matrices $\bar{A}_{h,i} \in \bar{\mathscr{A}}$ as in the following form

$$\begin{pmatrix} x_{n+1}(k+1) \\ x_1(k+1) \\ x_2(k+1) \\ \vdots \\ x_n(k+1) \end{pmatrix} = \bar{A}_{h,i} \begin{pmatrix} x_{n+1}(k) \\ x_1(k) \\ x_2(k) \\ \vdots \\ x_n(k) \end{pmatrix}, \tag{5.16}$$

which according to the special structure assumed for $\bar{A}_{h,i}$ in (5.15), is valid if and only if the following set of equations hold

$$\begin{pmatrix} x_1(k+1) \\ x_2(k+1) \\ \vdots \\ x_n(k+1) \end{pmatrix} = A_{h,i} \begin{pmatrix} x_1(k) \\ x_2(k) \\ \vdots \\ x_n(k) \end{pmatrix} \quad \textit{and} \quad x_{n+1}(k+1) = \sum_{j=1}^{n} c_{hi,j} x_j(k). \tag{5.17}$$

It is apparent from this last equation that the higher dimensional switching system with $n+1$ states explicitly contain the original switching system with n states. We will show in the 3^{rd} step of the proof below that for any solution $\bar{x}(k) = (x_{n+1}(k), x_1(k), x_2(k), \ldots, x_n(k))$ of the augmented switching system (5.16),

$$lim_{k\to\infty}(x_1(k), x_2(k), \ldots, x_n(k)) = 0$$

will be guaranteed for any solution $x(k) = (x_1(k), x_2(k), \ldots, x_n(k))$ of the original switched system (5.1) with the special structure, thus proving global attractivity of the origin.

Step-2 : Now for a given $i \in \{1, 2, \ldots, n+1\}$ we consider the $n+1$ linearly independent columns of $\bar{M}_i$. These form an $n+1$ dimensional coordinate system which includes τ as one of the axes. We consider the projection of the state $\bar{x}(k)$ onto each coordinate systems (columns of $\bar{M}_i$) as the dynamics of the system (5.16) evolve. This projection is given by the vectors

$$g_i(k) = \bar{M}_i^{-1}\bar{x}(k), \quad i = 1, 2, \ldots, n+1, \tag{5.18}$$

at each discrete time step k. We denote the j^{th} component of $g_i(k)$ as $[g_i]_j(k)$ for each $i = \{1, 2, \ldots, n+1\}$. We further define $G(k)$ as the set consisting of the first components of $n+1$ coordinate projections at the discrete time step k as follows

$$G(k) = \begin{pmatrix} [g_1]_1(k) & [g_2]_1(k) & [g_3]_1(k) & \ldots & [g_{n+1}]_1(k) \end{pmatrix}, \tag{5.19}$$

where $[g_i]_1(k)$ denotes the first component of the i^{th} projection vector $g_i(k)$, and it is the projection of $\bar{x}$ onto τ, that is the first column of $\bar{M}_i$ as seen in (5.11).

Now suppose that the system dynamics of the augmented system (5.16) are described by the following LTI discrete-time system

$$\bar{x}(k+1) = \bar{A}_{h,i}\bar{x}(k) \tag{5.20}$$

during some arbitrary discrete time interval $[k_1, k_2]$, where $k_2 = k_1 + s$ for some positive integer s representing the number of discrete time steps. Note that by making use of the

definitions of $\bar{A}_{h,i}$ in (5.15) and the coordinate projections $g_i(k)$ from (5.18), we can express the evolution of this LTI system by

$$g_i(k+1) = \bar{D}_h g_i(k). \tag{5.21}$$

Now we denote $\lambda_{h,m}$ as the m^{th} diagonal element of the $n \times n$ diagonal matrices D_h for some $m \in \{1,2,\ldots,n\}$ and for some $h \in \{1,2,\ldots,p\}$, where p is the total number of diagonal matrices. Notice here that according to the definition (5.13), $\lambda_{h,m}$ is the $(m+1)^{th}$ diagonal element of $\bar{D}_h$. Suppose further that each eigenvalue $\lambda_{h,m}$ is on the right half of the unit circle satisfying (5.8). Under these assumptions, each component of the projection vector (5.21) has the following dynamic characteristics

$$[g_i]_m(k+1) = \begin{cases} 0 & for \quad m = 1 \\ \lambda_{h,m-1}[g_i]_m(k) & for \quad m = 2,3,\ldots,n \end{cases}. \tag{5.22}$$

Given any fixed interval $[k_1,k_2]$ the solutions to above dynamical equations can be expressed as

$$[g_i]_m(k) = (\lambda_{h,m-1})^{k-k_1}[g_i]_m(k_1) \quad for \quad m \neq 1 \tag{5.23}$$

Note here that $[g_i]_1(k)$ is a constant function of the discrete time step k, while each $[g_i]_m(k)$ for $m \neq 1$ varies according to dynamic relationship (5.23) above over the discrete interval $[k_1,k_2]$. We will now look at how the first component of the projection vector, $[g_i]_1(k)$ varies over the discrete intervals when the system matrices $\bar{A}_{h,i}$ switch.

We denote the first component of the projection vector (which is constant) over the discrete interval $[k_2,k_3]$ as $[g_j]_1(k)$. We further define the "distance" $d_{i,j}(k)$ between the first components of the projection vector for the two switching systems as follows

$$d_{i,j}(k) = |[g_i]_1(k) - [g_j]_1(k)|. \tag{5.24}$$

Note that using the following identity

$$g_i(k) = \bar{M}_i^{-1}\bar{M}_j g_j(k), \tag{5.25}$$

one can conveniently calculate the distance $d_{i,j}(k)$ as the first component of the vector

$$|(\bar{M}_i^{-1}\bar{M}_j - I)g_j(k)|,$$

where I is the identity matrix in $\mathbb{R}^{(n+1)\times(n+1)}$. Looking at the structure of the matrix $F_{i,j} = \bar{M}_i^{-1}\bar{M}_j$ for $i \neq j$, we observe that the first-row first-column entry of this matrix is always unity. Next, we give a lemma which establishes that there is only one other nonzero entry in the first row of $F_{i,j}$ matrix.

Lemma 5.4.2 *If we exclude the first column of the matrix $F_{i,j} = \bar{M}_i^{-1}\bar{M}_j$, for $i \neq j$, then there is only one non-zero entry denoted by $c_{i,j,\delta}$ in the first row, where δ is an integer representing the column index. δ depends on the i, j indexes, and the relationship is given as*

$$\delta = \begin{cases} j & when \quad i = 1 \\ i & when \quad i = 2,3,\ldots,n \end{cases}.$$

Note that δ is never 1.

See [112] for a proof of this lemma. Using this lemma and the identity (5.25) it is straightforward to show that

$$[g_i]_1(k) = [g_j]_1(k) + c_{i,j,\delta}[g_j]_\delta(k) \quad for \quad 1 \leq i \leq n+1, \quad i \neq j, \tag{5.26}$$

which is valid irrespective of the switched system that we are in at any given discrete interval. Now using this last equation that is valid in any of the switched systems, along with the dynamic relationships for each component of the projection vector (5.23) that are valid for a given discrete interval $[k_1, k_2]$, we obtain

$$[g_i]_1(k) - [g_j]_1(k) = c_{i,j,\delta}(\lambda_{h,\delta-1})^{k-k_1}[g_j]_\delta(k_1) \quad for \quad i \neq j. \tag{5.27}$$

Substituting this relationship in $d_{i,j}(k)$, which is the distance as defined in (5.24) yields

$$d_{i,j}(k) = |c_{i,j,\delta}|(\lambda_{h,\delta-1})^{k-k_1}[g_j]_\delta(k_1) \quad for \quad k_1 \leq k \leq k_2 \quad and \quad i \neq j. \tag{5.28}$$

We will show in the 3^{rd} and the last step below that the distances $d_{i,j}(k)$ either stay constant or become smaller after each consequent switching of the corresponding dynamical system expressed by (5.10).

Step-3 : In this last step we show that $\lim_{k\to\infty}|[g_i]_1(k)-[g_j]_1(k)|=0$, for all $i,j\in\{1,...,n+1\}$. From this fact we will deduce that $\lim_{k\to\infty}(x_1(k),\ldots,x_n(k))=0$, which is sufficient to demonstrate the global attractivity of the origin of the switching discrete-time system (5.1) with the set $\mathscr{A}$ as defined in the statement of the Theorem.

We first denote the maximum and minimum values of the set $G(k)$ from (5.19), with $max[G(k)]_m$ and $min[G(k)]_m$ respectively, where the subscript m denotes the m^{th} fixed discrete interval spanning $[k_m,k_{m+1}]$. Now we consider the evolution of largest distance d_{max}, among the maximum and minimum values of $G(k)$ for the first interval $[k_1,k_2]$, which can expressed as

$$^1d_{max}\triangleq|max[G(k)]_1-min[G(k)]_1|\triangleq|[g_i]_1(k)-[g_r]_1(k)|,$$

for some $i,r\in\{1,2,\ldots,n+1\}$. Here $^1d_{max}$ denotes the largest distance for the first interval. Also note that for some random element j of the set $G(k)$ such that $j\in\{1,2,\ldots,n+1\}$ the following is true in the interval $[k_1,k_2]$

$$^1d_{max}=|[g_i]_1(k)-[g_j]_1(k)+[g_j]_1(k)-[g_r]_1(k)|.$$

Using the equation (5.27) one can express this last relationship as follows

$$^1d_{max}=|c_{i,j,\delta}[g_j]_\delta(k_1)(\lambda_{h,\delta-1})^{k-k_1}+c_{j,r,\rho}[g_r]_\rho(k_1)(\lambda_{h,\rho-1})^{k-k_1}|, \tag{5.29}$$

where integer column indexes δ,ρ vary as described in Lemma 5.4.2. Note that if $[g_j]_1(k)$ is a maximum or minimum value of $G(k)$, then the last line above collapses to just one term instead of two, and in this case the following arguments will also work.

Remembering that all the eigenvalues of the system are on the right half of the unit circle, we denote λ_{max} as the largest eigenvalue defined formally as follows

$$\lambda_{max}=max\{\lambda_{h,j}:\ 1\le h\le p\ ,\ 1\le j\le n\}. \tag{5.30}$$

Now utilizing this last expression and the subadditivity property of absolute value of real numbers (i.e., triangle inequality) given as $|a+b| \leq |a|+|b|$, we can express the largest distance (5.29) with the following inequality

$$\begin{aligned} {}^1d_{max} &\leq |c_{i,j,\delta}||[g_j]_\delta(k_1)|(\lambda_{h,\delta-1})^{k-k_1} + |c_{j,r,\rho}||[g_r]_\rho(k_1)|(\lambda_{h,\rho-1})^{k-k_1} \\ &\leq \left[|c_{i,j,\delta}||[g_j]_\delta(k_1)| + |c_{j,r,\rho}||[g_r]_\rho(k_1)|\right]\lambda_{max}^{k-k_1} \end{aligned} \tag{5.31}$$

We emphasize that in this last inequality the expression $|c_{i,j,\delta}||[g_j]_\delta(k_1)|$ denotes the distance between $[g_i]_1(k_1)$ and $[g_j]_1(k_1)$. Similarly, $|c_{j,r,\rho}||[g_r]_\rho(k_1)|$ denotes the distance between $[g_j]_1(k_1)$ and $[g_r]_1(k_1)$. Then,

$$\begin{aligned} {}^1d_{max} &\leq \left[|c_{i,j,\delta}||[g_j]_\delta(k_1)| + |c_{j,r,\rho}||[g_r]_\rho(k_1)|\right]\lambda_{max}^{k-k_1} \\ &\leq |max[G(k_1)]_1 - min[G(k_1)]_1|\lambda_{max}^{k-k_1}. \end{aligned} \tag{5.32}$$

The last inequality follows from the fact that, over the discrete time interval $[k_1,k_2]$, $[g_i]_1(k)$ remains on the same side of the constant $[g_j]_1(k)$, and $[g_r]_1(k)$ remains on the other side of $[g_j]_1(k)$. This is because the right hand side of (5.27) does not change sign as time changes in the interval $[k_1,k_2]$.

Note that at the terminal step of the interval, that is $k=k_2$, we have

$$|max[G(k)]_1 - min[G(k)]_1| \leq |max[G(k_1)]_1 - min[G(k_1)]_1|\lambda_{max}^{k_2-k_1}. \tag{5.33}$$

Suppose now we switch to the second interval $[k_2,k_3]$ such that the dynamics now evolve according to another discrete-time LTI system described by

$$\overline{x}(k+1) = \overline{A}_{c,w}\overline{x}(k), \quad for\ all \quad k_2 \leq k \leq k_3. \tag{5.34}$$

We again denote the extremal elements of the set $G(k)$ for this interval with $max[G(k)]_2$ and $min[G(k)]_2$, while we define the largest distance ${}^2d_{max}$ as follows

$${}^2d_{max} \triangleq |max[G(k)]_2 - min[G(k)]_2| \triangleq |[g_i]_1(k) - [g_r]_1(k)|,$$

for some $i, r \in \{1, 2, \ldots, n+1\}$. Then a similar analysis results in

$$^{2}d_{max} = |max[G(k)]_2 - min[G(k)]_2| \leq |max[G(k_2)]_2 - min[G(k_2)]_2| \lambda_{max}^{k-k_2}$$

Since k_2 is both the terminal step of the interval $[k_1, k_2]$ and the initial step of $[k_2, k_3]$ then we can substitute (5.33) in the last expression, which yields

$$\begin{aligned} |max[G(k)]_2 - min[G(k)]_2| &\leq |max[G(k_2)]_2 - min[G(k_2)]_2| \lambda_{max}^{k-k_2} \\ &\leq |max[G(k_1)]_1 - min[G(k_1)]_1| \lambda_{max}^{k_2-k_1} \lambda_{max}^{k-k_2}. \end{aligned}$$

This last inequality then implies that

$$^{2}d_{max} = |max[G(k)]_2 - min[G(k)]_2| \leq |max[G(k_1)]_1 - min[G(k_1)]_1| \lambda_{max}^{k-k_1}. \tag{5.35}$$

After another switching of the system to the 3^{rd} interval $[k_3, k_4]$, the procedure can be applied to arrive at

$$^{3}d_{max} = |max[G(k)]_3 - min[G(k)]_3| \leq |max[G(k_1)]_1 - min[G(k_1)]_1| \lambda_{max}^{k-k_1}. \tag{5.36}$$

For the general situation, when we have switched for the m^{th} time, the system is described by m^{th} discrete-time LTI system $\bar{x}(k+1) = \bar{A}_{z,l}\bar{x}(k)$ over the time interval $[k_m, k_{m+1}]$. Then as above we get

$$^{m}d_{max} = |max[G(k)]_m - min[G(k)]_m| \leq |max[G(k_1)]_1 - min[G(k_1)]_1| \lambda_{max}^{k-k_1}. \tag{5.37}$$

Therefore, as $0 < \lambda_{max} < 1$, then we conclude that

$$\lim_{k \to \infty} (\max\ [G(k)] - \min\ [G(k)]) = 0, \tag{5.38}$$

where $max[G(k)]$ and $min[G(k)]$ denote the maximum and minimum values of $G(k)$ for any time step $k \geq k_1$. Thus,

$$\lim_{k \to \infty} |[g_i]_1(k) - [g_j]_1(k)| = 0, \quad for\ all \quad i, j \in \{1, 2, \ldots, n+1\}. \tag{5.39}$$

Also substituting (5.27) in the last expression we arrive at the expression

$$\lim_{k\to\infty} |c_{i,j,\delta}||[g_j]_\delta(k)| = 0, \quad \textit{where} \quad \begin{cases} \delta = j \quad if \quad i = 1 \\ \delta = i \quad if \quad i \neq 1 \quad and \quad i \neq j \end{cases}, \tag{5.40}$$

which then implies

$$\lim_{k\to\infty} |[g_j]_\delta(k)| = 0, \tag{5.41}$$

for $j \in \{1,2,\ldots,n+1\}$, and $\delta \in \{2,3,\ldots,n+1\}$. Note that this last expression follows from the fact that the $c_{i,j,\delta}$ values form a finite collection of non-zero numbers when $i \neq j$. Also the equation (5.41) might not hold for $\delta = 1$ because then $i = j = 1$. Therefore, because $\lim_{k\to\infty} \bar{x}(k) = \lim_{k\to\infty} \bar{M}_j g_j(k)$, then we obtain

$$\lim_{k\to\infty} \begin{pmatrix} x_{n+1}(k) \\ x_1(k) \\ x_2(k) \\ \vdots \\ x_n(k) \end{pmatrix} = \lim_{k\to\infty} \begin{bmatrix} 1 & b & 1 & \ldots & 1 \\ 0 & & & & \\ 0 & & M_j & & \\ \vdots & & & & \\ 0 & & & & \end{bmatrix} \begin{pmatrix} [g_j]_1(k) \\ [g_j]_2(k) \\ \vdots \\ [g_j]_{n+1}(k) \end{pmatrix}, \tag{5.42}$$

which then implies that

$$\lim_{k\to\infty} \begin{pmatrix} x_1(k) \\ x_2(k) \\ \vdots \\ x_n(k) \end{pmatrix} = \lim_{k\to\infty} \begin{bmatrix} 0 & & \\ 0 & M_j & \\ \vdots & & \\ 0 & & \end{bmatrix} \begin{pmatrix} [g_j]_1(k) \\ [g_j]_2(k) \\ \vdots \\ [g_j]_{n+1}(k) \end{pmatrix} \tag{5.43}$$

$$= \begin{pmatrix} 0 \\ 0 \\ \vdots \\ 0 \end{pmatrix}. \tag{5.44}$$

Thus

$$\lim_{t\to\infty}(x_1, x_2, \ldots, x_n) = 0, \tag{5.45}$$

which proves the global attractivity of the origin for the switching system (5.1).

Q.E.D.

Remark 5.4.1 The following facts can be deduced for the set $\mathscr{A}$ defined in Theorem 5.4.1:

(i) Every matrix in $\mathscr{A}$ is Schur stable and diagonalizable.

(ii) Any matrix pair in $\mathscr{A}$ share at least $(n-1)$ linearly independent common real eigenvectors.

(iii) Every matrix pair in $\mathscr{A}$ can simultaneously be triangularized. (See [118] for the proof of this.)

Remark 5.4.2 We can not simply replace Hurwitz stable matrices for the continuous-time case in Theorem 3.1 of [112] with Schur stable matrices and arrive at the same conclusions of global attractivity of the origin. In the discrete-time case we need the condition given in equation (5.8) on the eigenvalues of D_h for $1 \leq h \leq p$. Because otherwise, we do not get the global asymptotic stability of the origin. This is demonstrated in the following example.

Example 5.4.1 Let the set $\mathscr{V} = \{v_1, v_2, v_3, v_4\}$ be given as

$$v_1 = \begin{bmatrix} 1 & 0 & 0 \end{bmatrix}^T, \quad v_2 = \begin{bmatrix} 0 & 1 & 0 \end{bmatrix}^T,$$
$$v_3 = \begin{bmatrix} 0 & 0 & 1 \end{bmatrix}^T, \quad v_4 = \begin{bmatrix} 1 & 1 & 1 \end{bmatrix}^T.$$

Further assume that $M_i \in \mathbb{R}^{3\times 3}$ matrices are constructed as follows

$$M_1 = \begin{bmatrix} v_1 & v_2 & v_3 \end{bmatrix}, \quad M_2 = \begin{bmatrix} v_4 & v_2 & v_3 \end{bmatrix},$$
$$M_3 = \begin{bmatrix} v_1 & v_4 & v_3 \end{bmatrix}, \quad M_4 = \begin{bmatrix} v_1 & v_2 & v_4 \end{bmatrix}.$$

Moreover select a 3×3 diagonal Schur stable matrix D as follows

$$D = \begin{bmatrix} 0.9 & 0 & 0 \\ 0 & 0.8 & 0 \\ 0 & 0 & -0.6 \end{bmatrix}.$$

Now consider the following Schur stable LTI systems

$$\Sigma_{A_i} : x(k+1) = A_i x(k),\ A_i \in \mathbb{R}^{3\times 3}, \tag{5.46}$$

where A_i matrices are constructed from

$$A_i = M_i D M_i^{-1}, \quad i = 1,..,4. \tag{5.47}$$

It is sufficient to show that there exists a switching sequence between A_i's such that the resulting system has eigenvalues outside the unit circle. We simply consider the incremental switching sequence $A_1 \to A_2 \to A_3 \to A_4$; then the dynamics of the system evolve according to the matrix product

$$A = A_1 A_2 A_3 A_4. \tag{5.48}$$

Since the eigenvalues of A are $\{1.1899, 0.1058, 0.2766\}$, then with one eigenvalue outside the unit circle, this switching sequence is unstable. It is also interesting to note that if D is chosen such that all of its eigenvalues are on the right half of the unit circle, i.e., $D = diag\{0.9, 0.8, 0.6\}$, then the A matrix corresponding to the switching sequence (5.48) has eigenvalues $\{0.5861, 0.1517, 0.3917\}$ and is stable by Theorem 5.4.1.

Remark 5.4.3 For the class of linear discrete time switched systems that satisfy the conditions of Theorem 5.4.1, one does not necessarily require the existence of a CQLF to show the global attractivity of the origin. In other words, it is possible to find switching systems that are stable by Theorem 5.4.1, and that **do not have a CQLF**. We emphasize that the class of such systems (i.e., the subclass of pairwise triangularizable systems) is strictly larger than the class of simultaneously triangularizable systems. Indeed, Example 5.5.1 introduced in

the next section presents such a switching system, which arises from a practical problem related to automotive control.

In what follows, we give two separate controller synthesis procedures for enhancing automotive roll dynamics based on the main results of this section; we also note that the first application we introduce was the main motivation for initiating the study on the current chapter.

5.5 A stabilizing switched controller synthesis procedure for configurable driving experience of automotive vehicles

As an example of the application of the results presented in the previous section we consider the design of an automobile dynamics enhancement system. The aim of the control design given here is to configure the driving experience based on active suspension actuators alone, and at the same time, to guarantee switching stability in the roll dynamics of the vehicle subject to sudden changes in the dynamical characteristics. Software configurable driving experience enhancement technologies utilizing active control systems is a topical subject for many luxury car manufactures. In fact, there are already some passenger vehicles on the market that give the drivers the option to select comfort and sporty driving experience settings with a press of a button, and/or modify the suspension settings as a function of speed. For example the IVDC (Interactive Vehicles Dynamics Control) technology from Ford (see *http://www.ford.ie/ie/smax/smax_interior/smax_drive*), and the AirMATIC (Adaptive Intelligent Ride System) technology from Mercedes-Benz (see *http://www3.mercedes-benz.com/techlex/ 2006/main_de.html*), both utilize semi-active suspension technologies to achieve these functions. In this section we show how such a strategy

may be implemented such that stability is guaranteed irrespective of switching[1]. For illustrative purposes, we assume vertical changes in CG position as the only source of switching in the dynamical characteristic of the vehicle, which can result from passenger and load movement. Thus, the driving experience enhancement control design described in the sequel is based on a simplified roll dynamics model of a car and aims to adjust the suspension settings as a function of CG position and without introducing any switching instabilities.

We first present the simplified roll plane model of an automobile with a second order linear parameter varying (LPV) structure. The model presented in the sequel is the simplest model that captures the roll dynamics of a car and it is free from the effects of uncertainties originating from unknown tire parameters. Assuming all vehicle mass is sprung, effective linear torques exerted by the suspension system about the roll center are defined as follows

$$T_{spring} = k\,\phi, \quad T_{damper} = c\,\dot{\phi}, \tag{5.49}$$

where k, c denote the linear spring stiffness and damping coefficients, respectively. We further define the roll torque input about the roll center (R.C.) as u, which is assumed to be provided by suitable active suspension actuators. For the sake of simplicity we assume no internal actuator dynamics or constraints. Using these notations and assumptions, we can apply a torque balance in the roll plane of the vehicle in terms of the effective suspension torques and control torque inputs (see Figure 5.1 and Table 5.1 for further notations of the roll plane model), and obtain the following 2^{nd} order relationship

$$J_{x_{eq}}\ddot{\phi} + c\dot{\phi} + k\phi = mh(a_y cos\phi + gsin\phi) + u. \tag{5.50}$$

Note that for simplicity, it is assumed in this model that, relative to the ground, the sprung

[1]Switching in the dynamical characteristic of road vehicles can occur due to a number reasons such as sudden changes in the vehicle mass, sudden changes in the loading configuration (i.e, shifting CG position), sloshing of liquid loads, a failure in the chassis components or the active safety systems, a sudden switching of the gear during a high speed cornering maneuver, or any other sources of high/low frequency oscillations, all of which may cause a sudden change in the lateral and roll dynamics response of the vehicle.

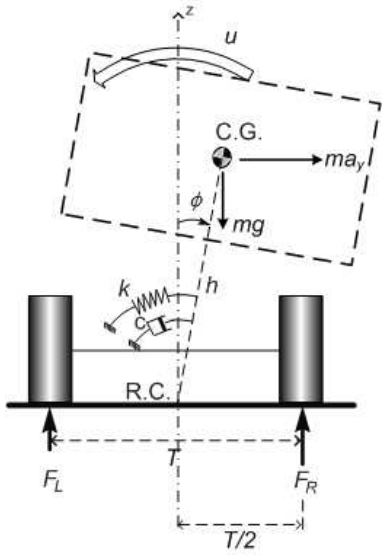

Figure 5.1: Second order roll plane model.

mass rolls about a fixed horizontal roll axis which is along the centerline of the body and at ground level. In the last equation $J_{x_{eq}}$ denotes the equivalent roll moment of inertia derived using the parallel axis theorem of mechanics taking into account the CG height variation as described below

$$J_{x_{eq}} \triangleq J_{xx} + mh^2. \tag{5.51}$$

For small roll angles, i.e., $\phi \ll$, we can approximate the nonlinear terms in equation (5.50) as $cos\phi \approx 1$, $sin\phi \approx \phi$. Further defining the state as $x = [\ \phi\ ,\ \dot{\phi}\ ]^T$, we can represent (5.50) as in the following state space form

$$\dot{x} = A_c x + G_c a_y + B_c u,\ \ with \tag{5.52}$$

$$A_c = \begin{bmatrix} 0 & 1 \\ -\frac{k-mgh}{J_{x_{eq}}} & -\frac{c}{J_{x_{eq}}} \end{bmatrix},\ G_c = \begin{bmatrix} 0 \\ \frac{mh}{J_{x_{eq}}} \end{bmatrix},\ B_c = \begin{bmatrix} 0 \\ \frac{1}{J_{x_{eq}}} \end{bmatrix}, \tag{5.53}$$

where a_y is the lateral acceleration measured at the center of gravity. Next we construct a discrete time approximation for this state space system. To this end consider the continuous

Table 5.1: Model parameters and definitions

Parameter	Description	Unit
m	Vehicle mass	$[kg]$
g	Gravitational constant	$[m/s^2]$
J_{xx}	Roll moment of inertia measured at the CG	$[kg \cdot m^2]$
T	Track width	$[m]$
h	CG height measured over the ground	$[m]$
c	suspension damping coefficient	$[kg \cdot m^2/s]$
k	suspension spring stiffness	$[kg \cdot m^2/s^2]$
ϕ	Roll angle measured at the roll center	$[rad]$
$\dot{\phi}$	Roll rate measured at the roll center	$[rad]$
u	Torque input about the roll center	$[Nm]$
a_y	Lateral acceleration measured at CG	$[m/s^2]$

time system of the form

$$\dot{\xi}(t) = F\xi(t) + H\omega(t) + Gu(t), \tag{5.54}$$

where $\xi(t) \in \mathbb{R}^n$ is the state, and $F \in \mathbb{R}^{n\times n}$, $H \in \mathbb{R}^n$, $G \in \mathbb{R}^n$ are the corresponding system matrices. Also $\omega \in \mathbb{R}$, and $u \in \mathbb{R}$ denote the disturbance and the control inputs for the this generic state space system, respectively. Then the discrete time equivalent of this system can be expressed by

$$\xi(k+1) = A\xi(k) + B_1\omega(k) + B_2u(k), \tag{5.55}$$

where, denoting the discrete time step by Δt, the matrices A, B_1, B_2 are computed from

$$A = e^{F\Delta t}, \quad B_1 = \int_0^{\Delta t} e^{F(\Delta t-\tau)}Hd\tau, \quad B_2 = \int_0^{\Delta t} e^{G(\Delta t-\tau)}Hd\tau. \tag{5.56}$$

Note here that $\xi(k) \in \mathbb{R}^n$ is the corresponding discrete time state, and $A \in \mathbb{R}^{n\times n}$, $B_1 \in \mathbb{R}^n$, $B_2 \in \mathbb{R}^n$ are the accompanying system matrices. Considering the roll plane model given with (5.52), (5.53) and using a first order approximation for the matrix exponentials above, the discrete time equivalent can be expressed with the following state space form

$$x(k+1) = A_d x(k) + G_d a_y(k) + B_d u(k), \;\; with \tag{5.57}$$

$$A_d = \begin{bmatrix} 1 & \Delta t \\ -\frac{(k-mgh)\Delta t}{J_{x_{eq}}} & 1-\frac{c\Delta t}{J_{x_{eq}}} \end{bmatrix}, \; G_d = \begin{bmatrix} 0 \\ \frac{mh\Delta t}{J_{x_{eq}}} \end{bmatrix}, \; B_d = \begin{bmatrix} 0 \\ \frac{\Delta t}{J_{x_{eq}}} \end{bmatrix}. \tag{5.58}$$

It is important here to note that the roll plane model introduced above depends on the CG height in a nonlinear fashion. It is known that the change in this parameter significantly affects the roll dynamics of a vehicle [124], [125] and if these changes are not accounted for in the active safety control implementations, they can cause accidents such as the rollover of the vehicle, during extreme driving situations. This is why we consider the changes in the CG position here, which can potentially result from shifting loads inside the vehicle due to inertial forces exerted during high speed maneuvers. Given that these changes in the CG position can be detected in real time (see Chapter 2 for an example of a real time CG estimation algorithm), we give next a synthesis method for a stable switched linear control design procedure for driving dynamics enhancement system based on active suspension actuators, and making use of the results obtained in Section 5.4. For the sake of exposition, we only consider changes in the vertical position of CG here; however these ideas can be extended to more general implementations, where changes in the CG position in 3 dimensions are all accounted for.

The switched control structure is shown in Figure 5.2, where there are N different controllers that switch based on the current CG height (i.e., the CG height change is the switching criteria). We emphasize that one of the goals of the controller design advocated in the sequel is to guarantee that the feedback system is able to cope with the instabilities that might be induced by switching of dynamics as a result of detectable changes in the system parameters (in this case the CG height of the vehicle).

Remark 5.5.1 For the ease of exposition it is assumed here that the changes in CG height can be detected instantaneously. In general this is not a realistic assumption as this parameter can not be measured directly in automotive vehicles. However, it is possible to estimate CG height based on sensor data as described in Chapter 2, as well as in recent publications [122], [121], [123]. Inherent delays in estimating the CG height using these or other alternative methods can be compensated by the control design suggested in the sequel, and this shall be considered in the future extensions of the present chapter.

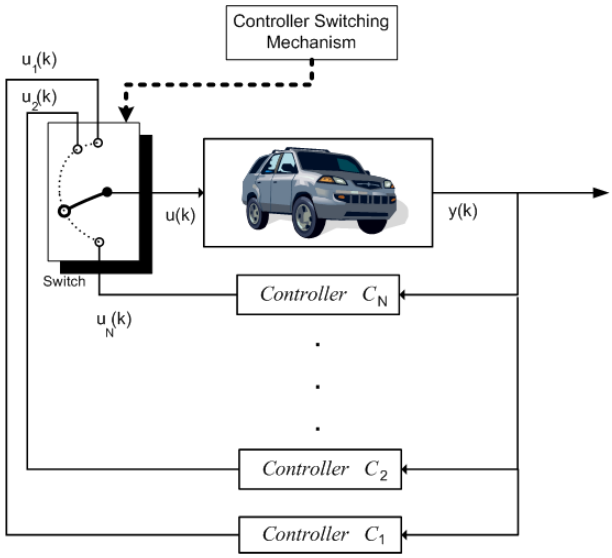

Figure 5.2: Switched controller structure.

To keep the following discussion as simple as possible we assume $N = 3$, yielding an expression for the closed loop dynamics given by

$$x(k+1) = A_{d,i}x(k) + G_{d,i}a_y(k) + B_{d,i}u(k) \qquad for \qquad i \in \{1,2,3\}, \tag{5.59}$$

where

$$A_{d,i} = \begin{bmatrix} 1 & \Delta t \\ -\frac{(k-mgh_i)\Delta t}{J_{x_{eq,i}}} & 1-\frac{c\Delta t}{J_{x_{eq,i}}} \end{bmatrix}, \; G_{d,i} = \begin{bmatrix} 0 \\ \frac{mh_i\Delta t}{J_{x_{eq,i}}} \end{bmatrix}, \; B_{d,i} = \begin{bmatrix} 0 \\ \frac{\Delta t}{J_{x_{eq,i}}} \end{bmatrix}. \tag{5.60}$$

We propose the following switched linear state feedback control structure for the above set of dynamical systems

$$C_i: \; u_i(k) = -K_i x(k), \qquad i \in \{1,2,3\} \tag{5.61}$$

where $K_i = [\ \kappa_{i1},\ \ \kappa_{i2}\ ]$ with $\kappa_{i1}, \kappa_{i2} \in \mathbb{R}$, are fixed control gains corresponding to each CG height configuration. Under this feedback controller, the closed loop system becomes

$$x(k+1) = \tilde{A}_i x(k) + G_{d,i} a_y(k) \tag{5.62}$$

where

$$\tilde{A}_i = A_{d,i} - B_{d,i} K_i = \begin{bmatrix} 1 & \Delta t \\ -\frac{(k - mgh_i + \kappa_{i1})\Delta t}{J_{x_{eq,i}}} & 1 - \frac{(c+\kappa_{i2})\Delta t}{J_{x_{eq,i}}} \end{bmatrix}, \tag{5.63}$$

for each $i \in \{1,2,3\}$. We have now the following result which is useful for the control design.

Lemma 5.5.1 *Let the matrices $\tilde{A}_i \in \mathbb{R}^{2\times 2}$ for $i \in \{1,2,3\}$ be given as defined in (5.63). Consider the diagonal matrices $D_1, D_2, D_3 \in \mathbb{R}^{2\times 2}$ with positive real entries given as below*

$$D_1 = \begin{bmatrix} \lambda_1 & 0 \\ 0 & \lambda_2 \end{bmatrix}, \quad D_2 = \begin{bmatrix} \lambda_3 & 0 \\ 0 & \lambda_2 \end{bmatrix}, \quad D_3 = \begin{bmatrix} \lambda_1 & 0 \\ 0 & \lambda_3 \end{bmatrix}, \tag{5.64}$$

where the diagonal elements are such that $0 < \lambda_j < 1$ and $\lambda_i \neq \lambda_j$ for every $i, j \in \{1,2,3\}$ and $i \neq j$. Suppose further that invertible matrices $M_1, M_2, M_3 \in \mathbb{R}^{2\times 2}$ are defined as follows

$$M_1 = \begin{bmatrix} \nu_1 & \mu_1 \\ \nu_2 & \mu_2 \end{bmatrix}, \quad M_2 = \begin{bmatrix} \eta_1 & \mu_1 \\ \eta_2 & \mu_2 \end{bmatrix}, \quad M_3 = \begin{bmatrix} \nu_1 & \eta_1 \\ \nu_2 & \eta_2 \end{bmatrix}, \tag{5.65}$$

where all the entries $\nu_1, \eta_1, \mu_1, \nu_2, \eta_2, \mu_2$ are real numbers. Then the following choice of control gains κ_{i1}, κ_{i2} for $i \in \{1,2,3\}$

$$\left.\begin{aligned} \kappa_{11} &= mgh_1 - k - \tfrac{J_{x_{eq,1}}}{\Delta t^2}(\lambda_1 - 1)(\lambda_2 - 1) \\ \kappa_{12} &= -c + \tfrac{J_{x_{eq,1}}}{\Delta t}\tfrac{(\lambda_1-1)^2 - (\lambda_2-1)^2}{\lambda_2 - \lambda_1} \end{aligned}\right\} \quad for \quad i = 1 \tag{5.66}$$

$$\left.\begin{array}{l} \kappa_{21} = mgh_2 - k - \frac{J_{x_{eq,2}}}{\Delta t^2}(\lambda_3 - 1)(\lambda_2 - 1) \\ \kappa_{22} = -c + \frac{J_{x_{eq,2}}}{\Delta t}\frac{(\lambda_3-1)^2-(\lambda_2-1)^2}{\lambda_2-\lambda_3} \end{array}\right\} \quad for \quad i = 2 \tag{5.67}$$

$$\left.\begin{array}{l} \kappa_{31} = mgh_3 - k - \frac{J_{x_{eq,3}}}{\Delta t^2}(\lambda_1 - 1)(\lambda_3 - 1) \\ \kappa_{32} = -c + \frac{J_{x_{eq,3}}}{\Delta t}\frac{(\lambda_1-1)^2-(\lambda_3-1)^2}{\lambda_3-\lambda_1} \end{array}\right\} \quad for \quad i = 3 \tag{5.68}$$

guarantee that the unforced closed loop system matrices $\tilde{A}_1$, $\tilde{A}_2$ and $\tilde{A}_3$ can be expressed as

$$\tilde{A}_i = M_i D_i M_i^{-1} \qquad for \qquad i \in \{1,2,3\} \tag{5.69}$$

and that $\tilde{A}_1, \tilde{A}_2, \tilde{A}_3$ satisfy the conditions of Theorem 5.4.1.

Proof of Lemma 5.5.1: We first show the result for $i = 1$. Using the definitions of D_1 and M_1 in (5.64) and (5.65), respectively, the similarity transformation for $\tilde{A}_1$ in equation (5.69) can be expressed as follows

$$\tilde{A}_1 \;=\; \frac{1}{\nu_1\mu_2 - \mu_1\nu_2}\begin{bmatrix} \lambda_1\nu_1\mu_2 - \lambda_2\mu_1\nu_2 & (\lambda_2 - \lambda_1)\nu_1\mu_1 \\ (\lambda_1 - \lambda_2)\mu_2\nu_2 & \lambda_2\nu_1\mu_2 - \lambda_1\mu_1\nu_2 \end{bmatrix}. \tag{5.70}$$

Comparing the last equation with (5.63) for $i = 1$ results in the following relationships

$$\lambda_1\nu_1\mu_2 - \lambda_2\mu_1\nu_2 = \nu_1\mu_2 - \mu_1\nu_2, \tag{5.71}$$

$$(\lambda_2 - \lambda_1)\nu_1\mu_1 = (\nu_1\mu_2 - \mu_1\nu_2)\Delta t, \tag{5.72}$$

$$J_{x_{eq,1}}(\lambda_1 - \lambda_2)\mu_2\nu_2 = -(k - mgh_1 + \kappa_{11})(\nu_1\mu_2 - \mu_1\nu_2)\Delta t, \tag{5.73}$$

$$J_{x_{eq,1}}(\lambda_2\nu_1\mu_2 - \lambda_1\mu_1\nu_2) = (J_{x_{eq,1}} - c - \kappa_{12})(\nu_1\mu_2 - \mu_1\nu_2)\Delta t. \tag{5.74}$$

Arranging equations (5.71) and (5.72), the following set of identities can be obtained

$$\frac{\nu_1\mu_2}{\mu_1\nu_2} = \frac{1-\lambda_2}{1-\lambda_1}, \qquad \frac{\nu_1\mu_1}{\nu_1\mu_2 - \mu_1\nu_2} = \frac{\Delta t}{\lambda_2 - \lambda_1} \tag{5.75}$$

$$\nu_1 = \frac{\Delta t}{\lambda_1 - 1}\nu_2, \qquad \mu_1 = \frac{\Delta t}{\lambda_2 - 1}\mu_2, \tag{5.76}$$

Also solving for κ_{11} from (5.73), κ_{12} from (5.74) and making use of the above identities, we obtain the corresponding relations for the controller gains given by (5.66).

For $i = 2$, we again use the definitions of D_2 and M_2 from (5.64) and (5.65), respectively and obtain the following expression for $\tilde{A}_2$

$$\tilde{A}_2 = \frac{1}{\eta_1\mu_2 - \mu_1\eta_2}\begin{bmatrix} \lambda_3\eta_1\mu_2 - \lambda_2\mu_1\eta_2 & (\lambda_2-\lambda_3)\eta_1\mu_1 \\ (\lambda_3-\lambda_2)\mu_2\eta_2 & \lambda_2\eta_1\mu_2 - \lambda_3\mu_1\eta_2 \end{bmatrix}. \tag{5.77}$$

Comparing the last equation with (5.63) for $i = 2$ results in the following relationships

$$\lambda_3\eta_1\mu_2 - \lambda_2\mu_1\eta_2 = \eta_1\mu_2 - \mu_1\eta_2, \tag{5.78}$$

$$(\lambda_2-\lambda_3)\eta_1\mu_1 = (\eta_1\mu_2 - \mu_1\eta_2)\Delta t, \tag{5.79}$$

$$J_{x_{eq,2}}(\lambda_3-\lambda_2)\mu_2\eta_2 = -(k - mgh_2 + \kappa_{21})(\eta_1\mu_2 - \mu_1\eta_2)\Delta t, \tag{5.80}$$

$$J_{x_{eq,2}}(\lambda_2\eta_1\mu_2 - \lambda_3\mu_1\eta_2) = (J_{x_{eq,2}} - c - \kappa_{22})(\eta_1\mu_2 - \mu_1\eta_2)\Delta t. \tag{5.81}$$

Arranging equations (5.78) and (5.79), the following set of identities can be obtained

$$\frac{\eta_1\mu_2}{\mu_1\eta_2} = \frac{1-\lambda_2}{1-\lambda_3}, \qquad \frac{\eta_1\mu_1}{\eta_1\mu_2 - \mu_1\eta_2} = \frac{\Delta t}{\lambda_2-\lambda_3} \tag{5.82}$$

$$\eta_1 = \frac{\Delta t}{\lambda_3 - 1}\eta_2, \qquad \mu_1 = \frac{\Delta t}{\lambda_2 - 1}\mu_2, \tag{5.83}$$

Also solving for κ_{21} from (5.80), κ_{22} from (5.81) and making use of the above identities, we obtain the corresponding relations for the controller gains given with (5.67). Similarly, the expressions (5.68) can be obtained as above for $i = 3$ and using the appropriate set of matrices. It is trivial to show also that, due to the chosen structure for $\tilde{A}_i$, the resulting set of closed loop unforced system matrices for $\tilde{A}_1, \tilde{A}_2, \tilde{A}_3$ satisfy the conditions of the Theorem 5.4.1.

Q.E.D.

Next we give a technical lemma from [102] to relate the exponential stability of the unforced system $x(k+1) = \tilde{A}_i x(k)$ to the bounded stability of the solutions of the forced system (5.62).

Lemma 5.5.2 *Consider the following LPV discrete time system*

$$x(k+1) = A(k)x(k) + B(k)u(k), \tag{5.84}$$

$$y(k) = C(k)x(k). \tag{5.85}$$

Let the above system be exponentially stable, and further suppose that there exists finite constants β and γ such that

$$\| B(k) \| \leq \beta, \qquad \| C(k) \| \leq \gamma \tag{5.86}$$

for all k. Then the discrete time LPV system is uniformly bounded-input, bounded-output (BIBO) stable.

See [102] for the proof of the lemma. Next we demonstrate the suggested control design with a numerical example.

Example 5.5.1 Let the positive constants $\lambda_1, \lambda_2, \lambda_3$ be given as $0.994, 0.6, 0.3$, respectively. Without loss of generality, we choose the constants ν_2, μ_2, η_2 as $1, 2, 3$, respectively. Note that the eigenvalues and the choice of ν_2, μ_2, η_2 affect the amount of attenuation of the dynamics under feedback; so these can be considered as the tuning parameters. Also, we set the discrete time step as $\Delta t = 0.05$. The vehicle model parameters used in the example are given in Table 5.2, and they correspond to a compact class vehicle. In this example we assume that the CG height of the vehicle can switch between any of the values h_1, h_2 or h_3 specified in Table 5.2 at any instant. Now utilizing the Lemma 5.5.1 and using the matrix definitions in (5.64) we obtain the following set of D_i matrices, which contain the target closed loop eigenvalues of the roll plane models corresponding to each CG height position

$$D_1 = \begin{bmatrix} 0.994 & 0 \\ 0 & 0.6 \end{bmatrix}, \quad D_2 = \begin{bmatrix} 0.3 & 0 \\ 0 & 0.6 \end{bmatrix}, \quad D_3 = \begin{bmatrix} 0.994 & 0 \\ 0 & 0.3 \end{bmatrix}.$$

The corresponding M_i matrices are obtained making use of (5.65) and utilizing the identities

Table 5.2: Simulation parameters

Parameter	Description	Unit
m	1200	$[kg]$
g	9.81	$[m/s^2]$
J_{xx}	300	$[kg \cdot m^2]$
c	5000	$[kg \cdot m^2/s]$
k	30000	$[kg \cdot m^2/s^2]$
h_1	0.5	$[m]$
h_2	0.7	$[m]$
h_3	0.9	$[m]$

(5.76) and (5.83), which result in

$$M_1 = \begin{bmatrix} -8.333 & -0.25 \\ 1 & 2 \end{bmatrix}, M_2 = \begin{bmatrix} -0.2143 & -0.25 \\ 3 & 2 \end{bmatrix}, M_3 = \begin{bmatrix} -8.333 & -0.2143 \\ 1 & 3 \end{bmatrix}.$$

Also according to (5.66),(5.67) and (5.68) the controller gains for each CG height position are computed as follows

$$\left.\begin{array}{rcl} \kappa_{11} & = & -23538 \\ \kappa_{12} & = & -128 \end{array}\right\} \quad for \quad i = 1, \quad (CG\ height - 1), \tag{5.87}$$

$$\left.\begin{array}{rcl} \kappa_{21} & = & 77696.4 \\ \kappa_{22} & = & 14536 \end{array}\right\} \quad for \quad i = 2, \quad (CG\ height - 2), \tag{5.88}$$

$$\left.\begin{array}{rcl} \kappa_{31} & = & -17268.24 \\ \kappa_{32} & = & 12960.64 \end{array}\right\} \quad for \quad i = 3, \quad (CG\ height - 3). \tag{5.89}$$

Then according to (5.69), the closed loop system matrices $\tilde{A}_1, \tilde{A}_2$ and $\tilde{A}_3$ corresponding to

the controller gains above are given as

$$\tilde{A}_1 = \begin{bmatrix} 1 & 0.05 \\ -0.048 & 0.594 \end{bmatrix}, \quad \tilde{A}_2 = \begin{bmatrix} 1 & 0.05 \\ -5.6 & -0.1 \end{bmatrix}, \quad \tilde{A}_3 = \begin{bmatrix} 1 & 0.05 \\ -0.084 & 0.294 \end{bmatrix} \tag{5.90}$$

Then evolution of dynamics corresponding to any periodic switching sequence between the unforced closed loop system matrices $\tilde{A}_1, \tilde{A}_2$ and $\tilde{A}_3$ are stable by Theorem 5.4.1. That is, the resulting switched unforced discrete time dynamical systems expressed as follows

$$x(k+1) = A(k)x(k), \quad A(k) \in \{\tilde{A}_1, \tilde{A}_2, \tilde{A}_3\},$$

have positive real eigenvalues in the unit circle, and thus are stable. This inherently implies that with the suggested switched control structure, where controller switching is based on the current CG height, results in stable roll dynamics of the vehicle regardless of the switching parameters. Also, it follows from Lemma 5.5.2 that the closed loop forced switched roll model given in (5.62) is uniformly BIBO stable for bounded lateral acceleration $a_y(k)$ inputs.

Remark 5.5.2 As mentioned earlier, it is important to note here that the closed loop system matrices $\tilde{A}_i$ for $i \in \{1,2,3\}$ obtained above in (5.90) **do not have a CQLF**, but is nevertheless exponentially stable. The non-existence of a CQLF can be confirmed numerically using LMI solvers. Therefore, the stability of this specific switched system needs to be tested with non-CQLF techniques such as the one described here.

We finally give the numerical simulation results corresponding to the suggested controller in feedback loop with a simple vehicle model. We generate the simulated vehicle behavior with a model commonly known as the “single track model with roll degree of freedom", which we initially introduced in Chapter 2. The model as illustrated in Figure 5.3 is the simplest model with coupled lateral and roll dynamics, which assumes that the steering angle δ, roll angle ϕ, and sideslip angle β are small, and also that all vehicle mass is

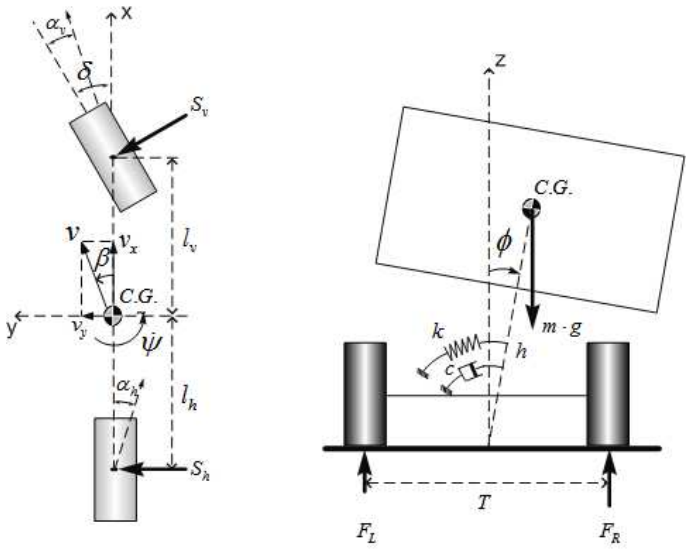

Figure 5.3: Linear bicycle model with roll degree of freedom.

sprung. We can write the equations of motion for the single track model with roll degree of freedom and with active roll torque input as follows

$$\dot{x} = \begin{bmatrix} -\frac{\sigma}{mv_x}\frac{J_{xeq}}{J_{xx}} & \frac{\rho}{mv_x^2}\frac{J_{xeq}}{J_{xx}} - 1 & -\frac{hc}{J_{xx}v_x} & \frac{h(mgh-k)}{J_{xx}v_x} \\ \frac{\rho}{J_{zz}} & -\frac{\kappa}{J_{zz}v_x} & 0 & 0 \\ -\frac{h\sigma}{J_{xx}} & \frac{h\rho}{v_x J_{xx}} & -\frac{c}{J_{xx}} & \frac{mgh-k}{J_{xx}} \\ 0 & 0 & 1 & 0 \end{bmatrix} x + \begin{bmatrix} \frac{C_v}{mv_x}\frac{J_{xeq}}{J_{xx}} \\ \frac{C_v l_v}{J_{zz}} \\ \frac{hC_v}{J_{xx}} \\ 0 \end{bmatrix} \delta + \begin{bmatrix} \frac{h}{J_{xx}v_x} \\ 0 \\ \frac{1}{J_{xx}} \\ 0 \end{bmatrix} u, \quad (5.91)$$

where $x = \begin{bmatrix} \beta & \dot{\psi} & \dot{\phi} & \phi \end{bmatrix}^T$ is the state vector, and $u \in \mathbb{R}$ is the roll torque input introduced earlier. Also

$$\begin{aligned} \sigma &\triangleq C_v + C_h \\ \rho &\triangleq C_h l_h - C_v l_v \\ \kappa &\triangleq C_v l_v^2 + C_h l_h^2. \end{aligned} \quad (5.92)$$

are the auxiliary parameters in terms of the tire cornering stiffnesses C_v and C_h. Further notations and definitions are given in Table 5.3. For a more detailed introduction and derivation

Table 5.3: Model parameters and definitions

Parameter	Description	Value	Unit
m	Vehicle mass	1200	$[kg]$
g	Gravitational constant	9.81	$[m/s^2]$
v_x	Vehicle longitudinal speed	20	$[m/s]$
δ	Steering angle	varying	$[rad]$
J_{xx}	Roll moment of inertia at the CG	300	$[kg \cdot m^2]$
J_{zz}	Yaw moment of inertia at the CG	1300	$[kg \cdot m^2]$
l_v	longitudinal CG position w.r.t. front axle	1.2	$[m]$
l_h	longitudinal CG position w.r.t. rear axle	1.4	$[m]$
h	CG height measured over the ground	varying	$[m]$
c	suspension damping coefficient	5000	$[kg \cdot m^2/s]$
k	suspension spring stiffness	30000	$[kg \cdot m^2/s^2]$
C_v	linear tire stiffness coefficient for the front tire	30000	$[N/rad]$
C_h	linear tire stiffness coefficient for the rear tire	50000	$[N/rad]$
β	Sideslip angle at vehicle CG	varying	$[rad]$

of this model see [50]. We used this model to represent the real vehicle in simulation and in a feedback loop with the discrete time control design introduced earlier. The reference maneuver is a steady state cornering maneuver with a gradual step steering input as shown in Figure 5.4, where the steering input starts at 4 seconds into the simulation and reaches its peak steady state value of 80° at 6 seconds. Note here that we assumed a steering ratio of $1:20$ between the wheel and driver's steering wheel. Also the vehicle velocity during the simulation was fixed at $v_x = 20m/s$. In order to represent the switching in the dynamics we assumed the CG height profile shown in the lower part of Figure 5.4, which we as-

sume results from loads falling over inside the vehicle during the maneuver (which makes sense). As specified in the control design, the CG height switches between $0.9[m], 0.7[m]$, and $0.5[m]$ only; also to simulate a gradual falling of loads inside the vehicle we assumed a switching sequence of $0.9[m] \rightarrow 0.7[m] \rightarrow 0.5[m]$ in the CG height.

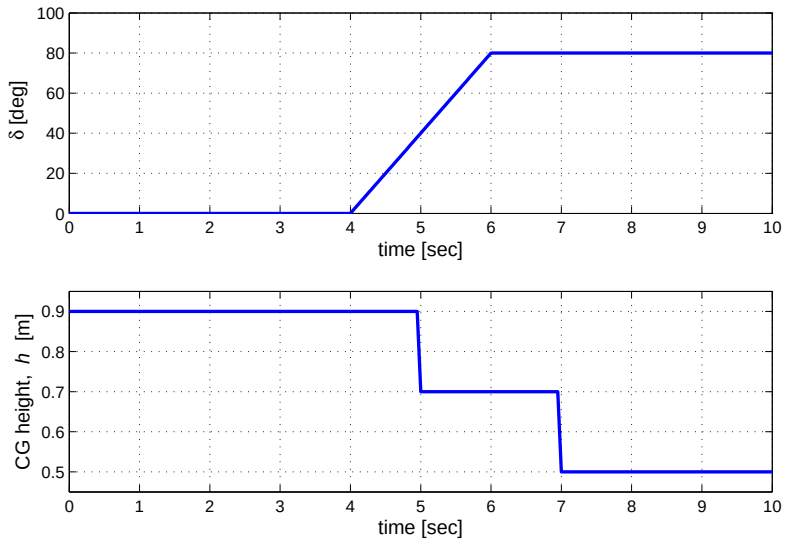

Figure 5.4: Driver steering wheel input δ (where steering ratio is $1/20$) and the time varying CG height during the maneuver.

Using the controller gains (5.87),(5.88) and (5.89) corresponding to each CG height configuration, results in the state histories during the maneuver shown in Figure 5.5 for the closed loop single track model. Note also in the figure that these states are compared to those of an uncontrolled vehicle subject to the same parameter switching, and the effectiveness of the controller is evident from the results. Specifically, it is observed from the roll angle and the roll rate profiles shown in the left half of figure that the suggested switched controller reduces the controlled roll angle significantly while preserving the vertical response characteristics. Similar conclusions can be made from the corresponding yaw rate and sideslip angle plots shown in the right half of the same figure, where it is also observed that the control action results in a reduced side slip angle whereas it causes an increased yaw rate

values as compared to the vehicle with no control. These imply that for a given steering input, the controlled vehicle can tolerate higher yaw rates without having as much sideslip as compared to the vehicle with no control.

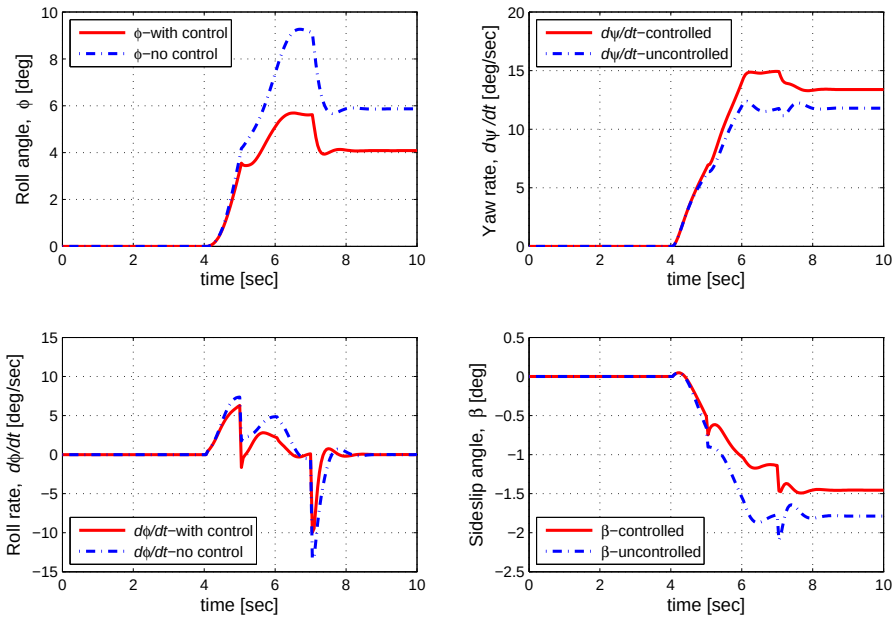

Figure 5.5: Comparisons of the states for vehicles with and without control.

It also is interesting to see how the suggested controller affect the vehicle path. To do this, we note that the coordinates (x, y) of the vehicle CG relative to the road satisfy

$$x(k+1) = x(k) + v_x \cos(\beta(k) + \psi(k))\Delta t\,, \tag{5.93}$$

$$y(k+1) = y(k) + v_x \sin(\beta(k) + \psi(k))\Delta t\,, \tag{5.94}$$

where we choose the initial coordinates $(x(0), y(0))$ to be zero. In Figure 5.6 the CG trajectories of the controlled and the uncontrolled vehicles are compared, where we observe that due to higher yaw rate values of the controlled vehicle, the corresponding trajectory has a smaller turn radius, which is favorable in terms of the cornering capability.

Comment: We observe based on the simulation results that, the state feedback control

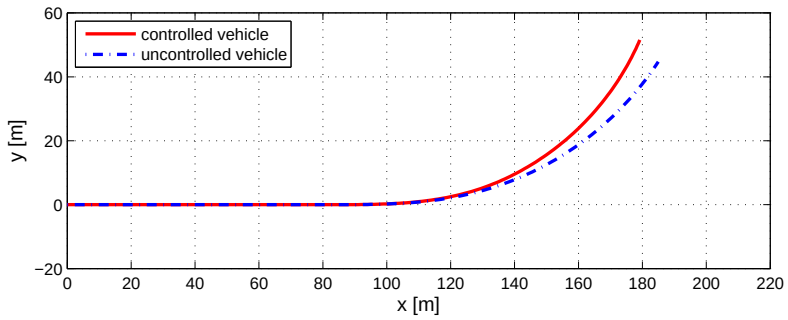

Figure 5.6: Comparison of controlled and uncontrolled vehicle trajectories.

structure suggested in this section suppresses the roll motion of the controlled vehicle under parameter switching, which in return causes an increased yaw rate and reduced sideslip values as compared to the vehicle without control. These characteristics are reminiscent of a sporty vehicle response in terms of increased responsiveness in the lateral dynamics and higher cornering performance. Therefore, the suggested controller can be used used to emulate sporty driving dynamics in a generic vehicle, as well as guaranteeing the switched stability with respect to changing CG height.

5.6 A stabilizing switched controller synthesis procedure for transient-free emulation of roll dynamics of automotive vehicles

As a second example of the application of the main results presented in Section 5.4, we now consider a problem related to the roll stabilization introduced in the previous section, but this time there are added demands on the controller that include following a given reference state trajectory, providing a means for transient free switching as well as guaranteeing the

switching stability due to changing CG height. Applications of such a switching stabilizing controller is abundant; to name a few, it can be used to modify vertical and roll dynamics of a vehicle for various applications such as the dynamical emulation of other vehicles (generic prototyping) [2], as well as optimization of the dynamics for driving comfort or sporty response settings.

Remark 5.6.1 It is possible to use the control implementation described in this section as an automotive vehicle rollover prevention system. For a detailed description and discussion of the automotive rollover problem, see Chapter 3 as well as [124] and [125]. It is possible to specify the reference roll angle trajectory used here for tracking such that a dynamical metric related to rollover occurrence (such as the dynamic load transfer ratio, LTR_d) is upper bounded for given bounded disturbance inputs. However, since we are mainly concerned with the emulation of roll dynamics here, this is outside the scope of the current section. We will report an extension of this work for rollover prevention problem in the near future.

In the preceding section we introduced a simplified second order model for the roll dynamics of an automobile in (5.50). Surprisingly, there are many other dynamical processes in automotive systems as well as in other engineering systems, which can be represented with the same dynamical structure. Before we give the controller synthesis procedure for such class of systems, we need to express the roll dynamics model given with (5.50) in a more suitable form so that it serves as a prototype for such class of systems. One can possibly express the second order roll plane model under the small angles assumption in the following form

$$\ddot{\phi} + \frac{c}{J_{x_{eq}}}\dot{\phi} + \frac{k - mgh}{J_{x_{eq}}}\phi = \frac{mh}{J_{x_{eq}}}a_y + \frac{1}{J_{x_{eq}}}u, \tag{5.95}$$

where the lateral acceleration $a_y \in \mathbb{R}$ is the disturbance input from lateral dynamics, and $u \in \mathbb{R}$ is the control torque imposed by the active suspension actuators. We further define

the following time varying parameters as functions of the CG height

$$a0_g = \frac{k - mgh_g}{J_{x_{eq,g}}}, \qquad a1_g = \frac{c}{J_{x_{eq,g}}}, \tag{5.96}$$

$$\omega_g = \frac{mh_g}{J_{x_{eq,g}}}, \qquad L_g = \frac{1}{J_{x_{eq,g}}}, \tag{5.97}$$

where the subscript $g \in \{1,2,\cdots,m\}$ denotes the current (detectable) CG height setting. Note also that the parameter $J_{x_{eq,g}}$ is a function of the CG height, and the dependence of it on the current CG height, h_g is clear from its definition given in (5.51). Substituting these definitions in the roll plane model above, we obtain the following second order linear parameter varying (LPV) model structure,

$$\frac{d^2\phi}{dt^2} + a1_g\frac{d\phi}{dt} + a0_g\phi = \omega_g a_y + L_g u, \qquad g \in \{1,2,\cdots,m\}. \tag{5.98}$$

Using this prototype model structure, we next give the control synthesis procedure.

The control strategy advocated here is similar to the one described in the preceding section in that, it consists of a bank of linear controllers (one for each CG position) along with a switching mechanism that are connected in feedback as depicted in Figure 5.7. We adopt the following type of control strategy for each individual controller, which we denote by C_i that correspond to the i^{th} CG position setting

$$C_i: \ \frac{du_i}{dt} = -b_i u_i + K1_i e + K2_i \frac{de}{dt}, \tag{5.99}$$

where $b_i \in \mathbb{R}, K1_i \in \mathbb{R}, K2_i \in \mathbb{R}$ are the derivative, proportional and integral gains, respectively. A controller of this form is a standard lead-lag (also known as proportional-integral-derivative or PID) controller that is described in elementary text-books [98]. As a side remark, we here note that this type of control implementations are commonly used in automotive control applications; for example in the context of control of vertical dynamics see [127], which uses a PI (proportional-integral) approach for tracking control design. For the ease of exposition of the suggested control structure given in (5.99), we here consider the tracking (i.e., emulation) of the roll angle only. Therefore $e = r - \phi$ designates the roll angle tracking error, where $r \in \mathbb{R}$ is the reference roll angle trajectory for the maneuver. As

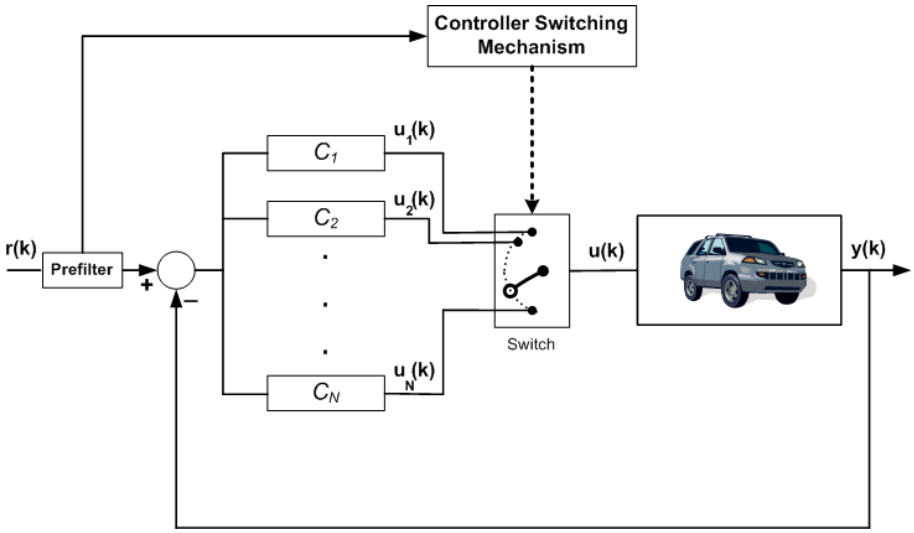

Figure 5.7: Reference tracking, switched roll dynamics emulation controller structure.

a further simplification, we also assume the switching logic selects the appropriate individual controller at the instant of a change in the CG height. It is important to note that the task of the emulation controller suggested here is not only the tracking of desired reference states relevant to roll dynamics, but also maintaining the stability of the nominal switched closed loop system. Therefore, we demonstrate here how the results presented in Section 5.4 may be used as the basis for a switched controller design, which consists of a bank of linear controllers (one for each CG height configuration) along with a switching mechanism as depicted in Figure 5.7, and that accommodates all of the design considerations.

To keep the discussion in the sequel as simple as possible, we assume that there are only three configurations that the CG height can switch to, that is $m = 3$, yielding an expression for the closed loop dynamics given by,

$$\dot{x} \quad = \quad A_g x + B_g r + G_g a_y, \quad A_g \in \{A_1, A_2, A_3\}, \tag{5.100}$$

where the state is defined as $x = [\ \phi,\ d\phi/dt,\ u_1,\ u_2,\ u_3\ ]^T$ and the system matrices A_g, B_g and G_g are given as below

$$A_g = \begin{bmatrix} 0 & 1 & 0 & 0 & 0 \\ -a0_g & -a1_g & L_1d_1 & L_2d_2 & L_3d_3 \\ -K1_1 & -K2_1 & -b_1 & 0 & 0 \\ -K1_2 & -K2_2 & 0 & -b_2 & 0 \\ -K1_3 & -K2_3 & 0 & 0 & -b_3 \end{bmatrix}, B_g = \begin{bmatrix} 0 \\ 0 \\ K1_1 \\ K1_2 \\ K1_3 \end{bmatrix}, G_g = \begin{bmatrix} 0 \\ \omega_g \\ 0 \\ 0 \\ 0 \end{bmatrix}. \quad (5.101)$$

Note here that $d_g = 1$ if the g^{th} controller is engaged at any instant, and it is zero otherwise. A discrete time equivalent for this dynamical system follows from (5.54), which is of the same form as (5.100) for each g. Utilizing a first order approximation for the matrix exponentials (5.56), the following discrete time version for the forced roll plane model can be obtained

$$x(k+1) = A_{d,g}x(k) + B_{d,g}r(k) + G_{d,g}a_y(k), \quad A_{d,g} \in \{A_{d,1}, A_{d,2}, A_{d,3}\}, \quad (5.102)$$

where

$$A_{d,g} = \begin{bmatrix} 1 & \Delta t & 0 & 0 & 0 \\ -a0_g\Delta t & 1-a1_g\Delta t & L_1d_1\Delta t & L_2d_2\Delta t & L_3d_3\Delta t \\ -K1_1\Delta t & -K2_1\Delta t & 1-b_1\Delta t & 0 & 0 \\ -K1_2\Delta t & -K2_2\Delta t & 0 & 1-b_2\Delta t & 0 \\ -K1_3\Delta t & -K2_3\Delta t & 0 & 0 & 1-b_3\Delta t \end{bmatrix}, \quad (5.103)$$

$$B_{d,g} = \begin{bmatrix} 0 & 0 & K1_1\Delta t & K1_2\Delta t & K1_3\Delta t \end{bmatrix}^T, \quad (5.104)$$

$$G_{d,g} = \begin{bmatrix} 0 & \omega_h\Delta t & 0 & 0 & 0 \end{bmatrix}^T, \quad (5.105)$$

for each $g \in \{1,2,3\}$. We emphasize that the choice of $m = 3$ is motivated by a desire to aid exposition; the arguments and results obtained generalize to m arbitrary and finite. Next

we give a technical lemma that is useful for controller synthesis for the class of systems introduced above.

Lemma 5.6.1 *Let $A_{d,g} = \{A_{d,1}, A_{d,2}, A_{d,3}\}$ with $A_{d,g}$ defined as in (5.103) be given. Suppose that the characteristic polynomials of $A_{d,1}, A_{d,2}, A_{d,3}$ are denoted by $p_1(\lambda)$, $p_2(\lambda)$, and $p_3(\lambda)$ respectively, with,*

$$\begin{aligned} p_1(\lambda) &= (\lambda - 1 + b_2\Delta t)(\lambda - 1 + b_3\Delta t)H_1(\lambda), \\ p_2(\lambda) &= (\lambda - 1 + b_1\Delta t)(\lambda - 1 + b_3\Delta t)H_2(\lambda), \\ p_3(\lambda) &= (\lambda - 1 + b_1\Delta t)(\lambda - 1 + b_2\Delta t)H_3(\lambda), \end{aligned} \tag{5.106}$$

where

$$H_g(\lambda) = (\lambda - 1)^3 + \tilde{a}_g(\lambda - 1)^2 + \tilde{b}_g(\lambda - 1) + \tilde{c}_g, \tag{5.107}$$

and the constants $\tilde{a}_g, \tilde{b}_g, \tilde{c}_g$ are defined as

$$\tilde{a}_g = (a1_g + b_g)\Delta t, \tag{5.108}$$

$$\tilde{b}_g = (a0_g + a1_g b_g + L_g K2_g)\Delta t^2, \tag{5.109}$$

$$\tilde{c}_g = (a0_g b_g + L_g K1_g)\Delta t^3. \tag{5.110}$$

We choose the controller gains $K1_g, K2_g, b_g$ such that $H_1(\lambda) = H_2(\lambda) = H_3(\lambda) = H(\lambda)$ for all λ. We consider the case where the roots of the polynomial $P(\lambda) = (\lambda - 1 + b_1\Delta t)(\lambda - 1 + b_2\Delta t)(\lambda - 1 + b_3\Delta t)H(\lambda)$ are distinct. Then each pair of matrices $A_{d,1}$, $A_{d,2}$ and $A_{d,3}$ have exactly $n-1$ linearly independent common eigenvectors, where "n" is the dimension of the closed loop system (that is, 5).

Proof of Lemma 5.6.1: First we show the result for $A_{d,1}$ and $A_{d,2}$. Identical arguments can be developed for the matrix pairs $(A_{d,1}, A_{d,3})$ and $(A_{d,2}, A_{d,3})$. Note that $A_{d,1}$ and $A_{d,2}$ are

identical matrices except in the second row as it is apparent from

$$A_{d,1} = \begin{bmatrix} 1 & \Delta t & 0 & 0 & 0 \\ -a0_1\Delta t & 1-a1_1\Delta t & L_1\Delta t & 0 & 0 \\ -K1_1\Delta t & -K2_1\Delta t & 1-b_1\Delta t & 0 & 0 \\ -K1_2\Delta t & -K2_2\Delta t & 0 & 1-b_2\Delta t & 0 \\ -K1_3\Delta t & -K2_3\Delta t & 0 & 0 & 1-b_3\Delta t \end{bmatrix},$$

$$A_{d,2} = \begin{bmatrix} 1 & \Delta t & 0 & 0 & 0 \\ -a0_2\Delta t & 1-a1_2\Delta t & 0 & L_2\Delta t & 0 \\ -K1_1\Delta t & -K2_1\Delta t & 1-b_1\Delta t & 0 & 0 \\ -K1_2\Delta t & -K2_2\Delta t & 0 & 1-b_2\Delta t & 0 \\ -K1_3\Delta t & -K2_3\Delta t & 0 & 0 & 1-b_3\Delta t \end{bmatrix}.$$

We need to show that for each common eigenvalue, the matrices $A_{d,1}$ and $A_{d,2}$ have a common eigenvector, and that for the eigenvalue that is not common, the matrices have no common eigenvector. We also note that, by definition, $A_{d,1}$ and$A_{d,2}$ have $n-1$ distinct common eigenvalues. These eigenvalues correspond to the roots of $H(\lambda)$ and $\lambda = 1-b_3\Delta t$. The eigenvalues $\lambda = 1-b_2\Delta t$ (corresponding to $A_{d,1}$) and $\lambda = 1-b_1\Delta t$ (corresponding to $A_{d,2}$) are not common to both matrices. We first look at the eigenvectors corresponding to common eigenvalues.

Common eigenvalues:

The form of $A_{d,1}$ and $A_{d,2}$ implies that the common eigenvector corresponding to $\lambda = 1-b_3\Delta t$ is given by $v_1 = [\ 0\ \ 0\ \ 0\ \ 0\ \ 1\ ]^T$. Now let λ be an eigenvalue that is common to both matrices that is not equal to $1-b_3\Delta t$. The eigenvector of $A_{d,1}$ that corresponds to the

eigenvalue λ can be obtained by determining the null space of $\lambda I - A_{d,1}$:

$$\lambda I - A_{d,1} = \begin{bmatrix} \lambda - 1 & -\Delta t & 0 & 0 & 0 \\ a0_1\Delta t & \lambda - 1 + a1_1\Delta t & -L_1\Delta t & 0 & 0 \\ K1_1\Delta t & K2_1\Delta t & \lambda - 1 + b_1\Delta t & 0 & 0 \\ K1_2\Delta t & K2_2\Delta t & 0 & \lambda - 1 + b_2\Delta t & 0 \\ K1_3\Delta t & K2_3\Delta t & 0 & 0 & \lambda - 1 + b_3\Delta t \end{bmatrix}.$$

Let $[rA1_1, rA1_2, rA1_3, rA1_4, rA1_5]$ denote the row vectors of the matrix $\lambda I - A_{d,1}$, where $rA1_i$ is the i^{th} row vector. As should be clear from the above discussion the eigenvalues under interest here are such that $\lambda \neq 1 - b_g\Delta t$ where $g \in \{1,2,3\}$, that is λ is a root of $H(\lambda)$. It is clear that the row vectors $[rA1_1,\ rA1_3,\ rA1_4,\ rA1_5]$ are linearly independent, therefore it immediately follows that $\lambda I - A_{d,1}$ is singular. Hence, it must be possible to write $rA1_2$ as a linear combination of $[rA1_1,\ rA1_3,\ rA1_4,\ rA1_5]$. This implies that the eigenvector corresponding to λ is completely specified by the vectors $[rA1_1,\ rA1_3,\ rA1_4,\ rA1_5]$.

Now consider the matrix $A_{d,2}$. The eigenvector of $A_{d,2}$ that corresponds to the eigenvalue λ defined above can be obtained similarly by determining the null space of $\lambda I - A_{d,2}$:

$$\lambda I - A_{d,2} = \begin{bmatrix} \lambda - 1 & -\Delta t & 0 & 0 & 0 \\ a0_2\Delta t & \lambda - 1 + a1_2\Delta t & 0 & -L_2\Delta t & 0 \\ K1_1\Delta t & K2_1\Delta t & \lambda - 1 + b_1\Delta t & 0 & 0 \\ K1_2\Delta t & K2_2\Delta t & 0 & \lambda - 1 + b_2\Delta t & 0 \\ K1_3\Delta t & K2_3\Delta t & 0 & 0 & \lambda - 1 + b_3\Delta t \end{bmatrix}.$$

As before, let $[rA2_1, rA2_2, rA2_3, rA2_4, rA2_5]$ denote the row vectors of the matrix $\lambda I - A_{d,2}$, where $rA2_i$ is the i^{th} row vector. Again, $\lambda \neq 1 - b_g\Delta t$ where $g \in \{1,2,3\}$, that is λ is a root of $H(\lambda)$. Clearly the row vectors $[rA2_1,\ rA2_3,\ rA2_4,\ rA2_5]$ are linearly independent, and the matrix $\lambda I - A_{d,2}$ is singular. Hence, it is possible to write $rA2_2$ as a linear

combination of $[rA2_1,\ rA2_3,\ rA2_4,\ rA2_5]$. This implies that the eigenvector corresponding to λ is completely specified by the vectors $[rA2_1,\ rA2_3,\ rA2_4,\ rA2_5]$. However, the matrices $A_{d,1}$ and $A_{d,2}$ are identical except for the second row. Hence, it follows that $rA1_i = rA2_i,\ \forall\, i = \{1,3,4,5\}$, and that the matrices $A_{d,1}$ and $A_{d,2}$ have a common eigenvector for all common eigenvalues λ, where $\lambda \neq 1 - b_g\Delta t$ for $g \in \{1,2,3\}$.

Eigenvalues that are not common to matrices $A_{d,1}$ and $A_{d,2}$:

Consider the matrix $A_{d,1}$. The eigenvalue of $A_{d,1}$ that is not common to $A_{d,2}$ is $1 - b_2\Delta t$. The eigenvector of $A_{d,1}$ that corresponds to this eigenvalue is $v_2 = [\ 0\ \ 0\ \ 0\ \ 1\ \ 0\ ]^T$. Now consider the matrix $A_{d,2}$. The eigenvalue of $A_{d,2}$ that is not common to $A_{d,1}$ is $1 - b_1\Delta t$. The eigenvector of $A_{d,2}$ that corresponds to this eigenvalue is $v_3 = [\ 0\ \ 0\ \ 1\ \ 0\ \ 0\ ]^T$. Clearly, $v_2 \neq v_3$.

Q.E.D.

We now note the following facts concerning the matrix $A_{d,g}$.

(i) $rank\{A_{d,i} - A_{d,j}\} = 1$, for $i \neq j$, and $i, j \in \{1,2,3\}$.

(ii) The characteristic polynomials $p_1(\lambda), p_2(\lambda)$, and $p_3(\lambda)$ share $n-1$ common roots (eigenvalues) if $H_i(\lambda) = H(\lambda),\ i \in \{1,2,3\}$.

(iii) Let $H_i(\lambda) = H(\lambda)$, for $i \in \{1,2,3\}$. Then the matrices $A_{d,i}$ and $A_{d,j}$, for $i \neq j$ and $i, j \in \{1,2,3\}$, satisfy Lemma 5.6.1, and they share $n-1$ common real linearly independent eigenvectors.

The following corollary summarizes the sufficient conditions for the closed loop switched system stability for this problem.

Corollary 5.6.1 The sufficient conditions for the matrices $A_{d,g} \in \{A_{d,1}, A_{d,2}, A_{d,3}\}$ to satisfy the conditions of Theorem 5.4.1, and hence for the stability of the unforced system,

$$x(k+1) = A_{d,g}x(k), \qquad A_{d,g} \in \{A_{d,1}, A_{d,2}, A_{d,3}\} \tag{5.111}$$

are given by:

(i) the target polynomials $H_i(\lambda)$ have positive real eigenvalues in the unit circle for all $i \in \{1,2,3\}$;

(ii) $H_i(\lambda) = H_j(\lambda)$, $\forall i, j \in \{1,2,3\}$;

(iii) $1 > 1 - b_i\Delta t > 0$, $\forall i \in \{1,2,3\}$;

(iv) the roots of the polynomial $P(\lambda) = (\lambda - 1 + b_1\Delta t)(\lambda - 1 + b_2\Delta t)(\lambda - 1 + b_3\Delta t)H(\lambda)$ are distinct.

When these conditions are satisfied, one can easily verify that any 5 of the 6 linearly independent eigenvectors given by the eigenvectors of $A_{d,1}, A_{d,2}, A_{d,3}$, are linearly independent. Therefore, the hypothesis of Theorem 5.4.1 is satisfied, and the origin of the switched system representing the unforced roll plane dynamics model given in (5.102) with $r = 0$ and $a_y = 0$, is globally attractive and asymptotically stable. BIBO stability of the forced system with $r \neq 0$ and $a_y \neq 0$ follows directly from elementary arguments given in Lemma 5.5.2 (also see [102]).

We next give the following corollary that is useful in obtaining roll dynamics emulation controllers that satisfy Lemma 5.6.1.

Corollary 5.6.2 Suppose that the discrete time roll dynamics model with three switches as described in (5.102) along with the matrices (5.103),(5.104), and (5.105) is given. Noting that each constituent switched system is of 5^{th} order, we assume that the closed loop system matrices $A_{d,1}, A_{d,2}, A_{d,3}$ share three real common eigenvalues and the corresponding real eigenvectors. We denote these common eigenvalues as $\gamma_1, \gamma_2, \gamma_3$, and further assume that they satisfy $0 < \gamma_g < 1$ for each $g \in \{1,2,3\}$. Then with the following choice of the gains

for the PID controller given in (5.99) for each $g \in \{1,2,3\}$

$$b_g = \frac{3-(\gamma_1+\gamma_2+\gamma_3)}{\Delta t} - a1_g, \tag{5.112}$$

$$K2_g = \left[\frac{-3+2\tilde{a}_g+(\gamma_1\gamma_2+\gamma_1\gamma_3+\gamma_2\gamma_3)}{\Delta t^2} - a0_g - a1_g b_g\right]\frac{1}{L_g}, \tag{5.113}$$

$$K1_g = \left[\frac{1-\tilde{a}_g+\tilde{b}_g-\gamma_1\gamma_2\gamma_3}{\Delta t^3} - a0_g b_g\right]\frac{1}{L_g}, \tag{5.114}$$

results in three closed loop switched systems (5.102) that satisfy the conditions of Lemma 5.5.1 and Theorem 5.4.1. The definitions of $\tilde{a}_g, \tilde{b}_g, \tilde{c}_g$ appearing in the above expressions are as described in (5.108),(5.109), and (5.110) and they utilize the roll model parameters given with (5.96) and (5.97) above.

Remark 5.6.2 ***(Condition for transient free switching)***

It is known that a switched control structure such as the one introduced here can induce undesirable transients, which result from state transitions after the switching of a controller [139]. However, in a recent thesis [140] it is shown that when the constituent systems corresponding to different controllers in the feedback loop have a common steady-state for a given constant input signal, then the overall switched system has no transients, given that the switching occurs during steady state. In order obtain a more refined control design, we can also make use of this result. Note that, for the emulation controller synthesis procedure we developed so far, we made no specific mention of the fact that each of the individual switched controllers C_i defined in (5.99) can result in a different steady state roll angle for a given constant lateral acceleration input. Denoting the steady-state for the g^{th} controller by $\hat{x}_g(k)$, the steady state requirement for the discrete time switched forced roll plane model given in (5.102) is that $\hat{x}_g(k+1) = 0$, which yields the following expression

$$\hat{x}_g(k) = -A_{d,g}^{-1}B_{d,g}r(k) - A_{d,g}^{-1}G_{d,g}a_y(k), \tag{5.115}$$

for $g \in \{1,2,3\}$. In order to make the steady state roll angle uniform for each C_i, one can possibly multiply the reference roll angle $r(k)$ by a gain such that the first element of the steady-state $\hat{x}_g(k)$ is constant for each g. That is, instead of using $r(k)$ as the reference roll

angle signal, a modified signal $\hat{r}_g(k)$ can be used for each of the constituent systems, which is defined as follows

$$\hat{r}_g(k) = \alpha_g r(k), \tag{5.116}$$

where $\alpha_g \in \mathbb{R}$ are a set of scalars. Fixed gains α_g are chosen such that the first element of the steady-state (i.e., the steady state roll angle), which we denote by $[\hat{x}_g]_1(k)$ is constant. That is

$$[\hat{x}_i]_1(k) = [\hat{x}_j]_1(k), \tag{5.117}$$

for all $i, j \in \{1,2,3\}$. Note that this condition is easily implemented in the control design through a pre-filtering of the reference roll angle signal, which is shown in Figure 5.7.

With this background in mind, and making use of Corollary 5.6.2 we next demonstrate the roll dynamics emulation controller design with a numerical example.

Example 5.6.1 In this example we assume a similar simulation scenario to that of Section 5.5. That is, we assume the single track model with roll degree of freedom given in (5.91) to represent the real vehicle in simulation with a constant velocity at $v_x = 20m/s$. Also the driver's gradual step steering input with a peak magnitude of 80° was assumed to be the same. For the ease of exposition we assumed that the CG height of the vehicle switches between three distinct positions; this reflects a possible situation where the loads dislocate inside the vehicle vertically as a result of the inertial forces induced during a maneuver. Without loss of generality, we assumed a repeating switching sequence between $0.9[m] \rightarrow 0.7[m] \rightarrow 0.5[m]$ in the CG height as shown in Figure 5.8 along with the driver steering input. Also, we set the discrete time step as $\Delta t = 0.005$ and the rest of the vehicle model parameters used in the example are as specified in Table 5.2, which are representative of a compact class vehicle. Next we give the results of the discrete time controller advocated here for roll dynamics emulation based on Corollary 5.6.2, and in a feedback loop with the single track model with roll degree of freedom as the plant model.

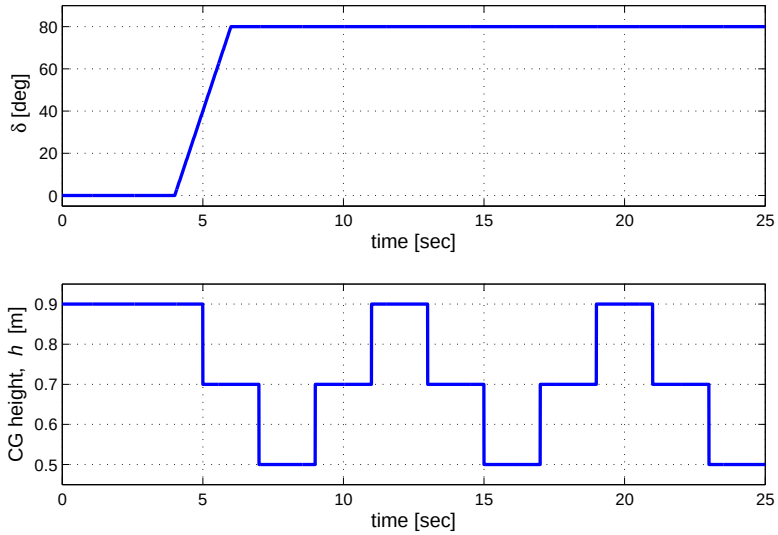

Figure 5.8: Driver steering wheel input δ (where steering ratio is $1/20$) and the time varying CG height during the maneuver.

Without loss of generality, we set the three eigenvalues that are common to each of the $A_{d,1}, A_{d,2}, A_{d,3}$ matrices as follows

$$\gamma_1 = 0.9, \qquad \gamma_2 = 0.7, \qquad \gamma_3 = 0.5.$$

Utilizing the Corollary 5.6.2 we then obtained the the following controller gains

$$\begin{array}{lllllllll} b_1 & = & 151.6667 & b_2 & = & 154.3694 & b_3 & = & 156.0692 \\ K1_1 & = & 4.4343\times 10^7 \ , & K1_2 & = & 6.7681\times 10^7 \ , & K1_3 & = & 9.8731\times 10^7 \ . \\ K2_1 & = & 3.2976\times 10^6 & K2_2 & = & 5.2448\times 10^6 & K2_3 & = & 7.8498\times 10^6 \end{array}$$

Assuming a forward difference approximation for the derivatives in (5.99) and applying a Z-transform with zero initial conditions, we implemented the switched controllers as discrete time transfer functions given below

$$\frac{u_g(z)}{e(z)} = \frac{K2_g z + K1_g \Delta t - K2_g}{z - 1 + b_g \Delta t}, \quad for \quad g \in \{1,2,3\}, \tag{5.118}$$

where $u_g(z) = \mathbf{Z}[u_g(k)]$, and $e(z) = \mathbf{Z}[e(k)]$.

In Figure 5.9 the resulting state histories are shown for the controlled and uncontrolled vehicles during the maneuver. Note that we also show the reference roll angle signal in this figure. Based on the simulation results, the roll angle tracking performance of the controller demonstrates the effectiveness of the controller. An important observation based on the

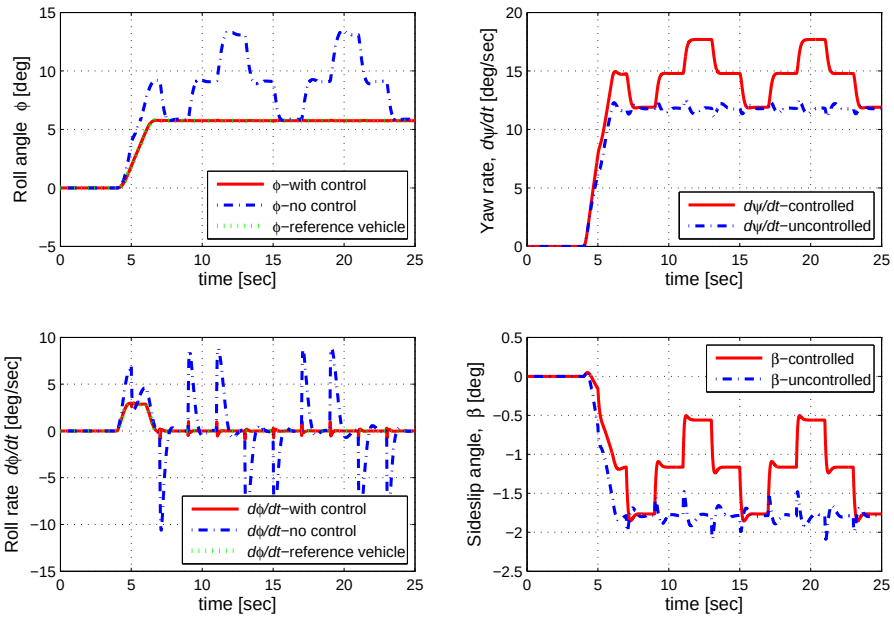

Figure 5.9: Comparisons of the model states for the vehicles with and without the emulation controller.

simulation results as seen in the figure is that the roll torque input generated by the active suspension actuators affect the lateral dynamics of the vehicle significantly. In particular, the yaw rate of the controlled vehicle as seen at the top right of the figure shows significant changes in the steady state value of the controlled vehicle. Although the switching in the side slip angle of the controlled vehicle seen in the bottom right of the figure has a small magnitude, the switching in yaw rate has very large magnitude and is likely to change the cornering behavior of the vehicle. Also, it might be uncomfortable (or even dangerous) for the driver when the steady state yaw rate switches as a result of the control action. In order to prevent this, the effect of the roll torque input on the steady state value of the yaw rate can

be compensated utilizing active steering inputs in a second control loop. This requires the availability of active steering actuators in the front wheels, and we here assume a specific type of such actuators commonly known as the “mechatronic-angle-superposition" steering actuator. This type of actuators contain a physical steering column and act cooperatively with the driver, while they permit various functions such as speed dependent steering ratio modification, and active response to mild environmental disturbances (see [125] for an extensive discussion of active steering actuators). Using this type actuators, the effective steering input to the vehicle can be expressed as

$$\delta = \delta_{driver} + \delta_{active}. \tag{5.119}$$

The effect of the roll torque input on the steady state yaw rate can be calculated analytically using the closed-loop single track model with roll degree of freedom given in (5.91). At steady state the closed loop model becomes

$$x_{ss} = -A^{-1}B\delta - A^{-1}Gu, \tag{5.120}$$

where $x_{ss} = \begin{bmatrix}\beta_{ss} & \dot{\psi}_{ss} & \dot{\phi}_{ss} & \phi_{ss}\end{bmatrix}^T$ is the value of the steady state. Also, $A \in \mathbb{R}^4$ is the system matrix given (5.91), and B, G are defined as follows from the same equation

$$B = \begin{bmatrix} \frac{C_v}{mv_x} & \frac{J_{xeq}}{J_{xx}} & \frac{C_v l_v}{J_{zz}} & \frac{hC_v}{J_{xx}} & 0 \end{bmatrix}^T, \qquad G = \begin{bmatrix} 0 & 0 & \frac{1}{J_{xx}} & 0 \end{bmatrix}^T. \tag{5.121}$$

In order to obtain the required active steering input to cancel the steady state contribution of u on the yaw rate, one can use (5.120) with δ_c as the only steering input and also set $\dot{\psi}_{ss}$ to zero. This then yields the following switched active steering compensator

$$S_g: \quad \delta_{c,g} = \frac{\rho h_g m}{J_{xx} C_v (\rho + \sigma l_v)} u, \tag{5.122}$$

where the subscript $g \in \{1, 2, \cdots, m\}$ denotes the current (detectable) CG height setting. The resulting integrated control structure with both active suspension and active steering inputs are schematically represented in Figure 5.10.

Implementation of this simple active steering compensation to the simulation scenario described above results in the effective steering input shown in Figure 5.11, where the resultant

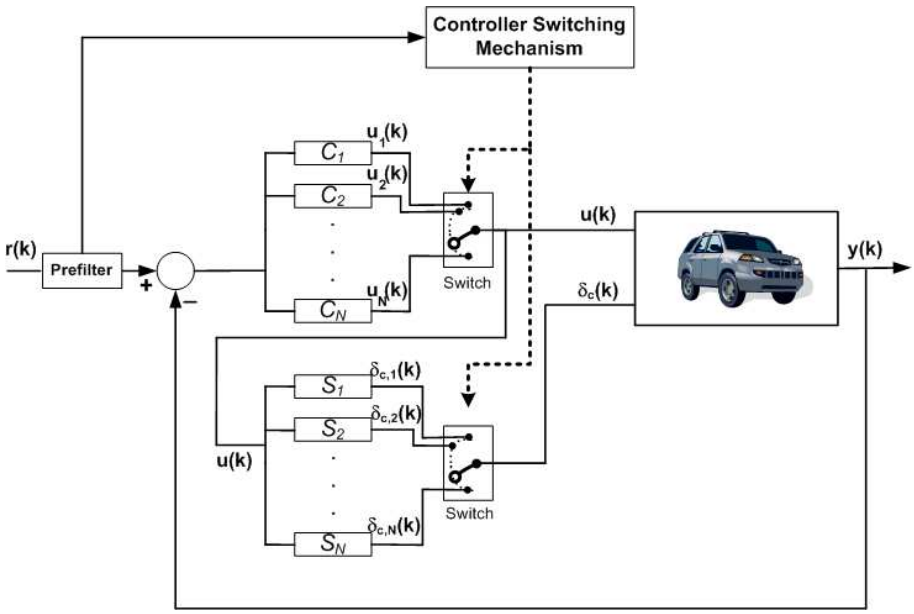

Figure 5.10: Integrated roll dynamics emulation controller structure with active suspension and active steering.

steering input is also compared with the driver input. In Figure 5.12 the resulting roll angle and roll rate history is shown for the controlled and uncontrolled vehicles during the maneuver. Note that we also show the reference roll angle signal in this figure. Based on the simulation results, the tracking performance of the controller demonstrates the effectiveness of the suggested controller. The corresponding yaw rate and side slip plots for the controlled and uncontrolled vehicles are shown in Figure 5.13, where the effect of the active steering compensation on the yaw rate and sideslip trajectories are obvious when compared to the simulation results given in Figure 5.9 for the emulation controller without the active steering compensation. Note here that there is still some visible switching in the side slip however its magnitude is very small and it would probably be undiscernible for the driver. We emphasize that the aim of the active steering compensation here is to cancel the effect suspension controller on the steady state yaw rate, this was achieved as observable from the simulation results. Finally, in order to see how the suggested controllers affect the vehicle path, we again used (5.93) and (5.94) to calculate the vehicle path during the maneuver,

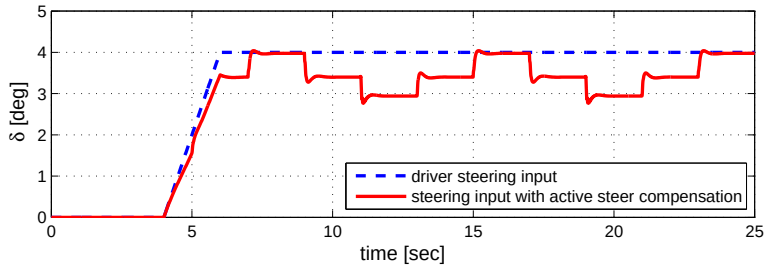

Figure 5.11: Comparison of the driver steering wheel input δ_d and the effective steering input $\delta = \delta_d + \delta_c$ as a result of active steer compensation.

where we choose the initial coordinates $(x(0), y(0))$ to be zero for both the controlled and the uncontrolled vehicles. In Figure 5.14 the trajectories of the CG position of the controlled (with and without active steering compensation) and the uncontrolled vehicles on a lateral plane representing the road surface is shown. We observe that due to the high magnitude switching in the controlled vehicle with no active steer compensation, the corresponding trajectory has diverged greatly from the uncontrolled vehicle. It is also observed from the same trajectory that the switching in yaw rate causes significant changes in the lateral motion of the vehicle and therefore the resulting path is non-circular. However, none of these occur in the controlled vehicle with the active steering compensation, and the corresponding vehicle trajectory is almost identical to the uncontrolled one. This is more apparent from Figure 5.15, where the instantaneous distances of the controlled vehicles with and without the active steering compensation relative to the uncontrolled vehicle trajectory are compared. Note that, we compute the instantaneous relative distance according to

$$distance(k) = \sqrt{(x_{cont}(k) - x_{nocont}(k))^2 + (y_{cont}(k) - y_{nocont}(k))^2} \tag{5.123}$$

for vehicles with either of the emulation controllers, where the pair $(x_{cont}(k), y_{cont}(k))$ denote the instantaneous coordinates of the controlled vehicle, whereas $(x_{nocont}(k), y_{nocont}(k))$ denote that of the uncontrolled one. As seen from from this last figure, the vehicle with the emulation controller and with the active roll compensation stays very close to uncontrolled vehicle. This is favorable in the sense that the suggested controller does not interfere with

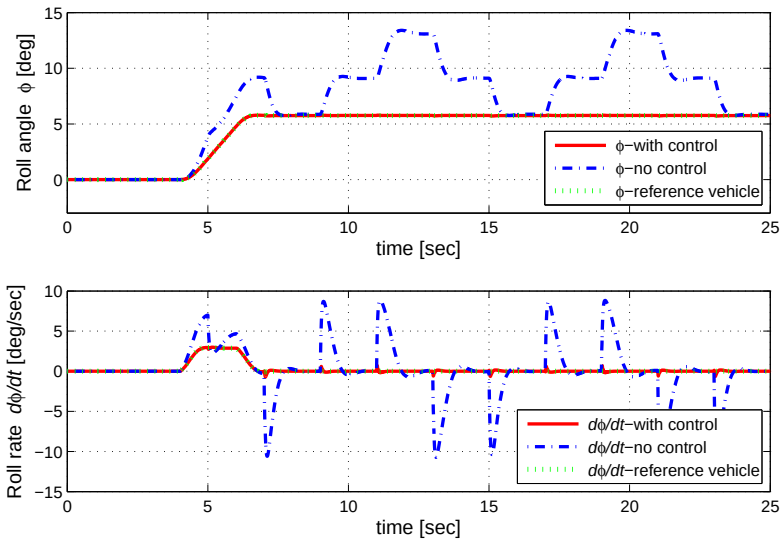

Figure 5.12: Roll angle and and roll rate history of the emulation controller with active steering compensation.

the vehicle path for tracking a certain reference roll signal, and thus the vehicle retains its natural lateral response. Moreover these characteristics are not effected from the switches in the CG height.

Remark 5.6.3 As a final comment, it is important to mention about the robustness of the control design methods introduced so far. We assumed neither uncertainty in the system matrices, nor inexact knowledge of the switching instants for either of the applications introduced so far. When automotive applications are considered, such certainty would practically be overly optimistic and uncertainty must always be taken into account. It has been shown in [113] that, uncertainty in the eigenvectors and eigenvalues of the switched system matrices can lead to instability for a related class of continuous time systems to those introduced in Theorem 5.4.1. The theoretical and numerical analysis of robustness for the class of discrete time switched systems introduced in this chapter is still an open question. Our future work will include a detailed analysis of the robustness for these systems, and the control syntheses will include compensation of uncertainty.

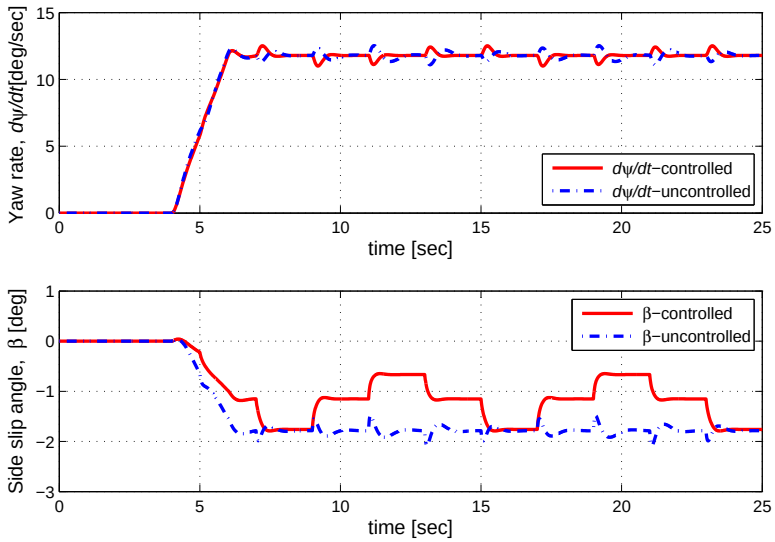

Figure 5.13: Yaw rate and side slip history of the emulation controller with active steering compensation.

5.7 Conclusions and possible future directions

In this chapter we have shown that the global attractivity results for a class of discrete-time switching systems is not necessarily equivalent to continuous time systems with this property. Hence, in cases when the existence of a CQLF is unknown for the switched set of LTI systems, qualitative statements concerning the system stability for the continuous-time as well as the discrete-time systems must be validated separately using non-CQLF techniques. One such technique for a specific class of discrete time systems is presented in the current chapter; namely, a technique which proves global attractivity by embedding the original (n-dimensional) state space in a higher $(n+1)$ dimensional state space. This result can be translated into practical control design laws for switched systems. As a motivation for the applications of this main result, we presented two examples where this result is used to design controllers that are robust with respect to switching action. Both design examples are related to automotive roll dynamics stabilization problem that involves switching as a result of changing CG height. We have shown in the first application numerically that,

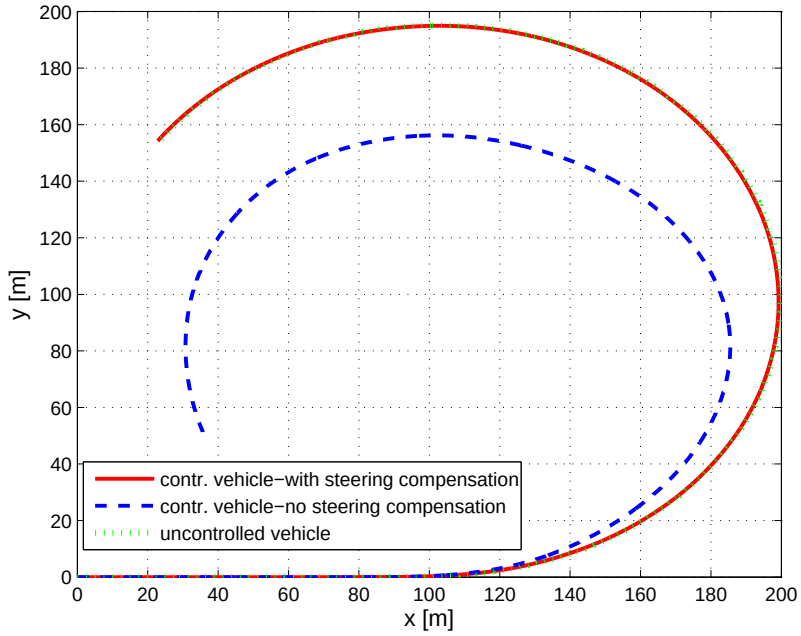

Figure 5.14: Comparison of controlled and uncontrolled vehicle trajectories for the suggested emulation controllers.

for a simplified version of the problem that is constrained to only three switches in the plant parameters, the chosen switched unforced system had no CQLF; for this problem we presented a stabilizing controller synthesis procedure utilizing the non-CQLF technique that is the main result of this chapter. In the second application we presented a PID control synthesis procedure for the emulation of roll dynamics, where tracking a reference signal related to roll dynamics was the main goal. Based on the numerical simulation results, both examples demonstrate the efficacy of the suggested design techniques.

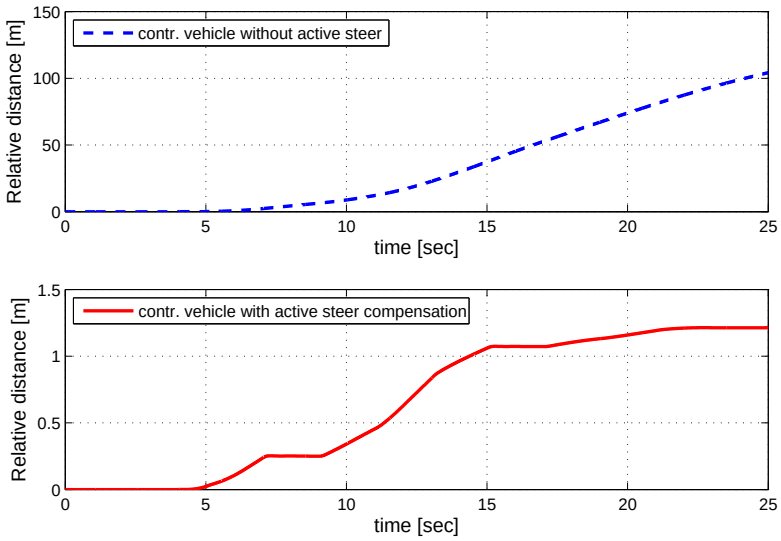

Figure 5.15: Comparison of relative distances of the controlled vehicles with and without active steering with respect to the uncontrolled vehicle.

Chapter 6

Integrated Decentralized Automotive Dynamics Tracking Controllers that Account for Structural Uncertainty

In this chapter we present a method for decentralized control design for systems with multiple dynamical modes, which guarantees robustness with respect to structural uncertainty. We consider the implementation of this method to the decentralized control designs for the automotive lateral and roll reference dynamics tracking. The respective control rules that we utilize are based on simplified, 2-state roll and lateral dynamics models of the vehicle. We utilize a method for checking the overall stability of the integrated controllers based on a frequency domain criterion. We also give a numerical example for the integrated automotive tracking control designs based on PI feedback, which utilize active suspension and active steering actuators. Finally, we show how this result can preserve robustness with respect to sensor failure in such applications. We acknowledge that the work in this chapter is an application

of some recent results by Shorten and Narendra reported in [119] and Shorten, Curran, Wulff, King and Zeheb reported in [109] and [110]; also it is a joint work between ourselves, Dr. Mark Readman and Carlos Villegas as part of the EU funded project CEmACS.

6.1 Chapter contributions

It is a known fact that most real-life engineering systems have dynamical subsystems that interact. With this perspective, the contribution of this chapter is in considering a novel integration method for simplified decentralized controllers, each of which are designed for controlling different dynamical modes of a complicated dynamical system. This is an important problem as most engineering systems can be modelled with many simplified dynamical subsystems that interact with each other. In the context of automotive vehicle dynamics control, we encountered the effects of dynamical interactions during the roll dynamics tracking problem analyzed in Section 5.6. Thus, another major contribution of the chapter in implementing the suggested decentralized control design for the problem of simultaneous control of the vehicle roll and lateral dynamics, which can be considered as a means to dynamically imitate other vehicle types. Based on the results we showed that the suggested method can provide robustness with respect to structural uncertainty, which can be considered as a failure mitigation method in the case of sensor and/or subsystem failure in automotive vehicles.

6.2 Introduction

It is an irrefutable fact that decentralized control is a feature of the control engineering practice. A basic problem in the design of control systems is the lack of simple methods for designing decentralized controllers that are robust with respect to certain types of struc-

tural uncertainties. Most complex engineering systems can be described by a number of interacting dynamical modes and sub-processes. When control of such systems are considered, the engineering practice is to utilize a number of control systems, each of which are designed to control a particular sub-process or a dynamical mode. Such designs arise for a number of reasons. Firstly, it is human nature to divide a complicated problem into a set of simpler ones, each of which can be solved independently of each other. Second, even when a centralized controller is possible, in practice, a low order decentralized controller is often preferred due to their simplicity and ease of implementation. Third, when networked control systems are considered, it is often the case that interconnected subsystems must be designed to be individually stable, even when interconnected together, so that they are robust to the effects of unreliable communication between each of the subsystems. Finally, from the perspective of the industry, it is often the case that different sub-contractors are assigned separate parts of a complex control task; the automotive industry provides a very good example of this latter point. In terms of vehicle dynamics control applications, it is common in the automotive industry that some parts suppliers design and manufacture the roll over prevention systems, and some other manufacturers supply the lateral dynamics control systems (such as the ESP®) for the same vehicle. Even though each of these control systems affect one another[1], and even sometimes these utilize common sensor and actuator units, they are often designed independently of each other. Also, it is a common practice in the automotive industry to utilize sensor measurements to artificially decouple dynamical interactions of the vehicle, and the control task at hand then becomes the development of methods for the integration of these units so that the overall performance objectives, and also a certain degree of robustness are met with respect to unreliable sensor measurements.

Motivated by these facts, our objective in this chapter is to present one such method and to explore how some of the methods developed in this thesis can be integrated with other

[1]We have seen in the preceding chapters that the lateral and the roll dynamics of the vehicle interact at various levels. Therefore, controllers designed to control these also interact, as we have clearly seen in Section 5.6.

automotive control systems in a structured manner. To aid the exposition, we utilize decentralized controllers based on the two-state single track model and the two-state roll plane model to simultaneously track reference vehicle states. Therefore, here we discuss about how to integrate a controller for the roll degree of freedom, with that for the lateral degree of freedom in a vehicle equipped with both active suspension and active front wheel steering actuators, while at the same time achieving a decentralized design that is not restricted by the structural constraints and uncertainties imposed on the problem.

6.3 A decentralized control design methodology

In an abstract setting, the basic task of the control approach we utilize is to find a decentralized control structure that simultaneously stabilizes a number of subsystems and the integrated overall system, as well as it guarantees robustness with respect to certain types of structural (possibly time-varying) uncertainty. A basic mechanism for achieving this objective is to select decentralized feedback structures such that the linearized closed loop system admits a block diagonal Lyapunov function. The existence of such a Lyapunov function is not only sufficient for guaranteeing the stability of the constituent subsystems and the interconnected system (i.e., the integrated overall system), but it is also sufficient that the overall system is stable with respect to uncertain measurements, which affect certain regions of the system matrix, and whose bounds can be quantified. In what follows, we formally describe the problem and then present our approach for the decentralized controller design task.

Let $A \in \mathbb{R}^{n \times n}$ be a Hurwitz[2] stable matrix, which represents the overall closed loop system matrix of a dynamical process with two interacting constituent subsystems, which have the

[2]This means that all the eigenvalues of the matrix A have strictly negative real parts. This also implies that the LTI system $\dot{x} = Ax$ is exponentially stable.

following structure

$$\dot{x} = Ax \qquad \text{with} \qquad A = \begin{bmatrix} A_{11} & A_{12} \\ A_{21} & A_{22} \end{bmatrix}, \tag{6.1}$$

where both $A_{11} \in \mathbb{R}^{(n-m)\times(n-m)}$ and $A_{22} \in \mathbb{R}^{m\times m}$ are assumed to be Hurwitz stable also. For example, this equation can be considered to represent the error dynamics of a given closed loop system. A basic question that arises for this feedback system is whether one can find a positive, block diagonal matrix $P = P^T > 0$, such that

$$\left.\begin{aligned} A_{11}^T P_{11} + P_{11} A_{11} < 0 \\ A_{22}^T P_{22} + P_{22} A_{22} < 0 \\ A^T P + PA < 0 \end{aligned}\right\} \tag{6.2}$$

with

$$P = \begin{bmatrix} P_{11} & 0 \\ 0 & P_{22} \end{bmatrix}, \tag{6.3}$$

where $P_{11} \in \mathbb{R}^{(n-m)\times(n-m)}$ and $P_{22} \in \mathbb{R}^{m\times m}$. In other words we want to stabilize each of the constituent subsystems, and the entire interconnected system, simultaneously. If such a block diagonal, positive matrix $P = P^T > 0$ exists, then not only is the system stable, but also it is stable with respect to structural uncertainties in A_{12} and A_{21},which in effect, can be considered as robustness with respect to system failure. Despite having a long history in control theory, this problem, namely the problem of finding vector Lyapunov functions, remains open to this day. Fortunately, in our situation, one may find feedback strategies to ensure a block diagonal Lyapunov function as described in the sequel.

Let $B \in \mathbb{R}^{n\times m}$ be the matrix of all zeros except for the last m rows and m columns which are set to be the elements of $m \times m$ identity matrix, and which we denote by $I_m \in \mathbb{R}^{m\times m}$, such that B matrix is expressed as follows

$$B = \begin{bmatrix} 0_{n-m\times m} \\ I_m \end{bmatrix}. \tag{6.4}$$

Further we denote $s \in \mathbb{R}$, as the scalar variable in the frequency domain. Suppose now that one can find a symmetric matrix $\hat{P} = \hat{P}^T \in \mathbb{R}^{m\times m}$ such that

$$\hat{P}B^T(sI_n - A)^{-1}B, \tag{6.5}$$

is Strictly Positive Real (SPR).

Suppose further that the matrix pair (A,B) is controllable and at the same time, the matrix pair $(A,B\hat{P})$ is observable. Then, it follows from the KYP lemma [49] that the frequency domain condition (6.5) is sufficient for the existence of a matrix $P = P^T > 0$ that satisfies:

$$\left.\begin{array}{rcl} A^TP + PA & < & 0 \\ PB & = & B\hat{P} \end{array}\right\} \tag{6.6}$$

This in turns guarantees the existence of a block diagonal P matrix with $P_{22} = \hat{P}$. This simple idea translates into a decentralized design strategy for our application as follows.

Proposition 6.3.1 (**Decentralized control design procedure**)

Suppose that a feedback system structure of the form (6.1) is given, where the aim is to design controllers for the subsystems $\dot{x_1} = A_{11}x_1$ and $\dot{x_2} = A_{22}x_2$ such that the overall system $\dot{x} = Ax$ with $x = [x_1, x_2]^T \in \mathbb{R}^n$ is stable regardless of bounded structural uncertainties that might be present in the blocks A_{12} and A_{21}. The following design rule achieves this.

(a) Design a feedback strategy for block $\dot{x_2} = A_{22}x_2$, where $x_2 \in \mathbb{R}^m$, so that the basic design requirements for this subsystem are met over a range of operating conditions; this also specifies the matrix $\hat{P} \in \mathbb{R}^{m\times m}$.

(b) Select the control strategy for block $\dot{x_1} = A_{11}x_1$, where $x_1 \in \mathbb{R}^{n-m}$ such that

$$\hat{P}B^T(sI_n - A)^{-1}B, \tag{6.7}$$

is SPR.

6.4 Decentralized control design for vehicle dynamics tracking

To illustrate the technique introduced in Proposition 6.3.1, we use a problem that is initially considered in [2]. Specifically, here we implement the methodology described in the preceding section for synthesizing vehicle dynamics controllers for simultaneous tracking the reference lateral and roll dynamics. The motivation for this problem was described in detail in Chapter 5. While we considered the roll dynamics tracking to be the main focus in the preceding chapter, here we are concerned with the tracking of both roll and lateral dynamics based on decentralized controllers and utilizing active suspension and active steering actuators. In doing so, we take the dynamical interactions into account in the design such that the stability of the resulting controlled roll and lateral dynamics are unaffected from the interactions. To keep the discussion reasonably simple, we use simplified vehicle dynamics models, which have already been introduced in the preceding chapters in detail. Specifically, we design the lateral tracking controller based on the active steering actuator and using the two-state single track model, while we use the two-state roll plane model with active suspension actuator for designing the roll dynamics tracking controller. We then integrate both controllers based on the design methodology outlined in Proposition 6.3.1. We show the efficacy of the resulting integrated tracking controller with numerical simulations, and as applied to a four-state single track model with the roll degree of freedom.

6.4.1 Lateral PI controller design based on LQR

In this subsection we introduce a simple lateral dynamics reference tracking controller design utilizing the linear single track model with active front steering input. For this control design we assume that mechatronic-angle-superposition type active steering actuators on the front wheels provide the sole control input. We previously introduced these actuators

in Chapter 3 in the context of rollover prevention control design. Also we utilized the two-state single track model for vehicle parameter estimation in Chapter 2. Here we combine this model and the actuator to design a simple PI control law, where the control gains are obtained by LQR (Linear Quadratic Regulator) design techniques.

The two-state single track model[3] is the simplest model that represents the lateral dynamics of a car in the horizontal plane, where the effects of heave, roll, and pitch motions are all ignored [2]. It is also assumed that only the front tire is used for steering the vehicle, and that the steering angle is small. In this model, we represent the horizontal dynamics in terms of the state variables β and $\dot{\psi}$, that is the *sideslip angle* and the *yaw rate*, respectively. Both of these states are assumed to be small for linearization. The corresponding state space representation of the model with active steering input is given as follows

$$\begin{bmatrix} \dot{\beta} \\ \ddot{\psi} \end{bmatrix} = \begin{bmatrix} -\frac{\sigma}{mv_x} & \frac{\rho}{mv_x^2} - 1 \\ \frac{\rho}{J_{zz}} & -\frac{\kappa}{J_{zz}v_x} \end{bmatrix} \cdot \begin{bmatrix} \beta \\ \dot{\psi} \end{bmatrix} + \begin{bmatrix} \frac{C_v}{mv_x} \\ \frac{C_v l_v}{J_{zz}} \end{bmatrix} \delta_d, + \begin{bmatrix} \frac{C_v}{mv_x} \\ \frac{C_v l_v}{J_{zz}} \end{bmatrix} u_1, \tag{6.8}$$

where δ_d is the driver steering command, and u_1 is the steering command from the active steering actuator. Also, the auxiliary parameters $\sigma, \rho,$ and κ are defined as below

$$\left.\begin{aligned} \sigma &\triangleq C_v + C_h \\ \rho &\triangleq C_h l_h - C_v l_v \\ \kappa &\triangleq C_v l_v^2 + C_h l_h^2 \end{aligned}\right\} \tag{6.9}$$

For further description of the parameters of the model, refer to Table 2.1 and the Chapter 2.

The purpose of the control design we consider here is to follow a reference yaw rate trajectory[4]. This choice is motivated by the fact that the yaw rate $\dot{\psi}$, along with the lateral acceleration a_y are responsible for most of the *lateral handling feel*, (i.e., the lateral response) of

[3] See Figure 2.1 for the graphical representation and the notations of the model.

[4] It is possible to consider the tracking of both the yaw rate $\dot{\psi}$, and the sideslip angle β given that there is more control authority such as the differential braking and/or active front and rear wheel steering. However, we assume neither of these actuators in this discussion.

an automotive vehicle, and therefore are the natural targets for emulation. We can achieve this by introducing a new integrator state x_I as a function of the yaw rate tracking error

$$\dot{x}_I = \dot{\psi} - \dot{\psi}_{ref} = \dot{\psi} - \alpha\delta_d, \tag{6.10}$$

where $\dot{\psi}_{ref}$ denotes the reference yaw rate trajectory, which is a linear function of the driver steering input δ_d. Thus, the scalar α is the steady-state gain from the driver steering input δ_d to the reference yaw rate $\dot{\psi}_{ref}$ for the vehicle that we want to emulate. Further, we can define an augmented state $x_1 \in \mathbb{R}^3$ given as below

$$x_1 = \begin{bmatrix} \beta & \dot{\psi} & x_I \end{bmatrix}^T, \tag{6.11}$$

which results in the following augmented feedback system description

$$\left.\begin{aligned} &\dot{x}_1 = A_{11}x_1 + B_1\delta_d + B_2u_1 \quad \text{with} \\ &A_{11} = \begin{bmatrix} -\frac{\sigma}{mv_x} & \frac{\rho}{mv_x^2} - 1 & 0 \\ \frac{\rho}{J_{zz}} & -\frac{\kappa}{J_{zz}v_x} & 0 \\ 0 & 1 & 0 \end{bmatrix}, \quad B_1 = \begin{bmatrix} \frac{C_v}{mv_x} \\ \frac{C_v l_v}{J_{zz}} \\ -\alpha \end{bmatrix}, \quad B_2 = \begin{bmatrix} \frac{C_v}{mv_x} \\ \frac{C_v l_v}{J_{zz}} \\ 0 \end{bmatrix} \end{aligned}\right\} \tag{6.12}$$

Now in order to track the reference yaw rate trajectory, it is possible to design a PI linear state feedback rule based on the active steering input u_1 of the form below

$$u_1 = Kx_1 = \begin{bmatrix} K_{p1} & K_{p2} & K_I \end{bmatrix} x_1, \tag{6.13}$$

where K_{p1}, K_{p2} are the proportional gains for the first two states, and K_I is the control gain corresponding to the integrator state. While there are many ways to specify these gains, we use a quadratic cost optimization technique known as the LQR for designing the control input. This choice is motivated by the fact LQR is a well known method for state feedback design and also that there are convenient numerical tools developed for this purpose (such as the Matlab® control system toolbox). Just to briefly explain, for a linear system $\dot{x} = Ax + Bu$ with $x \in \mathbb{R}^n$, $u \in \mathbb{R}^m$ and $x(0) = x_0$, the LQR design method for choosing a state feedback

controller $u = Kx$ amounts to finding the fixed control gain vector

$$K = \begin{bmatrix} K_{11} & \dots & K_{1n} \\ \vdots & \ddots & \vdots \\ K_{m1} & \dots & K_{mn} \end{bmatrix},$$

such that the closed loop system is stable, and also that the quadratic cost function

$$J(x_0, u(\cdot)) = \int_0^\infty \left[x(t)^T Q x(t) + u(t)^T R u(t) \right] dt, \tag{6.14}$$

is minimum for the choice symmetric matrices $Q = Q^T \geq 0 \in \mathbb{R}^{n \times n}$ and $R = R^T > 0 \in \mathbb{R}^{m \times m}$. The matrices Q and R are known as the *weighting matrices* and are the tuning parameters in this design approach. We shall present the numerical implementation of this controller in Section 6.4.3 below, where we will choose the matrices Q and R such that SPR condition given in (6.7) are satisfied.

6.4.2 Roll PID controller design based on pole placement

In this subsection we use the second order roll plane model derived in Section 2.3.2 in detail, for designing the roll angle reference tracking controller based on the active suspension actuators. We note that the control design approach suggested here is based largely on the pole placement controller introduced in Section 5.6; the difference is in that we here consider the continuous-time version with fixed and known system parameters[5].

Assuming that the sprung mass of the vehicle rolls about a fixed horizontal roll axis along the centerline of the vehicle body relative to the ground, and also that all angles are small, the equations describing the roll plane motion of an automotive vehicle can be expressed in

[5]We emphasize that it is also possible to consider linear time varying systems in the scope of the control design approach introduced in this Chapter, which shall be future direction.

the following state space form with reference to Figure 5.1

$$\begin{bmatrix} \dot{\phi} \\ \ddot{\phi} \end{bmatrix} = \begin{bmatrix} 0 & 1 \\ -\frac{k-mgh}{J_{x_{eq}}} & -\frac{c}{J_{x_{eq}}} \end{bmatrix} \cdot \begin{bmatrix} \phi \\ \dot{\phi} \end{bmatrix} + \begin{bmatrix} 0 \\ \frac{mh}{J_{x_{eq}}} \end{bmatrix} a_y + \begin{bmatrix} 0 \\ \frac{1}{J_{x_{eq}}} \end{bmatrix} u_2, \tag{6.15}$$

where a_y is the lateral acceleration and u_2 is the roll torque input generated by the active suspension actuator. Also, $J_{x_{eq}}$ denotes the equivalent roll moment of inertia defined as

$$J_{x_{eq}} = J_{xx} + mh^2.$$

For further description of the parameters of the model, refer to Table 5.1.

The purpose of the control design we consider in this subsection is to follow a reference roll angle trajectory. In order to achieve this we propose the following PID control structure

$$\frac{du_2}{dt} = -K_{r3}u_2 + K_{r1}e + K_{r2}\frac{de}{dt} \qquad \text{with} \qquad e = \phi_{ref} - \phi, \tag{6.16}$$

where K_{r1}, K_{r2}, K_{r3} are the PID gains, e is the roll angle tracking error, and ϕ_{ref} is the reference roll trajectory. Now we can define an augmented state $x_2 \in \mathbb{R}^3$ given as below

$$x_2 = \begin{bmatrix} \phi & \dot{\phi} & u_2 \end{bmatrix}^T, \tag{6.17}$$

which results in the following augmented feedback system description

$$\left.\begin{aligned} &\dot{x}_2 = A_{22}x_1 + B_3 a_y + B_4 \phi_{ref} \quad \text{with} \\ &A_{22} = \begin{bmatrix} 0 & 1 & 0 \\ -a_0 & -a_1 & a_2 \\ -K_{r1} & -K_{r2} & -K_{r3} \end{bmatrix}, \quad B_3 = \begin{bmatrix} 0 \\ \frac{mh}{J_{x_{eq}}} \\ 0 \end{bmatrix}, \quad B_4 = \begin{bmatrix} 0 \\ 0 \\ K_{r1} \end{bmatrix} \end{aligned}\right\} \tag{6.18}$$

where

$$a_0 = \frac{k-mgh}{J_{x_{eq}}}, \qquad a_1 = \frac{c}{J_{x_{eq}}}, \qquad a_2 = \frac{1}{J_{x_{eq}}}. \tag{6.19}$$

The characteristic polynomial corresponding to the closed loop system matrix A_{22} is

$$p(s) = s^3 + (a_1 + K_{r3})s^2 + (a_0 + a_2K_{r2} + a_1K_{r3})s + (a_0K_{r3} + K_{r1}a_2). \tag{6.20}$$

Denoting the closed loop eigenvalues (i.e., the target poles) as $\lambda_1, \lambda_2, \lambda_3$, the target characteristic polynomial of the closed loop system can be expressed as

$$p(s) = s^3 - (\lambda_1 + \lambda_2 + \lambda_3)s^2 + (\lambda_1\lambda_2 + \lambda_1\lambda_3 + \lambda_2\lambda_3)s - \lambda_1\lambda_2\lambda_3. \tag{6.21}$$

Comparing (6.21) with (6.20) we obtain the following fixed control gains in terms of the target poles and the elements of the system matrix

$$\begin{aligned} K_{r1} &= \frac{a_0 a_1 + a_0(\lambda_1 + \lambda_2 + \lambda_3) - \lambda_1\lambda_2\lambda_3}{a_2}, \\ K_{r2} &= \frac{a_1^2 + a_1(\lambda_1 + \lambda_2 + \lambda_3) - a_0 + \lambda_1\lambda_2 + \lambda_1\lambda_3 + \lambda_2\lambda_3}{a_2}, \\ K_{r3} &= -a_1 - (\lambda_1 + \lambda_2 + \lambda_3). \end{aligned} \tag{6.22}$$

Now taking the Laplace transform of the controller (6.16) we can express the resulting PID controller in frequency domain as follows

$$u_2(s) = \frac{K_{r1} + K_{r2}s}{s + K_{r3}} e(s),$$

where $u_2(s) = \mathscr{L}\{u_2(t)\}$, and $e(s) = \mathscr{L}\{e(t)\}$ are the Laplace transforms of the control input, and the tracking error, respectively. As a final remark we note that the design parameters for this tracking controller are the target poles $\lambda_1, \lambda_2, \lambda_3$; in order for the closed loop system to be stable these are set be negative real. In what follows, we implement the integrated control methodology based on the decentralized control designs introduced in the current and the preceding subsections.

6.4.3 Robust integration of controllers

In this subsection we give an implementation of the design methodology described in Proposition 6.3.1 for simultaneous, and structurally robust emulation [2] of the reference vehicle states related to the lateral and the roll dynamics. In doing so, we utilize the simple decentralized control structures introduced in the preceding two subsections and show that the

resulting controller integration approach is robust with respect to certain types of structural uncertainties.

For the controller integration we consider the four-state single track model with the roll degree of freedom to represent the real vehicle. This choice is motivated by the fact that the four-state single track model is the simplest model that considers the interactions of both the roll and the lateral dynamics, and thus it is an ideal choice for exposing the control integration idea. We utilize the version of the model with the states $\xi = \begin{bmatrix}\beta & \dot{\psi} & \phi & \dot{\phi}\end{bmatrix}^T$, and the model assumes control inputs from both the active front wheel steering actuator and the active suspension actuator. Then, the linearized equations of motion corresponding to this model with two inputs can be expressed follows

$$\dot{\xi} = A\xi + G_1\delta_d + G_1u_1 + G_2u_2 \quad \text{with} \tag{6.23}$$

$$A = \begin{bmatrix} -\frac{\sigma J_{x_{eq}}}{mv_xJ_{xx}} & \frac{\rho J_{x_{eq}}}{mv_x^2J_{xx}} - 1 & \frac{h(mgh-k)}{v_xJ_{xx}} & -\frac{hc}{v_xJ_{xx}} \\ \frac{\rho}{J_{zz}} & -\frac{\kappa}{v_xJ_{zz}} & 0 & 0 \\ 0 & 0 & 0 & 1 \\ -\frac{h\sigma}{J_{xx}} & \frac{h\rho}{v_xJ_{xx}} & \frac{mgh-k}{J_{xx}} & -\frac{c}{J_{xx}} \end{bmatrix}, \tag{6.24}$$

$$G_1 = \begin{bmatrix} \frac{C_vJ_{x_{eq}}}{mv_xJ_{xx}} & \frac{C_vl_v}{J_{zz}} & 0 & \frac{hC_v}{J_{xx}} \end{bmatrix}^T, \quad G_2 = \begin{bmatrix} \frac{h}{v_xJ_{xx}} & 0 & 0 & \frac{1}{J_{xx}} \end{bmatrix}^T, \tag{6.25}$$

where u_1 represents the mechatronic-angle-superposition type active steer input, and u_2 represents the active suspension roll torque input. For further definitions of all the parameters and notations appearing above, see Table 2.1 as well as the Chapters 2 and 3, where variants of this model have been utilized extensively. Also see [50] for a detailed derivation of this model.

The task of the integrated controller considered here is to follow reference roll angle ϕ_{ref}, and reference yaw rate $\dot{\psi}_{ref}$ trajectories corresponding to a different vehicle. In our numerical studies we simulate this scenario by utilizing two four-state single track models, each with a different parametrization; we shall refer to the vehicle that we want to emulate as the *reference vehicle*, which generates the reference trajectories, and the other vehicle

Table 6.1: Fixed model parameters

Parameter	**Reference Vehicle**	**Controlled Vehicle**	unit
m	1400	1224.1	$[kg]$
J_{xx}	500	362	$[kg \cdot m^2]$
J_{zz}	1500	1279	$[kg \cdot m^2]$
l_v	1.4	1.102	$[m]$
l_h	1.5	1.254	$[m]$
h	0.6	0.375	$[m]$
c	6000	4000	$[kg \cdot m^2/s]$
k	39000	36075	$[kg \cdot m^2/s^2]$
C_v	80000	90240	$[N/rad]$
C_h	175000	180000	$[N/rad]$
α	4.019		$[1/s]$

is referred to as the *controlled vehicle*. In Table 6.1 we give the numerical values for the model parameters corresponding to each vehicle. Figure 6.1 below shows a gradual step steering input δ_d of the the driver that is applied to both vehicles at a constant speed of $v_x = 20m/s$ (where a constant steering ratio of 1/20 assumed for both); this results in the dynamical responses shown on Figure 6.2, which clearly indicates that both vehicles have distinct dynamical characteristics.

Now in order to implement the controller integration procedure described in Proposition 6.3.1, we need to express the full state feedback system as a function of the control gains. To do so, we first introduce a new state $x \in \mathbb{R}^6$ representing the full controlled vehicle states

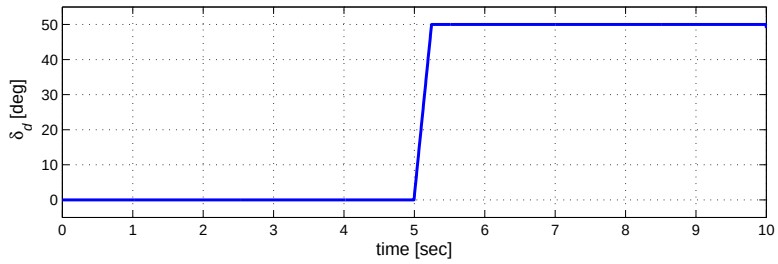

Figure 6.1: Gradual driver step steer input.

as defined below

$$x = \begin{bmatrix} x_1 \\ x_2 \end{bmatrix}, \quad \text{with} \quad \begin{cases} x_1 = \begin{bmatrix} \beta & \dot{\psi} & x_I \end{bmatrix}^T \\ x_2 = \begin{bmatrix} \phi & \dot{\phi} & u_2 \end{bmatrix}^T \end{cases} \tag{6.26}$$

Next we substitute u_1 from (6.13) and u_2 from (6.16) in the four-state vehicle model given in (6.23)-(6.25), which results in the following closed loop state space system describing the vehicle dynamics

$$\dot{x} = \tilde{A}x + \tilde{B}_1\delta_d + \tilde{B}_2\phi_{ref} \quad \text{with} \tag{6.27}$$

$$\tilde{A} = \begin{bmatrix} \tilde{A}_{11} & \tilde{A}_{12} \\ \tilde{A}_{21} & \tilde{A}_{22} \end{bmatrix}, \quad \tilde{B}_1 = \begin{bmatrix} \frac{C_v J_{xeq}}{m v_x J_{xx}} & \frac{C_v l_v}{J_{zz}} & -\alpha & 0 & \frac{hC_v}{J_{xx}} & 0 \end{bmatrix}^T, \quad \tilde{B}_2 = \begin{bmatrix} 0 & 0 & 0 & 0 & K_{r1} \end{bmatrix}^T, \tag{6.28}$$

where

$$\tilde{A}_{11} = \begin{bmatrix} (-\frac{\sigma}{mv_x} + \frac{C_v}{mv_x}K_{p1})\frac{J_{xeq}}{J_{xx}} & (\frac{\rho}{mv_x^2} + \frac{C_v}{mv_x}K_{p2})\frac{J_{xeq}}{J_{xx}} - 1 & \frac{C_v}{mv_x}\frac{J_{xeq}}{J_{xx}}K_I \\ \frac{\rho}{J_{zz}} + \frac{C_v l_v}{J_{zz}}K_{p1} & -\frac{\kappa}{J_{zz}v_x} + \frac{C_v l_v}{J_{zz}}K_{p2} & \frac{C_v l_v}{J_{zz}}K_I \\ 0 & 1 & 0 \end{bmatrix}, \tag{6.29}$$

$$\tilde{A}_{12} = \begin{bmatrix} \frac{h(mgh-k)}{v_x J_{xx}} & -\frac{hc}{v_x J_{xx}} & -\frac{h}{v_x J_{xx}} \\ 0 & 0 & 0 \\ 0 & 0 & 0 \end{bmatrix}, \tag{6.30}$$

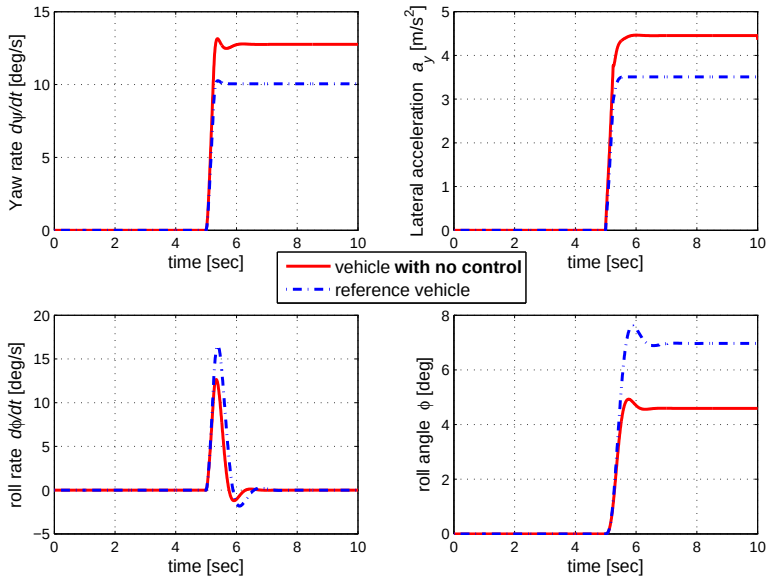

Figure 6.2: Comparison of the lateral and the roll dynamics responses of the reference and the uncontrolled vehicles.

$$\tilde{A}_{21} = \begin{bmatrix} 0 & 0 & 0 \\ (-\sigma + C_v K_{p1})\frac{h}{J_{xx}} & (\frac{\rho}{v_x} + C_v K_{p2})\frac{h}{J_{xx}} & -\frac{hC_v}{J_{xx}} K_I \\ 0 & 0 & 0 \end{bmatrix}, \tag{6.31}$$

$$\tilde{A}_{22} = \begin{bmatrix} 0 & 1 & 0 \\ \frac{(mgh-k)}{J_{xx}} & -\frac{c}{J_{xx}} & -\frac{1}{J_{xx}} \\ -K_{r1} & -K_{r2} & -K_{r3} \end{bmatrix}. \tag{6.32}$$

In Figure 6.3 below the integrated control structure and the corresponding closed loop feedback system is shown schematically.

Now we are in a position to numerically implement the control design as outlined in Proposition 6.3.1. First, we start with designing the roll tracking controller based on Section 6.4.2. Recall that the target poles (eigenvalues) are the only design parameters for the roll controller. Without loss of generality we set $\lambda_1 = -40,\ \lambda_2 = -50,\ \lambda_3 = -60$ as the target

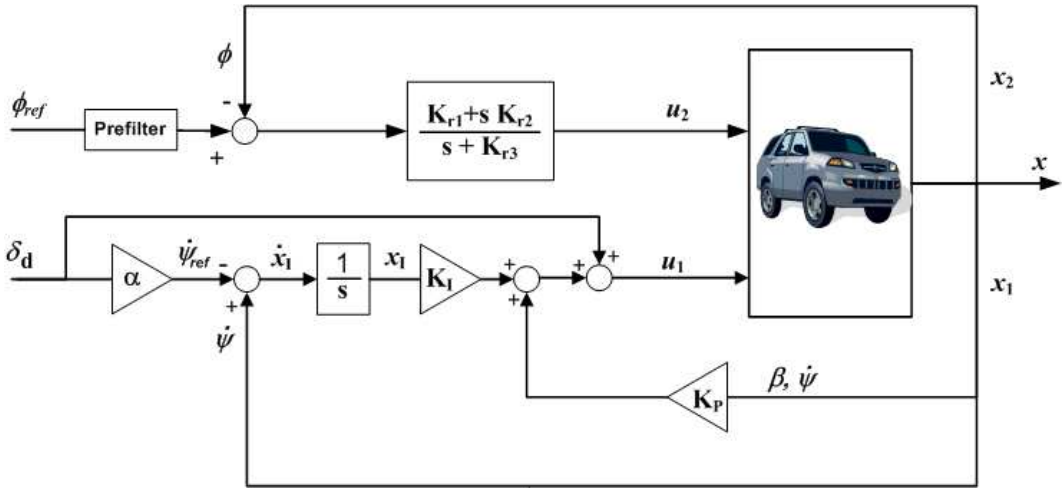

Figure 6.3: Schematic representation of the integrated decentralized control structure.

poles; then from (6.22) the PID control gains are calculated as

$$K_{r1} = 6.0533 * 10^7, \qquad K_{r2} = 3.3614 * 10^6, \qquad K_{r3} = 142.5195. \tag{6.33}$$

Then in order to find $\hat{P}$ we solve the following Lyapunov equation numerically

$$A_{22}^T \hat{P} + \hat{P} A_{22} = -Q_{22}.$$

For this numerical solution, without loss of generality, we set $Q_{22} = 10 * I_3$, where I_3 denotes the identity matrix in $\mathbb{R}^{3\times 3}$. This solution results in

$$P = \begin{pmatrix} 1.276 * 10^{10} & 7.544 * 10^8 & -8.763 * 10^2 \\ 7.544 * 10^8 & 4.830 * 10^7 & 65.919 \\ -8.763 * 10^2 & 65.919 & 0.364 \end{pmatrix} \tag{6.34}$$

Next we design the control gains for the lateral PI tracking controller described in Section 6.4.1, according to the item (b) of Proposition 6.3.1. In order to do so, we first utilized the Matlab® control system toolbox to compute the LQR controller gains described in (6.13), which minimizes the quadratic cost function (6.14). Again, without loss of generality, we assumed a diagonal structure for the *weighting matrices* Q and R in conjunction with the

LQR solution (note here that, as the lateral tracking controller is based on a single input, then R is a scalar). We used the following values for these;

$$Q = 18 * I_3, \qquad R = 550. \tag{6.35}$$

Then one can numerically show that condition (6.7) satisfied. We note that the resulting matrix pair $(\tilde{A}, B)$ is controllable and the pair $(\tilde{A}, B\hat{P})$ is observable. In Figure 6.4 we show the variation of the eigenvalues of $\hat{P}B^T((j\omega - \varepsilon)I_n - \tilde{A})^{-1}B + (\hat{P}B^T((j\omega - \varepsilon)I_n - \tilde{A})^{-1}B)^*$ demonstrating SPR condition in a section of the frequency domain for varying $\omega \in \mathbb{R}$, where ε is an arbitrarily small scalar [49].

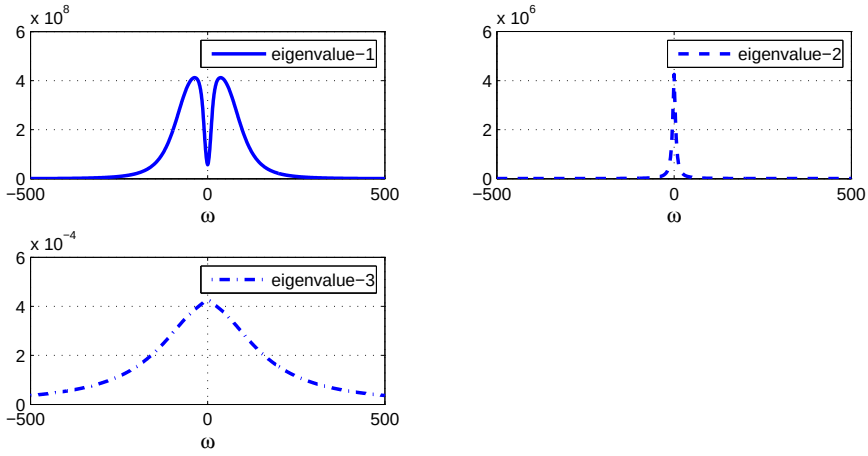

Figure 6.4: Eigenvalues of $\hat{P}B^T((j\omega - \varepsilon)I_n - \tilde{A})^{-1}B + (\hat{P}B^T((j\omega - \varepsilon)I_n - \tilde{A})^{-1}B)^*$ in frequency domain, for $\varepsilon = 10^{-15}$.

Comment: Note that SPR condition is easily checked using spectral methods [110], [109], or by solving a generalized eigenvalue problem. Here we give an approximate graphical frequency domain check to illustrate that the problem of the existence of block diagonal Lyapunov functions can be reduced to a frequency domain search. Our motivation in doing this is that we can quantify the uncertainty in our model over frequency ranges that are of interest in our design. Note also that the limiting conditions given in [49] are also satisfied and have been checked numerically. It is also easily verified that our controllability and

observability conditions are satisfied.

In order to test the integrated controller, we considered an obstacle avoidance maneuver scenario conducted by the driver. The vehicle speed was assumed to be fixed at $v_x = 20m/s$ during the course of the maneuver and the driver steering input is shown in Figure 6.5. The resulting dynamical responses of the reference and the controlled vehicles is shown in Figure 6.6, where we observe a good agrement in the reference and the controlled states. Note here that the lateral acceleration in simulations was computed using the following relationship

$$a_y = v_x(\dot{\beta} + \dot{\psi}). \tag{6.36}$$

Based on the simulation results, we observe that the decision of following a yaw rate reference $\dot{\psi}_{ref}$ was a reasonable one, as this also resulted in good tracking results for the lateral acceleration of the reference vehicle. Considering the fact that the lateral acceleration is one of the most important variables for the lateral dynamics response, the effectiveness of the controller is evident.

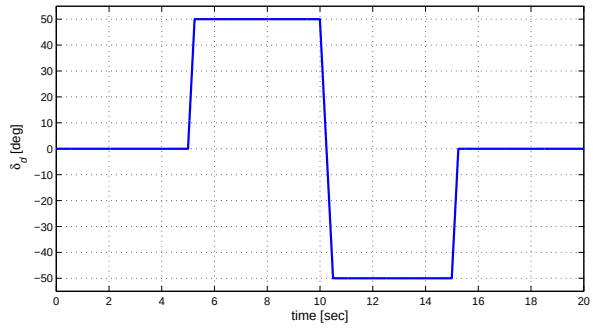

Figure 6.5: Driver steering input.

It is also interesting to look at how the suggested integrated controller affect the vehicle path. To do this, we recall that the coordinates (x, y) of the vehicle CG relative to the road

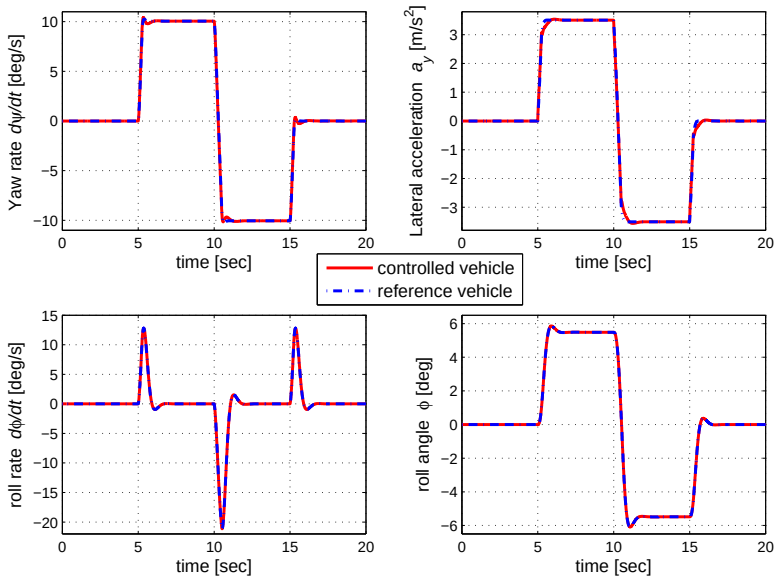

Figure 6.6: Comparison of the lateral and the roll dynamics responses of the reference and the controlled vehicles.

satisfy

$$\dot{x} = v\cos(\beta+\psi), \tag{6.37}$$

$$\dot{y} = v\sin(\beta+\psi), \tag{6.38}$$

where we choose the initial coordinates $(x(0), y(0))$ to be zero. In Figure 6.7 the trajectories over the road plane for the reference, the controlled, and the uncontrolled vehicles are compared. Again we observe a good agreement between the reference and the controlled vehicle trajectories.

As part of the numerical analysis, we finally look at the robustness of the suggested controller with respect to structural uncertainty. In order to simulate such uncertainties, we artificially multiplied the blocks $\tilde{A}_{12}$ and $\tilde{A}_{21}$ with a scalar constant. Without loss of generality we chose this number to be -3 such that the closed loop system matrix $\tilde{A}$ corresponding to

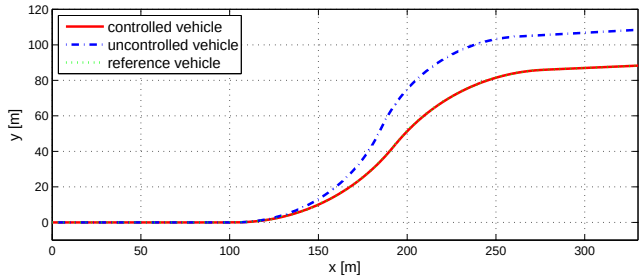

Figure 6.7: Comparison of the horizontal trajectories for the reference, controlled and the uncontrolled vehicles.

the controlled vehicle is now expressed with

$$\tilde{A} = \begin{bmatrix} \tilde{A}_{11} & -3\tilde{A}_{12} \\ -3\tilde{A}_{21} & \tilde{A}_{22} \end{bmatrix}$$

Under this uncertainty we repeated our simulations for the same driving scenario as before where the steering input is as given in Figure 6.5. The resulting dynamical responses of the controlled vehicle is shown in Figure 6.8 where we observe that the controlled vehicle is stable, however the tracking performance of the states have been degraded due to the structural uncertainty, which is expected. In Figure 6.9 we show the trajectories of the controlled and the uncontrolled vehicles with the structural uncertainty as compared with the reference vehicle trajectory. We observe from this plot that the controlled vehicle maintains a close tracking of the reference vehicle for a range of structural uncertainty, while the uncontrolled vehicle shows an infeasible and a divergent behavior.

6.5 Conclusions and possible future directions

In this chapter we presented a novel approach for decentralized control design for systems with multiple interacting dynamical modes. We applied the suggested design technique

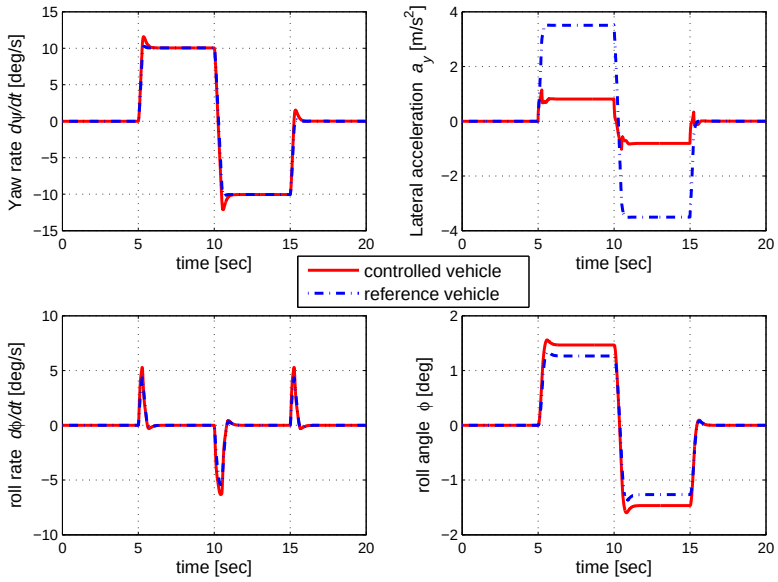

Figure 6.8: Comparison of the lateral and the roll dynamics responses of the reference vehicle and the controlled vehicle **with structural uncertainty**.

for the robust integration of the decentralized control designs for the lateral and the roll reference tracking controllers for an automotive vehicle. We presented the efficacy of the integrated vehicle emulation controller with numerical simulations, which showed high performance and accurate tracking results. Finally, we showed numerically that the suggested control design preserves robustness of the closed loop system with respect to structural uncertainty in such applications.

As a future direction we shall look into extending our results to the case where the plant is subject to parameter variations and/or undergoes discrete switches. Also, we shall look into extensions of the integrated vehicle emulation control design that utilize combinations of the active four-wheel steering, the active suspension as well as the differential braking actuators in conjunction with our decentralized control design approach.

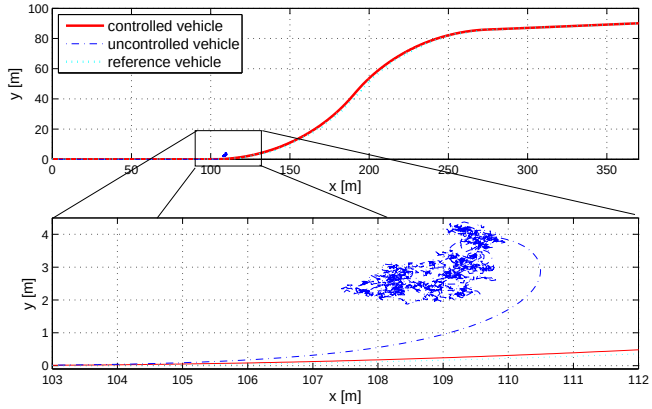

Figure 6.9: Comparison of the horizontal trajectories for the reference vehicle, and the controlled and uncontrolled vehicles **with structural uncertainty**.

Chapter 7

Two Problems on Existence of Common Lyapunov Solutions for Switched Linear Systems: Interval Uncertainty & Regular Inertia

In this chapter we give some results on common Lyapunov solution (CLS) existence for certain classes of switched linear systems. For a subclass of switched Hurwitz systems with bounded uncertainties in the matrix elements, we show that the quadratic stability can be verified using simple algebraic conditions. We also illustrate this with numerical examples. For another switched system class, which involves a pair of switching system matrices with the same regular inertia and in companion form, we extend the classical Lefschetz version of the Kalman-Yacubovich-Popov (KYP) lemma to derive an easily verifiable spectral condition to have a CLS. As a final extension, we combine these two results for a particular switched system class.

7.1 Chapter contributions

The scientific contribution of this chapter over the state of the art is mainly in the area of stability theory. While most of the achievements of the chapter have theoretical motivations, some of the results have applications to control design for uncertain systems. The first major contribution of the chapter was the extension of recent results on existence of common quadratic Lyapunov functions (CQLF) for the class of switched linear systems that involve a pair of Hurwitz matrices in companion form. We extended these results to a particular class of switching linear systems, where the elements of the switched system matrices have bounded interval uncertainties. Particularly, we showed that quadratic stability of such uncertain systems is easily verified by checking the eigenvalues of only 8 matrix products. Also, we gave a numerical example of this result for checking the stability of the automotive roll dynamics subject to parametric uncertainties and switching. The second contribution of the chapter was the derivation of a simple algebraic condition that is equivalent to common Lyapunov solution (CLS) existence for a significant class of pairs of matrices in companion form and with the same regular inertia. We achieved this by extending the classical Lefschetz version of the Kalman-Yacubovich-Popov (KYP) lemma for matrices with regular inertia; we then utilized this lemma to derive a result on CLS existence for this specific class of switching systems. The final contribution of the chapter was to fuse these two results to obtain CLS existence conditions for switched pair of matrices with regular inertia and with interval uncertainty.

The work contained in this chapter has resulted in the following publications:

(i) Zeheb E., Mason O., Solmaz S., Shorten R.,"*On the quadratic stability of switched interval systems: Preliminary results*", Proceedings of the 2005 IEEE International Symposium on Intelligent Control, and 2005 Mediterranean Conference on Control and Automation, Page(s):12 - 17, 2005.

(ii) Zeheb E., Mason O., Solmaz S., Shorten R.,"*Some results on quadratic stability of*

switched systems with interval uncertainty", International Journal of Control, Vol. 80, No. 6, Page(s):825-831, June 2007.

(iii) Mason O., Shorten R., Solmaz S., "*On the Kalman-Yakubovich-Popov lemma and common Lyapunov solutions for matrices with regular inertia*", Linear Algebra and its Applications, Vol. 420, Issue 1, Page(s):183-197, January 2007.

(iv) Solmaz S., Mason O., Shorten R., "*General Inertia and Circle Criterion*", Proceedings in Applied Mathematics and Mechanics", Vol. 6, Issue 1, Page(s):845-846, December 2006. (Initially presented at 77th Annual Meeting of the Gesellschaft für Angewandte Mathematik und Mechanik e.V., March 27th - 31st, 2006.)

7.2 Introduction

Classical Lyapunov theory provides a strong method for checking the exponential stability of linear time-invariant (LTI) systems of the form $\dot{x} = Ax$, $A \in \mathbb{R}^{n\times n}$ without explicitly calculating the eigenvalues of A [26, 43]. The result is that, the zero state of $\dot{x} = Ax$ is asymptotically stable if and only if the solution of the Lyapunov equation

$$A^T P + PA = -Q,$$

is a symmetric positive definite matrix P for all $Q = Q^T > 0$. Here, the matrix $P = P^T > 0$ is called a *Lyapunov solution* for A. Also, the asymptotic stability of $\dot{x} = Ax$ implies that all the eigenvalues of A have strictly negative real parts, where such matrices are said to be *Hurwitz* .

In this chapter we consider certain subclasses of the switched linear systems of the form

$$\Sigma : \dot{x} = A(t)x, \tag{7.1}$$

where $x(t) \in \mathbb{R}^n$, $A(t) \in \mathbb{R}^{n\times n}$, $A(t) \in \{A_1, ..., A_m\}$. One way of establishing the stability of such systems is to show that for some positive definite matrix P the quadratic Lyapunov

function $V(x) = x^T Px$ is decreasing in time; namely that $A_i^T P + PA_i < 0$ for all $1 \leq i \leq m$. When such a function exists, then the associated LTI systems

$$\Sigma_{A_i} : \dot{x} = A_i x \quad 1 \leq i \leq m \tag{7.2}$$

are said to have a common quadratic Lyapunov function (CQLF). Also P is referred to as a common Lyapunov solution (CLS) for the inequalities $A_i^T P + PA_i < 0$, $1 \leq i \leq m$. Recently, motivated by the stability of switched systems [59], the problem of determining compact conditions for the existence of a CQLF for a finite number of LTI systems has assumed a position of great theoretical importance in the mathematics and engineering communities; see [9, 115, 116, 29, 30, 90, 75, 6] for some of the recent work in this area. Also in an earlier publication, CQLF existence problem has been investigated in conjunction with the stability of LTI systems with uncertain parameters in [41]. Drawing from these results, in this chapter, we give some extensions of the CLS existence results for certain subclasses of the switched linear systems of the form (7.1).

As a first extension we consider, in Section 7.3, the exponential stability of a certain class of switching systems, which involves Hurwitz system matrices in companion form and with elements having bounded interval uncertainties. We show that it is possible to obtain analogs of the CQLF existence results in [116, 115] for this particular system class. This extension has significant implications for control engineering, as many real life systems involve controllers based on simplified dynamical models with uncertainties; we have seen some examples of these in Chapter 2 in the context of automotive systems. In a second extension in Section 7.4, we consider a pair of LTI systems with regular inertia, meaning that the system matrices can have nonzero eigenvalues on either side of the imaginary axis (but not on it), thus are not necessarily Hurwitz. We extend the classical Lefschetz version of the KYP lemma and utilize it to show that the algebraic conditions for existence of a CLS (with a regular inertia) can readily be verified for this system class. Finally in Section 7.5, we combine these two results to obtain a CLS existence result for a switched system class that involves matrices with both interval uncertainty and regular inertia.

7.3 CQLF existence problem for interval matrix families

In this section we consider the stability of a certain subclass of the switched linear systems given in (7.1). Although great progress has been made on the general CQLF existence problem in recent years, the problem of determining whether or not a set of LTI systems subject to interval uncertainty has a CQLF has received relatively little attention, despite its obvious considerable practical importance. Our objective in this section is to study this problem for a restricted class of switching systems subject to interval uncertainty; namely the class of switching systems given by $\dot{x} = A(t)x$, $A(t) \in \{A, A - gh^T\}$, where g, h are vectors[1] in $\mathbb{R}^n$, and the system matrices $A, A - gh^T$ are subject to interval uncertainty of the form $\underline{a}_{ij} \leq a_{ij} \leq \overline{a}_{ij}$.

The class of switched linear systems that we study is thus restricted in two ways:

(i) We consider switching between two LTI systems, Σ_{A_1}, Σ_{A_2};

(ii) the system matrices A_1 and A_2 differ by rank one ($A_2 = A_1 - gh^T$).

The first restriction, although a special case of the general problem of switching between an arbitrary number of LTI systems, is important, has numerous applications, and has been extensively treated in the literature (see e.g. [90, 30]). Also, this restriction is relevant to control systems which include a relay with two states e.g. "on" and "off", or other linear dynamical systems containing a single switch whose position is assumed to take on values from a discrete set of the form $\{0, 1\}$ according to a certain rule. Moreover, many dynamical systems with nonlinearities due to saturation, hysteresis, or backlash can be described as switching between two linear systems.

Obviously, a necessary condition for the existence of a CQLF for a finite set of LTI systems

[1] We emphasize that the vectors $g, h \in \mathbb{R}^n$ are not necessarily fixed.

is that every pair of systems belonging to the set has a CQLF. Moreover, there can exist system classes for which the existence of a CQLF for any pair of systems in a finite family implies the existence of a CQLF for the entire family. This was shown to be the case for the class of second order positive systems in [37]. This fact provides further motivation for the study of the problem of CQLF existence for pairs of systems.

With regard to the second restriction, pairs of systems differing by rank one have historically occupied a position of great importance in systems theory, and several classical results on absolute stability for single-input single-output (SISO) systems such as the *Popov Criterion* and *Circle Criterion* can be considered in this framework. Also, this class of systems includes pairs of systems whose system matrices are in companion form as a subclass. Furthermore, switching between systems differing by rank one arises in a number of practical applications. For example, in [134] a control system for four-wheel steer-by-wire vehicles is described, which involves switching between a pair of LTI systems differing by rank one, and whose parameters are subject to interval uncertainty. It should also be noted that systems differing by rank one have received a considerable amount of attention in the literature [115, 76, 51].

It should be emphasized that, in compensation to these restrictions, this paper extends results for the class of systems under study in a very important direction. Every mathematical model of a physical system is inaccurate and includes uncertainties. These are either inherent to the model or a result of measurement inaccuracies or environmental changes, etc. These uncertainties can often be characterized by interval parameters in the model, examples of which were analyzed in Chapters 3 and 4. Such “interval models” are, however, difficult to analyze and thus are frequently neglected unjustifiably. Alternatively, numerical methods are used, as was the case in Chapters 3 and 4, where we used numerical LMI solvers to find Lyapunov solutions satisfying certain matrix inequalities. In this section we treat such interval uncertainty in a systematic analytic way, which is independent of the uncertainty.

7.3.1 Mathematical preliminaries

Throughout the current chapter, we adopt the convention that vectors in $\mathbb{R}^n$ are assumed to be column vectors. Also, j is used in the chapter to denote the complex number satisfying $j^2 = -1$. Moreover, for a vector x in $\mathbb{R}^n$, we denote x_i as the i^{th} component of x, and for a matrix A in $\mathbb{R}^{n\times n}$, we denote the entry in the (i,j) position by a_{ij}. Also, we use $\sigma(A)$ to denote the spectrum (i.e., the set of eigenvalues) of a given square matrix A. Finally, we denote I_n as the $n \times n$ identity matrix. We have the following definitions and results that will be useful for the rest of the chapter.

Companion matrices:

We say that a matrix $A \in \mathbb{R}^{n\times n}$ is in *companion form* [102, 42] if

$$A = \begin{pmatrix} 0 & 1 & 0 & \dots & 0 \\ 0 & 0 & 1 & \dots & 0 \\ \vdots & & & & \\ 0 & 0 & 0 & \dots & 1 \\ -a_0 & -a_1 & -a_2 & \dots & -a_{n-1} \end{pmatrix}, \tag{7.3}$$

where $a_0, \dots, a_{n-1}$ are real numbers. It is straightforward to verify that if A is in the form (7.3), then the characteristic polynomial of A is

$$\det(sI_n - A) = s^n + a_{n-1}s^{n-1} + \cdots + a_1 s + a_0.$$

In this chapter, for notational convenience, we shall denote the companion matrix (7.3) by $C(a_0, \dots, a_{n-1})$.

The Circle Criterion and CLS existence for systems differing by rank one:

One of the most fundamental results on the stability of dynamical systems in the engineering literature is the Circle Criterion. The relevance of the Circle Criterion [76] in our present context stems from the fact that it provides a necessary and sufficient condition for two fixed

Hurwitz matrices in companion form to have a common Lyapunov solution (or a CQLF). Formally, if A, $A-gh^T$ are two Hurwitz matrices in $\mathbb{R}^{n\times n}$ in companion form, where h,g are vectors in $\mathbb{R}^n$, then they have a CLS if and only if the rational function

$$1+h^T(sI_n-A)^{-1}g \tag{7.4}$$

is strictly positive real (SPR), meaning that

$$1+\mathrm{Re}\{h^T(j\omega I_n-A)^{-1}g\}>0 \quad \text{for all } \omega\in\mathbb{R}. \tag{7.5}$$

Moreover, it follows from Meyer's extension of the KYP Lemma in [67] that the condition (7.5) is also sufficient for CQLF existence for two LTI systems Σ_A, Σ_{A-gh^T} where A, $A-gh^T$ are Hurwitz matrices differing by rank one, but not necessarily in companion form. Recently in [115, 114], it has been established that the frequency domain condition (7.5) is equivalent to a simple condition on the eigenvalues of the matrix product $A(A-gh^T)$. This equivalence was first demonstrated in [115] for matrices in companion form and then extended to the case of a general pair of Hurwitz matrices A_1, A_2 with $\mathrm{rank}(A_2-A_1)=1$ in [114]. We state the most general form of the result here.

Theorem 7.3.1 *Let A, $A-gh^T$ be Hurwitz matrices in $\mathbb{R}^{n\times n}$, where $g,h\in\mathbb{R}^n$. Then*

$$1+\mathrm{Re}\{h^T(j\omega I_n-A)^{-1}g\}>0 \text{ for all } \omega\in\mathbb{R}$$

if and only if the matrix product $A(A-gh^T)$ has no negative real eigenvalues.

See Appendix C for the proof of this theorem.

Combining the result of Theorem 7.3.1 with Meyer's extension of the KYP Lemma [67], yields the following spectral condition for CLS existence for Hurwitz matrices differing by rank one.

Theorem 7.3.2 *[114] Let A, $A-gh^T$ be two Hurwitz matrices in $\mathbb{R}^{n\times n}$ where g,h are vectors in $\mathbb{R}^n$. A necessary and sufficient condition for the existence of a common Lyapunov*

solution for the matrices A, $A-gh^T$ is that the matrix product $A(A-gh^T)$ does not have any negative real eigenvalues.

In the remainder of this section, we shall show how Theorem 7.3.2 may be used to obtain results on CQLF existence for pairs of LTI systems subject to interval uncertainty.

Kharitonov's theorem and rational transfer functions:

In obtaining the main results of this section, we shall make use of a version of Kharitonov's Theorem for rational functions that was derived in [24]. Let $\mathscr{P}$ be the family of interval polynomials of order n given by

$$p(s) = p_0 + p_1 s + \cdots + p_n s^n, \tag{7.6}$$

where $\underline{p}_i \leq p_i \leq \overline{p}_i$ for $0 \leq i \leq n$. Then define the four Kharitonov polynomials associated with $\mathscr{P}$:

$$k_1^{\mathscr{P}}(s) = \underline{p}_0 + \underline{p}_1 s + \overline{p}_2 s^2 + \overline{p}_3 s^3 + \cdots \tag{7.7}$$

$$k_2^{\mathscr{P}}(s) = \underline{p}_0 + \overline{p}_1 s + \overline{p}_2 s^2 + \underline{p}_3 s^3 + \underline{p}_4 s^4 \cdots \tag{7.8}$$

$$k_3^{\mathscr{P}}(s) = \overline{p}_0 + \underline{p}_1 s + \underline{p}_2 s^2 + \overline{p}_3 s^3 + \overline{p}_4 s^4 + \cdots \tag{7.9}$$

$$k_4^{\mathscr{P}}(s) = \overline{p}_0 + \overline{p}_1 s + \underline{p}_2 s^2 + \underline{p}_3 s^3 + \cdots \tag{7.10}$$

If $\mathscr{P}$ and $\mathscr{Q}$ are two families of interval polynomials of order n and m respectively with $n \leq m$, then $\mathscr{P}/\mathscr{Q}$ denotes the family of proper rational functions of the form

$$\frac{p(s)}{q(s)} \tag{7.11}$$

where $p \in \mathscr{P}$ and $q \in \mathscr{Q}$. The following result on the strict positive realness of all of the rational functions in $\mathscr{P}/\mathscr{Q}$ was derived in [24].

Theorem 7.3.3 *Every transfer function in the family $\mathscr{P}/\mathscr{Q}$ is strictly positive real if and*

only if the following eight transfer functions are strictly positive real.

$$\left.\begin{array}{l} \frac{k_2^{\mathscr{P}}(s)}{k_1^{\mathscr{Q}}(s)}, \frac{k_3^{\mathscr{P}}(s)}{k_1^{\mathscr{Q}}(s)}, \frac{k_1^{\mathscr{P}}(s)}{k_2^{\mathscr{Q}}(s)}, \frac{k_4^{\mathscr{P}}(s)}{k_2^{\mathscr{Q}}(s)}, \\ \frac{k_1^{\mathscr{P}}(s)}{k_3^{\mathscr{Q}}(s)}, \frac{k_4^{\mathscr{P}}(s)}{k_3^{\mathscr{Q}}(s)}, \frac{k_2^{\mathscr{P}}(s)}{k_4^{\mathscr{Q}}(s)}, \frac{k_3^{\mathscr{P}}(s)}{k_4^{\mathscr{Q}}(s)}, \end{array}\right\} \tag{7.12}$$

where $k_i^{\mathscr{P}}$, $k_i^{\mathscr{Q}}$, $1 \leq i \leq 4$, are the Kharitonov polynomials corresponding to the interval polynomial families $\mathscr{P}$ and $\mathscr{Q}$ respectively.

In what follows, we give the main result of this section.

7.3.2 CQLF existence for interval matrices in companion form

In this subsection, we derive a result on CQLF existence for a pair of LTI systems, which involve interval matrix families in companion form as the system matrices. Particularly, we consider the case when each matrix family is independently subject to interval uncertainty. Based on results from two different areas and applications for this particular type of switching systems, we give necessary and sufficient conditions expressed *explicitly* in terms of eight fixed coefficient matrices.

We denote $\mathscr{A}$ and $\mathscr{B}$ as real interval matrix families in $\mathbb{R}^{n\times n}$ consisting of companion matrices as defined below

$$\left.\begin{array}{l} \mathscr{A} = \{C(a_0,\ldots,a_{n-1}) \in \mathbb{R}^{n\times n} : \underline{a}_i \leq a_i \leq \overline{a}_i \text{ for } 0 \leq i \leq n-1\} \\ \mathscr{B} = \{C(b_0,\ldots,b_{n-1}) \in \mathbb{R}^{n\times n} : \underline{b}_i \leq b_i \leq \overline{b}_i \text{ for } 0 \leq i \leq n-1\} \end{array}\right\} \tag{7.13}$$

In Theorem 7.3.4 below, we consider the following problem.

> *Determine necessary and sufficient conditions for any pair of LTI systems Σ_A, Σ_B with $A \in \mathscr{A}$, $B \in \mathscr{B}$ to have a CQLF.*

We are concerned with CQLF existence for pairs of systems Σ_A, Σ_B with $A \in \mathscr{A}$, $B \in \mathscr{B}$. Hence, we shall assume that all of the matrices belonging to the families $\mathscr{A}$, $\mathscr{B}$ are Hurwitz.

The problem of determining whether or not a family of interval matrices consists entirely of Hurwitz matrices has itself been the subject of a considerable amount of research [108, 100, 142], and in the case of interval matrices in companion form, Kharitonov's Theorem can be used to test for stability.

For the interval matrix family $\mathscr{A}$, construct the four matrices

$$\left.\begin{aligned} A_1 &= C(\underline{a}_0, \underline{a}_1, \overline{a}_2, \overline{a}_3, \ldots) \\ A_2 &= C(\underline{a}_0, \overline{a}_1, \overline{a}_2, \underline{a}_3, \underline{a}_4, \ldots) \\ A_3 &= C(\overline{a}_0, \underline{a}_1, \underline{a}_2, \overline{a}_3, \overline{a}_4, \ldots) \\ A_4 &= C(\overline{a}_0, \overline{a}_1, \underline{a}_2, \underline{a}_3, \ldots), \end{aligned}\right\} \tag{7.14}$$

in analogy with the Kharitonov polynomials given by (7.7)–(7.10). The matrices B_1, B_2, B_3, B_4 are defined in the same manner for the family $\mathscr{B}$. We are now ready to state the main result of this subsection.

Theorem 7.3.4 *Consider the interval matrix families $\mathscr{A}$, $\mathscr{B}$ given by (7.13), and assume that all the matrices belonging to $\mathscr{A}$, $\mathscr{B}$ are Hurwitz. Then for every pair of LTI systems of the form Σ_A, Σ_B with $A \in \mathscr{A}$, $B \in \mathscr{B}$ to have a CQLF, it is necessary and sufficient that none of the eight matrix products*

$$A_1B_2, A_1B_3, A_2B_1, A_2B_4,$$

$$A_3B_1, A_3B_4, A_4B_2, A_4B_3,$$

has a negative real eigenvalue.

Proof of Theorem 7.3.4: Let $A = C(a_0, \ldots, a_{n-1})$, $B = C(b_0, \ldots, b_{n-1})$ be two matrices in the families $\mathscr{A}$ and $\mathscr{B}$ respectively, and write $B = A - gh^T$ where $g = (0, 0, \ldots, 1)^T$, and $h = (b_0 - a_0, \ldots, b_{n-1} - a_{n-1})^T$. Then it follows from the Circle Criterion that the LTI systems Σ_A, Σ_B have a CQLF if and only if the rational function

$$1 + h^T(sI_n - A)^{-1}g$$

is strictly positive real. It is known that for any vector $f = (f_0, \ldots, f_{n-1})^T$ in $\mathbb{R}^n$,

$$f^T(sI_n - A)^{-1}g = \frac{f_0 + f_1 s + \ldots + f_{n-1}s^{n-1}}{det(sI_n - A)}, \tag{7.15}$$

for $s \in \mathbb{C}$ [47, 102]. Utilizing this result, it can be verified by direct computation that

$$1 + h^T(sI_n - A)^{-1}g = b(s)/a(s) \tag{7.16}$$

where the polynomials $a(s)$, $b(s)$ are given by

$$\left.\begin{aligned} a(s) &= a_0 + a_1 s + \cdots a_{n-1}s^{n-1} + s^n \\ b(s) &= b_0 + b_1 s + \cdots b_{n-1}s^{n-1} + s^n \end{aligned}\right\} \tag{7.17}$$

It now follows that every pair of LTI systems Σ_A, Σ_B with $A \in \mathscr{A}$, $B \in \mathscr{B}$ will have a CQLF if and only if all of the rational functions $b(s)/a(s)$ are strictly positive real where $a(s)$ and $b(s)$ belong to the interval polynomial families

$$a(s) = a_0 + a_1 s + \cdots a_{n-1}s^{n-1} + s^n \quad \text{with} \quad \underline{a}_i \leq a_i \leq \overline{a}_i \quad \text{for} \quad 0 \leq i \leq n-1,$$

and

$$b(s) = b_0 + b_1 s + \cdots b_{n-1}s^{n-1} + s^n \quad \text{with} \quad \underline{b}_i \leq b_i \leq \overline{b}_i \quad \text{for} \quad 0 \leq i \leq n-1,$$

respectively. By a slight abuse of notation, we shall use the notation $\mathscr{A}$, $\mathscr{B}$ to denote these polynomial families also.

Now, Theorem 7.3.3 establishes that all of the rational functions in $\mathscr{B}/\mathscr{A}$ are strictly positive real if and only if the functions

$$\frac{k_2^{\mathscr{B}}(s)}{k_1^{\mathscr{A}}(s)}, \frac{k_3^{\mathscr{B}}(s)}{k_1^{\mathscr{A}}(s)}, \frac{k_1^{\mathscr{B}}(s)}{k_2^{\mathscr{A}}(s)}, \frac{k_4^{\mathscr{B}}(s)}{k_2^{\mathscr{A}}(s)},$$
$$\frac{k_1^{\mathscr{B}}(s)}{k_3^{\mathscr{A}}(s)}, \frac{k_4^{\mathscr{B}}(s)}{k_3^{\mathscr{A}}(s)}, \frac{k_2^{\mathscr{B}}(s)}{k_4^{\mathscr{A}}(s)}, \frac{k_3^{\mathscr{B}}(s)}{k_4^{\mathscr{A}}(s)},$$

are strictly positive real. The result now follows from Theorem 7.3.1.

Q.E.D.

Remark 7.3.1 The above result provides simple conditions that are necessary and sufficient for CQLF existence for a pair of LTI systems in companion form subject to interval uncertainty. In fact, it is only necessary to calculate the eigenvalues of eight matrix products, whereas testing for strict positive realness requires evaluating transfer functions at infinitely many values of ω.

7.3.3 Applications of the results

In this subsection we present two numerical examples to illustrate the use of Theorem 7.3.4. The first example is based on a hypothetical switched system with interval uncertainty. The second example is motivated by automotive roll dynamics that is analyzed in detail within this thesis. In this example we show how the results of this chapter can be utilized to check whether the roll dynamics is stable under switching and subject to parameter uncertainties.

Example-1: (*Hypothetical switching plant with interval uncertainty*)

Consider the following stable family of matrix pairs in companion form and with interval uncertainty, as expressed in terms of our notation given in (7.13),

$$\begin{aligned} \mathscr{A} &= \{C(a_0,a_1,a_2) : a_0 \in [1,2], a_1 \in [5,6], a_2 \in [3,4]\} \\ \mathscr{B} &= \{C(b_0,b_1,b_2) : b_0 \in [1,1], b_1 \in [1,2], b_2 \in [3,4]\} \end{aligned} \tag{7.18}$$

where $C(a_0,a_1,a_2)$ denotes the companion matrix whose last row is $(-a_0,-a_1,-a_2)$. We are interested in the stability of arbitrarily switching linear systems Σ_A, and Σ_B, where $A \in \mathscr{A}$, $B \in \mathscr{B}$. We emphasize that this problem originates from an example in [24], where they consider the following stable family of transfer functions with interval uncertainty,

$$G(s) = \frac{1+b_1 s+b_2 s^2+s^3}{a_0+a_1 s+a_2 s^2+s^3}, \quad with \quad \begin{cases} b_0 \in [1,1], b_1 \in [1,2], b_2 \in [3,4] \\ a_0 \in [1,2], a_1 \in [5,6], a_2 \in [3,4] \end{cases}$$

Here we express this transfer function family as a rational function of two interval families of companion matrices, $\mathscr{A}, \mathscr{B} \in \mathbb{R}^{3\times 3}$ as described in (7.18).

For this problem, the corresponding Kharitonov family of companion matrices defined by (7.14) are as follows

$$\left.\begin{array}{l} A_1 = C(1,5,4)\ ,\ A_2 = C(1,6,4)\ ,\ A_3 = C(2,5,3)\ ,\ A_4 = C(2,6,3) \\ B_1 = C(1,1,4)\ ,\ B_2 = C(1,2,4)\ ,\ B_3 = C(1,1,3)\ ,\ B_4 = C(1,2,3) \end{array}\right\} \tag{7.19}$$

Then, both $\mathscr{A}$ and $\mathscr{B}$ consist of Hurwitz matrices and the eigenvalues of the eight matrix products of Theorem 7.3.4 utilizing (7.19) are presented in Figure 7.1.

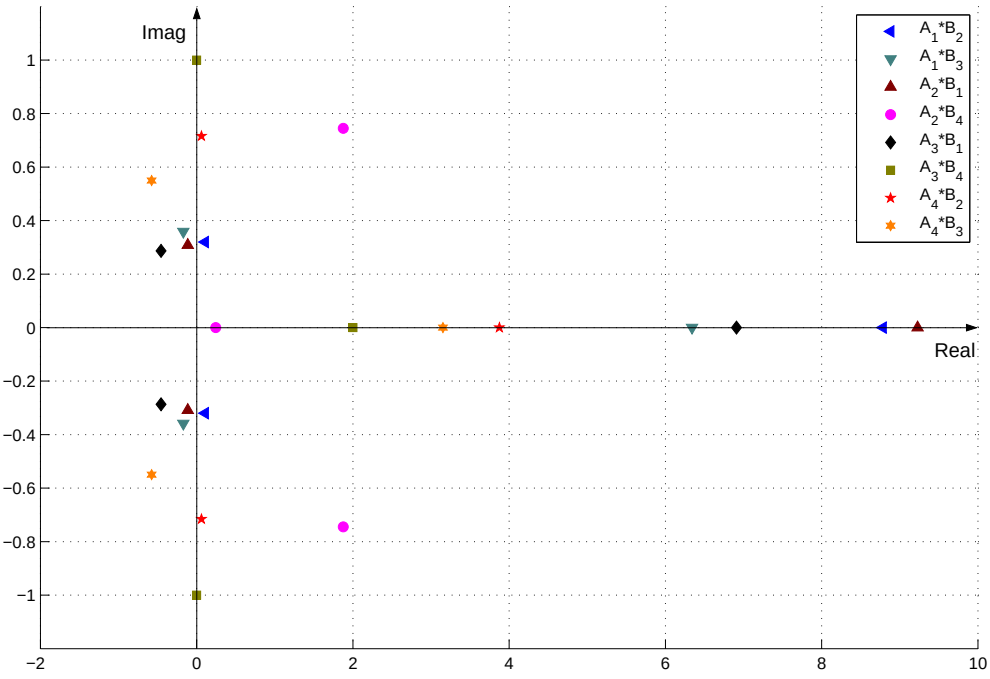

Figure 7.1: Eigenvalues of the matrix products of Theorem 7.3.4.

As can be seen from the plot none of the matrix products have negative real eigenvalues. Theorem 7.3.4 therefore guarantees the existence of a CQLF for any pair of LTI systems Σ_A, Σ_B where $A \in \mathscr{A}$, $B \in \mathscr{B}$.

Example-2: (*Switching automotive roll dynamics subject to interval uncertainty*)

In this example we show how the results of the current section can be utilized to check whether the roll dynamics of an automotive vehicle is stable under switching when also subject to parametric uncertainties. The example is motivated by the fact that the roll dynamics of a vehicle can change as a result sudden switches in the vehicle's center of gravity (CG) height. Also, the suspension parameters and/or the roll center can change depending on many factors[2]. When using linearized models to analyze the problem, it is possible to model these variations as bounded interval uncertainties.

Assuming that the sprung mass of the vehicle rolls about a fixed horizontal roll axis along the centerline of the vehicle body relative to the ground, and also that all angles are small, the equations describing the roll plane motion of an automotive vehicle can be expressed in the following state space form with reference to Figure 2.2

$$\begin{bmatrix} \dot{\phi} \\ \ddot{\phi} \end{bmatrix} = \begin{bmatrix} 0 & 1 \\ -\frac{k-mgh}{J_{x_{eq}}} & -\frac{c}{J_{x_{eq}}} \end{bmatrix} \cdot \begin{bmatrix} \phi \\ \dot{\phi} \end{bmatrix} + \begin{bmatrix} 0 \\ \frac{mh}{J_{x_{eq}}} \end{bmatrix} a_y \tag{7.20}$$

where a_y is the lateral acceleration, and $J_{x_{eq}}$ denotes the equivalent roll moment of inertia defined as

$$J_{x_{eq}} = J_{xx} + mh^2. \tag{7.21}$$

For further description of the parameters of the model, refer to Table 2.1.

Now we consider a scenario where the CG height can switch between two values $h = [h_1, h_2]$. Further we assume that the uncertainties in the linear suspension stiffness k, and the linear damping coefficient c can be expressed as bounded interval uncertainties such

[2]In a real vehicle, the suspension parameters are nonlinear functions of the vehicle speed, aerodynamic forces, suspension geometry and varying roll center, as well as other factors such as the tire pressure, temperature etc. However these factors do not appear in the simple, linearized roll plane model (7.20), which motivates the consideration of parametric uncertainty in k and c.

that $k \in [\underline{k}, \overline{k}]$ and $c \in [\underline{c}, \overline{c}]$. We are interested in stability of the roll dynamics subject to the switching in the CG height h, and uncertainties in the linear suspension parameters k, c.

Under these assumptions, the roll dynamics evolve according to two matrix families $A \in \mathscr{A}$ and $B \in \mathscr{B}$ depending on the two possible CG positions, and they have the following form

$$A = \begin{bmatrix} 0 & 1 \\ -\frac{k-mgh_1}{J_{x_{eq,1}}} & -\frac{c}{J_{x_{eq,1}}} \end{bmatrix}, \qquad B = \begin{bmatrix} 0 & 1 \\ -\frac{k-mgh_2}{J_{x_{eq,2}}} & -\frac{c}{J_{x_{eq,2}}} \end{bmatrix}, \tag{7.22}$$

where

$$J_{x_{eq,i}} = J_{xx} + mh_i^2, \quad for \quad i = \{1,2\}. \tag{7.23}$$

Further we define the following auxiliary parameters

$$\left.\begin{aligned} a_0 &= \tfrac{k-mgh_1}{J_{x_{eq,1}}}, \qquad a_1 = \tfrac{c}{J_{x_{eq,1}}} \\ b_0 &= \tfrac{k-mgh_2}{J_{x_{eq,2}}}, \qquad b_2 = \tfrac{c}{J_{x_{eq,2}}} \end{aligned}\right\} \tag{7.24}$$

where $k \in [\underline{k}, \overline{k}]$ and $c \in [\underline{c}, \overline{c}]$. Then, we can cast the resulting family of system matrices from (7.20) into our notation given in (7.13) as two interval families of companion matrices, $\mathscr{A}$, $\mathscr{B}$ defined below

$$\left.\begin{aligned} \mathscr{A} &= \{C(a_0,a_1) : a_0 \in [\underline{a}_0, \overline{a}_0], a_1 \in [\underline{a}_1, \overline{a}_1]\} \\ \mathscr{B} &= \{C(b_0,b_1) : b_0 \in [\underline{b}_0, \overline{b}_0], b_1 \in [\underline{b}_1, \overline{b}_1]\} \end{aligned}\right\} \tag{7.25}$$

For the numerical analysis we assumed the parameters given Table 7.1, which results in the following companion matrix family from (7.25)

$$\left.\begin{aligned} \mathscr{A} &= \{C(a_0,a_1) : a_0 \in [30.1425, 42.6425], \quad a_1 \in [5,10]\} \\ \mathscr{B} &= \{C(b_0,b_1) : b_0 \in [16.2322, 24.1186], \quad b_1 \in [3.1546, 6.3091]\} \end{aligned}\right\} \tag{7.26}$$

The corresponding Kharitonov family of companion matrices defined by (7.14) are then

Table 7.1: Model parameters for numerical analysis

Parameter	Numerical Value	unit	definition
m	1200	$[kg]$	vehicle mass
J_{xx}	500	$[kg \cdot m^2]$	roll moment of inertia about CG
h_1	0.5	$[m]$	CG height configuration-1
h_2	0.8	$[m]$	CG height configuration-2
$\overline{k}$	40000	$[kg \cdot m^2/s^2]$	spring stiffness (upper bound)
$\underline{k}$	30000	$[kg \cdot m^2/s^2]$	spring stiffness (lower bound)
$\overline{c}$	8000	$[kg \cdot m^2/s]$	roll damping coefficient (upper bound)
$\underline{c}$	4000	$[kg \cdot m^2/s]$	roll damping coefficient (lower bound)

given as follows

$$\left.\begin{array}{l} A_1 = C(30.1425, 5)\ ,\ A_2 = C(30.1425, 10) \\ A_3 = C(42.6425, 5)\ ,\ A_4 = C(42.6425, 10) \\ B_1 = C(16.2322, 3.1546)\ ,\ B_2 = C(16.2322, 6.3091) \\ B_3 = C(24.1186, 3.1546)\ ,\ B_4 = C(24.1186, 6.3091) \end{array}\right\} \tag{7.27}$$

Then, both $\mathscr{A}$ and $\mathscr{B}$ consist of Hurwitz matrices and the eigenvalues of the eight matrix products of Theorem 7.3.4 utilizing (7.19) are presented in the figure 7.2 below.

As none of the matrix products have negative real eigenvalues, Theorem 7.3.4 guarantees the existence of a CQLF for any pair of matrices $A \in \mathscr{A}$, $B \in \mathscr{B}$; thus the described roll dynamics model subject to random switches in CG height as well as interval uncertainty in the suspension parameters is stable.

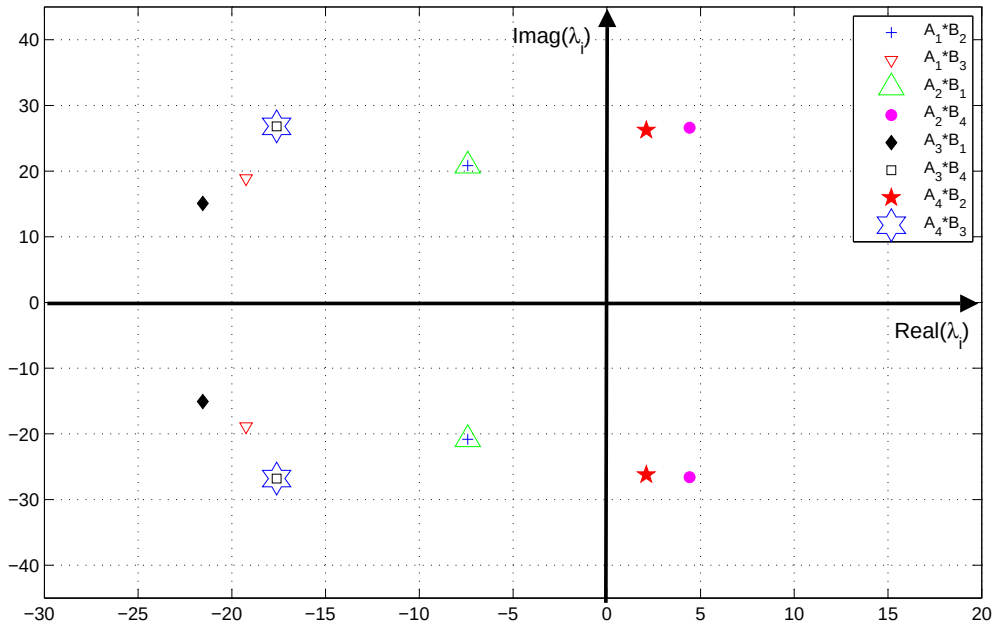

Figure 7.2: Eigenvalues of the matrix products of Theorem 7.3.4 for the roll dynamics.

7.4 Generalized KYP lemma and common Lyapunov solutions for matrices with regular inertia

In the preceding section we considered an extension of some recent results on CQLF existence for a set of Hurwitz matrices to switched systems with interval uncertainty. We will consider a further extension here for a particular subclass of a pair of switched linear systems. Recall that, for the case of a pair of systems, the CQLF existence problem amounts to determining necessary and sufficient conditions for the existence of a positive definite symmetric matrix $P = P^T > 0$, $P \in \mathbb{R}^{n\times n}$ that simultaneously satisfies the matrix inequalities

$$A_1^T P + PA_1 < 0 \quad , \qquad A_2^T P + PA_2 < 0 \tag{7.28}$$

where all eigenvalues of the given matrices $A_1, A_2 \in \mathbb{R}^{n\times n}$ lie in the open left half of the complex plane, that is A_1, A_2 are Hurwitz. When there exists a $P = P^T > 0$ satisfying the above inequalities, then the scalar function $V(x) = x^T Px$ is said to be a common quadratic Lyapunov function (CQLF) for the dynamical systems $\Sigma_{A_i} : \dot{x} = A_i x \;\; i \in \{1,2\}$, and the matrix P is a common Lyapunov solution (CLS) for the Lyapunov inequalities (7.28). In a slight abuse of notation, we shall often refer to such a P as a CLS for the matrices A_1, A_2. The existence of CQLFs is of considerable importance in a number of engineering problems [58] and consequently the CQLF existence problem has assumed a pivotal role in research on stability theory.

It is generally accepted that determining the existence of a CQLF for a finite set of LTI systems is very difficult to solve analytically. However, in certain situations as in the case of switching between two LTI systems, elegant conditions for the existence of a CQLF may be obtained when restrictions are placed on the matrices A_1 and A_2. Recently, one such result was obtained for the case where A_1 and A_2 are Hurwitz and $rank(A_1 - A_2) = 1$; in this case a CQLF exists for Σ_{A_1} and Σ_{A_2} if and only if the matrix product A_1A_2 does not have any real negative eigenvalues. Furthermore, it has been shown recently in [115] that this result can be seen as a time-domain version of the Kalman-Yacubovich-Popov (KYP) lemma which was introduced by Kalman in [47].

Our primary aim in this section is to extend this result on CLS existence to the case where the matrices A_1 and A_2 are no longer Hurwitz, but rather have regular inertia [43]. Note that the general problem of CLS existence for matrices with regular inertia has been considered by various authors before [39, 29, 30, 9, 99], and, in particular, results linking CLS existence to the inertia of so-called *convex invertible cones* of matrices have been established for the cases of Hermitian and triangular matrices in $\mathbb{R}^{n\times n}$ and for matrix pairs in $\mathbb{R}^{2\times 2}$. In this section, we shall extend the KYP lemma from classical stability theory to matrices with regular inertia and show that, in analogy with the classical case of Hurwitz matrices [76], this extension leads to elegant conditions for CLS existence for matrices with regular inertia

also.

7.4.1 Mathematical Preliminaries

In this subsection we present a number of basic definitions and results that are required for the discussions in the remainder of this chapter.

Matrix Inertia:

The inertia of a matrix $A \in \mathbb{R}^{n\times n}$ is the ordered triple

$$In(A) = (i_+(A), i_-(A), i_0(A)) \tag{7.29}$$

where $i_+(A), i_-(A), i_0(A)$ are the number of eigenvalues of A in the open right half plane, the open left half plane, and on the imaginary axis, respectively. We say that A has regular inertia if $i_0(A) = 0$.

The Matrix Ray $\sigma_{\gamma[0,\infty)}[A_1, A_2]$:

Later in the current section, we shall refer to the *matrix ray* $\sigma_{\gamma[0,\infty)}[A_1, A_2]$. Formally, this is the parameterized family of matrices of the form

$$\sigma_{\gamma[0,\infty)}[A_1, A_2] = \{A_1 + \gamma A_2 : \ \gamma \in [0,\infty)\}. \tag{7.30}$$

We shall say that $\sigma_{\gamma[0,\infty)}[A_1, A_2]$ is *non-singular* if $A_1 + \gamma A_2$ is non-singular for all $\gamma \geq 0$; otherwise it is said to be *singular*. It is trivial to show that singularity of the matrix ray $\sigma_{\gamma[0,\infty)}[A_1, A_2]$ is equivalent to the matrix product $A_1^{-1}A_2$ having a negative real eigenvalue if A_1 and A_2 are non-singular. Also, we say that $\sigma_{\gamma[0,\infty)}[A_1, A_2]$ has constant inertia if there are fixed non-negative integers n_+, n_-, n_0 such that $In(A_1 + \gamma A_2) = (n_+, n_-, n_0)$ for all $\gamma \geq 0$.

Technical lemmas:

We next record some basic technical facts that shall be used in proving the principal results of this section.

Lemma 7.4.1 *Suppose that $A \in \mathbb{R}^{n\times n}$ and has regular inertia, such that $In(A) = (n_+, n_-, 0)$. Then*

$$det(\omega^2 I_n + A^2) > 0, \tag{7.31}$$

for all $\omega \in \mathbb{R}$.

Proof of Lemma 7.4.1: As the matrix A has real entries and has regular inertia, it follows that for any $\omega \in \mathbb{R}$,

$$\det(\omega^2 I_n + A^2) = |\det(j\omega I_n + A)|^2 > 0. \tag{7.32}$$

Q.E.D.

Lemma 7.4.2 *[47] Let $A \in \mathbb{R}^{n\times n}$ and $A - gh^T \in \mathbb{R}^{n\times n}$ be in companion form, where $h, g \in \mathbb{R}^n$ with $g = [0, \ldots 0, 1]^T$. Then we can write*

$$1 + Re\{h^T (j\omega I_n - A)^{-1} g\} = 1 - h^T A(\omega^2 I_n + A^2)^{-1} g$$

The next lemma verifies the fact that any symmetric matrix P, which satisfies the Lyapunov inequality for a matrix A, also satisfies the Lyapunov inequality for its inverse, A^{-1}.

Lemma 7.4.3 *[29] Let $A \in \mathbb{R}^{n\times n}$ be non-singular. Then for any symmetric $P = P^T$ in $\mathbb{R}^{n\times n}$ with $In(P) = In(-A)$,*

$$A^T P + PA < 0 \tag{7.33}$$

if and only if

$$(A^{-1})^T P + P(A^{-1}) < 0. \tag{7.34}$$

Proof of Lemma 7.4.3: This follows immediately from the observation that

$$(A^{-1})^T P + PA^{-1} = (A^{-1})^T (A^T P + PA) A^{-1}. \tag{7.35}$$

Q.E.D.

The principal contribution of the present section is to extend Theorem 7.3.2 to the case of pairs of matrices with the same regular inertia. First of all, we recall some fundamental facts on the existence of solutions to the Lyapunov inequality for a single matrix with regular inertia. The first part of Theorem 7.4.1 below is usually referred to as the *General Inertia Theorem* [43], while the second part follows from general results on the existence of solutions to the Sylvester equation $AX + XB = C$ (For instance, see Theorem 4.4.6 in [43]). While the General Inertia Theorem has been established for matrices with complex entries, we state it here for real matrices as we only consider the CLS existence problem for real matrices in this paper.

Theorem 7.4.1 *General Inertia Theorem [43]*

Let $A \in \mathbb{R}^{n\times n}$ be given. Then there exists a symmetric matrix $P = P^T$ in $\mathbb{R}^{n\times n}$ such that

$$A^T P + PA < 0 \tag{7.36}$$

if and only if A has regular inertia. In this case, $In(P) = In(-A)$.

Furthermore, if $\lambda_i + \lambda_j \neq 0$ for all eigenvalues λ_i, λ_j of A, then for every $Q = Q^T < 0$ in $\mathbb{R}^{n\times n}$, there is a unique $P = P^T$ with $In(P) = In(-A)$ and $A^T P + PA = Q < 0$.

In the sequel, the two main contributions of this section are described. First of all, in Theorem 7.4.2 we extend the classical Lefschetz [54] version of the Kalman-Yacubovich-Popov (KYP) lemma to the case of matrices with regular inertia[3] and in companion form. Historically, the KYP lemma has played a key role in stability theory and has led to a number of important results on Lyapunov function existence for dynamical systems including the *Circle Criterion* [76] and the *Popov Criterion* [97, 81]. We shall see below that the extension

[3]We note that in a recent publication [99] a generalized version of the KYP lemma has been reported, which does not impose some of the restrictions that we require in our version of the proof.

of the KYP lemma to the case of matrices with regular inertia also has implications for the existence of common Lyapunov solutions in this more general context. In particular, in Theorem 7.4.3 we derive a simple algebraic condition that is equivalent to CLS existence for a significant class of pairs of matrices in companion form, and with the same regular inertia.

7.4.2 The KYP Lemma for matrices with regular inertia

The classical KYP lemma considered the existence of constrained solutions to the Lyapunov inequality for Hurwitz matrices. More formally, the following question, which we shall address below for matrices with regular inertia, was considered.

Given, A$\in \mathbb{R}^{n\times n}$ Hurwitz, vectors $g,h \in \mathbb{R}^n$, a real constant $\tau > 0$, and a positive definite matrix $D = D^T > 0$, determine conditions for the existence of a vector $q \in \mathbb{R}^n$, a real number $\varepsilon > 0$ and a positive definite matrix $P = P^T > 0 \in \mathbb{R}^{n\times n}$ such that

$$A^T P + PA = -qq^T - \varepsilon D \tag{7.37}$$

$$Pg - h = \sqrt{\tau} q. \tag{7.38}$$

Before we proceed, we prove the following technical lemma which shall be needed later in this subsection.

Lemma 7.4.4 *Let $A \in \mathbb{R}^{n\times n}$ be a nonsingular matrix such that for all pairs λ_i, λ_j of eigenvalues of A,* $\mathrm{Re}(\lambda_i + \lambda_j) \neq 0$. *Further suppose that g,h are column vectors in $\mathbb{R}^n$ such that for any h, the matrices A ,and $A - gh^T$ can simultaneously be transformed to companion forms using similarity transformations. Then*

$$\mathrm{Re}\{h^T (j\omega I_n - A)^{-1} g\} = 0 \text{ for all } \omega \in \mathbb{R} \tag{7.39}$$

implies that $h = 0$.

Proof of Lemma 7.4.4: Without loss of generality, we can assume that A is in companion form and that $g = (0,\ldots,1)^T$. We shall argue by contradiction. Assume now that (7.39) holds and that $h = (h_0,\ldots,h_{n-1})^T$ is non-zero, and consider the rational function $R(z) = h^T(zI_n - A)^{-1}g$. Then we can write

$$R(z) = \frac{h_0 + h_1 z + \cdots + h_{n-1}z^{n-1}}{\det(zI_n - A)}, \tag{7.40}$$

and moreover, under our assumptions the following facts must hold:

(i) $R(z)$ is not uniformly zero;

(ii) $R(z)$ has at least one pole and any such pole must be an eigenvalue of A;

(iii) $R(z)$ takes strictly imaginary values on the imaginary axis.

From (iii), it follows that the function $R_1(z) = jR(jz)$ takes real values for real z, and hence that $R_1(z)$ is a real rational function. Thus, the poles of $R_1(z)$ must be real, or else occur in complex conjugate pairs. Moreover, if λ is any pole of $R_1(z)$, then $j\lambda$ is a pole of the original function $R(z)$. From this it follows that $R(z)$ must either have a pole on the imaginary axis or else that there are two poles, λ_i, λ_j of $R(z)$ with $\mathrm{Re}(\lambda_i + \lambda_j) = 0$. Remembering that any pole of $R(z)$ must be an eigenvalue of A, this is a contradiction. Thus h must be zero as claimed.

Q.E.D.

Remark 7.4.1

(i) The proof given above is based on an argument presented in Chapter 8 of [54], where it was shown that for a Hurwitz matrix $A \in \mathbb{R}^{n\times n}$ in companion form, and $g = (0,\ldots,1)^T$,

$$\mathrm{Re}\{h^T(j\omega I_n - A)^{-1}g\} = 0 \text{ for all } \omega \in \mathbb{R}$$

implies that $h = 0$. This is not in general true for a companion matrix A with regular inertia as can be seen from the simple example

$$A = \begin{pmatrix} 0 & 1 \\ 4 & 0 \end{pmatrix}, g = h = (0,1)^T.$$

Clearly, the additional assumption made in Lemma 7.4.4 , that $\mathrm{Re}(\lambda_i + \lambda_j)$ is non-zero, is automatically satisfied if A is Hurwitz.

(ii) The assumption, that $\mathrm{Re}(\lambda_i + \lambda_j)$ is non-zero, for all eigenvalues λ_i, λ_j of A is satisfied generically. More precisely, given any $A \in \mathbb{R}^{n\times n}$ in companion form with regular inertia which does not satisfy the assumption, and $\varepsilon > 0$, there exists a matrix $A' \in \mathbb{R}^{n\times n}$ in companion form with the same inertia as A such that $\|A - A'\| < \varepsilon$ and $\mathrm{Re}(\lambda_i + \lambda_j)$ is non-zero for all eigenvalues λ_i, λ_j of A'. (Here $\|.\|$ can be any matrix norm on $\mathbb{R}^{n\times n}$.)

(iii) It is important to note that if $\mathrm{Re}(\lambda_i + \lambda_j)$ is non-zero for all eigenvalues λ_i, λ_j of A, then it follows from the last part of Theorem 7.4.1 that for any negative definite matrix $Q = Q^T < 0$ in $\mathbb{R}^{n\times n}$, there is a unique symmetric $P = P^T$ with $In(P) = In(-A)$ such that $A^T P + PA = Q < 0$. We shall make use of this fact in the proof of Theorem 7.4.2 below.

We are now in a position to state the principal result of this subsection which is an extension of the classical KYP lemma to the case of matrices with regular inertia.

Theorem 7.4.2 *Let $A \in \mathbb{R}^{n\times n}$ be a companion matrix with regular inertia such that $\mathrm{Re}(\lambda_i + \lambda_j) \neq 0$ for all $\lambda_i, \lambda_j \in \sigma(A)$, and let $g, h \in \mathbb{R}^n$ be vectors such that $A - gh^T$ is also in companion form. Moreover, let $D = D^T > 0$ in $\mathbb{R}^{n\times n}$ and $\tau > 0$ in $\mathbb{R}$ be given. Then the following two statements are equivalent:*

(i) There exists a symmetric matrix $P = P^T$ in $\mathbb{R}^{n\times n}$ with $In(P) = In(-A)$, a vector

$q \in \mathbb{R}^n$ and a scalar $\varepsilon > 0$ such that

$$A^T P + PA = -qq^T - \varepsilon D \tag{7.41}$$

$$Pg - h = \sqrt{\tau} q. \tag{7.42}$$

(ii) $\tau + 2Re\{h^T (j\omega I_n - A)^{-1} g\} > 0$ *for all* $\omega \in \mathbb{R}$.

Proof of Theorem 7.4.2: For convenience, throughout the proof we shall use the notation $A_{j\omega}$ to denote $(j\omega I_n - A)$ and $m_{j\omega}$ shall denote the complex vector-valued function $A_{j\omega}^{-1} g$. It is then straightforward to check that for any $P = P^T$ in $\mathbb{R}^{n\times n}$,

$$A_{j\omega}^* P + PA_{j\omega} = -(A^T P + PA), \tag{7.43}$$

Moreover, multiplying the left and right hand sides of (7.43) by $g^T (A_{j\omega}^{-1})^*$ and $A_{j\omega}^{-1} g$ respectively, we see that

$$g^T P m_{j\omega} + m_{j\omega}^* P g = -m_{j\omega}^* (A^T P + PA) m_{j\omega}. \tag{7.44}$$

(i) $\Rightarrow$ (ii):

Suppose that the equations (7.41), and (7.42) hold. It follows immediately from (7.41) and (7.44) that

$$m_{j\omega}^* P g + g^T P m_{j\omega} \quad = \quad m_{j\omega}^* qq^T m_{j\omega} + \varepsilon m_{j\omega}^* D m_{j\omega}. \tag{7.45}$$

In (7.45) we can replace the Pg term using (7.42) and arrange to get

$$m_{j\omega}^* h + h^T m_{j\omega} + \sqrt{\tau}(m_{j\omega}^* q + q^T m_{j\omega}) = m_{j\omega}^* qq^T m_{j\omega} + \varepsilon m_{j\omega}^* D m_{j\omega}$$

or equivalently,

$$2Re\{h^T m_{j\omega}\} = m_{j\omega}^* qq^T m_{j\omega} - 2\sqrt{\tau} Re\{q^T m_{j\omega}\} + \varepsilon m_{j\omega}^* D m_{j\omega}. \tag{7.46}$$

It now follows that

$$2Re\{h^T m_{j\omega}\} = |q^T m_{j\omega} - \sqrt{\tau}|^2 - \tau + \varepsilon m_{j\omega}^* D m_{j\omega}, \tag{7.47}$$

and hence, as D is positive definite and A has regular inertia,

$$\tau + 2Re\{h^T m_{j\omega}\} > 0 \tag{7.48}$$

for all $\omega \in \mathbb{R}$.

(ii) ⇒ (i):

Without loss of generality, we can assume that A is in companion form, and $g = (0,0,\ldots,1)^T$. In this case, it can be verified by direct calculation [47, 102] that for any vector $f = (f_0,\ldots,f_{n-1})^T$ in $\mathbb{R}^n$,

$$f^T(zI_n - A)^{-1}g = \frac{f_0 + f_1 z + \ldots + f_{n-1}z^{n-1}}{det(zI_n - A)}, \tag{7.49}$$

for $z \in \mathbb{C}$.

For convenience, we shall use $\kappa(\omega)$ and $\pi(\omega)$ to denote

$$\kappa(\omega) = 2\mathrm{Re}\{h^T m_{j\omega}\}, \qquad \pi(\omega) = m_{j\omega}^* D m_{j\omega}, \tag{7.50}$$

for $\omega \in \mathbb{R}$. Then:

(i) $\tau + \kappa(\omega) > 0$ for all $\omega \in \mathbb{R}$, and $\tau + \kappa(\omega) \to \tau$ as $|\omega| \to \infty$;

(ii) $\pi(\omega) > 0$ for all $\omega \in \mathbb{R}$ and $\pi(\omega) \to 0$ as $|\omega| \to \infty$.

It follows from (i) there exists a positive constant $m_\kappa > 0$ such that $\tau + \kappa(\omega) > m_\kappa$ for all $\omega \in \mathbb{R}$. Also, (ii) implies that there is some constant $M_\pi > 0$ such that $\pi(\omega) < M_\pi$ for all $\omega \in \mathbb{R}$. If we now choose $\varepsilon > 0$ with $\varepsilon < \frac{m_\kappa}{M_\tau}$ then it follows that for all $\omega \in \mathbb{R}$,

$$\tau + 2\mathrm{Re}\{h^T m_{j\omega}\} - \varepsilon m_{j\omega}^* D m_{j\omega} > 0. \tag{7.51}$$

It can be verified by calculation that the left hand side of (7.51) can be written in the form:

$$\begin{aligned} &\tau + m_{j\omega}^* h + h^T m_{j\omega} - \varepsilon m_{j\omega}^* D m_{j\omega} \\ &\qquad = \frac{\eta(\omega)}{\det(\omega^2 I_n + A^2)} \end{aligned} \tag{7.52}$$

where $\eta(.)$ is a polynomial with the following properties.

(i) $\eta(.)$ is a polynomial of degree $2n$ with real coefficients and leading coefficient τ. Thus, any non-real zeroes of $\eta(.)$ occur as complex conjugate pairs.

(ii) Only the even coefficients of η are non-zero. Thus, for any zero z_0 of $\eta(.)$, $-z_0$ is also a zero with the same multiplicity as z_0.

(iii) $\eta(\omega) > 0$ for all $\omega \in \mathbb{R}$. Thus, for any real zero, ω_0, of $\eta(.)$, ω_0 and $-\omega_0$ have the same *even* multiplicity.

It follows from the above considerations that there exists a polynomial $\theta(.)$ of degree n with real coefficients, and leading coefficient $\sqrt{\tau}$, such that

$$\eta(\omega) = \theta(j\omega)\theta(-j\omega), \tag{7.53}$$

for all $\omega \in \mathbb{R}$. Now, if we define $\psi(z) = \det(zI_n - A)$, then, as the leading coefficient of θ is $\sqrt{\tau}$,

$$\sqrt{\tau} - \frac{\theta(z)}{\psi(z)} = \frac{\nu(z)}{\psi(z)} \tag{7.54}$$

where $\nu(z) = q_0 + q_1 z + \cdots + q_{n-1} z^{n-1}$ is a polynomial of degree at most $n-1$. Thus, from (7.49)

$$\frac{\nu(z)}{\psi(z)} = q^T (zI_n - A)^{-1} h \tag{7.55}$$

where $q = (q_0, \ldots, q_{n-1})^T$.

For this vector q, it follows from Theorem 7.4.1 that there exists a symmetric matrix $P = P^T$ with $In(P) = In(-A)$ such that

$$A^T P + PA = -qq^T - \varepsilon D. \tag{7.56}$$

Moreover, combining (7.52), (7.55) and (7.54), we see that

$$\tau + m_{j\omega}^* h + h^T m_{j\omega} - \varepsilon m_{j\omega}^* D m_{j\omega} = |\sqrt{\tau} - q^T m_{j\omega} h|^2 \tag{7.57}$$

It now follows immediately that

$$\begin{aligned} m_{j\omega}^* h &+ h^T m_{j\omega} - \varepsilon m_{j\omega}^* D m_{j\omega} \\ &= (-m_{j\omega}^* q + \sqrt{\tau})(-q^T m_{j\omega} + \sqrt{\tau}) - \tau \\ &= m_{j\omega}^* q q^T m_{j\omega} - \sqrt{\tau}(q^T m_{j\omega} + m_{j\omega}^* q). \end{aligned}$$

We can now use (7.44) and (7.56) to obtain

$$\begin{aligned} m_{j\omega}^* h + h^T m_{j\omega} &- \varepsilon m_{j\omega}^* D m_{j\omega} = m_{j\omega}^* P g + g^T P m_{j\omega} \\ &- \varepsilon m_{j\omega}^* D m_{j\omega} - \sqrt{\tau}(q^T m_{j\omega} + m_{j\omega}^* q). \end{aligned} \tag{7.58}$$

After suitably rearranging the equations above we see that

$$\begin{aligned} m_{j\omega}^* P g + g^T P m_{j\omega} &- m_{j\omega}^* h - h^T m_{j\omega} \\ &- \sqrt{\tau} q^T m_{j\omega} - \sqrt{\tau} m_{j\omega}^* q = 0 \end{aligned} \tag{7.59}$$

and hence,

$$\begin{aligned} & m_{j\omega}^*(Pg - h - \sqrt{\tau}q) + (Pg - h - \sqrt{\tau}q)^T m_{j\omega} = 0 \\ \Rightarrow \quad & 2Re\{(Pg - h - \sqrt{\tau}q)^T m_{j\omega}\} = 0. \end{aligned} \tag{7.60}$$

As (7.60) holds for any real value of ω, it now follows from Lemma 7.4.4 that $Pg - h = \sqrt{\tau}q$. This completes the proof of the theorem.

Q.E.D.

7.4.3 Common Lyapunov solutions and the generalized KYP lemma

We shall now show how Theorem 7.4.2 can be used to obtain simple algebraic conditions for CLS existence for a significant class of pairs of matrices with the same regular inertia in $\mathbb{R}^{n\times n}$. The following theorem establishes this result.

Theorem 7.4.3 *Let A, $A-gh^T$ be two matrices in $\mathbb{R}^{n\times n}$ in companion form and with the same regular inertia, $In(A) = In(A-gh^T) = (n_+, n_-, 0)$, where g,h are vectors in $\mathbb{R}^n$. Further, assume that for any pair of eigenvalues, λ_i, λ_j, of A, $\mathrm{Re}(\lambda_i+\lambda_j) \neq 0$. Then, the following statements are equivalent:*

(i) There exists a symmetric matrix $P = P^T$ in $\mathbb{R}^{n\times n}$ with $In(P) = In(-A) = In(-(A-gh^T))$, and positive definite matrices $Q_1 > 0$, $Q_2 > 0$ such that

$$\left.\begin{aligned} A^TP + PA &= -Q_1 \\ (A-gh^T)^TP + P(A-gh^T) &= -Q_2 \end{aligned}\right\} \tag{7.61}$$

(ii) The matrix rays $\sigma_{\gamma[0,\infty)}(A, A-gh^T)$ and $\sigma_{\gamma[0,\infty)}(A^{-1}, A-gh^T)$ have the same regular inertia.

(iii) The matrix $A(A-gh^T)$ has no real negative eigenvalues.

(iv) $1 + \mathrm{Re}\{h^T(j\omega I_n - A)^{-1}g\} > 0, \quad \forall \omega \in \mathbb{R}.$

Proof of Theorem 7.4.3: We shall obtain the result by showing that $(i) \Rightarrow (ii) \Rightarrow (iii) \Rightarrow (iv) \Rightarrow (i)$.

(i) $\Rightarrow$ (ii):

Suppose that there is a symmetric $P = P^T$ satisfying (7.61). From Lemma 7.4.3 we know that P also satisfies

$$((A-gh^T)^T)^{-1}P + P(A-gh^T)^{-1} < 0 \tag{7.62}$$

Hence for all $\gamma \in [0,\infty)$

$$(A+\gamma(A-gh^T))^TP + P(A+\gamma(A-gh^T)) < 0 \tag{7.63}$$

$$(A+\gamma(A-gh^T)^{-1})^TP + P(A+\gamma(A-gh^T)^{-1}) < 0 \tag{7.64}$$

It now follows immediately from Theorem 7.4.1 that (ii) is true.

(ii) $\Rightarrow$ (iii):

Assume that (ii) is true. Then, $A^{-1}+\gamma(A-gh^T)$ has regular inertia for all $\gamma>0$. In particular, $A^{-1}+\gamma(A-gh^T)$ is non-singular for all $\gamma>0$. It follows immediately that the matrix product $A(A-gh^T)$ has no negative real eigenvalues.

(iii) $\Rightarrow$ (iv):

Assume that $A(A-gh^T)$ has no real negative eigenvalues. As A, $A-gh^T$ have the same regular inertia, it follows that

$$det(\omega^2 I_n+(A-gh^T)A)>0 \tag{7.65}$$

for all $\omega\in\mathbb{R}$. This implies that

$$\begin{aligned} det(\omega^2 I_n+(A-gh^T)A) &> 0 \\ \Rightarrow det(I_n\omega^2+A^2-gh^TA) &> 0 \end{aligned}$$

and hence

$$det(\omega^2 I_n+A^2)det(I_n-(\omega^2 I_n+A^2)^{-1}gh^TA)>0.$$

In this last relation we know that $det(\omega^2 I_n+A^2)>0$ from Lemma 7.4.1. Thus we can conclude that

$$det(I_n-(\omega^2 I_n+A^2)^{-1}gh^TA)>0 \tag{7.66}$$

for all $\omega\in\mathbb{R}$. Now making use of the identity $det(I_n-AB)=det(I_m-BA)$, (where $A\in\mathbb{R}^{n\times m}$ and $B\in\mathbb{R}^{m\times n}$) we can express the last inequality as follows;

$$det(1-h^TA(\omega^2 I_n+A^2)^{-1}g)>0. \tag{7.67}$$

Notice that the argument in the last relation is a scalar, and hence that

$$1-h^TA(\omega^2 I_n+A^2)^{-1}g=T(\omega^2)>0. \tag{7.68}$$

Now comparing this last equation with the result of Lemma 7.4.2, we see that

$$T(\omega^2)=1+Re\{h^T(j\omega I_n-A)^{-1}g\}>0 \tag{7.69}$$

which proves (iv).

(iv) $\Rightarrow$ (i):

Finally, assume that (iv) is true. Choose some positive definite $D = D^T > 0$ in $\mathbb{R}^{n\times n}$. Then it follows from Theorem 7.4.2 (with $\tau = 2$) that there exists a symmetric $P = P^T$ with $In(P) = In(-A)$ and a vector q such that

$$A^T P + PA = -qq^T - \varepsilon D \tag{7.70}$$

$$Pg - h = \sqrt{2}q. \tag{7.71}$$

It can be verified by direct computation that this P is a common Lyapunov solution for A, $A - gh^T$. This completes the proof of the theorem.

Q.E.D.

Remark 7.4.2 It is sufficient that either one of A, or $A - gh^T$ satisfy the spectral assumption that $\mathrm{Re}(\lambda_i + \lambda_j) \neq 0$ for any pair of eigenvalues λ_i, λ_j of the matrix.

7.5 CLS existence for interval matrix families with regular inertia

In this section we give an extension of the common Lyapunov solution (CLS) existence result of Section 7.4 for a specific class of pairs of matrices in $\mathbb{R}^{n\times n}$ with the same regular inertia, and with bounded interval uncertainties in their entries. This also serves as a general inertia extension of Theorem 7.3.2 for interval matrices with regular inertia. We show that the generalization of the KYP lemma as recorded by Theorem 7.4.2 can be used again to obtain easily verifiable algebraic conditions for CLS existence for the interval matrices with regular inertia. The following theorem establishes this result.

Theorem 7.5.1 *Consider the interval matrix families $\mathscr{A}$, $\mathscr{B} \in \mathbb{R}^{n\times n}$ in companion form given by*

$$\left.\begin{array}{l} \mathscr{A} = \{C(a_0,\ldots,a_{n-1}) : \underline{a}_i \le a_i \le \overline{a}_i \quad for \quad 0 \le i \le n-1\} \\ \mathscr{B} = \{C(b_0,\ldots,b_{n-1}) : \underline{b}_i \le b_i \le \overline{b}_i \quad for \quad 0 \le i \le n-1\} \end{array}\right\} \tag{7.72}$$

and assume that all the matrices $A \in \mathscr{A}$, and $B \in \mathscr{B}$ have the same regular inertia, that is $In(A) = In(B) = (n_+, n_-, 0)$. Further, assume that any pair of eigenvalues, λ_i, λ_j, of $A \in \mathscr{A}$ (and/or $B \in \mathscr{B}$), satisfy that $\mathrm{Re}(\lambda_i + \lambda_j) \neq 0$. Then a necessary and sufficient condition for any pair (A,B) with $A \in \mathscr{A}, B \in \mathscr{B}$ to have a common Lyapunov solution $P = P^T \in \mathbb{R}^{n\times n}$ with $In(P) = In(-A) = In(-B)$ is that the following eight matrix products

$$\left.\begin{array}{l} A_1B_2, A_1B_3, A_2B_1, A_2B_4 \\ A_3B_1, A_3B_4, A_4B_2, A_4B_3 \end{array}\right\} \tag{7.73}$$

have no real negative eigenvalues, where each of the matrices $A_1,\ldots,A_4, B_1,\ldots,B_4$ are specified by

$$\left.\begin{array}{lll} A_1 = C(\underline{a}_0, \underline{a}_1, \overline{a}_2, \overline{a}_3, \ldots) & , & B_1 = C(\underline{b}_0, \underline{b}_1, \overline{b}_2, \overline{b}_3, \ldots) \\ A_2 = C(\underline{a}_0, \overline{a}_1, \overline{a}_2, \underline{a}_3, \underline{a}_4, \ldots) & , & B_2 = C(\underline{b}_0, \overline{b}_1, \overline{b}_2, \underline{b}_3, \underline{b}_4, \ldots) \\ A_3 = C(\overline{a}_0, \underline{a}_1, \underline{a}_2, \overline{a}_3, \overline{a}_4, \ldots) & , & B_3 = C(\overline{b}_0, \underline{b}_1, \underline{b}_2, \overline{b}_3, \overline{b}_4, \ldots) \\ A_4 = C(\overline{a}_0, \overline{a}_1, \underline{a}_2, \underline{a}_3, \ldots), & , & B_4 = C(\overline{b}_0, \overline{b}_1, \underline{b}_2, \underline{b}_3, \ldots) \end{array}\right\} \tag{7.74}$$

Proof of Theorem 7.5.1:

Without loss of generality, we can express the family of matrices $B \in \mathscr{B}$ as $B = A - gh^T$, where $g = (0,0,\ldots,1)^T$, and $h = (b_0 - a_0, \ldots, b_{n-1} - a_{n-1})^T$. Then it follows from Theorem 7.4.3 that the matrix pair (A,B) has a common Lyapunov solution $P = P^T$ with $In(P) = In(-A) = In(-B)$ if and only if the rational function

$$1 + Re\{h^T(j\omega I_n - A)^{-1}g\} > 0, \quad \forall \omega \in \mathbb{R},$$

that is, it is strictly positive for all $A \in \mathscr{A}$, and $B \in \mathscr{B}$. Using the fact that for any vector $f = (f_0, \ldots, f_{n-1})^T$ in $\mathbb{R}^n$,

$$f^T(zI_n - A)^{-1}g = \frac{f_0 + f_1 z + \ldots + f_{n-1}z^{n-1}}{det(zI_n - A)}, \tag{7.75}$$

for $z \in \mathbb{C}$ [47, 102], it can be verified by direct computation that

$$1 + Re\{h^T(j\omega I_n - A)^{-1}g\} = Re\{b(j\omega)/a(j\omega)\} \tag{7.76}$$

where the polynomials $a(j\omega)$, $b(j\omega)$ are given by

$$\left.\begin{aligned} a(j\omega) &= a_0 + a_1(j\omega) + \cdots a_{n-1}(j\omega)^{n-1} + (j\omega)^n \\ b(j\omega) &= b_0 + b_1(j\omega) + \cdots b_{n-1}(j\omega)^{n-1} + (j\omega)^n \end{aligned}\right\} \tag{7.77}$$

It now follows that every pair of matrices (A, B) with $A \in \mathscr{A}$, $B \in \mathscr{B}$ will have a CLS if and only if all of the rational functions $Re\{b(j\omega)/a(j\omega)\}$ are strictly positive, where $a(j\omega)$ and $b(j\omega)$ belong to the interval polynomial families

$$a(j\omega) = a_0 + a_1(j\omega) + \cdots a_{n-1}(j\omega)^{n-1} + (j\omega)^n \quad \text{with} \quad \underline{a}_i \le a_i \le \overline{a}_i, \tag{7.78}$$

and

$$b(j\omega) = b_0 + b_1(j\omega) + \cdots b_{n-1}(j\omega)^{n-1} + (j\omega)^n \quad \text{with} \quad \underline{b}_i \le b_i \le \overline{b}_i, \tag{7.79}$$

where $0 \le i \le n-1$. By a slight abuse of notation, we shall use the notation $\mathscr{A}$, $\mathscr{B}$ to denote these polynomial families also.

Now, considering the Kharitonov polynomials associated with the interval polynomials (7.78) and (7.79), Theorem 7.3.3 establishes that all of the rational functions in $Re\{\mathscr{B}/\mathscr{A}\}$ are strictly positive if and only if the functions

$$Re\left\{\frac{k_2^{\mathscr{B}}(s)}{k_1^{\mathscr{A}}(s)}\right\}, Re\left\{\frac{k_3^{\mathscr{B}}(s)}{k_1^{\mathscr{A}}(s)}\right\}, Re\left\{\frac{k_1^{\mathscr{B}}(s)}{k_2^{\mathscr{A}}(s)}\right\}, Re\left\{\frac{k_4^{\mathscr{B}}(s)}{k_2^{\mathscr{A}}(s)}\right\},$$
$$Re\left\{\frac{k_1^{\mathscr{B}}(s)}{k_3^{\mathscr{A}}(s)}\right\}, Re\left\{\frac{k_4^{\mathscr{B}}(s)}{k_3^{\mathscr{A}}(s)}\right\}, Re\left\{\frac{k_2^{\mathscr{B}}(s)}{k_4^{\mathscr{A}}(s)}\right\}, Re\left\{\frac{k_3^{\mathscr{B}}(s)}{k_4^{\mathscr{A}}(s)}\right\},$$

are strictly positive. Then for each of the rational functions above, Theorem 7.4.3 verifies the spectral condition for the corresponding matrix products in (7.73).

Q.E.D.

7.6 Conclusions and possible future directions

In the first half of this chapter, we have considered the stability of switched linear systems subject to interval uncertainty, and gave necessary and sufficient conditions for CQLF existence for pairs of LTI systems in companion form and with interval uncertainty in the entries of their system matrices. Particularly we gave an easily verifiable spectral condition for CQLF existence for this class of systems. We also gave two numerical examples to illustrate how the results of the section can be used in practice, where the second example was motivated by automotive roll dynamics. As an extension of this result we shall consider obtaining practical design laws for synthesizing stable switched controllers for uncertain systems arising from practical automotive control problems, particularly for the roll dynamics and the lateral dynamics control applications for improving driving comfort and vehicle safety.

In the second half of the chapter we derived a verifiable spectral condition for common Lyapunov solution (CLS) existence for pairs of matrices in $\mathbb{R}^{n\times n}$ in companion form, and with the same regular inertia; thereby extending a recent result for pairs of Hurwitz matrices in [115]. We then further extended these results to case when the elements of the matrices for this particular system class included bounded interval uncertainties also.

Chapter 8

Concluding Remarks

In the closing chapter of the thesis, we give a brief summary of the preceding chapters, and highlight the major contributions accomplished during the completion of the work reported within.

The starting point for this thesis was a practical problem related to automotive vehicles, which is known as the rollover. Statistically, rollover accidents have the highest fatality rate among all accident types, and they pose a real threat for top heavy vehicles such as trucks, busses, vans and SUVs. Based on these observations, we started this thesis by analyzing the roll motion of automotive vehicles and found that the two of the most important factors affecting rollover tendency of a vehicle are lateral acceleration and the height of the center of gravity (CG). While the former is a measurable quantity using standard sensor equipment on cars, the CG height is a time varying quantity that is not measurable directly.

Motivated by these, in Chapter 2 we successfully implemented a technique known as the MMST (which originates from adaptive control field), for the problem of real time CG position estimation, that makes use of multiple identification models to minimize a nonlinear cost function based on the identification errors. We used simplified linear models for roll and lateral motion of the vehicle in conjunction with the algorithm and showed that

this method can give good estimations of the longitudinal and the vertical position of CG, as well as the linear suspension and tire parameters. We also gave an implementation of the method off-line measurement data from a real vehicle with success. In order to assess the limitations of the suggested method, we made an analysis of the cost function (i.e., the switching criterion) of the estimation algorithm, and found that when the parameter space of the identification models does not contain the exact plant parameterizations, the algorithm may end up with wrong estimations. This problem is related to the fact that there is no 1-1 mapping between the output space (of identification errors) and the parameter space of the identification models. While using a dense number of identification models solves this problem, this solution might be infeasible for automotive applications due to computational overheads. As a remedy we suggested an adaptive algorithm to modify the model space of the multiple model algorithm in an iterative fashion, which resulted in a small number of identification models with good estimation accuracy. We demonstrated the efficacy of this method with numerical examples utilizing a scalar dynamical system as well as utilizing second order vehicle models in conjunction with the CG position estimation problem.

Having considered the parameter estimation related to the automotive rollover problem, in Chapter 3 we gave a robust controller design technique to mitigate rollover. The suggested controller design is based on a particular bounded-input bounded-output (BIBO) stability result, which considers bounded driver steering command as disturbance input, and load transfer ratio (LTR) as the performance output. We showed the relevance of LTR in terms of rollover occurrence and obtained a dynamical version of LTR in terms of the states of the vehicle. We also showed that our controller design guarantees robustness with respect to parameter uncertainty, subject to the condition that the uncertainty belongs to a convex hull. In numerical simulations we considered robustness with respect to CG height and vehicle velocity and showed that rollover can be prevented based on this approach. We implemented the controllers based on differential braking and active steering actuators and showed that both can be used to mitigate rollover effectively. In conjunction with the control design

we also considered a mode switch based on the imminence of rollover, which resulted in controllers that are not intrusive when the rollover potential is low.

In Chapter 4 we fused the CG position estimation method of Chapter 2 with the robust control design procedure of Chapter 3 to obtain adaptive rollover mitigation controllers in the sense of MMST framework. We showed numerically that the resulting adaptive switched controllers with active differential braking performed better than the robust controller alternative with fixed gains.

In Chapter 5, we considered the discrete time extension of a recent non-Lyapunov result for the stability of a class of switched systems in continuous time. Specifically, we considered the asymptotic stability of a subclass of discrete-time switching linear systems, where each of the constituent subsystems is Schur stable among other conditions. We first presented an example to motivate our study, which illustrated that the bilinear (i.e., Tustin) transform does not preserve the stability between the discrete and continuous switched linear systems. This implies that the continuous time stability results cannot always be transformed to discrete time analogs using this transformation. We then presented a subclass of discrete-time switching systems with globally asymptotic origin, which arise frequently in practical applications. We showed that global attractivity can be established without requiring the existence of a common quadratic Lyapunov function (CQLF) for the switched linear systems. Utilizing this result we then gave constructive procedures to synthesize switching stabilizing controllers for two separate problems in automotive control based on active suspension actuators; the first problem was related to the stabilization of road vehicle roll dynamics subject to changes in the center of gravity (CG) height; we showed that this controller can also be used to change driver experience. The second problem concerned the design of PID tracking controllers for emulating reference roll dynamics while guaranteeing transient free switching as well as stability due to varying CG height.

During the course of the control designs for roll dynamics enhancement in Chapter 5, we observed interactions between the lateral roll dynamics of the controlled vehicle. These

required us to compensate the effects of the roll torque control inputs from the suspension actuators onto the lateral dynamics, which we partially achieved using active steering actuators. Motivated by these considerations, in Chapter 6 we applied a novel decentralized controller integration method for systems with multiple dynamical modes, which preserves robustness with respect to structural uncertainty. Based on some recent results in the literature, we utilized a method for checking the overall stability of the integrated controllers based on a frequency domain criterion. We then applied the design method for the integration of decentralized controllers for the simultaneous tracking of reference lateral and roll dynamics of an automotive vehicle. We designed the decentralized controllers based on simplified models utilizing active suspension and active front wheel steering actuators. We presented the efficacy of the integrated vehicle emulation controller with numerical simulations, which showed high performance and accurate tracking results. Finally, we showed numerically that the suggested control design preserves robustness of the closed loop system with respect to structural uncertainty in such applications.

Finally, in Chapter 7 we considered theoretical problems related to the switching linear systems. The first problem we considered was related to the stability of switched linear systems subject to interval uncertainty. Specifically we showed necessary and sufficient conditions for CQLF existence for pairs of LTI systems in companion form and with interval uncertainty in the entries of their system matrices. Then we gave a verifiable condition for CQLF existence for such uncertain systems. We also demonstrated the result with two numerical examples, where the second example was motivated by automotive roll dynamics. The second problem we considered in Chapter 7 was related to common Lyapunov solution (CLS) existence for pairs of matrices in companion form, and with the same regular inertia. As part of this problem, we extended the classical Lefschetz version of the Kalman-Yacubovich-Popov (KYP) lemma. Then, we derived an easily verifiable spectral condition for CLS existence for this class of systems. As a final problem, we considered interval matrices in companion form and with regular inertia; we showed that easily verifiable

CLS existence conditions can be obtained for this particular switched system class as well.

Appendix A

Proof of Theorem 3.5.1

We acknowledge that the proof given here follows [91] with minor modifications. Before we obtain the proof of Theorem 3.5.1, we give two results from literature that is helpful in obtaining the proof of the theorem. We first start with the definition of L_∞ stability that we utilize in the following discussion.

Definition (*L_∞ *Stability) [91]: Consider a general nonlinear input-output system below

$$\dot{x} = F(x,\omega) \tag{A.1}$$

$$z = H(x,\omega), \tag{A.2}$$

where $x(t) \in \mathbb{R}^n$ is the state vector at time t, and $\omega(t) \in \mathbb{R}^l$ is the exogenous (disturbance) input while $z(t) \in \mathbb{R}^p$ is the performance output. We define the input-output system above to be L_∞ **stable** with performance level γ if the following conditions are satisfied.

(i.) The undisturbed system $\dot{x} = F(x,0)$ is globally uniformly asymptotically stable about the origin.

(ii.) For every $\omega(t)$ and $x(t_0) = 0$ with $t_0 \geq 0$, we have

$$\|z(t)\| \leq \gamma \|\omega(t)\|_\infty, \qquad \forall t \geq t_0.$$

Note that scalar γ is an upper bound on the L_∞ gain of the system.

The following theorem from [91] records a sufficient condition for the L_∞ stability of the system described by (A.1), (A.2) with a level of performance γ.

Theorem A.0.1 *[91] Consider a general nonlinear input-output system described by (A.1) and (A.2). Suppose there exists a matrix P and positive scalars μ_0, μ_1 and μ_2 such that for all $x \in \mathbb{R}^n$ and $\omega \in \mathbb{R}^l$ we have*

$$x^T PF(x,\omega) < 0 \quad \text{when} \quad x^T Px > \mu_0 \|\omega\|^2 \tag{A.3}$$

and

$$\|H(x,\omega)\|^2 \leq \mu_1 x^T Px + \mu_2 \|\omega\|^2. \tag{A.4}$$

Then system (A.1), and (A.2) is L_∞ stable with level of performance

$$\gamma = \sqrt{\mu_0 \mu_1 + \mu_2}. \tag{A.5}$$

See [91] for the proof of this theorem. We next give the following well known theorem that is commonly referred to as the Schur complement result.

Theorem A.0.2 *[42] (Schur Complement Result): Suppose that a symmetric matrix $Q \in \mathbb{R}^{(n+m)\times(n+m)}$ is partitioned as follows*

$$Q = \begin{bmatrix} Q_{11} & Q_{12} \\ Q_{12}^T & Q_{22} \end{bmatrix}, \tag{A.6}$$

where $Q_{11} = Q_{11}^T \in \mathbb{R}^{n\times n}$, $Q_{22} = Q_{22}^T \in \mathbb{R}^{m\times m}$ are symmetric square matrices, and $Q_{12} \in \mathbb{R}^{n\times m}$. Then Q is positive definite, i.e., $Q > 0$, if and only if

$$Q_{11} > 0, \qquad Q_{22} > 0, \qquad Q_{11} - Q_{12} Q_{22}^{-1} Q_{12}^T > 0. \tag{A.7}$$

See [42] for the proof of this theorem.

Corollary A.0.1 *It is straightforward to show that the Schur complement result given with inequalities (3.22) corresponding $Q > 0$ implies also that*

$$\begin{aligned} Q &< 0 \iff Q_{11} < 0, \quad Q_{22} < 0, \quad Q_{11} - Q_{12}Q_{22}^{-1}Q_{12}^T < 0, \\ Q &\geq 0 \iff Q_{11} \geq 0, \quad Q_{22} \geq 0, \quad Q_{11} - Q_{12}Q_{22}^{-1}Q_{12}^T \geq 0, \\ Q &\leq 0 \iff Q_{11} \leq 0, \quad Q_{22} \leq 0, \quad Q_{11} - Q_{12}Q_{22}^{-1}Q_{12}^T \leq 0. \end{aligned} \tag{A.8}$$

Next, making use of these two theorems, we give the proof of the main theorem of Chapter 3. We emphasize that the proof given below follows that given in [91].

Proof of Theorem 3.5.1: Now consider a system described by (3.14)-(3.15) satisfying Assumption 3.5.1. Further suppose that there exist a matrix $S = S^T > 0$, a matrix L and scalars $\beta_1, \ldots \beta_N > 0$ and $\mu_0, \mu_{1j}, \mu_{2j} \geq 0$, for $j = 1, \ldots, r$ that satisfy the hypotheses of the Theorem 3.5.1. We will first show, based on the inequality (3.22), the sufficient condition for the stability of the dynamical system (3.14).

As the inequality (3.22) conforms to the hypotheses of Theorem A.0.2, we can use the Schur complement result on it, which yields

$$\beta_i(SA_i^T + A_iS + L^TB_{ui}^T + B_{ui}L) + S + \frac{\beta_i^2}{\mu_0}B_iB_i^T \leq 0.$$

Pre and post multiplying this inequality by $P = S^{-1}$ and arranging results in

$$A_i^TP + PA_i + PL^TB_{ui}^TP + PB_{ui}LP + \frac{1}{\beta_i}P + \frac{\beta_i}{\mu_0}PB_iB_i^TP \leq 0.$$

Again, we pre and post multiply the last relation by x^T and x, respectively; we also add and subtract $2x^TPB_i\omega$ to inequality, which results in the following expression

$$2x^TP(A_ix + B_i\omega + B_{ui}LPx) - 2x^TPB_i\omega + \frac{1}{\beta_i}x^TPx + \frac{\beta_i}{\mu_0}x^TPB_iB_i^TPx \leq 0.$$

Now denoting $\|.\|$ as the 2-norm, and substituting the definitions of $L = KS = KP^{-1}$ and $u = Kx$ in the last inequality, and after few arrangement steps we obtain

$$2x^TP(A_ix + B_i\omega + B_{ui}u) - 2x^TPB_i\omega + \frac{1}{\beta_i}x^TPx + \frac{\beta_i}{\mu_0}\|B_i^TPx\|^2 \leq 0.$$

In is straightforward to show that this last in equality can be written as follows

$$2x^T P(A_i x + B_i \omega + B_{ui} u) + \frac{\beta_i}{\mu_0}\left[G^T G - \frac{\mu_0^2}{\beta_i^2}\omega^T \omega\right] + \frac{1}{\beta_i} x^T P x \leq 0,$$

where $G = (x^T P \beta_i - \frac{\mu_0}{\beta_i}\omega)$. Now since $G^T G > 0$, and further β_i, μ_0 were chosen to be positive scalars, then removing the $\frac{\beta_i}{\mu_0} G^T G$ in the above inequality does not change semi-negativity, that is

$$2x^T P(A_i x + B_i \omega + B_{ui} u) - \frac{\mu_0}{\beta_i}\omega^T \omega + \frac{1}{\beta_i} x^T P x \leq 0,$$

which is equivalent to

$$2x^T P(A_i x + B_i \omega + B_{ui} u) + \frac{1}{\beta_i}(x^T P x - \mu_0 \|\omega\|^2) \leq 0 \qquad for \quad i = 1, \ldots, N \tag{A.9}$$

for all $x \in \mathbb{R}^n$, and $\omega \in \mathbb{R}$. Since $\beta_i > 0$ for $i = 1, \ldots, N$ it now follows that

$$x^T P(A_i x + B_i \omega + B_{ui} u) < 0 \quad when \quad x^T P x > \mu_0 \|\omega\|^2 \qquad for \quad i = 1, \ldots, N \tag{A.10}$$

Since it was assumed that the system matrices (3.14)-(3.15) satisfy the Assumption 3.5.1, then (A.10) implies that

$$x^T P(A(\theta) x + B(\theta)\omega + B_u(\theta) u) < 0 \quad when \quad x^T P x > \mu_0 \|\omega\|^2, \tag{A.11}$$

where θ is some parameter vector that captures the plant nonlinearity/uncertainty, which can depend on t, x, ω and u. Now defining $F(\theta) = A(\theta)x + B(\theta)\omega + B_u(\theta)u$ and substituting in the last inequality yields

$$x^T P F(\theta) < 0 \quad when \quad x^T P x > \mu_0 \|\omega\|^2, \tag{A.12}$$

which is same as the inequality (A.3) of Theorem A.0.1.

It remains to show that the inequality (3.23) of theorem holds so that the nonlinear/uncertain system (3.14)-(3.15) is L_∞ stable according to the theorem A.0.1. Now, pre and post multiplying the inequality (3.23) with

$$T = \begin{pmatrix} P & 0 & 0 \\ 0 & I & 0 \\ 0 & 0 & I \end{pmatrix},$$

and substituting $K = LP$ and $C_{cl_{j_i}} = C_{j_i} + D_{ju_i}K$, (where $C_{cl_{j_i}}$ denotes the closed loop system matrix for $i = 1,\ldots,N$ and $j = 1,\ldots,r$) results in the following inequality

$$\begin{bmatrix} -\mu_{1j}P & 0 & C_{cl_{j_i}}^T \\ 0 & -\mu_{2j} & D_{j_i}^T \\ C_{cl_{j_i}} & D_{j_i} & -I \end{bmatrix} \leq 0 \qquad i = 1,\ldots,N \qquad j = 1,\ldots,r. \tag{A.13}$$

Again, we can use Schur complement result to write this inequality in the following form

$$\begin{bmatrix} C_{cl_{j_i}}^T C_{cl_{j_i}} - \mu_{1j}P & C_{cl_{j_i}}^T D_{j_i} \\ D_{j_i}^T C_{cl_{j_i}} & D_{j_i}^T D_{j_i} - \mu_{2j}I \end{bmatrix} \leq 0, \tag{A.14}$$

Since it was assumed that the system matrices (3.14)-(3.15) satisfy the Assumption 3.5.1, then above inequality implies that

$$\begin{bmatrix} C_{cl_j}(\theta)^T C_{cl_j}(\theta) - \mu_{1j}P & C_{cl_j}(\theta)^T D_j(\theta) \\ D_j(\theta)^T C_{cl_j}(\theta) & D_j(\theta)^T D_j(\theta) - \mu_{2j}I \end{bmatrix} \leq 0, \qquad j = 1,\ldots,r, \tag{A.15}$$

where $C_{cl_j}(\theta) = C_j(\theta) + D_{ju}(\theta)K$, and θ is some parameter vector that captures the plant nonlinearity/uncertainty, which can depend on t, x, ω and u. Utilizing the Schur complement result on (A.15) and further arranging implies that

$$\begin{aligned} (C_j(\theta)x + D_j(\theta)\omega + D_{ju}(\theta)u)^T (C_j(\theta)x + D_j(\theta)\omega + D_{ju}(\theta)u) \\ -\mu_{1j}x^T Px - \mu_{2j}\|\omega\|^2 \leq 0 \end{aligned} \tag{A.16}$$

for all $x \in \mathbb{R}^n$ and $\omega \in \mathbb{R}$. Now setting $H(\theta) = C_j(\theta)x + D_j(\theta)\omega + D_{ju}(\theta)u$ and substituting in the last inequality yields

$$\|H(\theta)\|^2 \leq \mu_{1j}x^T Px + \mu_{2j}\|\omega\|^2, \tag{A.17}$$

which is the same inequality as (A.4) of Theorem A.0.1. Therefore the nonlinear/uncertain system given with equations (3.14)-(3.15) in compliance with Assumption 3.5.1 is L_∞ stable by Theorem A.0.1, with a level of performance γ_j, where

$$\gamma_j = \sqrt{\mu_0\mu_{1j} + \mu_{2j}}. \tag{A.18}$$

Q.E.D.

Appendix B

Iterative algorithm for robust control design

In our rollover controller design we attempt to minimize the level of performance γ_1 while keeping the level of performance γ_2 below some specified level $\bar{\gamma}_2$. Utilizing the structure of the data in the rollover control design problem, and making use of the Remark 3.5.4, one can solve the minimization problem described in Theorem 3.5.1 by solving the following problem:

Minimize $\mu_0\mu_{11}$ subject to

$$\left.\begin{array}{l}
\begin{bmatrix} \beta_i(SA_i^T + A_iS + L^TB_{u_i}^T + B_{u_i}L) + S & \beta_iB_i \\ \beta_iB_i^T & -\mu_0 I \end{bmatrix} \leq 0 \quad \text{for} \quad i = 1,\ldots,N \\
\begin{bmatrix} -S & SC_1^T \\ C_1S & -\mu_{11}I \end{bmatrix} \leq 0 \\
\begin{bmatrix} -S & L^T \\ L & -\mu_{12}I \end{bmatrix} \leq 0 \\
\mu_0\mu_{12} \leq \bar{\gamma}_2^2
\end{array}\right\} \quad \text{(B.1)}$$

and

$$\left.\begin{array}{rcll} S = S^T & > & 0 & \\ \mu_0, \mu_{11}, \mu_{12} & \geq & 0 & \\ \beta_i & > & 0 \quad \text{for} \quad & i = 1, \ldots, N \end{array}\right\} \tag{B.2}$$

Then $\gamma_1 = \sqrt{\mu_0 \mu_{11}}$ and $K = LS^{-1}$.

To solve the above optimization problem, one first needs a value of $\overline{\gamma}_2$ for which the above inequalities are feasible. To achieve this one can first minimize $\gamma_2^2 = \mu_0 \mu_{12}$ subject to all the inequalities above except those involving μ_{11} and $\overline{\gamma}_2$. After this first minimization ones obtain a value of γ_2 which we denote by γ_{2f}. Now choose $\overline{\gamma}_2 \geq \gamma_{2f}$; in this paper, $\overline{\gamma}_2 = 5\gamma_{2f}$. Having obtained a feasible value of $\overline{\gamma}_2$, one can can then minimize $\gamma_1 = \mu_0 \mu_{11}$.

The inequalities (B.1), (B.2) above and the objective functions $\mu_0 \mu_{11}$, $\mu_0 \mu_{12}$ are not linear functions of the variables. However if we separate the variables into two groups S, L, μ_{11}, μ_{12} and $\beta_1, \ldots, \beta_N, \mu_0$, the inequalities are linear with respect to each group of variables. Also, we can use commercially available software to solve optimization problems with linear objective functions and linear matrix inequality constraints. Based on these observations, we propose the following iterative algorithm in an attempt to solve the above optimization problems.

Algorithm To initiate the optimization of γ_2 one needs feasible symmetric matrices S and L. These can be found by solving the corresponding quadratic stabilizability problem using the following linear matrix inequalities

$$SA_i^T + A_i S + B_{u_i} L + L^T B_{u_i}^T + 2\eta S \quad \leq \quad 0 \quad \text{for} \quad i = 1, \ldots, N \tag{B.3}$$

for some $\eta > 0$. Notice that if there is no solution to this quadratic stabilization problem, then the first inequality in (B.1) does not have a solution.

The next part of the algorithm now iterates through Steps 1-3 in an attempt to minimize γ_2.

1. Fix S and L to those values obtained as a solution to (B.3) or from the previous iteration.

   Minimize μ_0 subject to

$$\begin{aligned}
\begin{bmatrix} \beta_i(SA_i^T + A_iS + L^TB_{u_i}^T + B_{u_i}L) + S & \beta_iB_i \\ \beta_iB_i^T & -\mu_0 I \end{bmatrix} &\leq 0 \quad \text{for} \quad i = 1,\ldots,N \\
\beta_i &> 0 \quad \text{for} \quad i = 1,\ldots,N \\
\mu_0 &\geq 0
\end{aligned}$$

2. Fix $\beta_1,...,\beta_N$ and μ_0 from the previous step.

   Minimize μ_{12} subject to

$$\begin{aligned}
\begin{bmatrix} \beta_i(SA_i^T + A_iS + L^TB_{u_i}^T + B_{u_i}L) + S & \beta_iB_i \\ \beta_iB_i^T & -\mu_0 I \end{bmatrix} &\leq 0 \quad \text{for} \quad i = 1,\ldots,N \\
\begin{bmatrix} -S & L^T \\ L & -\mu_{12} I \end{bmatrix} &\leq 0 \\
S = S^T &> 0 \\
\mu_{12} &\geq 0
\end{aligned}$$

3. Let $\gamma_2^2 = \mu_0\mu_{12}$ and return to Step 1 unless γ_2 has not decreased by a certain prespecified amount from the previous iteration.

Although the above steps may not achieve a global minimum for γ_2, a feasible value of γ_2 (which we denote by γ_{2f}) will be obtained along with corresponding feasible S and L matrices. We now fix γ_2 at $\overline{\gamma}_2 > \gamma_{2f}$; in this thesis, $\overline{\gamma}_2 = 5\gamma_{2f}$.

The next part of the algorithm attempts to minimize γ_1 subject to $\gamma_2 \leq \overline{\gamma}_2$. It iterates through Steps 4-6.

4. Fix matrices S and L from the previous stage or the previous iteration.

Minimize μ_0 subject to

$$\begin{aligned}
\begin{bmatrix} \beta_i(SA_i^T + A_iS + L^TB_{u_i}^T + B_{u_i}L) + S & \beta_iB_i \\ \beta_iB_i^T & -\mu_0 I \end{bmatrix} &\leq 0 \quad \text{for} \quad i = 1,\ldots,N \\
\beta_i &> 0 \quad \text{for} \quad i = 1,\ldots,N \\
\mu_0 &\geq 0
\end{aligned}$$

5. Fix $\beta_1,\ldots,\beta_N$ and μ_0 from the previous step.

   Minimize μ_{11} subject to

$$\begin{aligned}
\begin{bmatrix} \beta_i(SA_i^T + A_iS + L^TB_{u_i}^T + B_{u_i}L) + S & \beta_iB_i \\ \beta_iB_i^T & -\mu_0 I \end{bmatrix} &\leq 0 \quad \text{for} \quad i = 1,\ldots,N \\
\begin{bmatrix} -S & SC_1^T \\ C_1S & -\mu_{11}I \end{bmatrix} &\leq 0 \\
\begin{bmatrix} -S & L^T \\ L & -\mu_{12}I \end{bmatrix} &\leq 0 \\
\mu_0\mu_{12} &\leq \overline{\gamma}_2^2 \\
S = S^T &> 0 \\
\mu_{11},\mu_{12} &\geq 0
\end{aligned}$$

6. Let $\gamma_1^2 = \mu_0\mu_{11}$ and return to Step 4 unless γ_2 has not decreased by a certain prespecified amount from the previous iteration.

Note that although the iterations above may not achieve a global minimization of γ_1, each iteration of Steps 4-6 decreases γ_1.

Appendix C

Proof of Theorem 7.3.1

We acknowledge that the proof given here follows the one in [115]. The following lemma is helpful in obtaining the proof of this theorem.

Lemma C.0.1 *[46] Let $A, A-gh^T$ be Hurwitz matrices in $\mathbb{R}^{n\times n}$, where $g,h^T \in \mathbb{R}^n$. Then for any complex number s,*

$$1+h^T(sI-A)^{-1}g = \frac{det(sI-(A-gh^T))}{det(sI-A)}. \tag{C.1}$$

Proof of Theorem 7.3.1: Without loss of generality, we may assume that gh^T is in one of the following Jordan canonical forms

$$\text{(i)} \begin{pmatrix} c & 0 & \dots & 0 \\ 0 & \dots & \dots & 0 \\ \vdots & & & \\ 0 & \dots & \dots & 0 \end{pmatrix}, \qquad \text{(ii)} \begin{pmatrix} 0 & \dots & \dots & 0 \\ 1 & \dots & \dots & 0 \\ \vdots & & & \\ 0 & \dots & \dots & 0 \end{pmatrix}. \tag{C.2}$$

As A and $A-gh^T$ are both Hurwitz, their determinants will have the same sign, so it follows that the product $A(A-gh^T)$ has no negative real eigenvalues if and only if, for all $\lambda > 0$

$$det(\lambda I+(A-gh^T)A) = det(\lambda I+A^2-gh^TA) > 0$$

If gh^T is in Jordan form then it follows that the expressions

$$det(\lambda I + A^2 - gh^T A)$$

and

$$Re\{det(\lambda I + A^2 - gh^T A - \sqrt{\lambda}\, jgh^T)\},$$

are identical. Thus, writing $\lambda = \omega^2$ we have that for all real ω

$$Re\{det(\omega^2 I + A^2 - gh^T A - j\omega gh^T)\} > 0. \tag{C.3}$$

It now follows, after a short calculation (see [115],[89]) that for all $\omega \in \mathbb{R}$

$$Re\{\frac{det(j\omega I - (A - gh^T))}{det(j\omega I - A)}\} > 0. \tag{C.4}$$

Making use of Lemma C.0.1 It follows that for all real ω

$$1 + Re\{h^T (j\omega I - A)^{-1} g\} > 0$$

as claimed.

Q.E.D.

Bibliography

[1] Trafic safety facts 2004: A compilation of motor vehicle crash data from the fatality analysis reporting system and the general estimates system. Technical report, National Highway Trafic Safety Administration, 2006.

[2] Integrated Chasis Control - Deliverable D21 (*Final Report*), EU STREP Project CEmACS contract 004175. Technical report, Hamilton Institute, August, 2007.

[3] H. Abdellatif, B. Heimann, and J. Hoffmann. Identification of vehicle's coupled lateral and roll dynamics. Rhodes, Greece, 2003. Proc. of the 11th IEEE Mediterranean Conference on Control and Automation.

[4] Ackermann, J. and Odenthal, D. *Robust steering control for active rollover avoidance of vehicles with elevated center of gravity*, Amiens,France, July 1998. Proceeding of International Conference on Advances in Vehicle Control and Safety.

[5] T. Agnoli, D. Angeli, and E. Mosca. *Controller Falsification in Adaptive Multiple Model Control*. in *Adaptation and Learning In Control And Signal Processing 2001*,A Proceedings volume from the IFAC Workshop, Cernobbio-Como, Italy, 29-31 August 2001, Edited by S. Bittanti. Elsevier, 2002.

[6] A. A. Agrachev and D. Liberzon. Lie-algebraic stability criteria for switched systems. *SIAM Journal of Control and Optimization*, 40(1):253–269, 2001.

[7] Danish Ahmed. Parameter estimation of nonlinear systems using an extended kalman filter. Diploma thesis, Technische Universität Kaiserslautern, December 2004.

[8] R.W. Allen, D.H. Klyde, T.J. Rosenthal, and D.M. Smith. Estimation of passenger vehicle inertial properties and their effect on stability and handling. *Journal of Passenger Cars-Mechanical Systems*, 112, 2003.

[9] T. Ando. Sets of matrices with a common Lyapunov solution. *Archiv der Mathematik*, 77:76–84, 2001.

[10] D. Angeli and E. Mosca. Lyapunov-based switching supervisory control of nonlinear uncertain systems. *IEEE Transactions on Automatic Control*, 47(3):500–505, 2002.

[11] K.J. Åstrom and B. Wittenmark. *Adaptive Control 2nd ed.* Addison Wesley, 1995.

[12] M. Athans, D. Castanon, K. Dunn, C.S. Greene, W.H. Lee, N.R. Sandell, and A.S. Willsky. The stochastic control of the F-8C aircraft using a multiple model adaptive control (MMAC) method-part I: Equilibrium flight. *IEEE Transactions on Automatic Control*, AC-22(5):768–780, 1977.

[13] Paul Ayanendu. *Multi-Controller Adaptive Control (MCAC): Cost Detectibility, Stability and Some Applications*. PhD thesis, University of Southern California, 2005.

[14] J. Balakrishnan, K.S. Narendra, and M.K. Ciliz. Adaptation and learning using multiple models, switching, and tuning. *IEEE Control Systems Magazine*, 15(3):37–51, 1995.

[15] Y. Baram and Jr. Sandell, N.R. Consistent estimation on finite parameter sets with application to linear systems identification. *IEEE Transactions on Automatic Control*, AC-23(3):451–454, 1978.

[16] Y. Baram and N.R. Jr. Sandell. An information theoratic approach to dynamical systems modelling and identification. *IEEE Transactions on Automatic Control*, AC-23(1):61–66, 1978.

[17] Bošković, J.D. and Mehra, K. *Stable Adaptive Multiple Model-based Control Design for Accommodation of Sensor Failures*, Anchorage,AK, May 8-10 2002. Proceedings of the American Control Conference.

[18] R.G. Brown and P.Y.C. Hwang. *Introduction to Random Signals and Applied Kalman Filtering*. John Wiley & Sons, Inc., 3rd edition, 1997.

[19] P.B Brugarolas and M.G. Safonov. Learning about dynamical systems via unfalsification of hypotheses. *International Journal of Robust and Nonlinear Control, Special Issue on Robust Control Design from Data:Direct and Model Based Approaches*, 14 (11):933–943, 2004.

[20] Brugarolas, P.B. and Fromion, V. and Safonov, M.G. *Robust Switching Missile Autopilot*, Philadelphia, PA, Jun. 24-26 1998. Proceedings of the American Control Conference.

[21] Brugarolas, P.B and Safonov, M.G. *A Data Driven Approach to Learning Dynamical Systems*, Las Vegas, NV, Dec. 10-13 2002. Proceedings of the IEEE Conference on Decision and Control.

[22] Carlson, C.R. and Gerdes, J.C. *Optimal Rollover Prevention with Steer by Wire and Differential Braking*, number IMECE2003-41825 in Proceedings of IMECE'03, Washington, D.C., November 16-21 2003. ASME International Mechanical Engineering Congress and Exposition.

[23] Derek S. Caveney. *Multiple Model Techniques in Automotive Estimation and Control*. PhD thesis, University of California, Berkeley, 2004.

[24] H. Chapellat, M. Dahleh, and S. Bhattacharyya. On robust non-linear stability of interval control systems. *IEEE Transactions on Automatic Control*, 36(1):59–67, 1991.

[25] B. Chen and H. Peng. Differential-breaking-based rollover prevention for sport utility vehicles with human-in-the-loop evaluations. *Vehicle System Dynamics*, 36(4-5): 359–389, 2001.

[26] C. Chen. *Linear System Theory and Design*. Oxford University Press, 1984.

[27] C.C. Chou, R.W. McCoy, and J. Le. A literature review of rollover test methodologies. *Int. J. Vehicle Safety*, 1:200–237, 2005.

[28] C.C. Chou, F. Wu, L. Gu, and S.R. Wu. A review of mathematical models for rollover simulations. *Crashworthiness, Occupant Protection and Biomechanics in Transportation Systems*, AMD-Vol.230/BED-Vol.41, 1998.

[29] N. Cohen and I. Lewkowicz. Convex invertible cones and the Lyapunov equation. *Linear Algebra and its Applications*, 250(1):105–131, 1997.

[30] N. Cohen and I. Lewkowicz. A pair of matrices sharing common Lyapunov solutions - a closer look. *Linear Algebra and its Applications*, 360:83–104, 2003.

[31] Oswaldo Driollet. *Adaptive Control Using Multiple Estimation Models in the Presence of Random Disturbances*. PhD thesis, Yale University, 2003.

[32] Matthias Feiler. *Adaptative Control in the Presence of Disturbances*. PhD thesis, Lehrstuhl fur Elektrische Antriebssysteme, Technische Universitat Munchen, 2004.

[33] Fekri, S. and Athans, M. and Pascoal, A. *A New Robust Adaptive Control Method Using Multiple-Models*, Kusadasi,Aydin,Turkiye, Jun. 6-9 2004. Proceedings of the 12th Mediterranean Conference on Control and Automation.

[34] Fekri, S. and Athans, M. and Pascoal, A. *RMMAC: A Novel Robust Adaptive Control Scheme-Part I:Architecture,* Atlantis,Paradise Island,Bahamas, Dec. 14-17 2004. Proceedings of the 43rd IEEE Conference on Decision and Control.

[35] Fekri, S. and Athans, M. and Pascoal, A. *RMMAC: A Novel Robust Adaptive Control Scheme-Part II:Performance Evaluation*, Atlantis,Paradise Island,Bahamas, Dec. 14-17 2004. Proceedings of the 43rd IEEE Conference on Decision and Control.

[36] G.C. Griffin and P.S. Maybeck. Mmae/mmac control for bending with multiple uncertain parameters. *IEEE Transactions on Aerospace and Electronic Systems*, 33(3): 903–912, 1997.

[37] L. Gurvits, R. Shorten, and O. Mason. Preliminary results on the stability of switched positive linear systems. *Accepted for publcation in Mathematical Theory of Networks and Systems*, 2004.

[38] Hac, A. and Brown, T. and Martens, J. *Detection of Vehicle Rollover*, number 2004-01-1757 in SAE Technical Paper Series, Detroit,MI, March 8-11 2004. SAE 2004 World Congress & Exhibition.

[39] D. Herskowitz. On cones and stability. *Linear Algebra and its Applications*, pages 275–276, 1998.

[40] D. Hinrichsen and A.J. Pritchard. *Mathematical System Theory I: Modelling, State Space Analysis, Stability and Robustness*. Texts in Applied Mathematics. Springer, 2005.

[41] H. Horisberger and P. Belanger. Regulators for linear time invariant plants with uncertain parameters. *IEEE Transactions on automatic control*, 21:705–708, 1976.

[42] R. A. Horn and C. R. Johnson. *Matrix Analysis*. Cambridge University Press, Cambridge, UK, 1985.

[43] R. A. Horn and C. R. Johnson. *Topics in Matrix Analysis*. Cambridge University Press, Cambridge, UK, 1991.

[44] Jun, M. and Safonov, M.G. *Automatic PID Tuning:An Application of Unfalsified Control*, Kohala Coast, Hawaii, Aug. 22-27 1999. Proceedings of the IEEE Int. Syposium on Computer Aided Control System Design.

[45] Jun, M. and Safonov, M.G. *Controller Parameter Adaptation Algorithm using Unfalsified Control Theory and Gradient Method*, Barcelona, Spain, Jul. 21-26 2003. Proceedings of IFAC World Congress.

[46] T. Kailath. *Linear Systems*. Prentice-Hall, New Jersey, 1980.

[47] R. E. Kalman. Lyapunov functions for the problem of Lur'e in automatic control. *Proceedings of National Academy of Science*, 21(2):201–205, 1963.

[48] R. Kamnik, F. Böttiger, and K. Hunt. Roll dynamics and lateral load transfer estimation in articulated heavyfreight vehicles: A simulation study. *Proceedings of the Institution of Mechnaical Engineers*, Part D, 2003.

[49] H.K. Khalil. *Nonlinear Systems*. Prentice Hall, third edition, 2002.

[50] U. Kiencke and L. Nielsen. *Automotive Control Systems for Engine, Driveline and Vehicle*. Springer-Verlag & SAE Int., Berlin, 2000.

[51] C. King and M. Nathanson. On the existence of a common quadratic Lyapunov function for a rank one difference. *arXiv:math.OC/0403467*, 2004.

[52] Demetrios G. Lainiotis. Partinioning: A unifying framework for adaptive systems I:estimation. *Proceedings of the IEEE*, 64(8):1126–1143, 1976.

[53] Demetrios G. Lainiotis. Partinioning: A unifying framework for adaptive systems II:control. *Proceedings of the IEEE*, 64(8):1182–1198, 1976.

[54] S. Lefschetz. *Stability of Nonlinear Control Systems*. Academic Press, 1965.

[55] K.D. Leimbach and G. Wetzel. Procedure and device for determining a parameter related to the height of the centre of gravity of a vehicle, June 2006. European Patent EP 0 918 003 B1.

[56] D.J. Leith, R.N. Shorten, W.E. Leithead, O. Mason, and Curran P. Issues in the design of switched linear control systems: A benchmark study. *International Journal of Adaptive Control and Signal Processing*, 17:103–118, 2003.

[57] X.R. Li and Y. Bar-Shalom. Design of an interacting multiple model algorithm for air traffic control tracking. *IEEE Transactions on Control Systems Technology*, 1(3): 186–194, 1993.

[58] D. Liberzon. *Switching in Systems and Control*. Birkhauser, 2003.

[59] D. Liberzon and A. S. Morse. Basic problems in stability and design of switched systems. *IEEE Control Systems Magazine*, 19(5):59–70, 1999.

[60] H. Logemann and B. Mårtensson. Adaptive stabilization of infinite-dimensional systems. *IEEE Transactions on Autamatic Control*, 37(12):1869–1883, 1992.

[61] D.T. Magill. Optimal adaptive estimation of stochastic processes. *IEEE Transactions on Automatic Control*, AC-10(4):434–439, 1965.

[62] Mango, N. *Measurement & Calculation of Vehicle Center of Gravity Using Portable Wheel Scales*, number 2004-01-1076 in SAE Technical Paper Series, Detroit,MI, March 8-11 2004. SAE 2004 World Congress & Exhibition.

[63] Bengt Mårtennson. *Adaptive Stabilization*. Phd thesis, Lund Intitute of Technology, Department of Automatic Control, Lund, Sweden, Feb. 1986.

[64] Bengt Mårtennson. Switching function adaptive stabilization with a stability margin α. *Proceedings of the 28th Conference on Decision and Control*, 2:1561–1562, Dec. 1989.

[65] P.S. Maybeck and P.D. Hanlon. Performance enhancement of a multiple model adaptive estimator. *IEEE Transactions on Aerospace and Electronic Systems*, 31(4):1240–1253, 1995.

[66] P.S. Maybeck and R.D. Stevens. Reconfigurable flight control via multiple model adaptive control methods. *IEEE Transactions on Aerospace and Electronic Systems*, 27(3):470–479, 1991.

[67] K. Meyer. On the existence of Lyapunov functions for the problem of Lur'e. *J. SIAM Control*, 3(3):373–383, 1966.

[68] R.H. Middleton and G.C. Goodwin. Adaptive control of time-varying linear systems. *IEEE Transactions on Automatic Control*, 33(2):150–155, Feb. 1988.

[69] R.H. Middleton, G.C. Goodwin, D.J. Hill, and D.Q. Mayne. Design issues in adaptive control. *IEEE Transactions on Automatic Control*, 33(1):50–58, Jan. 1988.

[70] T. Mori, T.V. Nguyen, Y. Mori, and H. Kokame. Preservation of Lyapunov Functions under Bilinear Mapping. *Automatica*, 42:1055–1058, 2006.

[71] A.S. Morse. Supervisory control of families of linear set-point controllers. *Proceedings of the 32nd Conference on Decision and Control*, 2:1055–1060, Dec. 1993.

[72] A.S. Morse. Supervisory control of families of linear set-point controllers-part 1:exact matching. *IEEE Transactions on Automatic Control*, 41(10):1413–1431, Oct. 1996.

[73] A.S. Morse. Supervisory control of families of linear set-point controllers-part 2:robustness. *IEEE Transactions on Automatic Control*, 42(11):1500–1515, Nov. 1997.

[74] K. S. Narendra and A. M. Annaswamy. *Stable Adaptive Systems*. Prentice-Hall, 1989.

[75] K. S. Narendra and J. Balakrishnan. A common Lyapunov function for stable LTI systems with commuting $\mathscr{A}$-matrices. *IEEE Transactions on automatic control*, 39 (12):2469–2471, 1994.

[76] K. S. Narendra and R. M. Goldwyn. A geometrical criterion for the stability of certain non-linear non-autonomous systems. *IEEE Transactions on Circuit Theory*, 11(3):406–407, 1964.

[77] K.S. Narendra and J. Balakrishnan. Improving transient response of adaptive control systems using multiple models and switching. Technical Report 9212, Center for Systems Science, Dept. of EE, Yale University, New Haven, 1992.

[78] K.S. Narendra and J. Balakrishnan. Improving transient response of adaptive control systems using multiple models and switching. *IEEE Transactions on Automatic Control*, 39(9):1861–1866, 1994.

[79] K.S. Narendra and J. Balakrishnan. Adaptive control using multiple models. *IEEE Transactions on Automatic Control*, 42(2):171–187, 1997.

[80] K.S. Narendra, O.A. Driollet, M. Feiler, and K. George. Adaptative control using multiple models, switching and tuning. *International Journal of Adaptive Control and Signal Processing*, 17:87–102, 2003.

[81] K.S. Narendra and J.H. Taylor. *Frequency Domain Criteria for Absolute Stability*. Academic Press, 1973.

[82] K.S. Narendra and C. Xiang. Adaptive control of discrete-time systems using multiple models. *IEEE Transactions on Automatic Control*, 45:1669–1686, Sept. 2000.

[83] Kumpati S. Narendra. *From Feedback Control to Complexity Management: A Personal Perspective*, pages 1–30. in *Switching and Learning in Feedback Systems*, LNCS 3355, Edited by Murray-Smith R. and Shorten R. Springer, 2003.

[84] Narendra, K.S. and Balakrishnan, J. *Improving transient response of adaptive control systems using multiple models and switching*, volume 2, San Antonio, Texas, December 15-17 1993. Proceedings of the 32nd IEEE Conference in Decision and Control.

[85] Narendra, K.S. and Balakrishnan, J. *Intelligent Control using Fixed and Adaptive Models*, volume 1, Seattle, Washington, June 21-26 1995. Proceedings of the American Control Conference.

[86] Narendra, K.S. and Driollet, O.A. *Stochastic adaptive control using multiple estimation models*, volume 2, Las Vegas, Nevada USA, June 25-27 2001. Proceedings of the American Control Conference.

[87] Narendra, K.S. and George, K. *Adaptive Control of Simple Nonlinear Systems Using Multiple Models*, volume 3, Anchorage, AK, May 8-10 2002. Proceedings of the American Control Conference.

[88] Odenthal, D. and Bünte, T. and Ackermann, J. *Nonlinear steering and breaking control for vehicle rollover avoidance*, Karlsruhe, Germany, 1999. Proceeding of European Control Conference.

[89] Mason Oliver. *Switched systems, convex cones and common Lyapunov functions*. PhD thesis, Department of Electronic Engineering, National University of Ireland-Maynooth, Republic of Ireland, 2004.

[90] T. Ooba and Y. Funahashi. Two conditions concerning common quadratic Lyapunov functions for linear systems. *IEEE Transactions on automatic control*, 42(5):719–721, 1997.

[91] T. Pancake, M. Corless, and M. Brockman. Analysis and control methodology for a class of uncertain/nonlinear systems in the presence of bounded disturbance inputs. *In preperation*.

[92] Pancake, T. and Corless, M. and Brockman, M. *Analysis and control of polytopic uncertain/nonlinear systems in the presence of bounded disturbance inputs*, Chicago, IL, June 2000. Proceedings of the American Control Conference.

[93] Paul, A. and Akar, M. and Safonov, M.G. and Mitra, U. *Power Control for Wireless Networks Using Multiple Controllers and Switching*, Boston, MA, Jun.30-Jul.2 2004. Proceedings of the American Control Conference.

[94] Paul, A. and Safonov, M.G. *Model Reference Adaptive Control Using Multiple Controllers & Switching*, Maui, Hawaii, Dec. 9-12 2003. Proceedings of the IEEE Conference on Decision and Control.

[95] I. Petersen, T.A. Johansen, J. Kalkkuhl, and J. Ludemann. Wheel slip control in ABS brakes using gain scheduled constrained LQR. Porto, Portugal, 2001. Proc. of the European Control Conference.

[96] R. Pickhardt. Adaptive control of a solar power plant using a multi-model. *IEE Proceedings on Control Theory and Applications*, 147(5):493–500, 2000.

[97] V.M. Popov. On the absolute stability of nonlinear control systems. *Automatic Remote Control*, 22(8):961–979, 1961.

[98] H. Power and R. Simpson. *An Introduction to Dynamics and Control*. McGraw-Hill, New York, 1978.

[99] A. Rantzer. On Kalman-Yakubovic-Popov lemma. *Systems and Control Letters*, 28: 7–10, 1996.

[100] J. Rojas and J. Collada. Stability of interval matrices using the distance to the set of unstable matrices. *Proc. of the American Control Conference, Maryland*, pages 238–239, 1994.

[101] Walter Rudin. *Principles of Mathematical Analysis*. McGraw-Hill International, 3rd edition, 1976.

[102] Wilson J. Rugh. *Linear Systems Theory*. Information and System Sciences Series. Prentice-Hall, New Jersey, 2nd edition edition, 1996.

[103] M.G. Safonov and T. Tsao. The unfalsified control concept and learning. *IEEE Transactions on Automatic Control*, 42:843 – 847, June 1997.

[104] Erich Schindler. *Vehicle Dynamics, Lecture Notes*. FHTE Esslingen University of Applied Sciences, Esslingen-Germany, 2001.

[105] K.D. Schott and B.W. Bequette. *Multiple Model Adaptive Control*, pages 269–291. in *Multiple Model Approaches to Modelling and Control*, Edited by Murray-Smith R. and Johansen T.A. ,Taylor and Francis, 1997.

[106] Schott, K. and Bequette, B.W. *Control of Chemical Reactors Using Multiple-Model Adaptive Control (MMAC)*, Helsingor,Denmark, 1995. Proceedings of 4th IFAC Symposium on Dynamics and Control of Chemical Reactors,Distillation Columns and Batch Reactors.

[107] Á. Semsey, L. Palkovics, and Gerum. E. Roll-over prevention system for commercial vehicles-additional sensorless function of the electronic brake system. *Vehicle System Dynamics*, 32:285–297, 1999.

[108] M. Sezer and D. Siljak. On stability of interval matrices. *IEEE Transactions on automatic control*, 39(2):368–371, 1994.

[109] R. Shorten, P. Curran, K. Wulff, C. King, and E. Zeheb. On spectral conditions for positive realness of transfer function matrices. Technical report, TU Berlin, July 2007.

[110] R. Shorten, P. Curran, K. Wulff, and E. Zeheb. Spectral conditions for positive realness of transfer function matrices. Accepted for publication in *IEEE* Transactions on Automatic Control, July 2007.

[111] R. Shorten and F. Ó Cairbre. On the Stability of Pairwise Triangularisable and Related Switching Systems. volume 3, pages 1882 – 1883. Proceedings of the American Control Conference, 2001.

[112] R. Shorten and F. Ó Cairbre. A proof of global attractivity for a class of switching systems using a non-Lyapunov approach. *IMA Journal of Mathematical Control and Information*, 18:341–353, 2001.

[113] R. Shorten, F. Ó Cairbre, and P. Curran. On the dynamic instability of a class of switching systems. Budapest, Hungary, October 2-4 2000. IFAC Symposium on Artificial Intelligence in Real Time Control.

[114] R. N. Shorten, O. Mason, F. Ó Cairbre, and P. Curran. A unifying framework for the SISO Circle Criterion and other quadratic stability criteria. *International Journal of Control*, 77(1):1–8, 2004.

[115] R. N. Shorten and K. S. Narendra. On common quadratic Lyapunov functions for pairs of stable LTI systems whose system matrices are in companion form. *IEEE Transactions on automatic control*, 48(4):618–621, 2003.

[116] R. N. Shorten, K. S. Narendra, and O. Mason. A result on common quadratic Lyapunov functions. *IEEE Transactions on automatic control*, 48(1):110–113, 2003.

[117] R.N. Shorten and K.S. Narendra. Investigating the stability of a class of hybrit system. *IEE Computing and Control Engineering Journal*, 9(2):81–88, 1998.

[118] Robert N. Shorten. *A Study of Hybrid Dynamical Systems with Application to Automotive Control*. PhD thesis, Department of Electrical and Electronic Engineering, University College Dublin, Republic of Ireland, 1996.

[119] Shorten, R. and Narendra, K. S. *Strict positive realness and the existence of diagonal Lyapunov functions*, San Diego, CA, December 2006. Proceedings of the 45th IEEE Conference on Decision and Control.

[120] T. Söderström and P. Stoica. *System Identification*. International Series in Systems and Control Engineering. Prentice Hall International, Cambridge, Great Britain, 1989.

[121] S. Solmaz, M. Akar, and R. Shorten. Online Center of Gravity Estimation in Automotive Vehicles using Multiple Models and Switching. In *Proceedings of the 9th International Conference on Control, Automation, Robotics and Vision ICARCV06*, Singapore, Dec. 5-8 2006.

[122] S. Solmaz, M. Akar, and R. Shorten. Irish patent ref: (s2006/0162), method for determining the center of gravity for an automotive vehicle, February 2007. European Patent Pending.

[123] S. Solmaz, M. Akar, R. Shorten, and J. Kalkkuhl. Realtime Multiple-Model Estimation of Center of Gravity Position in Automotive Vehicles. *Vehicle System Dynamics Journal*, 2007. Accepted for publication.

[124] Solmaz, S. and Corless, M. and Shorten, R. *A methodology for the design of robust rollover prevention controllers for automotive vehicles: Part 1-Differential Braking*, San Diego, CA, December 2006. Proceedings of the 45th IEEE Conference on Decision and Control.

[125] Solmaz, S. and Corless, M. and Shorten, R. *A methodology for the design of robust rollover prevention controllers for automotive vehicles: Part 2-Active Steering*, New York, USA, July 11-13 2007. American Control Conference.

[126] E. Sontag. Smooth stabilization implies coprime factorization. *IEEE Transaction on Automatic Control*, 34(4):435–443, 1989.

[127] Ralph H. Streiter. *Entwicklung und Realisierung eines analytischen Regelkonzeptes für eine aktive Federung-(Active Body Control)*. PhD thesis, Technische Universtät Berlin, Germany, 1996.

[128] Takano, S. and Nagai, M. *Dynamics control of large vehicles for rollover prevention*, Tottori, Japan, September 25-28 2001. Proceedings of the IEEE International Vehicle Electronics Conference.

[129] T. Tsao and M.G. Safonov. Unfalsified direct adaptive control of a two-link robot arm. *International Journal of Adaptive Control and Signal Processing*, 15:319–334, May 2001.

[130] Tsao, T. and Brozenec, T. and Safonov M.G. *Unfalsified adaptive spacecraft attitude control*, Austin, Texas, Aug. 11-14 2003. Proceedings of AIAA Guidance, Navigation and Control Conference.

[131] A. Vahidi, A. Stefanopoulou, and H. Peng. Recursive least squares with forgetting for online estimation of vehicle mass and road grade: Theory and experiments. *Vehicle System Dynamics*, 43(1):31–55, 2005.

[132] Van Zanten, A. and Erhardt, R. and Pfaff, G. and Kost, F. and Hartmann, U. and Ehret, T. *Control Aspects of the Bosch-VDC*, Aachen, Germany, 1996. AVEC'96 Int. Symposium on Advanced Vehicle Control.

[133] Van Zanten, Anton T. *Evolution of Electronic Control Systems for Improving the Vehicle Dynamic Behavior*, Hiroshima, Japan, 2002. AVEC'02 Int. Symposium on Advanced Vehicle Control.

[134] M. Vilaplana, O. Mason, D. Leith, and W. Leithead. *Switching and Learning in Feedback Systems , chapter 'Control of yaw-rate and sideslip in 4-wheel steering cars with actuator constraints'*. Number LNCS 3355. Springer-Verlag, Lecture Notes in Computer Science, 2005.

[135] H.P. Whitaker. An adaptive system for control of the dynamics of performance aircraft and spaceraft. *Inst. Aeronatical Sciences*, pages 59–100, 1959.

[136] H.P. Whitaker, J. Yamron, and A. Kezer. Design of model reference adaptive control systems for aircraft. Technical Report R-164, Intrumentation Labaratory, MIT, Cambridge, Massachusetts, 1958.

[137] Wielanga, Thomas J. *A Method for Reducing On-Road Rollovers: Anti -Rollover Braking*, number 1999-01-0123 in SAE Technical Paper Series, Detroit,MI, March 1-4 1999. SAE 1999 World Congress & Exhibition.

[138] Wielanga, T.J. and Chace, M.A. *A Study of Rollover Prevention using Anti-Rollover Braking*, number 2000-01-1642 in SAE Technical Paper Series, Detroit,MI, May 2000. SAE 2000 World Congress & Exhibition.

[139] K. Wulff, F. Wirth, and R. Shorten. On the stabilisation of a class of switched single-input single-output systems. IEEE Conference on Decision and Control, 2005.

[140] Kai Wulff. *Quadratic and Non-Quadratic Stability Criteria for Switched Linear Systems*. PhD thesis, National University of Ireland-Maynooth, Republic of Ireland, 2004.

[141] Xiang, C. and Narendra, K.S. *Design Issues In Stochastic Adaptive Adaptive Control of Discrete-time Systems Using Multiple Models*, volume 2, Las Vegas, Nevada USA, Dec. 10-13 2002. Proceedings of the 41st IEEE Conference on Decision and Control.

[142] E. Zeheb. Necessary and sufficient conditions for robust stability of a continuous system-the continuous dependency case illustrated via multilinear dependency. *IEEE Transactions on Circuits and Systems*, 37(1):47–53, 1990.